

THESIS

ADDITIVE MANUFACTURE OF DISSOLVABLE TOOLING FOR AUTOCLAVE PROCESSING
OF FIBER REINFORCED POLYMER COMPOSITES

Submitted by

Isaac Morris

Department of Mechanical Engineering

In partial fulfillment of the requirements

For the Degree of Master of Science

Colorado State University

Fort Collins, Colorado

Summer 2022

Master's Committee:

Advisor: Donald Radford

Mostafa Yourdkhani
Paul Heyliger

Copyright by Isaac Michael Morris 2022

All Rights Reserved

ABSTRACT

ADDITIVE MANUFACTURE OF DISSOLVABLE TOOLING FOR AUTOCLAVE PROCESSING OF FIBER REINFORCED POLYMER COMPOSITES

Autoclave processing of advanced fiber reinforced polymer composites (AFRPC) uses applied heat and pressure to yield high quality composite components. Geometrically accurate and thermally stable molds or tools are used to maintain the part form until the part cures and rigidizes. For high-volume production runs, molds may be made from materials such as metals, ceramics, or AFRPCs. However, tooling made from these materials can be costly to manufacture and are not suitable for low volume production runs. This is especially true for complex geometries in trapped tooling situations where the cured composite shape prevents tool separation. In this situation, composite manufacturers rely on sacrificial washout tooling materials that are machined or cast to shape to create the tool. However, these sacrificial materials still come with significant challenges. For example, the surfaces of these tools are often porous and require sealing, and their washout can result in corrosive waste that makes disposal challenging. Additionally, these tools are brittle and monolithic in nature, making them fragile to handle and slow to heat up during cure.

An alternative may be to use high temperature, dissolvable thermoplastic materials in melt extrusion additive manufacturing to create complex washout tooling. However, there is a lack of information regarding the types of soluble materials and the structural configurations that make this type of tooling successful in autoclave use. To begin to address this, samples made from several materials, and one insoluble model material, were processed in stepwise fashion at increasing autoclave processing temperatures to evaluate the impacts of material and structure on autoclave robustness. Then, mid-sized composite specimens were produced on 3D-printed tooling that evaluated the interaction between the

composite and the tool, including surface quality and deformation. Finally, a trapped tooling geometry was used to manufacture several composites at processing conditions of 157°C at 414kPa, well above the use temperature of the tested materials. These trials focused on reducing deformation by adjusting the tool wall thickness and vacuum bagging configuration.

It was shown that 3D-printed dissolvable tooling can be used as an alternative to traditional washout tooling for autoclave processing. The materials Stratasys ST-130 and Infinite Material Solutions AquaSys 180 were used to manufacture tools that were processed at autoclave conditions of 121°C at 345kPa with minimal deformation. Surface quality was also found to be acceptable without machining or sealing, eliminating this step from the production of traditional washout tools. Finally, a modified tool design and vacuum bagging technique were demonstrated that significantly reduced the deformation of tooling at processing temperatures that significantly exceed the use temperature of the material.

ACKNOWLEDGMENTS

I would like to express my gratitude towards my advisor, Dr. Donald Radford, for having me complete my work at the Composite Materials, Manufacture and Structures lab, and his guidance and dedication throughout my graduate school experience. Even in trying times through the COVID-19 crisis, his goal was always aimed at towards helping me improve in school, in research, and in a professional setting. I also greatly appreciate the friendship, collaboration, and experiences shared with our entire lab group and others working at The Factory, including Jaren Fleischman, Steven Hogan, Rashedul Islam, Clement Brousse, Femi Ibitoye, Harry Ratkai, Sumaiya Tanu, Alex Preston, Morteza Ziaee, and Iman Naseri. Additionally, I'd like to thank Dr. Yourdkhani for always being a friendly face and having me volunteer in his lab group in my undergraduate career, which helped motivate me to pursue this degree. I am also so grateful for the unwavering support offered by my entire family throughout my college experience, and to my friends who were always free to help break up the long days and have some fun. Finally, I'm so thankful for the support of Kristen LeBar, who has made the days speed by.

This material is based on work supported by the U.S. Department of Energy's Office of Energy Efficiency and Renewable Energy under the support of Task 4.9 of the Institute for Advanced Composites Manufacturing Innovation, Award Number DE-EE006926. The views expressed in the article do not necessarily represent the views of the DOE or the U.S. Government. Funding was also provided by the Colorado Office of Economic Development and International Trade under grant number CTGG1 2020-2442. Additionally, much of this work was supported by Ability Composites, a composite manufacturing shop based out of Loveland, Colorado. Ability Composites provided traditional soluble tooling samples to compare to the 3D printed tools for the truncated pyramid and bent duct geometries. Additionally, they aided in the layup and autoclave processing of several composite components and completed 3D scans of the tooling to evaluate deformation.

TABLE OF CONTENTS

ABSTRACT.....	ii
ACKNOWLEDGMENTS	iv
LIST OF TABLES	vii
LIST OF FIGURES	viii
Chapter 1: Introduction and Background.....	1
Project Background.....	1
Introduction to Autoclave Production of Advanced Composites	1
General Overview of Composite Processing	1
Tooling for AFRPC Processing	4
Trapped Tooling.....	8
Autoclave Processing of AFRPC.....	10
Introduction to Additive Manufacturing	13
Additive Manufacturing Overview	13
Additive Processes for Composite Tooling.....	18
Additive Processes for Removable Tooling.....	23
Applying Melt Extrusion Technology to Autoclavable Composite Tooling	24
Thermal Stability	26
Thermal and Mechanical Anisotropy.....	28
Trapped Tooling.....	30
Problem Statement and Goals.....	31
Chapter 2: Material and Structure Evaluation for Autoclave Robustness and Dissolution	33
Temperature Pressure Vacuum Material Sample Testing.....	33
Experimentation.....	34
Results and Discussion	46
Temperature Pressure Vacuum Structural Sample Testing	57
Experimentation.....	57
Results and Discussion	62
Temperature Pressure Vacuum Structural Sample Testing – Infill and Road Width	68
Experimentation.....	68
Results and Discussion	70
Dissolution Studies	71
Experimentation.....	71
Results and Discussion	72

Chapter 3: Composite Manufacture on Partially Dense Truncated Pyramid Tooling	76
Composite manufacture On Truncated Pyramid Geometry	76
Experimentation	76
Truncated Pyramid Results and Discussion	82
Chapter 4: Composite Manufacture on Partially Dense Bent Duct Tooling	95
Experimentation	95
Results and discussion	102
Chapter 5: Composite Manufacture on Hollow Bent Duct Tooling	107
Experimentation	107
Materials	111
Equipment	112
Preparation of Hollow Duct Samples	116
Autoclave Processing of Composites on Hollow Bent Duct Tooling	120
Evaluation	123
Results and Discussion	123
Chapter 6: Conclusions	155
References	159
Appendices	168
Appendix A: Component Drawings	168
Appendix B: 3D Scans	174

LIST OF TABLES

Table 1	The additive manufacturing process categories defined by ASTM 2792-12a [16].	15
Table 2	Estimated print time for a 20mm cube with changing nozzle size	17
Table 3	The readily available material and processing parameters for the evaluated materials	35
Table 4	Dissolvable tooling candidate material 3D printing parameters	38
Table 5	A summary of material focused TPV tests conducted over the BVOH, CL-130, AQ-120, and ST-130.	45
Table 6	Photographs of the 1.3 mm thick CL-130 and BVOH samples during testing up to 121°C and 552 kPa.	48
Table 7	Photographs of the 1.3mm thick ST-130 and AQ-120 samples during testing up to 121°C and 552kPa.	49
Table 8	Photographs of the 1.3mm thick AQ-120, CL-130, and ST-130 samples during testing up to 121°C and 621kPa.	51
Table 9	Photographs of the 1.3mm thick AQ-180 and ST-130 samples during testing up to 121°C and 621kPa.	53
Table 10	Comparison of top surface deformation at 121°C and 621kPa conditions.	55
Table 11	Stability at 345kPa and temperature of 1.3mm surface thickness specimens.	56
Table 12	Summary of specimen failures based on visual examination.	56
Table 13	Test matrix for structural TPV testing of PETG specimens.	59
Table 14	Infill pattern test samples 1 and 2.	62
Table 15	Outer skin thickness test samples 1, 3, 4, and 5.	64
Table 16	The secondary support structure test samples 6 and 7.	65
Table 17	The effects of infill density are seen in samples 8, 1, and 9.	65
Table 18	Nozzle size test samples 12 and 13.	66
Table 19	PETG samples 10 and 11, with and without carbon fiber loading, respectively.	67
Table 20	Sample matrix for infill parameter testing.	69
Table 21	The washout time and information for each sample cube.	73
Table 22	The dissolution process is shown below for the AQ-120, AQ-180, and drilled AQ-180 samples.	75
Table 23	The surface profilometry data for the truncated pyramid tooling	93
Table 24	Various duct geometries and materials used for manufacturing composite parts for this project.	111
Table 25	The material usage, print time, and overall print rates for the 3D printed ducts.	120

LIST OF FIGURES

Figure 1	Two molds are used (left) for the manufacture of an AFRPC wind turbine blade (right) [2]. 3
Figure 2	The tool is first manufactured (1), then a mold is generated (2), and finally the final part is created in the mold (3). The high-quality outer surface on the tool is transferred to the final part. 5
Figure 3	An egg crate structure can be seen supporting the thin critical surface of this tool [4]. 7
Figure 4	A mold that acts as a diffusion barrier for a pressure vessel (a), a reusable, reformable shape memory mold (b), and a multi-part split mold made from composite materials (c) [9, 10, 11]. 9
Figure 5	A general composite layup for autoclave processing. 12
Figure 6	Cost vs. Complexity and Cost vs. Production volume relationships for additive and subtractive manufacturing approaches [18]. 16
Figure 7	Acetabular cup produced using a powder bed fusion process [24]. 18
Figure 8	Melt extrusion additive manufacturing platform [29]. 22
Figure 9	Sacrificial composite tooling can be made using binder jetting (a), vat photopolymerization (b, c), or melt extrusion (d, e) [13, 35, 31, 25]. 24
Figure 10	A 13-meter-long mold for a wind turbine blade manufactured using short carbon fiber filled thermoplastic feedstock in a melt extrusion process [2]. 25
Figure 11	In this image, both a shell-type tool (a) and a partially dense tool (b) are shown [40]. 27
Figure 12	The enclosed Ender 5 Plus showing the temperature controller (a) and water-cooling system (b). 36
Figure 13	The TPV specimen truncated cone geometry for the nominally 2.2mm thick top surface sample. 37
Figure 14	Underextrusion can be seen as a defect in the above AQ-120 samples with varying severity, sometimes stopping material extrusion entirely. Samples showing no underextrusion (a), some underextrusion (b), severe underextrusion (c), and a failed print caused by underextrusion (d). 40
Figure 15	Preliminary ST-130 sample showing poor surface roughness on side walls and discoloration on top surface compared to a high-quality ST-130 specimen, produced later in the study. 41
Figure 16	Representative images of samples made from BVOH (a), CL-130 (b), and AQ-180 (c). A line is marked across the top surface of the BVOH specimen (a), which was later used to aid in visualizing deformation. 41
Figure 17	TPV specimens in a vacuum bag configuration prior to testing. 42
Figure 18	A general TPV test, showing the various temperature and pressure cycles applied. 44
Figure 19	The TPV test configuration showing the entire tooling plate with all samples (a) and close-ups of specimens made from BVOH (b), CL-130 (c), AQ-120 (d), and ST-130 (e). 47
Figure 20	The samples with nominal top surface thicknesses of 1.3mm (a), 2.2mm (b), and 3.2mm thick (c). 50
Figure 21	Various tested specimens after the 121°C at 345kPa test run. 54
Figure 22	Print through failure mode. 57
Figure 23	The geometry used for samples 1-9 in the structural TPV tests. 58
Figure 24	A 3D Printed cylinder with gyroid infill and no outer skins. 60
Figure 25	Top view rendering of samples 1-9 during the manufacturing process. 61
Figure 26	The four ST-130 samples prepared for testing prior to being loaded into the autoclave. The top surfaces were marked to aid in visualizing deformation. 69
Figure 27	ST-130 specimens after testing including: control sample (1), increased infill density (2), decreased road width/spacing (3), and increased top surface thickness (4). 70
Figure 28	The ceramic washout tooling sample prior to dissolution (left) and during dissolution. 73
Figure 29	The gel-like substance forming on the surface of the ST-130 sample during dissolution trials. 74
Figure 30	Cross-section of truncated square pyramid specimen geometry. A complete drawing is in Appendix A. 78

Figure 31 One of the tools during manufacture inside the heated enclosure.	79
Figure 32 Representative layup (a), vacuum bagging (b), autoclave cure (c), and demolding (d) steps of the composite manufacturing process.	81
Figure 33 The approximate locations and orientations used to record the surface roughness data on the tool (left) and composite (right).	82
Figure 34 The as-printed Rough Pyramid tool (left) and the Smooth Pyramid tool (right).	83
Figure 35 The FaroArm scan of the Smooth Pyramid prior to composite manufacture.	84
Figure 36 The FaroArm scan of the ceramic tool prior to composite manufacture. Complete scans are listed in Appendix B.	85
Figure 37 The Rough Pyramid (left) and Smooth Pyramid (Right) tools shown after composite processing.	85
Figure 38 The Rough Pyramid tool and the resulting composite parts are shown before composite manufacture (a), after one production cycle (b, c), and after two production cycles (d, e).	86
Figure 39 The molded surfaces of the composites created by the Rough (a), Smooth (b), and Ceramic (d) Pyramid tools are shown.	87
Figure 40 The FaroArm scans of the 3D Printed Smooth Pyramid tool are shown before (a) and after (b) composite manufacture.	88
Figure 41 The FaroArm scan of the composite manufactured on the Smooth Pyramid tool showing the seam and region with excess material did transfer to the cured composite.	89
Figure 42 The Rough Pyramid tool scans after one processing cycle (a) and two processing cycles (b). ..	90
Figure 43 The first composite manufactured on the Rough Pyramid.	91
Figure 44 The second composite cured on the Rough Pyramid tool.	92
Figure 45 Geometry of the complex tooling.	96
Figure 46 The bent duct geometry showing the two halves.	97
Figure 47 Printing the Split ST-130 Duct (1).	98
Figure 48 The ST-130 Split Duct (1) was printed in two halves and utilized ironing on the surfaces indicated by the red arrows (a, b), had holes drilled in the bottom bonding surface (c), was bonded together (d) and clamped to cure (e).	99
Figure 49 The tool had a significant crack form during the post cure of the epoxy used to bond the two halves together (a). This crack was then filled, and post cured again (b). During the second post cure, a new crack formed (c) and can be seen traversing multiple layers (d).	100
Figure 50 The nominal autoclave conditions programmed for the cure of the Control Duct (0) and the Split ST-130 Duct (1), which used a carbon fiber plain weave with TCR UF3362 resin.	101
Figure 51 The FaroArm scan of the CNC machined Control Duct (0) both before (left) and after (right) autoclave processing.	102
Figure 52 The completed duct before and after washout tooling material removal.	103
Figure 53 The cured part and tool used for duct 1.	104
Figure 54 Cure cycle used to manufacture duct 1 showing a loss of vacuum.	105
Figure 55 Scans of the tool (left) and part (right) were made using a FaroArm by Ability Composites.	106
Figure 56 The hollow duct geometry and the new vacuum bagging approach, with a straightedge inserted through the vacuum bagged component to better visualize the approach.	108
Figure 57 Depiction of the vacuum bagging scheme on the hollow duct geometry.	109
Figure 58 The Bondtech CHT nozzle has three filament channels, increasing material flowrate.	114
Figure 59 The upgraded extruder can be seen with a water cooled heatsink (a), Berd Air Cooling (b), and a high flow 1mm Bondtech CHT nozzle (c).	114
Figure 60 The ends of the flexible plungers that contact the homing surfaces in the print chamber are circled in red (a). The limit switches are shown outside the enclosure (b).	115
Figure 61 This shows the solid tool geometry (a) and the modifier mesh (b) that was used to add an additional perimeter road to the sloped regions of the tool (c).	116
Figure 62 Hollow bent duct printing process for the Thick ST-130 Duct (2).	117
Figure 63 The speed and material flowrates for duct 7.	119

Figure 64 A representative composite manufacturing process of one of the hollow ducts at steps: bare tool (a), during layup (b), and during debulk (c).....	121
Figure 65 The nominal autoclave conditions programmed for the cure of ducts 2-7. This is the cure cycle that was used to process Ducts 0 and 1 in previous studies that also used prepreg with TCR UF3362 resin.....	122
Figure 66 The printed tool (a), the composite manufactured on the tool (b), and the composite part after the tooling was removed (c).....	124
Figure 67 FaroArm scans of the Thick ST-130 Tool (2) both before (left) and after (right) composite processing.	125
Figure 68 The top-down view of the Thick ST-130 Duct (2).....	126
Figure 69 The manufactured thin-walled ST-130 tool.....	127
Figure 70 The cured composite with the tool left inside.....	128
Figure 71 FaroArm scans of the Thin ST-130 Tool before (left) and after (right) composite manufacturing.	128
Figure 72 The manufactured tool for Duct 4.	130
Figure 73 The completed part and tool used to manufacture Duct 4.	131
Figure 74 The FaroArm scans of the Thick AQ-120 Duct (4) tool (left) and composite (right).	131
Figure 75 The manufactured tool for the Thin AQ-120 Duct (5).	132
Figure 76 The completed part and tool for the Thin AQ-120 Duct (5).....	133
Figure 77 The FaroArm scans of the Thin AQ-120 tool before (left) and after (right) composite manufacture.....	134
Figure 78 The manufactured Thin AQ-180 tool (6).....	135
Figure 79 Duct 6 had a rough surface texture on overhanging regions (left) and a wavy surface located where the color banding occurred (right).....	136
Figure 80 The cured composite cured on the Thin AQ-180 Duct (6).....	136
Figure 81 The FaroArm scans of the Thin AQ-180 Duct (6) before (left) and after (right) composite manufacture.....	137
Figure 82 The manufactured Extra Thick ST-130 Tool (7).....	138
Figure 83 The composite cured on the Extra Thick ST-130 Tool 7.	139
Figure 84 The FaroArm scans of the Extra Thick ST-130 Tool (7) both before (left) and after composite manufacture (right).	140
Figure 85 The manufactured Low Temperature Thin ST-130 Tool (7).....	141
Figure 86 The surface porosity caused by no retractions present on the backside of the tool.	141
Figure 87 The printing defect caused by insufficient cooling on overhanging regions (a), and the layer position at 195mm where the fan speed and extruder temperature were modified (b).	142
Figure 88 The composite cured on the Low Temperature Thin ST-130 Tool.	142
Figure 89 The FaroArm scans of the Low Temperature Thin ST-130 Duct (8) both before (top) and after composite manufacture (bottom).	143
Figure 90 The FaroArm scans of the hollow ducts 3-6. The remaining scans showed similar results but were scanned in different orientations. The entire set of scans can be found in Appendix B.....	144
Figure 91 The FaroArm scans for Ducts 7 and 8, which used scaling to adjust the size of the printed geometry.	146
Figure 92 The photograph of each cured duct can be compared for deformation.	148
Figure 93 The FaroArm scans of the ducts after composite processing.	150
Figure 94 Views showing relative distortions of the manufactured ducts 0-8.....	152
Figure A 1 Crush sample geometry	169
Figure A 2 Truncated square pyramid geometry for PETG sample studies	169
Figure A 3 Truncated pyramid geometry for composite manufacturing trials	170
Figure A 4 Bent duct tooling geometry	171
Figure A 5 Top half of longitudinally split bent duct	172
Figure A 6 Bottom half of longitudinally split bent duct.....	173

Figure B 1 The ceramic pyramid tool FaroArm 3D scan prior to composite manufacture.	174
Figure B 2 The Smooth Pyramid tool FaroArm 3D scan prior to composite manufacture.	174
Figure B 3 The Rough Pyramid tool FaroArm 3D scan after one composite was manufactured.	175
Figure B 4 The Smooth Pyramid tool FaroArm 3D scan after one composite was manufactured.	175
Figure B 5 The Rough Pyramid tool FaroArm 3D scan after two composites were manufactured	176
Figure B 6 The FaroArm scan of the first composite cured on the Rough Pyramid tool.....	177
Figure B 7 The FaroArm scan of the second composite cured on the Rough Pyramid tool.....	177
Figure B 8 The FaroArm scan of the composite cured on the Smooth Pyramid tool.	177
Figure B 9 The FaroArm scan of the top half of the tool used for the Control Duct (0).	178
Figure B 10 The FaroArm scan of the composite manufactured on the Control Duct Tool (0).	179
Figure B 11 The FaroArm scan of the Split ST-130 Tool (1).....	180
Figure B 12 The FaroArm scan of the composite manufactured on the Split ST-130 Tool (1).....	181
Figure B 13 The FaroArm scan of the Thick ST-130 Tool (2).....	182
Figure B 14 The FaroArm scan of the composite manufactured on the Thick ST-130 Tool (2).....	183
Figure B 15 The FaroArm scan of the Thin ST-130 Tool (3).....	184
Figure B 16 The FaroArm scan of the composite manufactured on the Thin ST-130 Tool (3).....	184
Figure B 17 The FaroArm scan of the Thick AQ-120 Tool (4).....	185
Figure B 18 The FaroArm scan of the composite manufactured on the Thick AQ-120 Tool (4).....	185
Figure B 19 The FaroArm scan of the Thin AQ-120 Tool (5).....	186
Figure B 20 The FaroArm scan of the composite manufactured on the Thin AQ-120 Tool (5).	186
Figure B 21 The FaroArm scan of the Thin AQ-180 Tool (6).....	187
Figure B 22 The FaroArm scan of the composite manufactured on the Thin AQ-180 Tool (6).	188
Figure B 23 The FaroArm scan of the Extra Thick ST-130 Tool (7).	189
Figure B 24 The FaroArm scan of the Extra Thick ST-130 Tool (7) after composite manufacture.....	189
Figure B 25 The FaroArm scan of the Low Temperature Thin ST-130 Duct (8).....	190
Figure B 26 The FaroArm scan of the composite manufactured on the Low Temperature Thin ST-130 Tool (8).	190

CHAPTER 1: INTRODUCTION AND BACKGROUND

PROJECT BACKGROUND

This project was supported by IACMI Project 4.9, Development of Additively Manufactured Complex Tools for Autoclave Cured Composites. A team was assembled for this project, including the industry lead, Ability Composites, as well as NREL and Colorado State University (CSU). Ability Composites had originally expressed interest in alternate methods of producing tooling for composite parts. In follow-up discussions, it became clear that one of their tooling challenges revolved around complex, small production volume composite parts that were tooled on washout material. To build an understanding of the potential for replacing conventional washout tooling with 3D printed thermoplastic tooling, several commercially available dissolvable thermoplastic printing materials were evaluated leading to tooling representative of commercial articles of interest to Ability Composites. Ultimately, Ability Composites was able to directly compare autoclave processed prepreg composite parts produced on conventional washout tooling to composite parts molded on 3D printed dissolvable tooling produced at CSU.

INTRODUCTION TO AUTOCLAVE PRODUCTION OF ADVANCED COMPOSITES

General Overview of Composite Processing

Advanced fiber reinforced polymer composite (AFRPC) materials have been used in many applications due to their high stiffness to weight ratio and their uniquely tailorable properties. These properties make their use ideal for structures requiring lightweight and stiff designs. Additionally, their development involves the parallel engineering of both the structure and material properties which makes their design and manufacture more versatile but also more difficult than traditional, isotropic materials. Composites gain their high specific properties from the combination of two or more constituent materials, commonly a reinforcing fiber and a matrix material. The reinforcing fibers act to provide stiffness and strength, and the matrix passes loads through shear between adjacent fibers. The properties can be tailored

by considering the orientation of the load-carrying fibers. The attention to fiber direction is what allows composites to develop unique or superior properties to either constituent alone.

AFRPC materials can be used in a variety of processes, and in most cases, they are molded to form the final shape. Some common applications of AFRPC materials include aircraft aerodynamic and structural components, parts for high performance motor or water sports, lightweight prosthetics, high performance consumer market sporting equipment (golf clubs, skis, tennis racquets, fishing rods, etc.), and wind turbine blades [1]. These applications all benefit greatly from AFRPC materials due to their complex curving surfaces and lightweight, stiffness-driven design.

Composite structures are created by placing both fiber reinforcement and matrix material into a geometrically accurate mold. The fibrous composite reinforcement materials may be loose, woven into a fabric, or stitched into a preformed geometry. The matrix material may take the form of a liquid, gel, powder, or fiber. Often, the reinforcement and matrix can also be acquired after being combined into a sheet in a highly controlled fashion, then partially cured to a gel-like state. In this state, called prepreg, the precursors are much easier to handle, cut, and assemble into the mold. After the precursor materials are placed into the mold, they are consolidated using external pressure or vacuum. This consolidation step is commonly used to eliminate voids and increase the packing density of the fiber reinforcement through the thickness of the part prior to and during processing. The consolidated composite is then cured, commonly by exposing the precursor materials to elevated temperatures in a ‘cure cycle’. Curing can also be completed at room temperature; however, the focus of this work will be on elevated temperature cure cycles. When heated, the matrix viscosity drops so that it may further flow to wet the reinforcement and eject voids. The increased temperature also accelerates crosslinking within the matrix material, forming a network of primary bonds that ultimately create a rigid composite structure.

There are many composite manufacturing processes that can meet the needs of various applications and resources. However, in all cases, some form of a mold or tool is used to form the composite part. The mold characteristics are critical to ensure the successful manufacture of the

component. The mold must, at minimum, maintain its shape during the cure cycle. Composite molds may be made from several different materials, and are commonly made from metals, ceramics, polymers, or composite materials. The molds may be manufactured by casting, machining, 3D printing, and many other processes. An example of a large 3D printed short fiber reinforced composite mold and the resulting part can be seen in figure 1.



Figure 1 Two molds are used (left) for the manufacture of an AFRPC wind turbine blade (right) [2].

The mold characteristics are so critical to the success of the composites manufacture because they create the final part geometry. The mold must also separate from the part once cured. Thus, draft angles are included for successful part release and the surface is held to vacuum tight standards and high-quality surface finishes. Mold designs must also consider the number of parts required and the associated durability of the mold. Finally, the thermal characteristics of the mold structure must be considered. Molds that have high coefficients of thermal expansion (CTE) may result in incorrect part sizes, which is especially important on large parts where small expansion ratios multiply over the length of the part. Additionally, molds should have high thermal conductivity and low thermal inertia, so that the part may be heated at the designed rates. Typically, a mold made with a combination of thermally stable materials, drafted surfaces, and a high-quality surface finish is sufficient to meet most of these requirements.

Contact molding is a common process in which only one surface of the part geometry is accurately formed by the mold. If the mold remains geometrically accurate and has a high-quality surface finish, then the molded side of the composite will share these characteristics. The other side of the

composite typically has less accurate thicknesses, and a lower quality surface finish. Alternatively, closed molding, or two-sided molding, approaches can provide two accurate and high-quality molded surfaces; however, they are much more complex. One-sided contact molding approaches are common and sufficient for many applications and will be the focus of this work.

Tooling for AFRPC Processing

One common way of creating parts is to use both a mold and a tool. The terms mold and tool are similar, but are often held to similar design requirements, so they can be used somewhat interchangeably. However, they do have distinct definitions. The tool is typically referred to as the master or plug and is used to create molds. A mold is then removed from the tool before being used to create the final composite component. There are numerous benefits gained from using both a tool and a mold related to production volume, durability, machinability, and surface finish. A common approach to increasing the production volume is to create several molds from one tool. Then each mold can be used to make several parts. Additionally, many commonly produced composite structures such as wind turbine blades use concave molds, so that the outer surface of the structure is the molded surface. However, manufacturing concave molds can be difficult, especially for deep geometries, because longer cutting tools are necessary to reach into deep cavities. So, it can be much easier to first manufacture a convex tool, reducing the machining complexity and cost. This approach still transfers the machined outer surface of the tool to the completed outer surface of the part. An example of this approach, as seen in figure 2, shows the typical manufacturing process for creating a master tool, a fiber reinforced composite mold, and a fiber reinforced composite part.

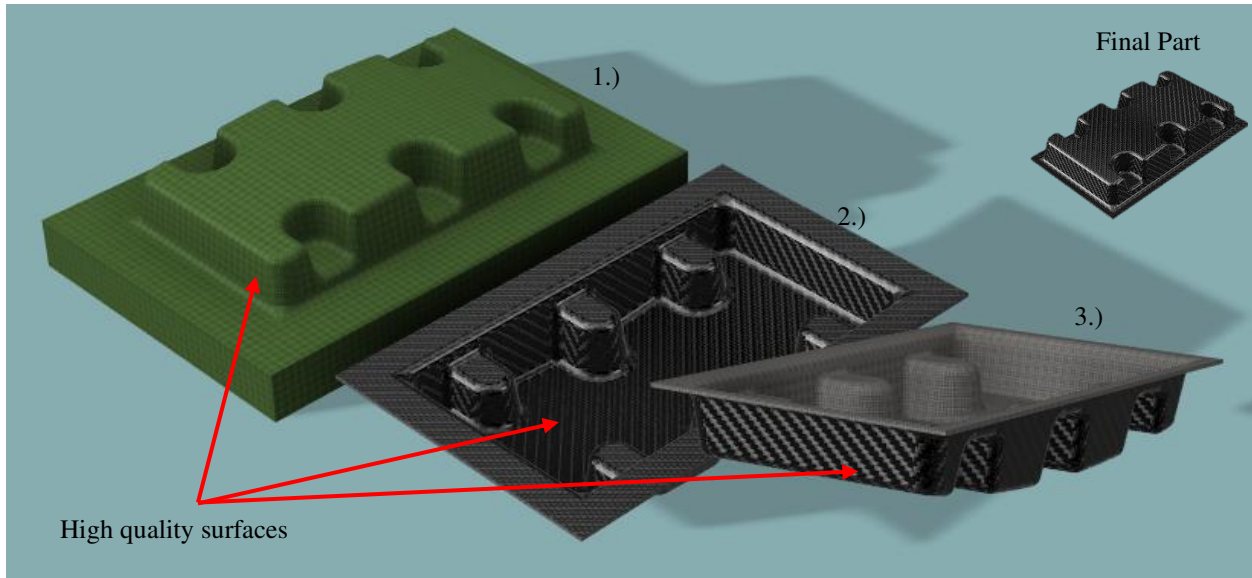


Figure 2 The tool is first manufactured (1), then a mold is generated (2), and finally the final part is created in the mold (3). The high-quality outer surface on the tool is transferred to the final part.

Manufacturing a master tool, then a mold, and finally a part is a great way of manufacturing components in medium to large production volumes. However, the process has a significant number of steps related to time spent setting up machines, developing fixturing, and manufacturing the tools and molds. High volume production runs can amortize these costs over many parts, but this process is unsuitable for low-production volume or prototyping scenarios. Instead, it can be advantageous to directly manufacture the mold, eliminating the cost of tool production from the total cost of manufacture. Additionally, the use of automated manufacturing processes using low-cost materials significantly reduces the cost of composite manufacture.

There are many tooling material options, and the choice is generally driven by the processing conditions of the composite part and the number of parts required. In low-temperature processing regimes, fiber reinforced composite tooling is common. If higher temperature processes are required, then materials such as metal or bulk graphite may be chosen. It is common to use metal tooling for high production volumes for the added durability [3]. However, for low production volumes or for prototype production, easily processed and inexpensive tooling materials are desired. Some material options include medium density fiberboard, plasters, 3D printed materials, tooling foam, and other similar economical

materials. Regardless of the tool material, the composite designer must additionally consider design requirements such as tool cost, life, accuracy, weight, machinability, strength, coefficient of thermal expansion (CTE), dimensional stability, surface finish, heat capacity, and thermal conductivity. It is often the case that the most desirable tooling materials are also expensive and challenging to manufacture [3].

It is important to consider the tool CTE, heat capacity, and thermal conductivity to determine the final part size and the appropriate heating rates. It is desirable for the CTE of the tool to be low so that at the cure temperatures when the mold is largest and the part becomes rigid, the size change of the tool does not impact the final geometry of the component. This size change can be accounted for, however the design methods to account for the size change can be complex. An additional challenge caused by high CTE tooling materials begins when the tool shrinks during cooldown. Upon cooling, the shrinking tool can break the part or lock the part into the tool. This common scenario occurs when the CTE of the composite is lower than the CTE of the tool. After the composite has become rigid and begins to cool, both the tool and the composite shrink; however, because the tool shrinks more than the composite, the tool mechanically traps the composite, and it becomes difficult (or impossible) to remove the composite without causing damage to the part or tool.

Efficient heat transfer during an elevated temperature cure is also desirable. A tool with a low thermal conductivity and a high heat capacity will respond slowly to temperature changes and may prevent the full cure of the composite part. Additionally, monolithic tools or thick layups slow the heating process further. The thermal characteristics of the tool, composite, and consumable materials can be accounted for in the design stages of the production using software that can predict the impact of these materials and their thicknesses on the cure progression by calculating the heating rates of the composite through the thickness of the layup. To reduce the impact of tooling thermal properties, structural or hardware choices can be made when designing the tooling that minimizes the impact of tooling thermal properties. These changes can include reducing the tool material thickness, incorporating heating channels or ducts, or utilizing an egg crate structure (see figure 3). The use of an egg crate structure can allow for

thinner tooling materials that heat up quickly and use less material (and therefore reduced cost and weight) as well as including jacking bolts for slightly adjusting the shape of the mold [3].



Figure 3 An egg crate structure can be seen supporting the thin critical surface of this tool [4].

Finally, one of the most crucial aspects of mold design is ensuring that the mold can be processed at the elevated temperatures used for the curing the composite. AFRPC can be cured at temperatures ranging from room temperature to as high as 400°C, necessitating mold materials with corresponding maximum use temperatures. Regardless of the material used, the mold must not soften, melt, outgas, or react at the process temperatures or else damage to the mold or composite may occur. In order of increasing use temperature, the common material options include AFRPCs, metals, and finally ceramics such as bulk graphite [3]. For polymeric tooling, two methods of determining the use temperature would be the glass transition temperature (T_g) and heat deflection temperature (HDT). The T_g indicates the state of the material and occurs when the polymer begins to behave rubbery instead of glassy. Above the T_g , the polymer can be easily deformed at low loads. Some engineering design guides indicate that 80% of the T_g (K) should be the maximum use temperature of the material; however, this is a general guideline and does not consider things like the structure or applied load. Alternatively, the HDT is a standardized measure of resistance to deformation at an applied load. In composite tooling applications where there is a known loading (pressure) condition, the HDT may be more useful. Additionally, it also responds to

modifications in the material and structure, such as the inclusion of fiber reinforcement, because it is a measure of the structural behavior of the sample.

Trapped Tooling

Another consideration is how the composite will be separated from the mold, and likewise, the mold from the tool. Some complex geometries or features on a component will mechanically lock the mold and component together, preventing simple removal. Components such as ducts, cable tracks, and pressure vessels often result in a trapped tool. A manufacturer has limited options if a tool is trapped by the geometry. The first option is to leave the tool within the part so that the tool may serve another purpose such as providing additional stiffness to the part or acting as a diffusion barrier, as is common in composite overwrapped pressure vessels [5, 6]. However, these options typically reduce the benefits of creating a component from lightweight composites.

The next option is to create a tool that can be separated from the part for reuse by considering shape-memory flexible bladders or multi-part tooling. Shape-memory polymer molds can be used at cure temperatures to form the component, then softened in a secondary heating cycle for extraction from the cured part. After softening they are removed from the part before being reformed in a secondary heating step using additional tooling, adding cost and time to the manufacturing process [7]. Multi-part metal tooling creates high quality and repeatable composite parts, but is typically complex in both design and implementation, and ultimately, best suited to large production volumes where the cost can be distributed over many composite parts [8]. Multi-part composite molds, or split molds, which have one or more parting planes can be used to separate the mold from the cured component. Examples of these types of molds are shown in figure 4.

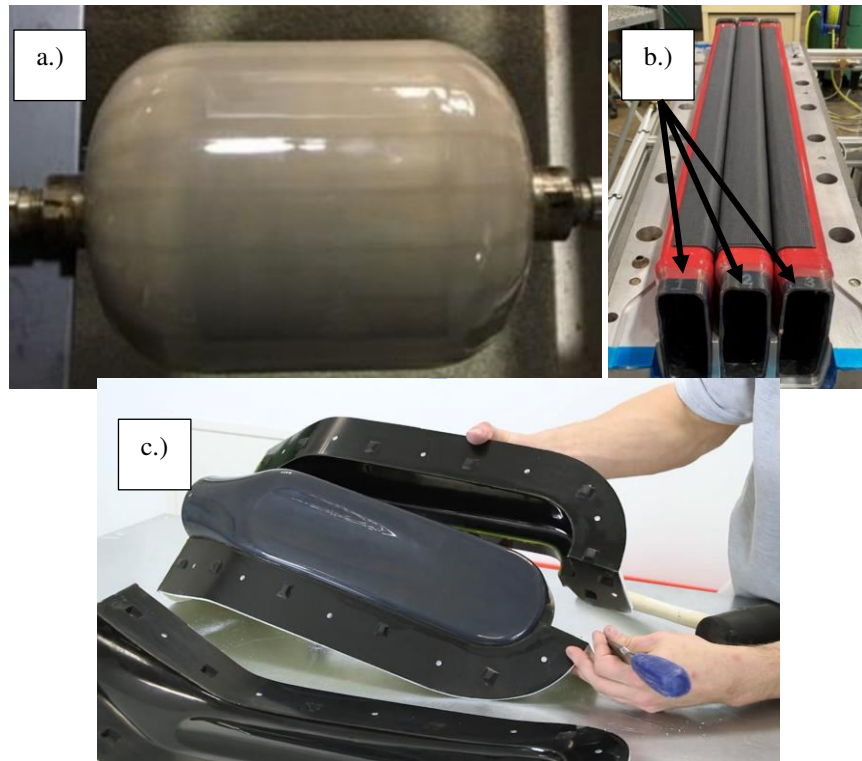


Figure 4 A mold that acts as a diffusion barrier for a pressure vessel (a), a reusable, reformable shape memory mold (b), and a multi-part split mold made from composite materials (c) [9, 10, 11].

While these approaches can be very effective, they also can be much more complex, making it desirable if the additional complexity and cost can be justified by the production volume of the part. One unique circumstance arises when a part design prevents removal, but low production volume cannot justify more complex reusable tooling. In this case, single-use sacrificial tooling that can be dissolved, broken out, or washed out from the cured component becomes an attractive choice [7].

A list of common sacrificial or washout tooling materials would include plasters, ceramics with soluble binder, expandable self-pressurizing tools, or eutectic salts [7, 12]. Plaster is a commonly used material because it is water soluble and easy to cast. However, molds made from plaster require another mold to create the casting, and the moisture inside the plaster mold must be removed using a heat cycle prior to composite manufacturing. If the water is not completely removed, it may result in manufacturing defects like voids or lowered glass transition temperatures in the cured composite [7]. Tools utilizing ceramic media with soluble binders are common as well and can be machined or cast to yield high quality

washout tools. Some soluble materials can be designed to expand during cure by utilizing a molded powder material that is made from a soluble polymer component and a microsphere-based blowing agent. This provides predictable internal pressures for hollow geometries [12]. Eutectic salts are also used to create complex geometries but require casting at high temperatures and result in slow washout times and corrosive waste [7]. Further complicating matters is the fact that washout tools tend to have porous surfaces that must be sealed to prevent resin infiltration during the cure of the composite part [7, 12]. One possible solution to address these challenges is the use of soluble 3D printed thermoplastic tools. These materials are promising because they may not require any secondary processing steps, such as machining, sealing, or molding prior to composite manufacturing, and they may reduce the costs of manufacture [13].

Autoclave Processing of AFRPC

One of the composite manufacturing processes that results in the highest quality components is autoclave processing. An autoclave is a piece of equipment used to provide the high temperatures and pressures to cure and consolidate the part. The use of controlled heating, external pressure, and vacuum is what makes autoclave processing so successful at producing high quality composite parts. They typically are designed as large, heated pressure vessels with forced convection on the inside. They also commonly include a vacuum source to provide an additional driving force to consolidate and remove voids from the component. Autoclaves are expensive pieces of equipment, especially when scaled to handle the size of large composite components. Some of these components include aircraft structures, necessitating autoclaves on the scale of 30m in diameter and 50m in length [3]. The autoclave production process involves several steps to produce the component. The first step includes both tool and material preparation, which involves tool manufacture and pre-trimming the materials to shape. The second step includes the layup of the materials and debulking, which is when vacuum is applied at intermediate steps to assist in consolidation. The third step is autoclave processing and includes curing and further consolidation of the component at elevated temperatures and pressures. The fourth step includes trimming

and other post processing or finishing steps. There are many possible variations of this process, but these are four common steps used in autoclave processing of composites [3].

The preparation for autoclave processing is a significant step in the process. It firstly involves creating a mold that can form the geometry accurately, has high quality surface finishes, allows part removal, can survive the processing conditions, and can produce the desired number of components. Then, materials are prepared by cutting them to the right size and collecting ancillary consumable materials for processing. Then, the composite precursor materials are laid into the mold in the layup step. There are many approaches to creating the composite layup, including both manual and automatic processes to deposit material on a tool or mold. However, due to the difficulty of justifying the financial investment of automated processes for small production volumes, manual hand-layup is one of the most versatile approaches to creating a component. This is relatively inexpensive and suited well to low production volumes because it uses skilled technicians who use their experience to create high quality layups. However, it lacks the repeatability of automated processes, so it can be less desirable in certain applications.

Once the composite material has been laid up on a mold, it is common to enclose the component in a bagging material prior to debulking. Debulking is a step where the air inside the bag is evacuated allowing the atmospheric pressure to consolidate the precursor materials. This step is often done multiple times during the layup. It requires removing the bag after debulking to add additional plies. In addition to the vacuum bag, other consumable materials may be included in the layup to distribute pressure, aid in composite removal, or control resin flow. After adding these materials to the mold, the vacuum bag is reapplied over the entire layup and loaded into the autoclave. After loading in the autoclave, pressure, temperature, and vacuum are applied to further consolidate the part, remove voids, and progress the cure. A general list of materials needed for this process include a vacuum bag, a porous material to create a continuous vacuum path (breather), a release layer to prevent the composite and consumable materials

from becoming adhered together, the composite precursor materials, and a mold. A very general composite stacking sequence can be seen in figure 5.

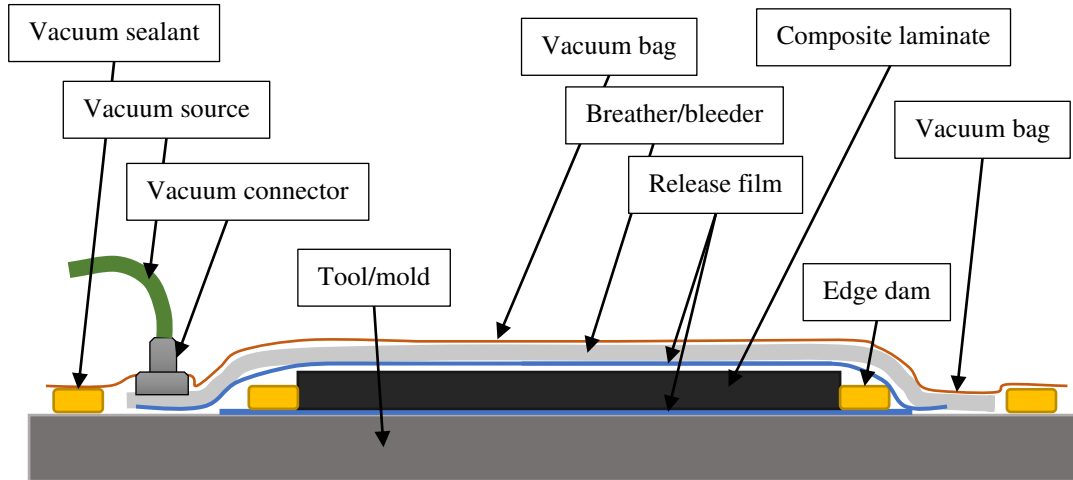


Figure 5 A general composite layup for autoclave processing.

This stacking sequence is commonly modified depending on the part requirements. One commonly used material system, and the material used in this work, is epoxy based prepreg. Prepreg is produced by impregnating a fiber reinforcement with the matrix material in a highly controlled fashion that results in a material feedstock with reliable and repeatable properties. The matrix material is then partially cured to a B-Stage, a highly viscous state where the previously liquid matrix becomes gel-like. The B-Stage matrix material is beneficial because it holds the fiber reinforcement together while remaining pliable enough that it can be manipulated for the layup. These sheets are tacky at room temperature, tend to stick together, and become difficult to move after assembly. When heated, the resin returns to a low viscosity state that allows for significant fiber movement and resin flow. This is critical for void removal and consolidation of the part [3]. Then, as the temperature is further increased, the matrix begins to cure or crosslink which results in a rigidized material. This high temperature step in the cure is what the mold or tool must undergo without losing its structural integrity and is the greatest challenge for the use of tooling materials like fiber reinforced polymer composites or 3D printed tools in

an autoclave process. When cured, the composite component is rigid and can be cooled and removed from the mold to continue with further post processing operations and assembly.

INTRODUCTION TO ADDITIVE MANUFACTURING

Additive Manufacturing Overview

Additive manufacturing (AM) was developed in the 1980s, and in recent years has gained traction in many industries and applications, including composite tooling [14]. One reason that AM has been so readily adopted because it enables highly complex geometries to be produced without significant increases in cost, especially in low volume applications. Some geometries that would typically be difficult or impossible to produce on multi-axis subtractive machines are trivial to produce using additive processes. The first step in an additive process is to create a surface model of the component, captured in an .STL, .OBJ, or .AMF file (among others), which contains information about the model geometry and can sometimes include information like texture or color. Then, this surface model is passed into a slicing software, which ‘slices’ the surface into the 2D cross sections that make up each layer. The slicing software is used to then generate a Numerical Control (NC) file that can be used by a CNC based motion platform. Typically, this NC file takes the form of G-Code, which lists the coordinates for the extruder to travel, as well as commands related to the process such as turning on or off heaters, setting the motion speed, or beginning extrusion.

Unlike subtractive manufacturing, the forces in AM are low, reducing the need for high rigidity machines and enabling increased scale at reduced cost. New AM materials are also constantly being developed, allowing applications requiring ceramics, metals, or polymers to be pursued. Unique materials and structures can be generated in AM, allowing manufacture using biocompatible materials, functionally graded materials, and structures created for their unique properties. Finally, rapidly iterating a part geometry allows parts to be refined much faster than in other processes. For example, if a flaw is found in the mold design for a casting process, the mold must be altered or scrapped and remade. However, in an additive process, a part can be reprinted with little wasted resources other than the

material and time required to reprint [14]. The iteration cycles in additive can occur multiple times a day, with fast turnaround on optimized geometries. The layer-by-layer approach to AM brings the low cost of complexity and the rapid prototyping characteristics associated with AM. However, it also brings challenges such as anisotropy, poor surface finish, and low production volumes.

Many approaches to AM produce components with varying degrees of anisotropy. This is caused by poor fusion at the boundaries between layers and adjacent printed roads. Roads, beads, and print paths are synonymous and refer to the thin strip of extruded material created by the printer along the print path [15]. Additionally, the parts produced can be sensitive to manufacturing parameters such as temperature, print speed, and print orientation, leading to reproducibility challenges. The distinct layers also tend to create a poor surface finish and loss of detail. AM processes are poorly suited to high production volumes when compared to formative or subtractive processes. AM machines can range in cost, but in many engineering applications high end systems are required which results in large upfront capital investments for industrial machines [14].

There are a variety of AM systems due to the large numbers of materials and techniques. This has resulted in a lack of standardization and terminology to describe these processes. This can make communicating information in both a technical and non-technical setting very challenging. However, the different processes were categorized and defined somewhat recently by ASTM F2792-12a and are listed in table 1. These processes include binder jetting, directed energy deposition, material extrusion, material jetting, powder bed fusion, sheet lamination, and vat photopolymerization [16].

Table 1 The additive manufacturing process categories defined by ASTM 2792-12a [16].

Additive Manufacturing Process Category	Definition
Binder Jetting	An additive manufacturing process in which a liquid bonding agent is selectively deposited to join powder materials.
Directed Energy Deposition	An additive manufacturing process in which focused thermal energy is used to fuse materials by melting as they are being deposited. Focused thermal energy means that an energy source (e.g., laser, electron beam, or plasma arc) is focused to melt the materials being deposited.
Material Extrusion	An additive manufacturing process in which material is selectively dispensed through a nozzle or orifice.
Material Jetting	An additive manufacturing process in which droplets of build material are selectively deposited. Example materials include photopolymer and wax.
Powder Bed Fusion	An additive manufacturing process in which thermal energy selectively fuses regions of a powder bed.
Sheet Lamination	An additive manufacturing process in which sheets of material are bonded to form an object.
Vat Photopolymerization	An additive manufacturing process in which liquid photopolymer in a vat is selectively cured by light-activated polymerization.

Some of these processes have shown success as methods for developing advanced composite tooling [17]. The recent interest in AM for composite tooling is that composite components are commonly complex and produced in low production volumes. Additive manufacturing is very well suited to these types of applications because complexity comes at a low cost, and the processes are well suited to low-volume situations. This is quite different from subtractive manufacturing, where subtractive manufacturing is better suited to higher production volumes and lower complexity, taking advantage of the economy of scale. The general cost/complexity and cost/volume relationships are shown graphically in figure 6 for both AM and subtractive processes.

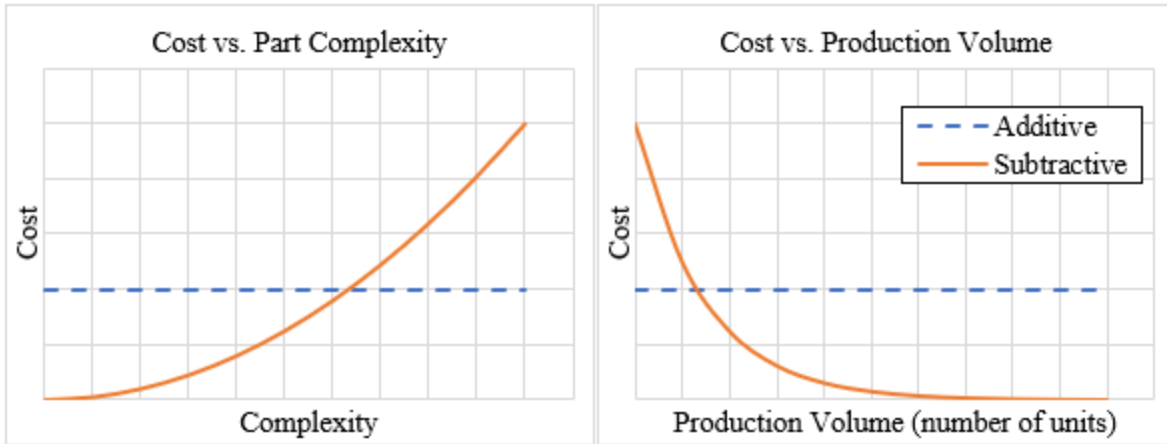
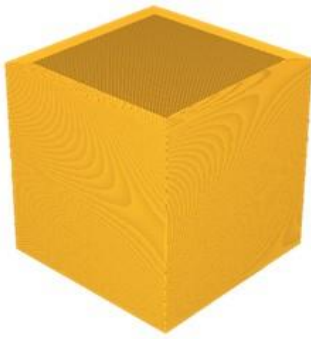
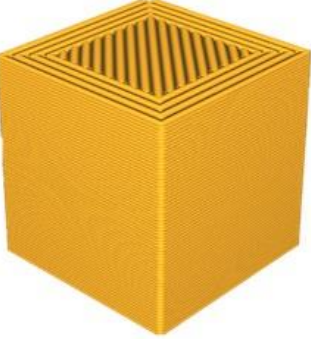


Figure 6 Cost vs. Complexity and Cost vs. Production volume relationships for additive and subtractive manufacturing approaches [18]

While primarily limited to low production volumes, AM processes such as binder jetting, melt extrusion, and DED can be quite scalable. These processes can be scaled by increasing the material deposition rates or by switching from single to multi-point deposition. The ability to scale an additive system allows applications such as construction, architecture, infrastructure, and art [19, 20, 21]. To scale a system, processes often move to larger orifice sizes, larger layer heights, and faster print speeds at the cost of increased minimum feature size and less detail. The exchange of resolution for print time is demonstrated in table 2 using estimated print times generated for a 20mm cube by changing the orifice size in a melt extrusion process.

Table 2 Estimated print time for a 20mm cube with changing nozzle size

Resolution	High	Medium	Low
Nozzle Size (mm)	0.2	0.5	1.0
Estimated Print Time (minutes)	251	63	23
Render			

It is typical for large geometries to be produced with poor surface detail, which is a type of approximation error associated with using discrete layers. This error is often referred to as the staircase effect [22]. It is typically addressed by ensuring critical surfaces are made to have the desired surface finish through secondary processing steps such as machining, sanding, or sealing [17]. Any of these post-processing steps add both cost and time to the production cycle, which is one of the significant challenges in the AM field.

When designing a component that uses additive manufacturing, there are certain practices that make AM particularly advantageous. These practices have been described as Design for Additive Manufacturing (DfAM), which aims to consider the characteristics of additive manufacturing in the design process to result in time and cost savings and improvements in function. This design approach takes advantage of the relatively low cost of increasing complexity in an additive process, allowing complex contours, lattice structures, and integrated functionality. Some exemplary DfAM approaches include topology optimization and generative design. Both processes attempt to optimize a component for performance and result in uniquely organic forms with improved structures. Another common example is the integration of complex lattice structures with unique properties and functions. These structures may

increase biocompatibility, induce auxetic material properties, or reduce the weight and material use [23]. Finally, approaches can be taken to embed electronics, create functionally graded structures, or include multiple materials to improve function with very little cost of implementation [23]. A great example of DfAM is the component shown in figure 7, which is utilized for hip replacements and considers both material selection and hierarchical structures. The acetabular cup utilizes Ti_6Al_4V for its high strength and biocompatibility and includes a networked surface texture to allow for bone ingrowth and a better integrated solution [24].



Figure 7 Acetabular cup produced using a powder bed fusion process [24].

Additive manufacturing can be made advantageous for composite tooling by using the strategies outlined by DfAM, taking advantage of the low cost of complexity to integrate unique designs and select from a large variety of materials to improve the manufacturing process.

Additive Processes for Composite Tooling

Additive manufacture of traditional composite tooling has shown some success by providing an opportunity to rapidly manufacture composite molds with high quality. For low volume applications, especially with complex geometries, additive manufacturing is very capable of competing with traditional manufacturing techniques in both time and cost investment in tooling production [25]. In all applications, additively manufactured tools, like traditional tooling, are held to the same requirements of surviving the process conditions. Thus, material and process selection are some of the most challenging aspects of AM

for composite tooling. Many additive manufacturing processes and materials have been used for composite tooling, but only binder jetting and material extrusion have been used to produce washout or soluble tooling. The processes that have been used to produce composite tooling include binder jetting, directed energy deposition, vat photopolymerization, and material extrusion. These processes are detailed below.

Binder Jetting

The first process listed in table 1 is binder jetting. This process involves the deposition of a binder into a powder bed, where the powder material can be metal, ceramic, or plastic. Originally, low-cost and fragile binder jetted parts were made from gypsum powder and used water as a binder [26]. Over time, these processes evolved to use binders such as polyvinyl alcohol (PVA) or cyanoacrylates, which remain commonly used. Now, colored parts can be produced by using colored binders. These machines typically include an inkjet print head attached to a positioning system. Then, the inkjet head sprays the binder into a powder bed, creating the structure only where the binder is deposited. After completion of a layer, the powder bed is moved away from the print head creating a gap, and a powder spreader deposits a fine layer of powder in that gap so that the process may be repeated. Some drawbacks of the binder jetting processes are the relatively poor surface quality and high porosity due to the powder substrate. This process is very flexible and can be used with almost any material type allowing a wide variety of applications. This type of additive manufacturing is originally what was marketed as Three-Dimensional Printing (3DP™) and the term has since been adopted for many other processes [14]. Binder jetting is a quickly growing field and has been used in many applications including the manufacture of molds for metal casting, tools for composites, full-color prototyping, functionally graded parts, and more.

Binder Jetting has proven useful for sacrificial washout composite tooling due to the ability to use a water-soluble binder and a reusable ceramic material to allow complete breakdown of the tool when soaked in water [13]. The applications for composite tooling are scalable and can utilize a wide variety of ceramic media, allowing varying CTE. Tools can be made that are robust in autoclave conditions up to

177°C (350°F) and 85psi. This is a fast process, with some machines being used for composite tooling having build volumes of up to 1.8x1.0x0.7m and build rates up to 125 liters/hour [27]. Multiple printed segments can be manufactured then assembled to make even larger tools. This process is capable of manufacturing tools that perform similarly to cast or machined traditional washout tools. However, like tools that are cast or machined from washout ceramic tooling material, binder jetted washout tools tend to require an additional step of sealing the surface to prevent resin impingement and to improve the surface finish. This is commonly done with an overwrap of PolyTetraFluoroEthylene (PTFE) tape or a soluble material spray coating. These tools also tend to be brittle and challenging to produce with intricate features. Finally, the ceramic, monolithic nature leads to poor thermal conductivity and low heat up rates.

Directed Energy Deposition

Directed energy deposition (DED) is a process that can be uniquely used to create fully dense metal parts with nearly no porosity. In DED, an energy source is used to melt metal feedstocks in processes like welding. The energy source used for this process may be LASER, electron beam, or plasma arc, which are directed into a spray of powdered metal or a wire feed to build components. Typically, an inert environment is used to prevent oxidation which can inhibit bonding. The high energy density and the use of metal feedstocks creates complex thermal environments that can develop different grain structures throughout the part [28]. This process can be very similar to welding, which has resulted in rapid standardization of DED processes and a fast adoption in highly regulated fields [29]. The machines that utilize DED are typically have at least 3 axes and systems with more than 3 axes are quite common. DED is uniquely suited to creating hard metal tooling for composites. The lack of porosity allows for high quality surfaces to be developed after a CNC machining operation, and the use of various feedstocks allow tools to be made of metals such as Invar. This is highly desirable for composite tooling due to its low CTE [4]. However, the use of complex systems typically makes DED cost prohibitive for low-volume composite tooling applications.

Vat Photopolymerization

Vat photopolymerization is a process that selectively cures photosensitive thermosetting resins to create solid objects. The first developed approach was vector scanning, in which a laser selectively scans across a resin bath to create a 2D part cross section in a layer-by-layer fashion. This was developed in 1984 and made commercial in 1986 by Charles Hull. This was the first commercial additive manufacturing process. An alternative approach uses mask projection, in which an entire layer can be cured at one time by using a liquid crystal mask that allows the entire layer to selectively be exposed to a light source [29]. These machines operate by raising or lowering a platform in a resin bath for the part to be built on. When the platform is moved, liquid resin flows into the gap that is created by the moving platform. Then, a light source selectively cures the resin in the small gap. This process can manufacture parts with very high detail but is better suited to small parts. The scale of component sizes produced using this process range from μm to cm, thus making large composite tooling impractical with the current technology [30].

Material Extrusion

Material extrusion is likely the process that is most associated with the terms 3D-printing and additive manufacturing. Material extrusion involves the deposition of a material through a nozzle onto a substrate and can be used with polymers, ceramics, and metals. There are many varieties of material extrusion, but they can typically be categorized into either melt extrusion or viscous extrusion systems. Viscous extrusion systems, also referred to as paste extrusion, applies to a wide variety of materials. Some examples of viscous extrusion systems used include ceramic pastes that can be sintered, cement or concrete for construction, foods such as chocolate, meat, or vegetarian meat alternatives, or bio-printed materials with live cells. Viscous extrusion and melt extrusion systems can both be used on very large scales like for construction or manufacturing large tooling for composites.

Melt extrusion systems commonly use plastic feedstocks with a variety of material characteristics that can be modified using additives such as metal, wood, or reinforcing fiber. It is common within melt

extrusion of complex geometries to incorporate 3D printed scaffold materials to support overhangs in a part during the printing process. These can be break-away or dissolvable structures [31], where dissolvable polymers are often chosen for their ease of use and the ability to support the component without significantly damaging the exterior surface. A diagram of a typical melt extrusion additive system is shown in figure 8, including both support and structural material spools.

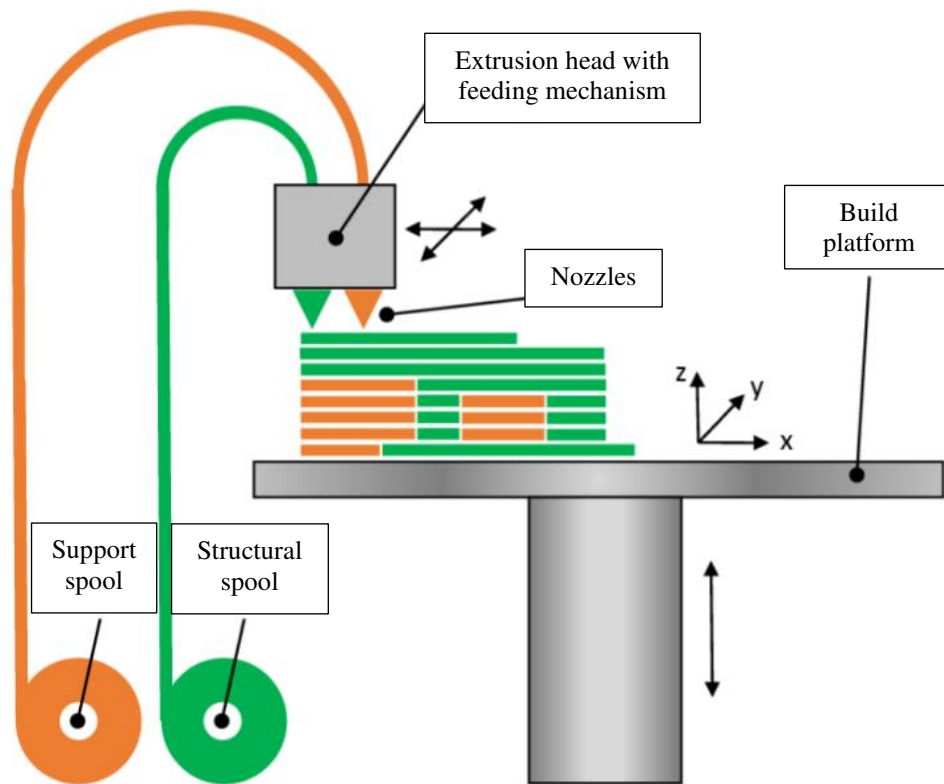


Figure 8 Melt extrusion additive manufacturing platform [29].

One challenge that these materials face, especially at high temperatures, is the dependence of thermoplastic properties on temperature. This presents a challenge for the use of melt extrusion AM for composite tooling applications, because the processing temperatures for composites are higher than the use temperature of many of the common materials used in AM. However, the low cost of thermoplastic feedstock and the scalability of melt-extrusion AM has created significant interest in the development of this technology for composite tooling.

Additive Processes for Removable Tooling

Independent of the approach to tooling manufacture, as the composite component geometry becomes more complex, removable tooling is often necessitated due to the inability to effectively remove a trapped tool. Soluble materials have been utilized in some additive processes, enabling the use of additive manufacture for trapped tooling situations. Since a new sacrificial tool must be manufactured for each composite part, automated processes like AM are advantageous. One AM approach is to use binder jet printing to create ceramic-based tools with soluble binders [13]. Unfortunately, these tools, like traditional ceramic-based washout tools, also require an additional step of sealing the surface, commonly with an overwrap of PTFE tape or a water-soluble surface coat. Further, these tools are monolithic in nature which leads to low heat up rates and the implementation of small intricate features is limited by the brittle nature of the tooling material. An additional approach is to use vat photopolymerization to create (non-soluble) tools that are very accurate and detailed but somewhat brittle in nature. Removable tools created through vat photopolymerization take advantage of the brittle tooling material, allowing the tool to be broken into pieces for removal. Sacrificial thermoplastic tooling made on melt extrusion systems have shown some success by including perforated breaking lines that facilitate tool destruction and removal. Finally, there have been attempts to utilize dissolvable thermoplastics that can be manufactured using melt extrusion [32, 33, 34]. Examples of each of these technologies are shown in figure 9.

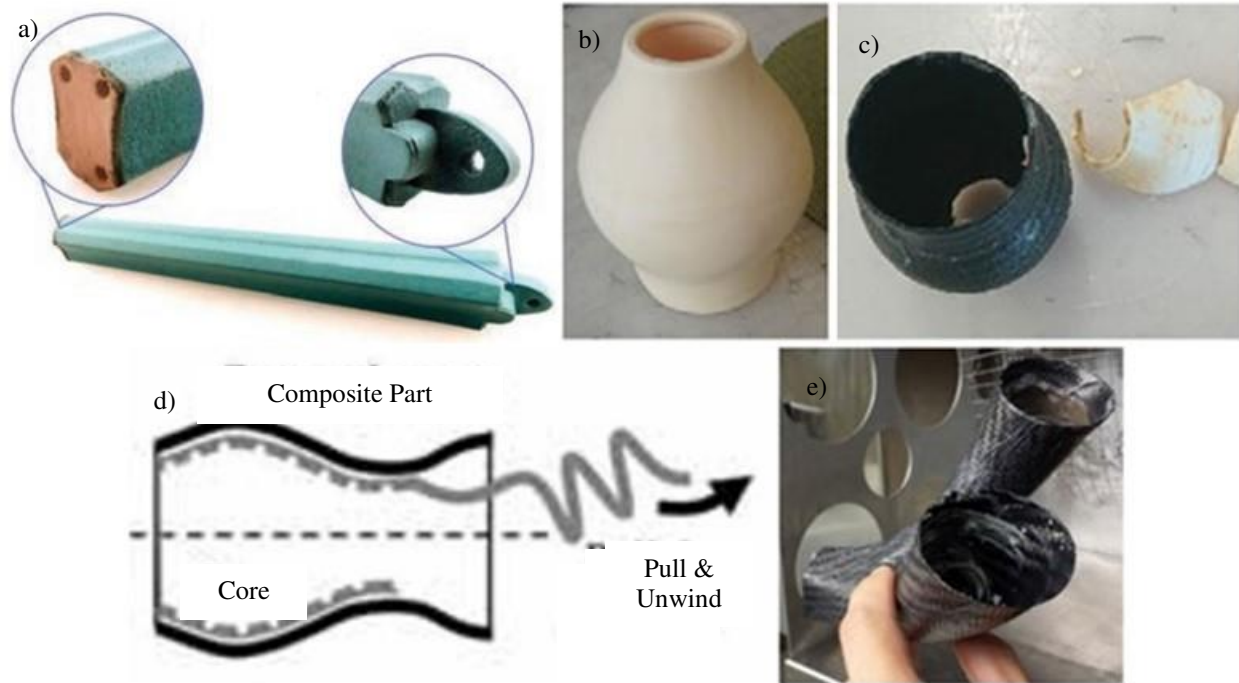


Figure 9 Sacrificial composite tooling can be made using binder jetting (a), vat photopolymerization (b, c), or melt extrusion (d, e) [13, 35, 31, 25].

APPLYING MELT EXTRUSION TECHNOLOGY TO AUTOCLAVABLE COMPOSITE TOOLING

Recently, melt extrusion additive manufacture (MEAM) has shown promise for the manufacture of molds for composites. Some of the advantages of MEAM for composites includes the scalability, the variety of materials, and the flexibility of production. Often, tooling can be first manufactured using MEAM then advanced fiber reinforced polymer composite (AFRPC) molds can be made from the printed tooling. However, the ability to directly manufacture the mold rather than manufacturing both a mold and a tool is another promising opportunity to save a significant amount of time in composite development process. Finally, the scalability of AM systems allows the application of MEAM to large composite structures. These attributes make MEAM an attractive process for the generation of autoclavable composite tooling.

Some 3D printing systems with very large build areas have been developed, allowing structures that are much larger than typically considered for 3D printing. These systems can include both a printing extruder and a spindle for machining and trimming. This allows near net shape components to be

completed using MEAM, then be machined to the final geometry with significantly reduced material waste. This two-step process is usually necessary for the large size of many composite structures, where the large quantities of rapidly deposited material result in a coarse approximation of the actual geometry with obvious layer lines. The largest system currently in use is a 30.5x6.7x3.0m printer that can output 227kg/hr and was developed by Ingersoll Machine Tools and the University of Maine [36]. Another system made by Thermwood is the LSAM 1040, which has a build volume of 4.5x12.2x1.5m with 95kg/hr material output [37]. Thermwood also states that their machines can be scaled to a size of 30.5x6.1x3.0m, approximately the same size as the University of Maine printer. At this scale, large tools could incorporate integrated functionality to ease and improve composite processing. Some features could include eggcrate structures, integrated heating/cooling channels, integrated resistive wires, forklift access points, air-tight vacuum bagging surfaces, and fiducial markings. The mold shown in figure 10 was manufactured using MEAM and used for resin infusion of a wind turbine blade. It included several channels for heated air as an alternative to resistive heating, potentially saving costs [2].



Figure 10 A 13-meter-long mold for a wind turbine blade manufactured using short carbon fiber filled thermoplastic feedstock in a melt extrusion process [2].

While the benefits of MEAM are valuable, there are also inherent challenges related to thermal stability. Thermoplastics, by nature, have structural integrity that is based on their temperature. This temperature dependence is what allows them to be used in melt-based processes like MEAM; however, thermoplastic tools quickly deform during composite processing if the process temperature exceeds the use-temperature of the material. There are also inherent tooling challenges caused by the additive process like the anisotropy of the printed structure or the high CTE of the available materials.

The following sections will discuss some potential approaches to improve or account for the reduced structural stability of 3D printed tools at elevated temperatures. Additionally, some of the processing challenges related to CTE and anisotropy will be discussed, as well as a specific scenario where dissolvable thermoplastics may provide a solution for trapped tooling. Finally, the aims of the work will be outlined with a project statement and several goals.

Thermal Stability

Many thermoplastics can be processed at low temperatures, making manufacture relatively easy. However, many of these are not suitable for autoclave processable composite tooling. This makes material selection and processing more challenging, as many high temperature materials are expensive and suffer from manufacturing challenges such as warping or cracking caused by thermal stresses developed upon extrusion and subsequent cooling. Some high temperature materials that have shown success as composite tooling materials include PPSU, PPS, PEI, or PC [38, 33, 39]. These plastics require high temperature process environments to prevent defects, so as an alternative, low temperature materials can be made with unique loading schemes and process changes.

There are many alterations to the composite production process that may allow tooling to be produced using additive manufacture that can result in higher temperature processing. The first modification to the process would be to manufacture a master tool using AM, then construct molds using low temperature curing tooling prepregs that can be post-cured to act as a suitable mold for high

temperature component manufacture. This approach works well but adds a significant mold manufacturing step to the process. Alternatively, AM molds may be printed completely solid. This can be a satisfactory solution, but it significantly increases the material use compared to partially dense 3D printing approaches and does not prevent deformation but instead limits it by increasing the stiffness of the mold. In most circumstances, a partially dense structure is preferable to a solid structure for the savings of material and cost. Alternatively, the tool structure may be modified to avoid partially dense tools by only manufacturing the external surfaces of the tool. This may be done by manufacturing a shell-type tool, so that pressures applied by the vacuum bag and autoclave on the tool are close to equal on both sides. An example of a shell-type tool is seen in figure 11.

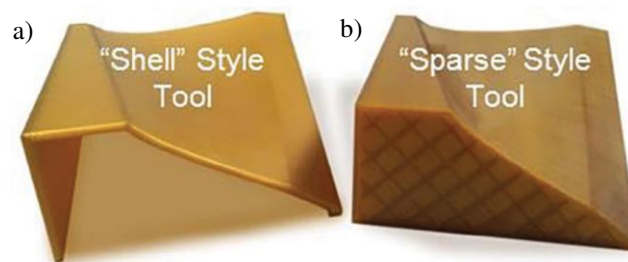


Figure 11 In this image, both a shell-type tool (a) and a partially dense tool (b) are shown [40].

The shell type tool allows the structure of the vacuum bag and the layup components to assist in maintaining a rigid layup during manufacturing once vacuum is pulled. However, the improved loading scheme may not be sufficient for large tools that may deform from their own weight as the material softens. Another approach that improves the loading scheme is by using a filler material in a hollow tool. For example, hollow geometries can be manufactured and then filled with thermally stable materials such as salt [31]. This significantly reduces the amount of AM feedstock material required for the tool but can also result in a monolithic structure with low heat up rates. However, as compared to the previously stated approaches, simply improving the material properties results in the greatest gains in performance. Rather than changing to high temperature engineering materials for tooling, modifications to commodity plastics can be a more common and cost-effective approach.

Compounding low temperature, easily processed materials with short fiber reinforcement is one approach to increase the use temperature of tooling material. This also helps avoid challenges in the tool manufacture. The addition of short reinforcing fibers to the material increases the stiffness significantly, even at elevated temperatures, allowing cheaper materials to be used at higher temperatures than would normally be appropriate. For example, the HDT of PET can be increased from 75°C to 225°C at 0.46MPa (67psi) loading by the addition of 30% glass fiber reinforcement [41]. The addition of short carbon fiber or short glass fiber can impact the CTE and thermal conductivity of the material. Short carbon fiber specifically has important benefits relating to the decrease in CTE of materials and increasing the thermal conductivity, which begins to address other problems related to 3D printed composite tooling [42].

Thermal and Mechanical Anisotropy

Anisotropy is developed in MEAM produced components due to poor fusion boundaries developing between printed paths. Typically, this results in the build direction being the weakest. This is primarily caused by the deposition of molten plastic on top of previously cooled and solidified plastic, and insufficient diffusion of the polymer chains at the boundary. Additionally, there is a need for anisotropic thermal expansion modeling for printed materials. PLA has a relatively isotropic thermal expansion, but ABS has been measured to have thermal expansion anisotropy of 35% between build and print-plane directions, that also varies with temperature. This may be a significant barrier for MEAM components being used in composite tooling applications, due to the changing temperature of tooling during processing causing nonlinear anisotropic size changes of the tools. However, it has been suggested that a transversely isotropic model could provide an appropriate solution that requires fewer elastic constants than an orthotropic model, providing an ability to account for the size changes of a tool during processing [43]. Further complicating matters is that there is anisotropy based on the printed road direction.

It has been shown that there is anisotropy in 3D printed structures both between layers, as well as between printed roads (beads). This is due to poor fusion boundaries of adjacent print paths. Thus, when

accounting for anisotropy, the print path directions should be accounted for. Worsening the anisotropy of printed material is the addition of reinforcing fibers. Fiber alignment with the deposition direction occurs due to the shearing forces present in the extruder. The stiffness and low CTE of carbon fibers constrains any thermal expansion in the deposition direction, but perpendicular to the fibers (in the deposition direction), the expansion is unconstrained, and matrix dominated. Similarly, the deposition direction also has increased modulus and increased thermal conductivity which can result in spring-in type effects [44]. Thus, accounting for anisotropic CTE may be advantageous within the printed road, in the varying road directions, and between layers. This has been shown to be effective for predicting the deformation of 3D-printed composite tooling [45]. Additionally, some process modifications have been developed that improve the anisotropy due to poor interlayer fusion of MEAM components.

Reducing anisotropy can be done by increasing the interaction between layers and adjacent roads by maintaining deposited material at high temperatures for longer or reheating the substrate prior to deposition. Some approaches to achieve this include heating the build environment or print substrate, as this increases interaction between the different layers and improves the fusion boundaries. This also has the added benefit of reducing CTE induced defects like warping by allowing thermal stresses to dissipate more easily. First, the print volume may be enclosed in a heated chamber. This area can then be heated by a variety of methods, but the goal is to have the chamber temperature approach the glass transition temperature of the material. Depending on the part size, the enclosure temperature should not exceed the T_g to avoid the component sagging or drooping during manufacture. The challenges with this approach include the need to move temperature sensitive components away from the heat source (like motors, limit switches, and fans), or provide air or water cooling to these components. Additionally, this approach is not easily scaled as large systems would be energetically expensive to heat [46]. Parts can also be manufactured in a vacuum environment, which reduces the effect of heat loss from convection and allows more time for interaction between layers [47]. However, this approach is again not scalable, due to the large size of vacuum chambers required for large parts. Another approach is to pre-heat the underlying

printed surfaces, which accomplishes the same goal of increasing the interaction between deposited material and the substrate. Up to two times increases in fracture energy of components have been demonstrated by preheating the print substrate with an infrared lamp which indicates much better bonding between layers. This approach is likely more scalable, as the substrate temperature is considered instead of the environment temperature [48]. Therefore, localized heating can be used to apply this technique to large systems and parts.

Additional challenges caused by the complex thermal expansion of 3D printed components are manufacturing defects include warping, cracking, and spring in. These severe printing defects are caused by shrinkage of the printed material after being applied to the previous, colder layer. The build process sequentially deposits warm layers that shrink and induce stresses into the previous cold layers, resulting in cracks and warping. These defects can again be reduced by improving the interaction between subsequent layers using heated enclosures and infrared preheating that were discussed above. These approaches reduce defects by heating the substrate to a higher temperature that is better suited to dissipating thermally induced stresses. If the previous layers are well below the glass transition temperature, the layers will not be suited to dissipate thermal stresses, and this will result in defects.

Trapped Tooling

The application of MEAM to removable composite tooling has little information available due to the lack of suitable materials for the application. Some water-soluble materials like PolyVinyl Alcohol (PVA or PVOH) and Butenediol Vinyl Alcohol copolymer (BVOH) are available and commonly used as soluble support materials for structural 3D printed components. However, these materials are unsuitable for use at elevated temperatures required for autoclave cured composites. There are commercially available materials that can be used for some autoclave cure cycles, such as ST-130 produced by Stratasys. However, this material requires dissolution in an 80°C bath of an approximately 13pH solvent.

The caustic nature of the solvent presents significant disposal challenges in and can reduce the composite properties. For example, it has been shown that after 6 hours in the solution required to dissolve ST-130, a 16°C decrease in cured composite glass transition temperature can occur, likely due to a plasticization effect from the basic solution [33]. However, similar degradation of properties may occur for both water and high-pH solvents. For example, a reduction of glass transition temperature, tensile modulus, and tensile strength were also observed in an aging study that used heated solutions of sodium hydroxide (13pH), hydrochloric acid (1pH), and water over 20-, 40-, and 80-day intervals. The NaOH and water reduced the properties of the composite matrix similarly, but less than the HCL. This reduction of properties occurred for all solutions and was more significant when held at elevated temperatures, like those in the dissolution of thermoplastic tooling materials [49]. Another study found contradictory results, indicating that specific material systems, time spent in solution, temperature, and other variables may affect the reduction of properties [50]. These studies were also over the course of weeks, and further information is needed regarding these effects on the relatively short timescales used for composite tooling dissolution (<24hr).

Recently, a high temperature support material called AquaSys 180 has become commercially available from Infinite Material Solutions that shows promise for use in trapped tooling applications that can be dissolved in a heated water bath [51]. If thermal stability and water solubility remain a focus for environmental or property degradation concerns, this material may be a good option for soluble tooling.

Problem Statement and Goals

There are many benefits of using melt extrusion additive manufacturing for the development of composite tooling, however one primary problem is the poor thermal stability of the tools. The primary goal of this work was to evaluate the thermal stability of dissolvable autoclave composite tooling and investigate structural and procedural changes that could elevate the use temperature of the tool without causing tool deformation. A thermal stability study was completed by testing various tooling material choices and the internal structure. It was also desired to evaluate internal structures that were partially

dense and continuous, allowing reduced material usage and print time as well as channels for dissolution media to pass through on the inside of the tooling. Additionally, the materials evaluated were dissolvable to focus on an alternative to traditional washout tooling materials for trapped tooling situations and to further understand the capabilities of these materials under autoclave conditions. If careful selection of tooling material, structure, and manufacturing approach are used, then tool thermal stability may be improved, which allows elevated autoclave processing conditions with minimized tool deformation in advanced fiber reinforced polymer composite manufacturing.

CHAPTER 2: MATERIAL AND STRUCTURE EVALUATION FOR AUTOCLAVE ROBUSTNESS AND DISSOLUTION

Given the limited information on the autoclave use of soluble 3D printed tooling, initial efforts were aimed to evaluate the effects of tool structure and material choice on autoclave robustness using small-scale samples under autoclave conditions. Throughout this study there was a specific focus on commercially available soluble materials; however, some small-scale samples were made from a low-cost insoluble model material, polyethylene terephthalate glycol (PETG), to further investigate the effects of structural modifications on autoclave robustness. Much of the knowledge gained in this study would apply to both soluble and insoluble tooling. Finally, a preliminary study of the washout characteristics of the selected materials was completed.

TEMPERATURE PRESSURE VACUUM MATERIAL SAMPLE TESTING

The use temperature of a thermoplastic material may be approximated using standardized tests to evaluate properties such as glass transition temperature (T_g) and heat deflection temperature (HDT). The HDT is important to consider for tool fidelity because it indicates the temperature the material will begin to deform at a given load. The T_g is useful because it indicates when a material will undergo a transition from a glassy to a rubbery state, and additionally important for determining the processing conditions for tool manufacture such as bed or enclosure temperature. Typically, both process temperatures should be near, but not exceed, the T_g .

While these metrics may be useful in many applications, the actual use temperature of a material depends on the applied loads and structure. So, the use temperature may be higher or lower than the T_g or HDT indicate, especially due to the use of additives such as short fibers. HDT testing is completed by applying a load on a sample and varying the temperature, so is a better indicator of autoclave performance than T_g . However, this test neglects the varying pressures and temperatures that a tool may undergo in an autoclave, so is still not a good representation of autoclave performance and an alternative testing approach was needed.

A testing approach coined Temperature Pressure Vacuum (TPV) testing was developed to evaluate the stability of the various candidate tooling materials and structural configurations under autoclave conditions. This approach was taken to determine tooling robustness, as opposed to HDT, T_g , or compressive testing at temperature, because it more closely mimics actual processing conditions a tool may experience during composite manufacturing. These samples were partially dense, rather than solid, to evaluate the impact of the printed internal structural configuration, or the infill, on the autoclave performance. These tools were not processed with composite materials. Instead, they were vacuum bagged directly and processed under conditions like those used for composite processing. The samples were exposed to temperature, pressure, and vacuum to represent the autoclave manufacturing process. After processing, the samples were unloaded from the autoclave and evaluated with a straightedge for deformation. Each test was repeated at a series of increasing temperatures to determine the approximate max use temperature of each material in autoclave conditions up to the target conditions of nominally 121°C (250°F) and 345kPa (50psi).

Experimentation

Materials

One of the primary objectives was to evaluate the stability of composite tooling materials made from commercially available dissolvable plastic feedstock under autoclave processing conditions. The materials tested included Verbatim Butenediol Vinyl Alcohol (BVOH), LAY-Filaments Chamberlay 130 (CL-130), Infinite Material Solutions AquaSys 120 (AQ-120) and AquaSys 180 (AQ-180), and Stratasys ST-130 (ST-130). BVOH was included as a baseline material as it is commonly used as a dissolvable scaffold or support material for 3D printing, and it has been used to manufacture dissolvable room-temperature curing composites in the past.

The ST-130 filament is marketed as a soluble composite tooling material, so it was expected to perform well. However, its dissolution involves a basic solution with 11-13pH. The other materials considered can be dissolved in water, which is a highly desirable trait for disposal and safety reasons, as

well as to avoid exposing the composite to caustic solutions. The CL-130, AQ-120, and AQ-180 filaments are marketed as water soluble support materials for high temperature 3D printing applications, where typical supports may be unstable due to elevated build chamber temperatures. AQ-180 became commercially available late in the study and is the high-temperature counterpart to AQ-120. AQ-180 was originally only marketed as a high temperature support material, but at the time of writing it has since been advertised as a composite tooling material as well.

The material properties and use temperatures that were readily available from the manufacturers are listed in table 3. The CTE determines the amount of size change the tooling material will undergo during both tool and composite manufacture, and a low value is desired.

Table 3 The readily available material and processing parameters for the evaluated materials

Material	Supplier	Maximum Build Chamber Temperature	CTE ($\mu\text{m}/\text{m}/^\circ\text{C}$)	HDT ($^\circ\text{C}$ at 461.9kPa)	T _g ($^\circ\text{C}$)	Solvent	Density (g/cm^3)	Cost ($\$/\text{kg}$)
BVOH	Verbatim	90	-	-	68	Water	1.14	160
CL-130	LAY-Filaments	130	-	-	-	Water	1.19	250
AQ-120	Infinite Material Solutions	120	-	-	92	Water	1.32	180
AQ-180	Infinite Material Solutions	180	42	70	92 ¹	Water	1.26	400
ST-130	Stratasys	130	107 (T<100 $^\circ\text{C}$) 177 (T>100 $^\circ\text{C}$)	121	132	Basic Solution	1.19	150

Equipment

The samples were printed on commercial 1.75mm filament melt extrusion printers including a Prusa i3 MK2s, a Creality Ender 3 Pro, a Lulzbot Mini 1.04, a large-format custom high temperature 3D-printer, and a modified Creality Ender 5 Plus. The large number of 3D-printers were used to manufacture

¹ The glass transition temperature for AquaSys 180 was not readily available, however in a discussion with the technical staff it was said to have a T_g near 90 $^\circ\text{C}$, and it is assumed that it has the same polymer matrix as AquaSys 120 so therefore has the same T_g.

samples in order to produce more samples quickly, and also to test various configurations that would provide good results. Originally, ST-130 samples were manufactured on a custom large format high temperature 3D printer, that was found to have significant challenges with vibration. Additionally, it was found that without a heated enclosure, significant warping could occur with ST-130. Therefore, substantial modifications were made to the Ender 5 Plus, including an updated all-metal hotend and a heated enclosure. By upgrading to an all-metal hotend, it became possible to achieve higher extruder temperatures that were required for processing ST-130 and AQ-180. The heated enclosure was built to reduce manufacturing defects such as warping and cracking. The enclosure was heated using a heat gun that was controlled using an Omega temperature controller. The maximum enclosure temperature was limited to 105°C, which allowed use without risking significant damage to the internal plastic components of the printer. However, internal cooling fans still needed regular replacing to maintain functionality at these temperatures. The modified Ender 5 Plus is shown in figure 12.

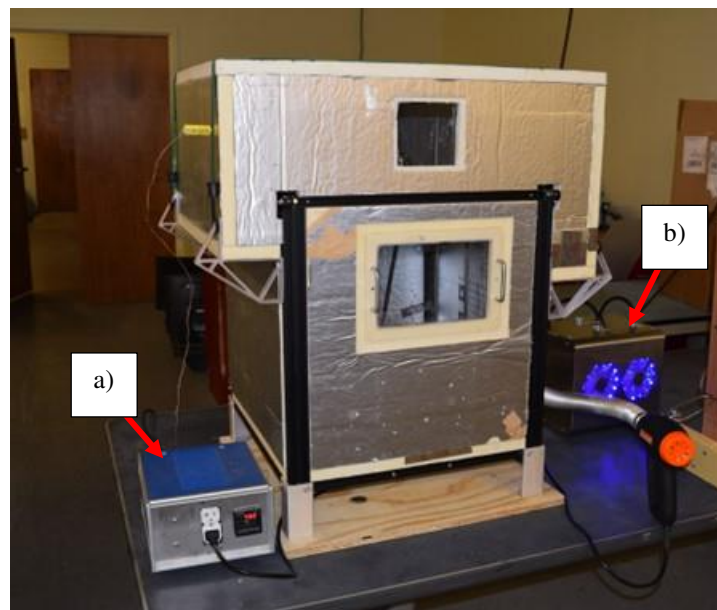


Figure 12 The enclosed Ender 5 Plus showing the temperature controller (a) and water-cooling system (b).

TPV testing was performed in an autoclave capable of 200°C (400°F) and 690kPa (100psi). Oilless vacuum pumps were used to create vacuum, which was sufficient and is standard for this type of composite processing.

Temperature Pressure Vacuum Sample Preparation

The TPV samples were designed to test tooling robustness under autoclave conditions and used a truncated conical geometry. The specimens were printed with 30% partially dense regions for benefits related to weight savings, material cost, and a reduction in washout time. The value 30% was arbitrarily chosen, as a starting point that would have improved characteristics compared to a monolithic tooling. The infill pattern chosen was called cubic and is a fast to print and quasi-isotropic (if the anisotropy caused by poor fusion boundaries between layers can be neglected) infill pattern.

A simulated view of the infill and a cross-section showing the sample geometry is shown in figure 13, with solid regions indicated by the cross-hatching and the unshaded region representing the 30% density cubic infill. The G-code was generated using the commercial 3D printing slicer, Cura Ultimaker 4.6.

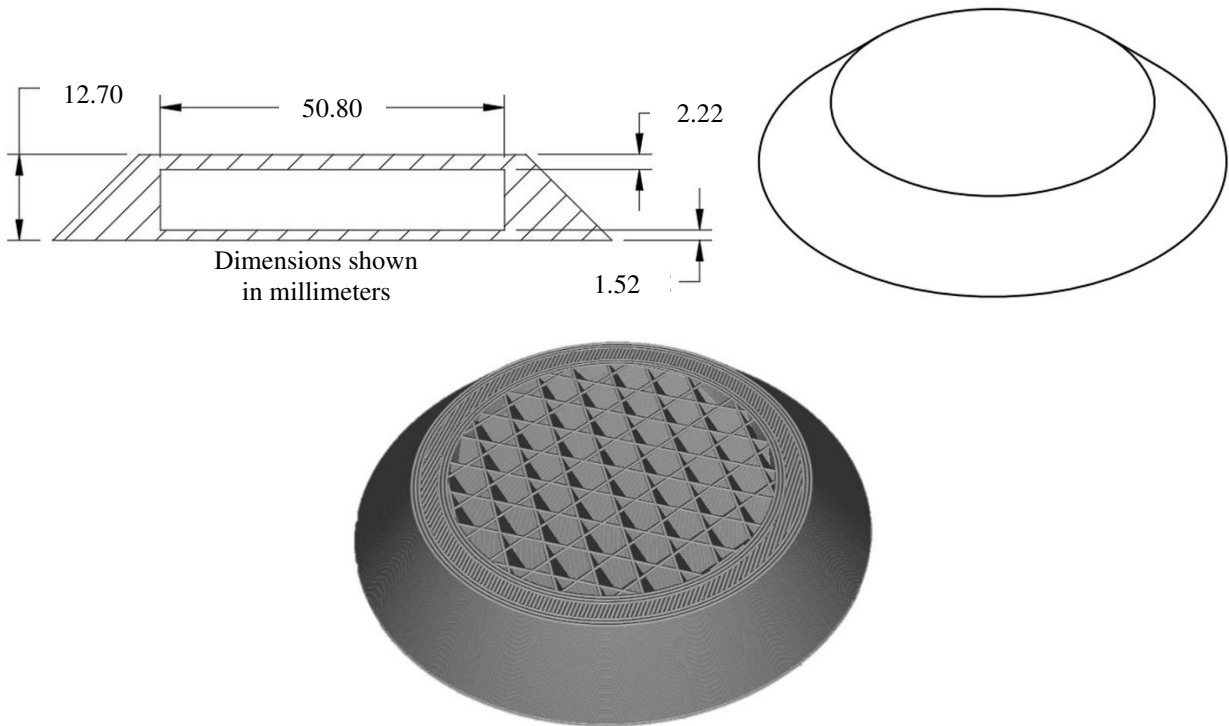


Figure 13 The TPV specimen truncated cone geometry for the nominally 2.2mm thick top surface sample.

The geometry for these specimens was chosen to simplify vacuum bagging and minimize pressure variations, as well as to leave a large flat surface that would be prone to deformation, as

compared to the sloped sides. The samples were printed from each material with nominal top surface thicknesses of approximately 3.3mm, 2.2mm, and 1.2mm, which resulted from 11, 7, and 4 top printed layers, respectively. These varying thicknesses were used to verify the impact of differing the outer surface thickness on resistance to deformation under autoclave conditions. The specimens were produced using a print speed of 30mm/s, a 0.6mm nozzle diameter, and a bottom surface thickness (against the build plate) of 1.6mm. The manufacturing temperatures that were determined by the end of the study and the successful hardware configuration used for manufacture are listed in Table 4 for each material. Any deviations in these manufacturing conditions will be listed in the results section.

Table 4 Dissolvable tooling candidate material 3D printing parameters

Material	Extruder Temperature (°C)	Print Bed Temperature (°C)	Enclosure Temperature (°C)	Hot-End	Filament Drive	Printer Used
BVOH	210	60	Ambient	Stock	Direct Drive	Lulzbot Mini 1.04, Prusa i3 MK2
Chamberlay 130	240	90	Ambient	Stock	Direct Drive/ Bowden	Prusa i3 MK2, Ender 3 Pro
AquaSys 120	235-255	100	Ambient	Stock	Direct Drive/ Bowden	Prusa i3 MK2, Ender 3 Pro, Ender 5 Plus
AquaSys 180	270-280	90	85-90	All-metal	Bowden	Ender 5 Plus
ST-130	270-285	126	105-122	All-metal	Bowden	Ender 5 Plus

There were manufacturing challenges related to the high process temperatures and CTE of ST-130 and AQ-180. If these materials were printed in ambient conditions, then poor interlayer fusion, warping, and cracking would develop. This was addressed by printing these materials in a heated enclosure, which was developed partway through the study. Additionally, worries of moisture absorption caused uncertainty of in some of the samples, so some tests were repeated after feedstock drying and storage procedures were developed. This process included first drying the feedstock for more than 4 hours at around 65°C, then loading the filament into desiccated storage containers that they could directly

supply the printers. These desiccated storage containers would maintain approximately 10-15% relative humidity.

Some samples, specifically made from AQ-120, were lighter in color which was initially attributed to moisture absorption. The moisture absorbed in the filament was thought to create small steam bubbles when heated, causing included voids, light colored, and opaque samples. However, after drying procedures were implemented, the sample quality was not improved. Based on this lack of improvement, under extrusion was determined to be responsible. Under extrusion is related to lower than desired extruder flow rates which result in a smaller than desired bead (road) cross section. This allows voids to be introduced between adjacent roads and layers, resulting in the opaque and lighter color. By measuring the mass of specimens with and without these characteristics, it was found that some underextruded specimens were almost half of the weight of correctly manufactured specimens. For example, in a comparison of two specimens that should have been identical, the measured mass of a faulty print and a nominal print were 26g and 45g, respectively. The cause of underextrusion was either due to a clogged nozzle or heat creep, which is a manufacturing problem caused by the filament melting prematurely and binding in the extruder. The underextruded specimens were lighter in color, had a rough surface texture, and were completely opaque as compared to the dark semi-translucent specimens that were printed correctly. Underextrusion was not a consistent issue with this material and would instead appear to occur randomly. The resulting specimen quality can be seen in figure 14.

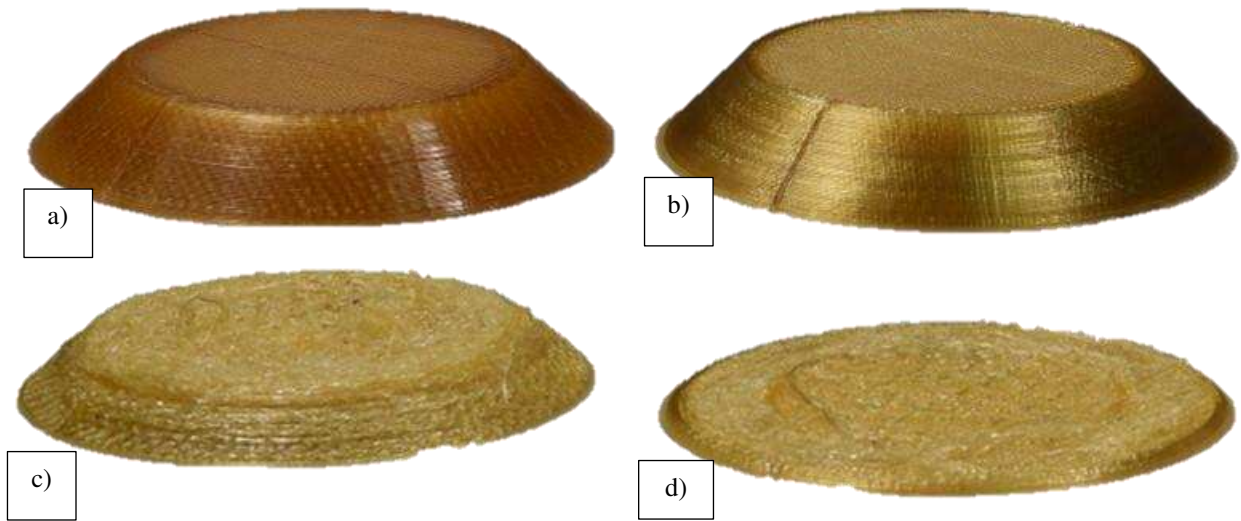


Figure 14 Underextrusion can be seen as a defect in the above AQ-120 samples with varying severity, sometimes stopping material extrusion entirely. Samples showing no underextrusion (a), some underextrusion (b), severe underextrusion (c), and a failed print caused by underextrusion (d).

Additionally, preliminary ST-130 samples had a light-colored ring on the outside of the top surface that is assumed to be from too high of extrusion temperatures that caused material degradation, discoloration, outgassing, and foaming as shown in figure 15. The perimeter of the top surfaces was likely the most affected because that is where the extruder was accelerating/decelerating as the turn was made and thus in contact with the material for a longer time. These preliminary ST-130 samples were printed at a nozzle temperature of 320°C, but with further process optimization it was determined that a temperature between 270 and 285°C was more appropriate. The use temperature was not provided by the manufacturer, as the material is proprietary and intended to be used only with Stratasys machines. The surface finish on the sloped walls of the ST-130 was also poor due to vibration and resonance issues in the original large format custom 3D printer used to make these samples.



Figure 15 Preliminary ST-130 sample showing poor surface roughness on side walls and discoloration on top surface compared to a high-quality ST-130 specimen, produced later in the study.

Materials made from BVOH and CL-130 did not have as many challenges in manufacturing, partly due to the reduced process conditions needed for manufacturing. AQ-180 was also straightforward to use, even though it required higher processing temperatures. Representative samples of each of these materials are shown in figure 16.

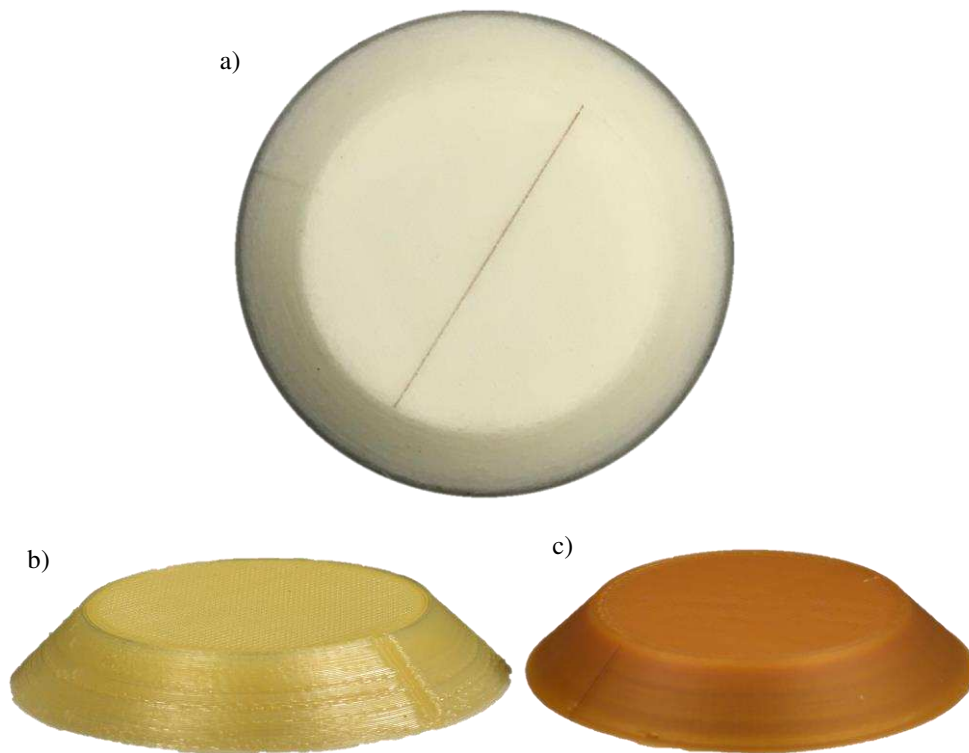


Figure 16 Representative images of samples made from BVOH (a), CL-130 (b), and AQ-180 (c). A line is marked across the top surface of the BVOH specimen (a), which was later used to aid in visualizing deformation.

It is likely that AQ-180 would have been a challenging material to print, but because it became available later in the study and had processing conditions like ST-130, the experience gained from ST-130 could be applied.

Temperature Pressure Vacuum Test Procedure

The TPV samples were first conditioned in a desiccated environment to maintain a low, consistent moisture content prior to being prepared for autoclave processing. The samples were then vacuum bagged to an aluminum tooling plate, with a layer of breather/bleeder cloth running up to the edge of the samples, as shown in figure 17. The top surfaces of the samples did not use breather/bleeder so that the surface could be photographed and referenced with a straightedge to observe deformation, without needing to remove the vacuum bagging material. The relative roughness of the surface of each sample was assumed to allow enough air flow to expose the sample surfaces to vacuum. Additionally, a line was drawn on either the top surface of the sample, or on the outside of the vacuum bag on the top side of the sample to aid in the visualization of any top surface deformation. After vacuum bagging, a 10-minute drop test was performed for each sample set to observe any drop in vacuum gauge pressure as a confirmation of vacuum quality.



Figure 17 TPV specimens in a vacuum bag configuration prior to testing.

Once loaded into the autoclave, the samples were exposed to a prescribed temperature, pressure, and vacuum cycle to mimic an autoclave processed composite part. The samples were ramped to

temperatures of 65, 93, 107, and 121°C in a stepwise fashion where they would undergo a 30-minute hold at that temperature. At the start of the hold, the pressure would be ramped to the hold pressure of 345kPa, which occurred over approximately 8 minutes. After the 30-minute hold, the autoclave was returned to ambient temperature and pressure. Then, the samples were removed from the autoclave and evaluated before being processed at the next highest temperature without being removed from the tooling plate or vacuum bag, and with vacuum applied throughout the entire process.

The rate used for heating and cooling was approximately 2.8°C/minute and the pressure ramp was initiated once the hold temperature was reached. The pressure ramp rate was at a maximum for the equipment used which was approximately 43kPa/minute (6.25psi/minute), lasting 8 minutes. The hold temperature duration was 30 minutes and, thus, the specimens were at the temperature and pressure of the test for approximately 22 minutes. A complete testing run with nominal temperature and pressure conditions is shown in figure 18. Note, there was not a set amount of time between cycles once the samples were cooled and removed from the autoclave, and sometimes the samples were left overnight under vacuum prior to testing at the next highest temperature.

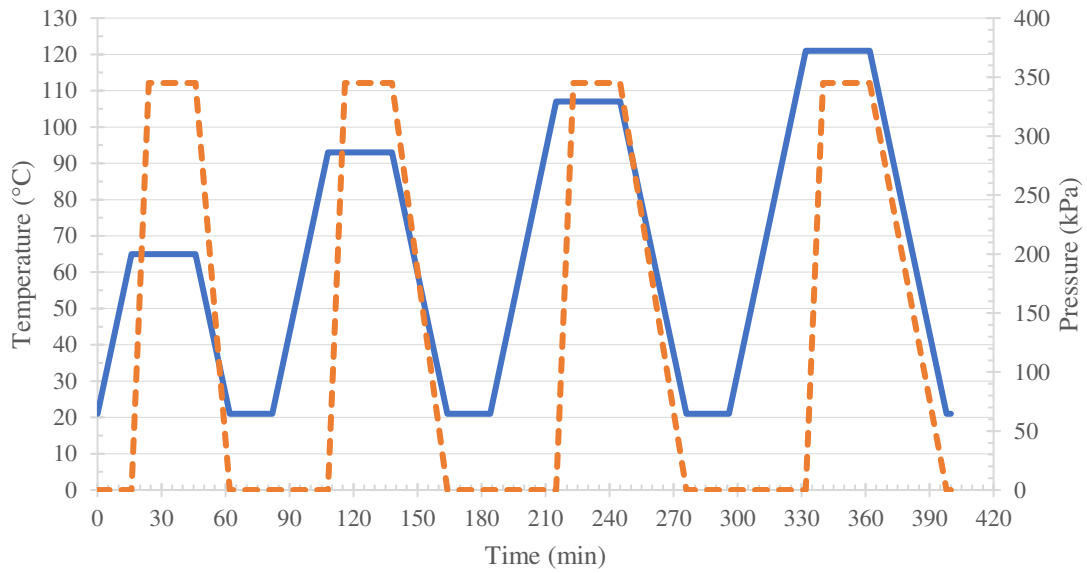


Figure 18 A general TPV test, showing the various temperature and pressure cycles applied.

After each cycle of the TPV test, the samples were removed from the autoclave and evaluated.

The series of TPV tests and any deviations from the process are detailed in table 5.

Table 5 A summary of material focused TPV tests conducted over the BVOH, CL-130, AQ-120, and ST-130.

Test:	Description:	Hold Temperatures Tested (°C)	Hold Pressures Tested (kPa)	Additional Notes
0	Tested ST-130, AQ-120, CL-130, and BVOH,	65, 93, 107, 121	345, 345, 345, 552	Final hold pressure was overshoot, leading to 552kPa hold pressure.
1	Tested AQ-120, CL-130, and ST-130 after drying had been implemented for AQ-120	93, 107, 121, 121	345, 345, 345, 621	121°C hold cycle was repeated at higher pressures that were of more interest to the industry partner Ability Composites.
2	Tested improved ST-130 samples against AQ-180	93, 107, 121	345, 345, 345	ST-130 samples were manufactured in a heated chamber on an Ender 5 Plus and were printed at lower nozzle temperatures, so they did not have defects caused by material degradation.
3	Compared ST-130 against AQ-120 samples after further drying efforts	121	345	AQ-120 filament feedstock was dried for 12-72 hours prior to manufacturing samples. ST-130 samples that had previously been tested in test 2 were reused.
4	Compared ST-130 against AQ-180 at even higher process pressure	121	621	The increased hold pressure was completed to accentuate the differences between ST-130 and AQ-120

Evaluation of TPV Material Samples

The tooling stability test samples were visually evaluated for deformation and photographed. There was a line marked across the top of each sample to provide a visual reference to aid in evaluation. Initially, a fixture was manufactured to assist in measuring the tool’s deformation, but it required a flat tool top surface that was often not available after the specimens had deformed at a given autoclave temperature and pressure step. As a result, the tooling stability test results were based only on visual observation of the deformation and were evaluated in terms of pass/fail at each processing step.

Evaluating the samples after each temperature and pressure cycle allowed for only intermittent observation of the samples. While the samples likely failed gradually as the temperature was increased and the specimens began to soften, data was only collected after each temperature/pressure cycle. This stepwise approach did enable an understanding of the development of shape loss, as some early stages of failure only showed print-through of the infill on the top surface. This type of failure would impact the surface finish of the completed composite but may not significantly impact the final geometry. However, for this study, infill print-through was considered a failure.

Results and Discussion

Test 0 – Preliminary Temperature Pressure Vacuum Test Results and Discussion

A preliminary test was completed that would include BVOH, CL-130, AQ-120, and ST-130 using three different top surface thicknesses of each material, nominally 1.2, 2.2, and 3.3mm. The test was completed prior to developing optimal manufacturing and environmental control procedures, however most of the results were still valuable. The ST-130 samples had some discoloration, likely due to the extrusion temperatures being too high and foaming caused by material degradation in small regions on the top surface of the sample. At this stage, the spools of filament were not stored with any consideration of moisture absorption. However, many of the samples were manufactured immediately after removing the filament spools from the original packaging, so moisture absorption was not considered significant at this point for most materials. However, a popping sound was noticed when printing AQ-120, indicating that moisture had been absorbed. Some of the AQ-120 samples also had underextrusion issues related to Bowden extrusion, indicated by lightweight samples with extremely poor adhesion between layers. Bowden extrusion is a setup where the extruder motor is separated from the extruder by a long flexible PTFE feed tube, which allows the weight of the extruder motor to be located off the machine but can cause issues with extrusion. These samples are shown in figure 19.

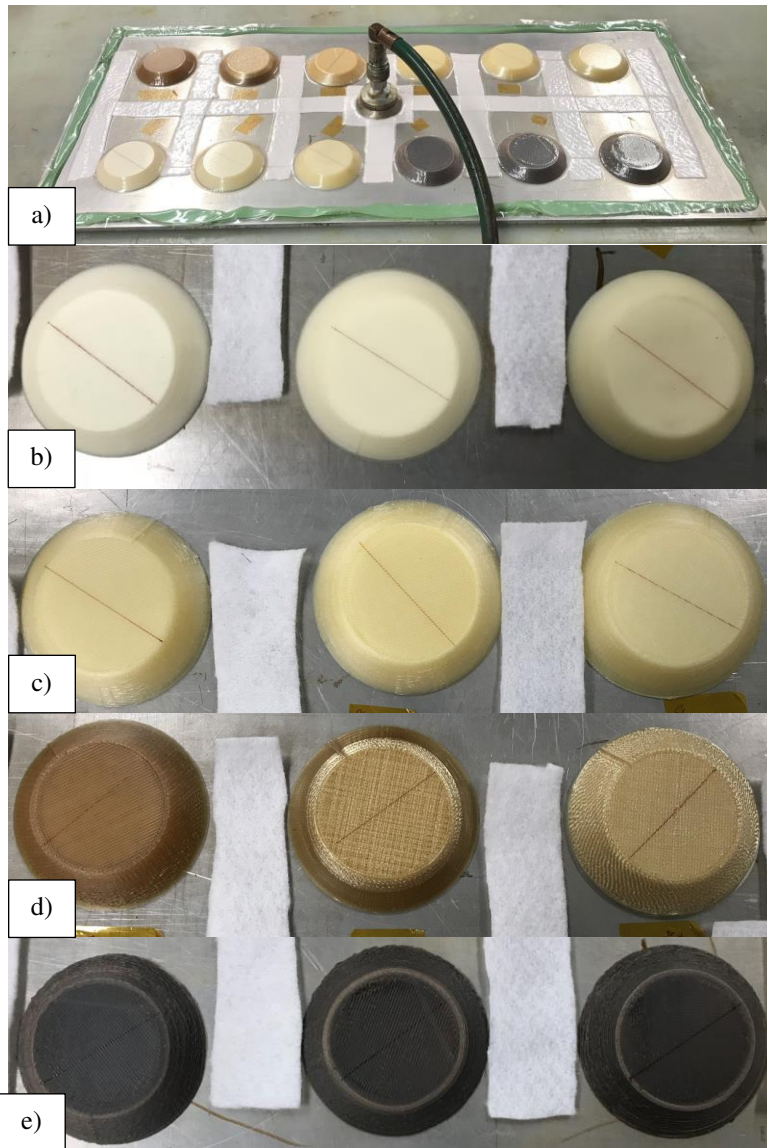
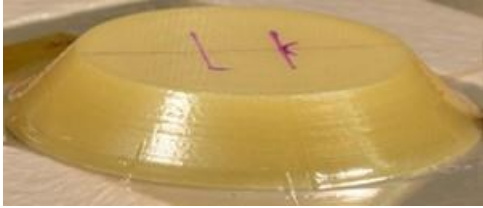


Figure 19 The TPV test configuration showing the entire tooling plate with all samples (a) and close-ups of specimens made from BVOH (b), CL-130 (c), AQ-120 (d), and ST-130 (e).

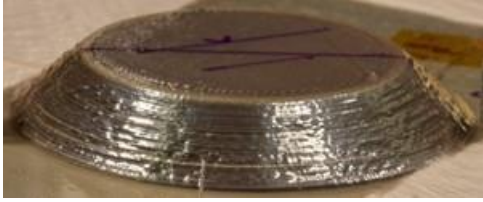
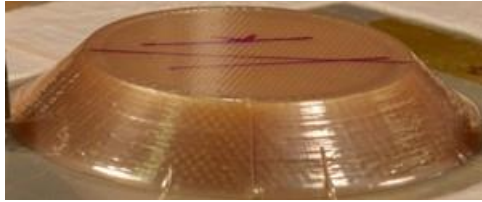
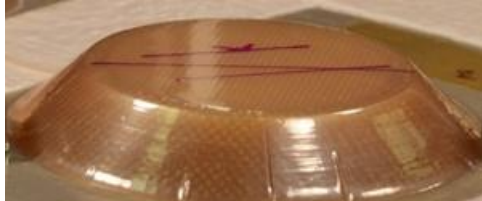
These samples were tested at 65, 93, 107, and 121°C at 345 kPa, except for the 121°C run, which was tested at 552 kPa. The photographed samples shown in Tables 6 and 7 have the thinnest of the three top surfaces tested, at 1.3mm thick, to better highlight the deformation. A visual representation of the sequence of tool deformation of is shown in Table 6 for CL-130 and BVOH.

Table 6 Photographs of the 1.3 mm thick CL-130 and BVOH samples during testing up to 121°C and 552 kPa.

Temperature (°C)/ Pressure (kPa)	CL-130	BVOH
65/345		
93/345		
107/345		
121/552		

The samples made from AQ-120 and ST-130 are shown in Table 7.

Table 7 Photographs of the 1.3mm thick ST-130 and AQ-120 samples during testing up to 121°C and 552kPa.

Temperature (°C)/ Pressure (kPa)	ST-130	AQ-120
65/345		
93/345		
107/345		
121/552		

The BVOH failed on the 65°C run. The CL-130 failed on the 93°C run. The ST-130 samples failed on the 121°C and 552kPa run. The AQ-120 specimen (only the 1.2mm thick sample) did not exhibit failure; however, this result was not reproducible in following tests. A significant effort was undertaken to determine printing parameters that could produce an AQ-120 specimen that could repeat this performance, but no further AQ-120 specimens resisted this temperature and pressure. Additionally, the two thicker specimens of AQ-120 tested during preliminary trials (that also showed obvious visual defects from underextrusion) performed poorly and failed at 93°C at 345kPa. The three AQ-120 specimens are shown in figure 20 after the 93°C cycle.

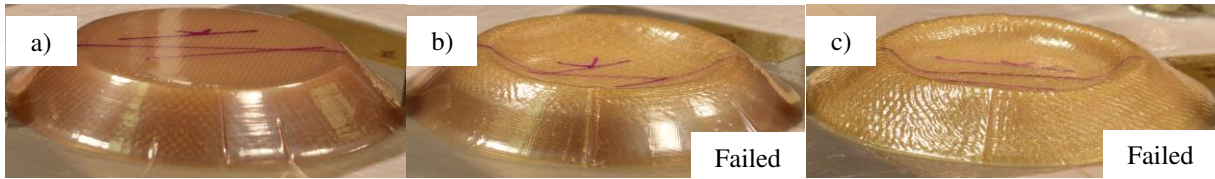


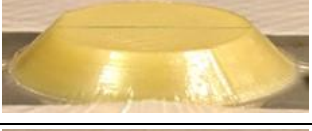
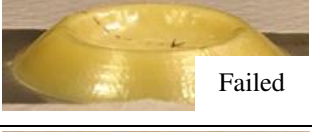
Figure 20 The samples with nominal top surface thicknesses of 1.3mm (a), 2.2mm (b), and 3.2mm thick (c).

The success of the 1.2 mm thick AQ-120 sample was assumed to be caused by processing errors during vacuum bagging. This was considered an outlier sample. After noticing the challenges printing AQ-120, the filament was dried and stored in a desiccated environment both before and during printing. BVOH was eliminated from further testing due to poor performance in this test, as well as its lower thermal properties indicating poor suitability as autoclave processable tooling.

Test 1 – Testing with Improved AQ-120 Feedstock Handling Results and Discussion

After beginning to dry AQ-120 filament, AQ-120, CL-130, and ST-130 samples were again manufactured and tested. The ST-130 samples were included, even though they still presented a discolored and rough surface, as a comparison to the new AQ-120 samples. CL-130 was included to attempt to repeat the previous results. The extensive drying procedure involved drying the AQ-120 filament at 70°C for at least 12 hours prior to each print. Then, the filament was stored in a desiccated environment both before and after printing. The results are shown in Table 8.

Table 8 Photographs of the 1.3mm thick AQ-120, CL-130, and ST-130 samples during testing up to 121°C and 621kPa.

Temperature/ Pressure (°C/kPa)	AQ-120	CL-130	ST-130
Pre-testing			
Pre-testing, bagged			
93/345	 Failed	 Failed	
107/345	 Failed	 Failed	
121/345	 Failed	 Failed	
121/621	 Failed	 Failed	

The results suggested that ST-130 would be the optimum material for thermal stability of autoclave tooling. The AQ-120 samples, even after being printed in a fully desiccated environment and lacking any visual defects which could cause failure, still failed at 93°C at 345kPa. While the ST-130 samples were still being printed at too high of a print temperature, they all survived the 121°C test at 345kPa with no noticeable deformation and survived the 121°C test at 621kPa with only minor deformation. It was necessary to further test ST-130 with improved manufacturing parameters to determine how the performance would change.

Both AQ-120 and CL-130 were carried this far into the study in hopes that adjustments in print parameters would enable use, as both were soluble in water. Solubility in water was considered very desirable compared to the high pH solution necessary to dissolve ST-130. However, none of the

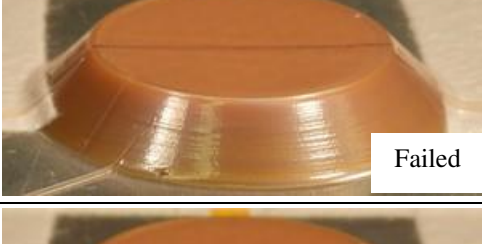
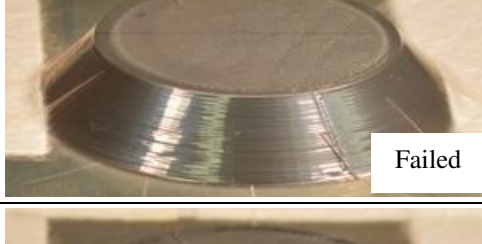
adjustments were successful and thus the CL-130 was removed from further processing trials. AQ-120 was still pursued in the hope that further optimization of processing conditions might allow use and potentially recreate the outlier result from test 0, where a single sample survived conditions of 121°C and 552psi.

Test 2 & 3 – Testing with Improved ST-130 samples, AQ-180, and Further Dried AQ-120 Results and Discussion

In this set of TPV test samples, a material candidate that was previously not on the market was made commercially available, so it was included for comparison with the ST-130 specimens. The ST-130 processing conditions were significantly improved by moving from a custom large-format printer in the laboratory to a heavily modified Ender 5 Plus. ST-130 specimens were printed in an enclosure temperature of 105°C with a nozzle temperature of 280°C, much cooler than the 320°C temperature used previously. Additionally, AQ-120 was still included but the filament underwent additional drying at 70°C for more than 72 hours before each sample was printed. The AQ-180 was manufactured with a nozzle temperature of 275°C and an enclosure temperature of 80°C, which was found to be sufficient to prevent warping.

These tests were completed in two TPV test runs. The first compared the ST-130 specimens to AQ-180 specimens while the second reused the ST-130 specimens and compared them against the remaining AQ-120 specimens printed for the project, as well as the specimens with additional drying time. The results comparing the AQ-180 and ST-130 are shown in Table 9.

Table 9 Photographs of the 1.3mm thick AQ-180 and ST-130 samples during testing up to 121°C and 621kPa.

Temperature/ Pressure (°C)/(kPa)	AQ-180	ST-130
Pre-test		
93/345		
107/345		
121/345		

It was noticed that during the 121°C at 345kPa run, and slightly on the 107°C at 345 kPa run, that the surface on ST-130 and AQ-180 samples deformed slightly so that the infill pattern could be seen through the part, although the top surface remained flatter for the ST-130 than the AQ-180 specimen. This test indicated that AQ-180 performed nearly as well as ST-130 and is an excellent choice for high temperature cures where mold water solubility is required; however, the performance of ST-130 was still marginally better. Infinite Material Solutions, the manufacturer of AQ-180, indicated during a public webinar that due to the make-up of the material and the associated fillers, the solubility should be

expected to decrease with extended time at elevated temperatures. This may be a concern for lengthy autoclave processing runs that may reduce the solubility of the mold.

The second part of this test included 72+ hour dried AQ-120 specimens and the previously tested ST-130 specimens. This test also included every AQ-120 specimen that had been printed, but not previously tested, to determine if one of the early samples of AQ-120 matched the performance of the single AQ-120 specimen that survived to 121°C at 345 kPa in the preliminary TPV test. Additionally, three AQ-120 specimens were printed and tested with filament drying conditions of 72+ hours at 70°C. This test was completed at 121°C at 345kPa, to see if any individual specimen could match the performance of ST-130. An image of the tooling plate after processing is shown in figure 21.

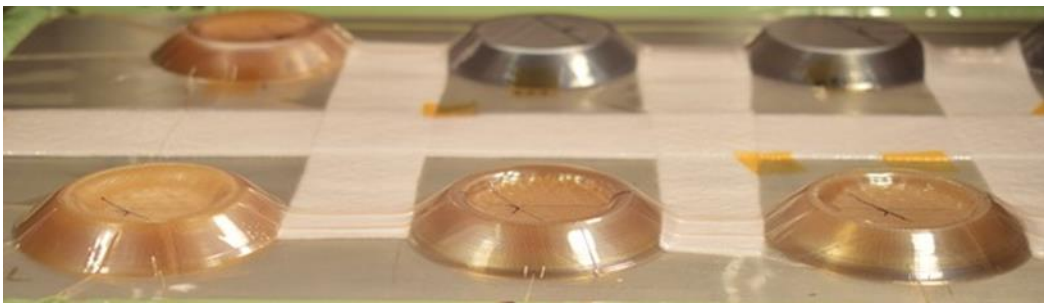


Figure 21 Various tested specimens after the 121°C at 345kPa test run.

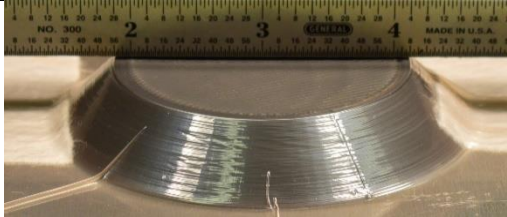
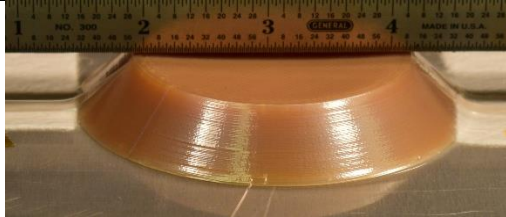
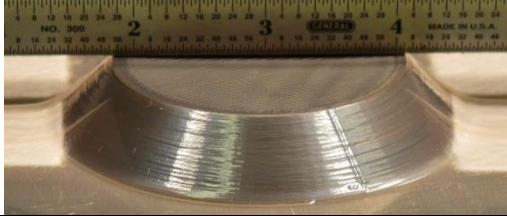
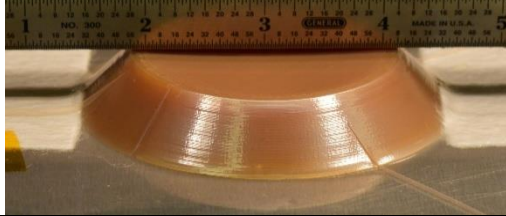
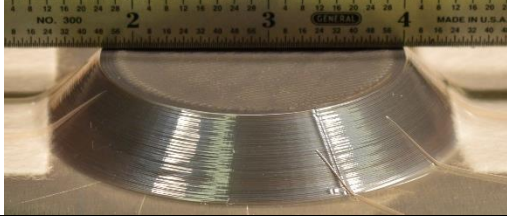
This test verified that independent of the printing conditions, none of the AQ-120 samples survived under the tested conditions. The ST-130 specimens once again were relatively undeformed after retesting at 121°C and 345kPa. By not having any of the AQ-120 specimens match the performance of the single 1.3 mm thick sample from the preliminary Temperature Pressure Vacuum test, it can be assumed that the single surviving sample was definitely an outlier, most likely due to inadequate vacuum distribution that caused reduced loading on the sample.

Test 4 – Comparing AQ-180 to ST-130 at Increased Pressure

The three thicknesses of the two most thermally stable samples made from AQ-180 and ST-130 were tested at a higher pressure still, with conditions of 121°C and 621kPa. This elevated pressure test

was completed to try to induce more obvious failures and differentiate the two materials. These results are shown in table 10 for the three different thickness specimens made using ST-130 and AQ-180.

Table 10 Comparison of top surface deformation at 121°C and 621kPa conditions.

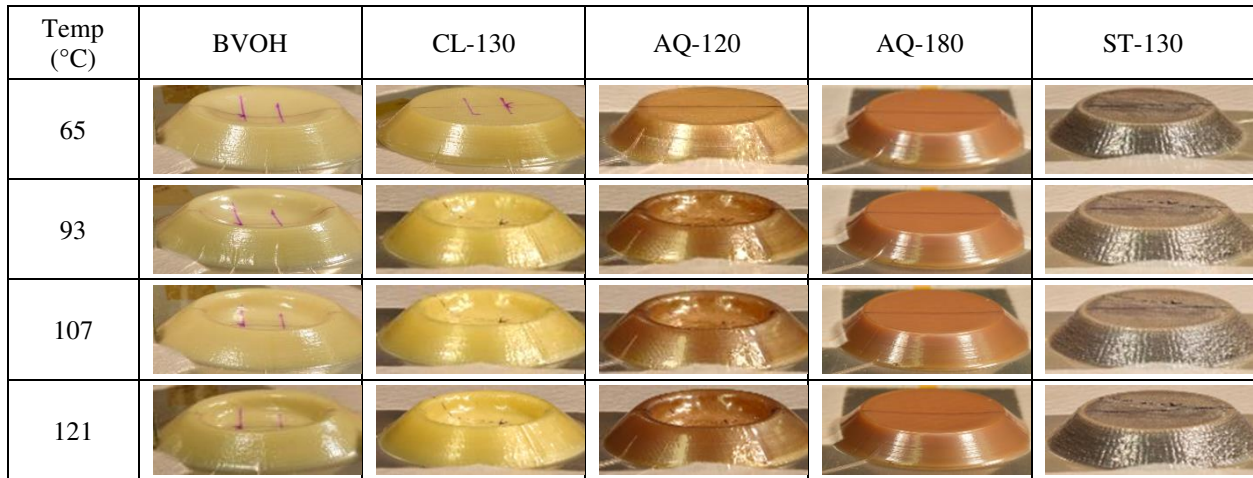
Thickness (mm)	ST-130	AQ-180
3.2		
2.2		
1.3		

Processing conditions of 121°C and 345kPa are likely at the edge of the stability range for both ST-130 and AQ-180. In a situation where high geometric fidelity is required, lower processing temperatures and pressures or higher infill densities would be required.

Summary of Results and Discussion

The deformation shown in Table 11 gives a sense of the effects of temperature and pressure on the various materials. The specimens shown have the thinnest (1.3mm) top surface to show the most severe deformation for any material sample set. Occasionally, the samples with thin top surfaces would fail where the samples with thick top surfaces would not.

Table 11 Stability at 345kPa and temperature of 1.3mm surface thickness specimens.



A summary of the results from these tests is given in Table 12.

Table 12 Summary of specimen failures based on visual examination.

Material		ST-130			AquaSys 180			AquaSys 120		
Thickness (mm)		3.2	2.2	1.3	3.2	2.2	1.3	3.2	2.2	1.3
Temperature (°C) at 345 kPa	65									
	93						X	X	X	X
	107					X	X	X	X	X
	121		X	X	X	X	X	X	X	X
Material		Chamberlay 130			BVOH			X = Failure		
Thickness (mm)		3.2	2.2	1.3	3.2	2.2	1.3			
Temperature (°C) at 345 kPa	65				X	X	X			
	93	X	X	X	X	X	X			
	107	X	X	X	X	X	X			
	121	X	X	X	X	X	X			

The results of the TPV tests indicate that ST-130 was the most robust 3D printing material for autoclave applications. However, AQ-180 also performed well during the 121°C autoclave cycles. The failures presented by the ST-130 and AQ-180 involved primarily infill print through, and slight sagging of the top surface for AQ-180. For this study, print-through type defects where the infill pattern could be seen in the sample top surface were considered failures. An example of this failure mode can be seen in figure 22, where the top surface shows the underlying cubic infill pattern.

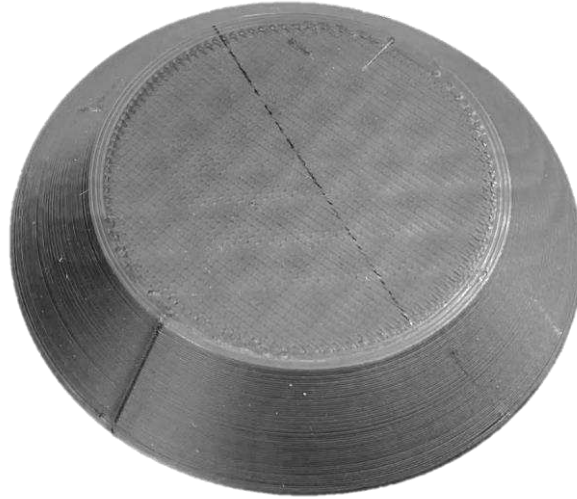


Figure 22 Print through failure mode.

The top surface thickness appeared to impact the severity of deformation, not necessarily the presence of deformation. For example, at 121°C, all the AQ-180 samples deformed slightly; however, the deformation was less significant for the specimens with the 3.2mm top surface thickness than those with the 1.3mm surface thickness.

TEMPERATURE PRESSURE VACUUM STRUCTURAL SAMPLE TESTING

Temperature Pressure Vacuum (TPV) testing was also completed to analyze a sample set that more closely focused on structure, rather than on the material. However, one of the parameters that was also evaluated in this sample set was the comparison of material with and without the inclusion of short carbon fiber and its impact on autoclave robustness. In this study, the infill type, infill percentage, top surface thickness, wall thickness, nozzle size, carbon fiber loading, and secondary infill structures were evaluated for their effects on the overall structural performance.

Experimentation

Materials and Equipment

This test was completed to evaluate the impacts of structural design on autoclave performance. These tests were completed with PETG, a low-cost material that is commonly used in the consumer 3D printing market due to its ease of manufacture and relatively high strength and toughness. PETG would

not be suitable for high temperature tooling applications, as its T_g is only 80°C . This material was printed with a nozzle temperature of 240°C and a bed temperature of 90°C . Samples were generated on a Prusa i3 MK2s printer from 1.75mm filament feedstock using a direct drive printer. The TPV testing was performed in the same autoclave capable of 200°C and 690kPa at the CMMS lab at CSU.

TPV Structural Sample Preparation

There were 13 samples generated for this portion of the study, 9 of which utilized a different geometry than the previous truncated conical geometry. Rather, samples 1-9 used a truncated pyramid geometry, nominally 76.2mm x 76.2mm x 12.7mm high with 45-degree inclined sides, as shown in figure 23.

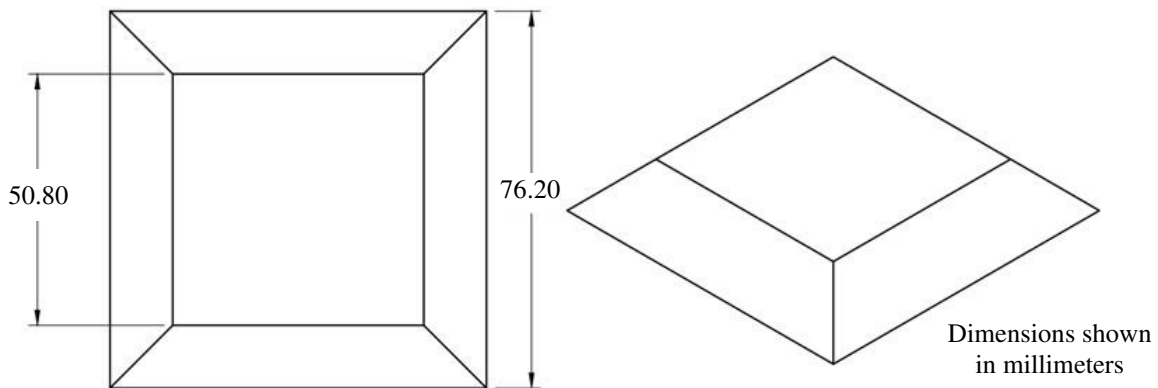


Figure 23 The geometry used for samples 1-9 in the structural TPV tests.

The samples were printed on the Prusa i3 MK2s and sized so that samples 1-9 could all fit onto the print bed of the printer and be printed simultaneously. This was desirable to eliminate any external variables, such as filament moisture absorption between prints. Samples 10-13 were printed separately and required changing nozzles or material between samples, so they were printed sequentially. Samples 10-13 also used the same truncated conical geometry that was used in the previous material focused TPV tests, as was shown in figure 13. The sample matrix is shown in table 13.

Table 13 Test matrix for structural TPV testing of PETG specimens.

Test Parameter	Infill Type (30% unless stated otherwise)	Perimeter Count	Top Layer Count	Solid Regions
1 Control	Gyroid	3	3	None
2 Compression Specific Infill	Stars (quarter isogrid)	3	3	None
3 Thick walls	Gyroid	6	3	None
4 Thick top layer	Gyroid	3	6	None
5 Thick top layer/ walls	Gyroid	6	6	None
6 Solid under angled surfaces	Gyroid	3	3	Under angled surfaces
7 Solid Ribs	Gyroid	3	3	Cross pattern through center of part
8 Low Infill Density	Gyroid 20%	3	3	None
9 High Infill Density	Gyroid 40%	3	3	None
10 Carbon Fiber Loading	Cubic	3	3	Under angled surfaces
11 No Carbon Fiber Loading	Cubic	3	3	Under angled surfaces
12 0.6mm nozzle	Cubic	3	3	Under angled surfaces
13 0.8mm nozzle	Cubic	3	3	Under angled surfaces

The gyroid and star infill patterns were changes from the previous TPV tests. Star infill was expected to perform well in compression, due to the vertical walls that would directly carry load like a honeycomb structure. Gyroid is a structure that has continuous open channels running throughout the part and this is desirable because for washout tooling this would allow dissolution media to infiltrate the entire structure at once. An example of the gyroid infill is shown in figure 24.

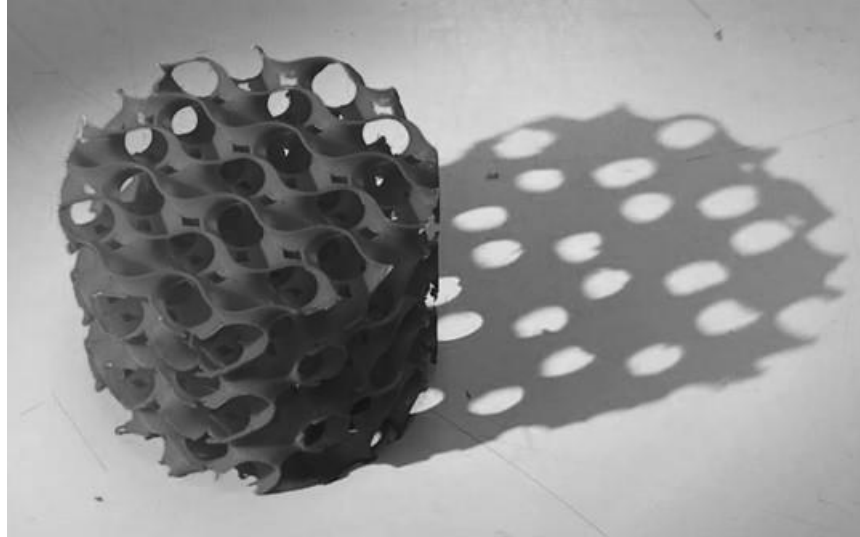


Figure 24 A 3D Printed cylinder with gyroid infill and no outer skins.

A rendering of the layout of samples 1-9 on the build plate can be seen in figure 25. This rendering was captured near the upper portion of the samples, prior to the solid top layers being deposited, so that the infill structures can be seen.

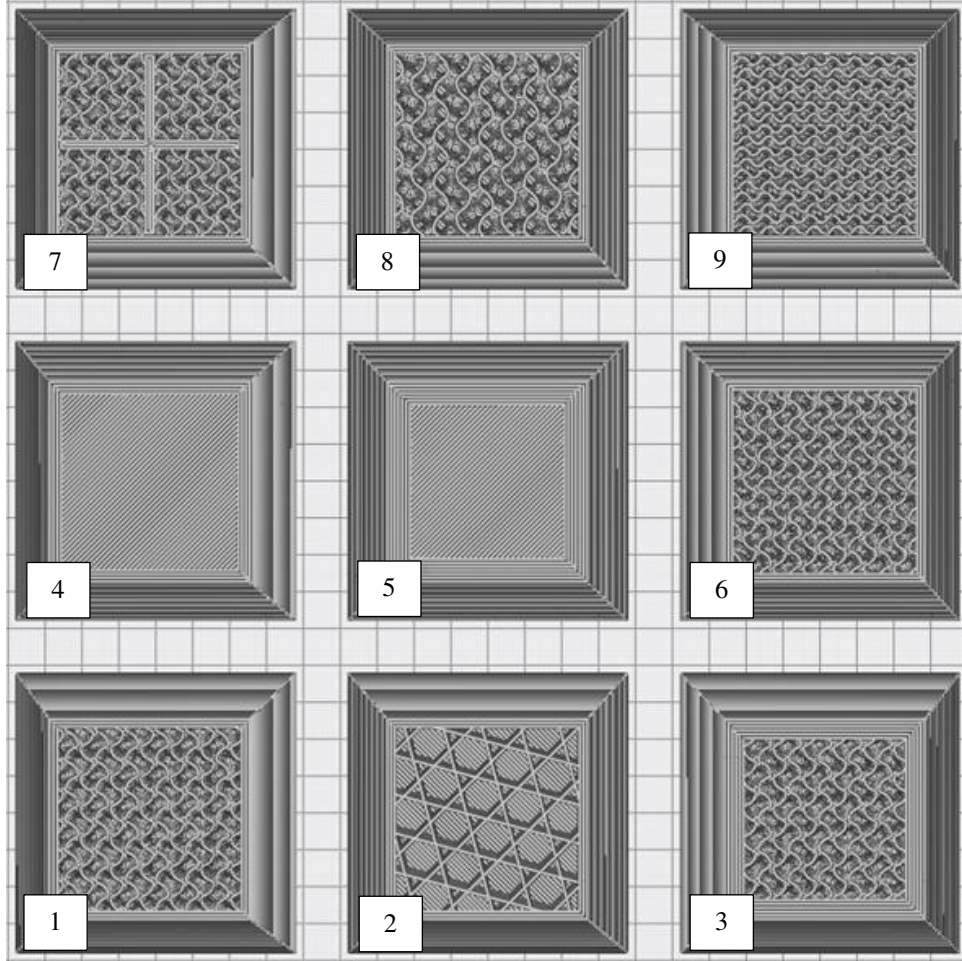


Figure 25 Top view rendering of samples 1-9 during the manufacturing process.

While the infill of most samples can be seen in figure 25, samples 4 and 5 show the thicker top surfaces. These samples still have underlying gyroid infill structure.

Temperature Pressure Vacuum Test Procedure

The TPV test procedure for this test was similar to the procedure described previously for the material TPV testing. However, it was completed at fractional temperatures of the T_g to show gradual deformation and so the results could still be used to guide tool design with higher temperature materials. The autoclave was, in a serial fashion, heated and pressurized to 60, 70, and 80°C at 345 kPa. Between test temperatures, the autoclave was cooled, and the samples were photographed and evaluated for deformation. Like the previous tests, the heating/cooling rate was approximately 2.8°C per minute and the

pressure ramp rate was approximately 43kPa per minute. The samples were at temperature for 30 minutes and the pressure ramp was initiated once the hold temperature was met.

Evaluation of TPV Structural Samples

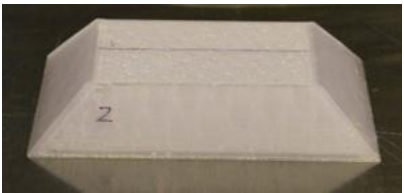
The structural TPV samples were evaluated in a similar fashion to previous tests. A line was marked on the top surface of each sample to assist in visualizing the deformation. The samples were photographed and evaluated to determine which parameters influenced the robustness of the samples.

Results and Discussion

The parameters tested were infill type, infill percentage, top surface thickness, wall thickness, nozzle size, carbon fiber loading, and secondary infill structures. In this section, these parameters will be compared to the control sample (sample 1) to determine the influence on structural performance.

Sample 1 and Sample 2 used gyroid and stars infill patterns, respectively, and can be seen in table 14.

Table 14 Infill pattern test samples 1 and 2.

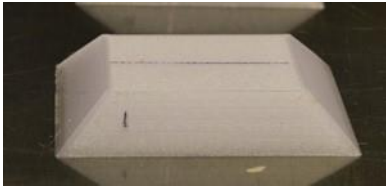
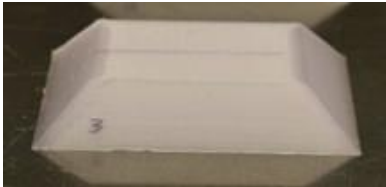
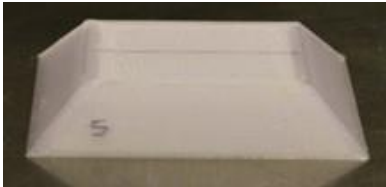
Temperature (°C)	Sample 1: Control	Sample 2: Stars (quarter-isogrid)
Pre-test		
70		
80		

The gyroid infill pattern had significantly better results than the stars infill pattern. In tangential work, the measured densities of various infill patterns were a few percent different than what was

specified in Cura Ultimaker; however, the difference small, so this is unlikely to be the cause for the significantly improved performance. Additionally, there may be some advantages to using gyroid infill related to print speed. Some infill patterns like honeycomb require the printhead to decelerate prior to changing directions, then accelerate again. However, gyroid is made up of smooth curving print paths, thus it can be created without slowing as much as other patterns. It was found that gyroid infill patterns are beneficial to improving the dimensional fidelity of autoclave tooling and had added benefits related to print speed.

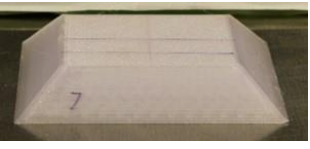
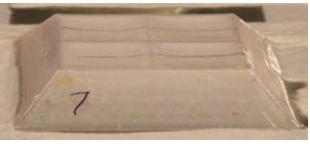
In table 15, samples 3, 4, and 5 are compared to the control sample. These samples had increased wall thickness, increased top surface thickness, and both increased wall and top surface thickness, respectively.

Table 15 Outer skin thickness test samples 1, 3, 4, and 5.

Temperature (°C)	Sample 1: Control	Sample 3: Thick Walls
Pre-test		
70		
80		
Temperature (°C)	Sample 4: Thick Top Surface	Sample 5: Thick Walls & Top Surface
Pre-test		
70		
80		

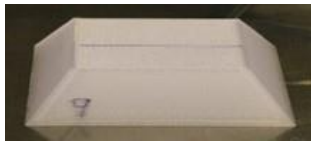
The outer skin thickness comparison showed that thicker walls and top surfaces are useful in increasing robustness. Another consideration was the addition of secondary support structures within the infill structure. These included solid regions under the walls and central solid supports in the part. The comparison of these samples is shown in Table 16.

Table 16 The secondary support structure test samples 6 and 7.

Temperature (°C)	Sample 1: Control Sample	Sample 6: Solid Under Sloped Walls	Sample 7: Solid Cross
Pre-test			
70			
80			

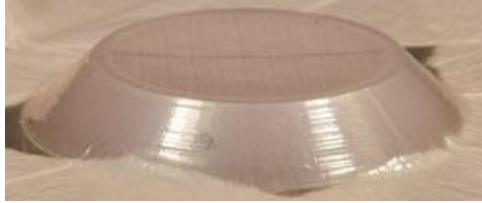
The addition of secondary support structures was not found to be worthwhile. While they did improve the deformation locally, they increased the material usage while leaving large regions of the sample unsupported. As an alternative to secondary support structures, increasing the infill density could be used to support the entire sample outer surface more evenly. In table 17, samples 8, 1, and 9, with infill densities of 20, 30, and 40% respectively, are compared.

Table 17 The effects of infill density are seen in samples 8, 1, and 9.

Temperature (°C)	Sample 8: 20% infill density	Sample 1: 30% infill density	Sample 9: 40% infill density
Pre-test			
70			
80			

The higher infill density samples performed the best. Infill density was determined to be the most influential parameter for autoclave robustness of all the parameters evaluated for these PETG samples. The next test was to understand the impact of a different nozzle size on performance. Both 0.6 mm and 0.8 mm nozzle sizes were used to create samples with similar features. Both samples used 30% infill, but the 0.8 mm nozzle created larger beads and these were printed farther apart to provide the same infill density. The geometry in this test was the truncated conical geometry. The results of this are in Table 18.

Table 18 Nozzle size test samples 12 and 13.

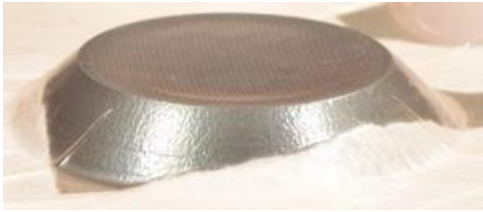
Temperature (°C)	Sample 12: 0.6 mm nozzle	Sample 13: 0.8 mm nozzle
Pre-test		
60		
70		

The nozzle size test showed that the infill printed with the thicker nozzle resulted in more deformation at 70°C. This can be explained by the spacing between infill roads being greater for the 0.8mm nozzle than for the 0.6mm nozzle to maintain the same infill density. For a simply supported beam, the span is an important factor in bending stiffness. There was likely worse performance for the 0.8mm nozzle due to the increased spans between supporting infill structures.

The final test compared a carbon fiber filled PETG and a neat PETG specimen. This test was designed to investigate the impact of carbon fiber filler on performance in autoclave conditions. The

hypothesis was that adding carbon fiber would increase the HDT of the material, resulting in improved performance. Table 19 shows the short carbon fiber filled PETG and neat PETG samples tested up to 80°C and 345kPa.

Table 19 PETG samples 10 and 11, with and without carbon fiber loading, respectively.

Temperature (°C)	Sample 10: Carbon Fiber PETG	Sample 11: Neat PETG
Pre-test		
70		
80		

This test showed that the neat PETG performed better than the carbon fiber loaded PETG, which can be seen in the 70°C test where measurable distortion is noted for the carbon filled specimen and not for the neat PETG specimen. The cause of this was assumed, after an analysis of the raw filament densities, to be due to an increased void content in the carbon fiber loaded filament. The carbon fiber filled filament had a lower-than-expected density, most likely due to poor fiber wetting during manufacturing and a high void content at the surface of the carbon fibers. This seemed to reduce the load transfer between the carbon fiber and the PETG resulting in poorer performance.

In summary, the parameter which made the greatest impact on the performance of the samples was the infill density. Following this, by using gyroid infill the sample performance was improved over

stars. Carbon fiber loading in PETG was not effective at reducing deformation. Finally, additional internal solid structures were deemed unnecessary for improved performance. While the increase in nozzle size worsened performance slightly, it also reduces the print time significantly. These results suggest that future prints should focus on increased infill percentage density and nozzle size.

TEMPERATURE PRESSURE VACUUM STRUCTURAL SAMPLE TESTING – INFILL AND ROAD WIDTH

After completing the structural tests with PETG and determining that infill percentage was an important parameter for improving the robustness of a 3D printed tool, it was desired to do a final small-scale test before moving on to larger composite tooling samples. The larger scale tools were expected to take much longer to manufacture, on the order of days, so there was a desire to investigate the nozzle diameter as that could reduce manufacturing time. The increase in nozzle size, as was seen in the PETG infill test prints tests with 0.6 vs. 0.8 mm nozzles, showed a widening of infill road spacing to maintain the same infill density, resulting in fewer passes to create the infill structure. Additionally, ST-130 was found to be the most robust tooling material from the material studies. Finally, the top surface thickness was also of interest to evaluate, to determine if increasing the top surface thickness could allow a reduced infill density with similar results. Therefore, this test was aimed to verify the impact of nozzle diameter, road (or bead/print path) width, top-surface thickness, and infill percentage using ST-130.

Experimentation

Materials and Equipment

Four specimens were manufactured from ST-130 using the Ender 5 Plus in a heated enclosure with a 0.8mm nozzle. These specimens were tested in the same autoclave used previously.

Sample Preparation

The specimens all used the same truncated conical geometry from previous TPV tests, shown in figure 13. They were manufactured with a nominal infill density of 40% using gyroid infill, the infill pattern that was determined to be most applicable for washout tooling with rapid manufacturing due to the

fast print speed and interconnected structure that would allow dissolution media to flow continuously through the infill regions. The samples manufactured are listed in table 20.

Table 20 Sample matrix for infill parameter testing.

Sample	Infill (%)	Infill Road Width (mm)	Infill Road Spacing (mm)	Top Surface Thickness (mm)
1	40	0.8	2	3.2
2	~53	0.8	1.5	3.2
3	40	0.6	1.5	3.2
4	40	0.8	2	4.6

Sample 1 was manufactured as a control sample, using the default infill road width and spacing, and the maximum top-surface thickness (3.2mm) tested in the material focused Temperature Pressure Volume (TPV) tests. Sample 2 was manufactured with reduced infill road spacing, without modifying the road width. This had the effect of increasing the density, from 40 to approximately 53%. Sample 3 had a reduced road width, using the same 0.8mm nozzle. This sample would then have a decreased road width and spacing, but it would maintain the same infill percentage. This was hypothesized to improve the robustness of the specimen, given the reduced span between infill passes. Finally, the fourth sample used a thick top surface. A representative sample is shown in figure 26.

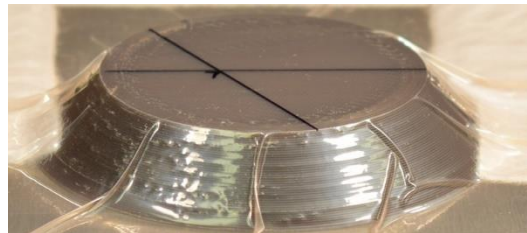


Figure 26 The four ST-130 samples prepared for testing prior to being loaded into the autoclave. The top surfaces were marked to aid in visualizing deformation.

Test Procedure and Evaluation

The samples were processed in a similar manner to previous tests. They were placed onto an aluminum tooling plate, vacuum bagged, loaded into an autoclave, and then processed at a cycle temperature. The conditions tested were at 121°C, with three pressures of 345, 483, and 621kPa (50, 70, and 90psi). The higher pressures were used to accentuate deformation, as ST-130 had been able to survive

the 345kPa tests with minimal deformation. Then they were allowed to cool and removed from the autoclave prior to evaluation. The samples were photographed and visually evaluated for deformation using a straightedge.

Results and Discussion

At 345 kPa (50 psi), the deformation was minimal. However, at 621 kPa, the deformation was slight, and could be seen by holding a straightedge across the sample. These results are shown in figure 27. The sample numbers in figure 9 correspond to those listed in Table 20.

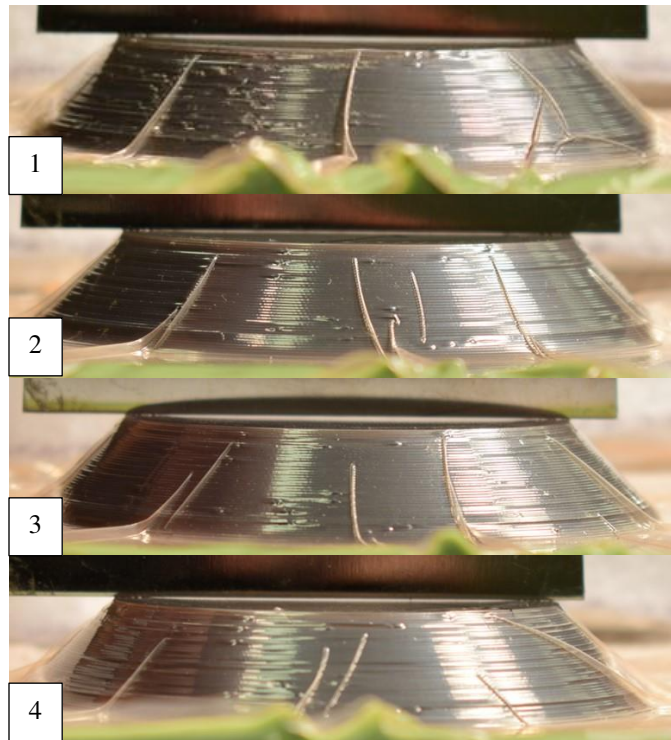


Figure 27 ST-130 specimens after testing including: control sample (1), increased infill density (2), decreased road width/spacing (3), and increased top surface thickness (4).

The four infill parameter samples tested showed that, like the PETG sample tests, the infill density had the greatest impact on the performance of the specimen. The samples showed good fidelity at 345kPa and additionally would only be tested to this value for the square pyramids. It is seen that sample 2 (~53% infill) performed the best, although marginally. This sample was the only sample with increased infill density. However, based on the marginal improvement and to conserve material and time, the default infill

parameters (2 mm road spacing) for a 0.8 mm nozzle with 40% infill (sample 1) were utilized for future specimen manufacture.

DISSOLUTION STUDIES

Experimentation

As a cursory study of the washout characteristics of some of the tooling materials, including ST-130, AQ-120, and AQ-180, several small test samples were manufactured to test the dissolution process. The washout characteristics were compared to Solcore 100, a ceramic tooling material that has a soluble binder and can be used for washout tooling applications.

Materials and Equipment

The 3D-printing materials that were carried forward into this portion of the study included ST-130, AQ-120, and AQ-180. The two other materials that were evaluated in the Temperature Pressure Vacuum (TPV) tests were CL-130 and BVOH, but these were excluded from the washout study because of their low thermal stability. However, both AQ-120 and CL-130 performed similarly in the TPV tests, but CL-130 seemed to have stopped being manufactured because it was no longer available for purchase. Future studies after this dissolution trial would require significant material quantities for testing so CL-130 was not considered for these trials.

Both AQ-120 and AQ-180 require a water bath for dissolution and the washout time is reduced significantly if the bath is heated. Infinite Material Solutions recommends a bath temperature of 80°C to increase the dissolution rate. ST-130 is soluble in a heated basic solution, which is a disadvantage due to challenges related to environmental safety. Stratasys recommends either WaterWorks or EcoWorks detergents to create a solution with 11-13 pH that is heated to 80°C. The approach taken by CSU was to use an aqueous solution of trisodium phosphate (TSP) to result in a solution of at least 12 pH. Aqueous TSP solution is a commonly used as an industrial cleaning agent and was investigated as an industrially scalable, inexpensive alternative to the Stratasys solutions. The ceramic washout tooling media can be left to soak in room temperature water, where the binder is dissolved, and the tooling can then be physically

removed rather than fully dissolving the tool. Alternatively, using high pressure water the tooling media can quickly be broken down. However, this process is made much easier by first allowing the tooling material to soak for some time. Ability Composites for example typically leaves ceramic washout tools soaking overnight in order to rapidly remove the tooling the next day.

The 3D-printed samples were printed on the modified Ender 5 Plus using nominal settings for each material. A 0.8mm nozzle diameter was used in the interest of increasing the manufacturing speed. After printing, the samples were weighed and then dissolution was completed using a laboratory heated bath with a magnetic stirrer, specifically a Corning Hot Plate Stirrer model PC-351. A type K thermocouple was submerged in the water bath and the heat setting on the hot plate was adjusted until the solution temperature stabilized at the desired value.

Sample Preparation, Testing, and Evaluation

To compare the dissolution of the ceramic washout tooling material and the 3D printed filaments, 25.4mm cubes were 3D printed. The samples were made with a nominally 3.2mm thick wall, top surface, and bottom surface. This corresponded to 4 perimeter print paths, 11 top layers, and 6 bottom layers. The interior of the sample was a 40% gyroid infill. Additionally, two AQ-180 samples were manufactured and one of them had holes drilled into both top and bottom surfaces of the sample, exposing the infill region. This would allow rapid infiltration of the sample with the dissolution media, reducing the washout time.

The samples were submerged in the heated bath and the washout time was recorded as the time at which the cube could be broken apart with tweezers. The ceramic tooling material, for example, was left in the solution for 24 hours with only slight change in shape. However, upon agitation it could readily be broken apart.

Results and Discussion

The mass, solution conditions, and washout time of each material are shown in Table 21.

Table 21 The washout time and information for each sample cube.

Material	Initial Mass (g)	Solution Temperature (°C)	Washout Time (hours)
Ceramic cube	11.3	18	1.0
ST-130	14.5	80	17.5
AQ-120	14.6	80	1.6
AQ-180	14.6	80	7.2
AQ-180, with holes	13.9	80	3.0

By using tweezers to agitate the samples, it could be estimated when the tooling material would be removable in a typical application. For example, after only 1 hour or less in the water bath, the Solcore 100 test cube could be agitated and broken down. However, without agitation the cube retained its shape for over 24 hours. Figure 28 shows a sample of the ceramic tooling media.

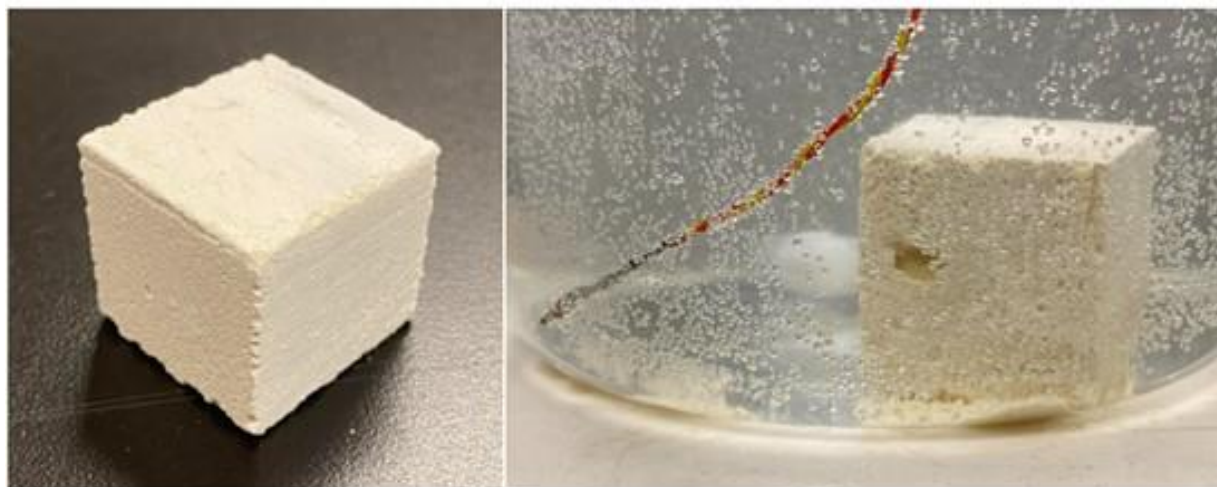


Figure 28 The ceramic washout tooling sample prior to dissolution (left) and during dissolution.

The ST-130 cube was placed in a solution composited of 200 g trisodium phosphate (TSP) dissolved in 750 mL of water (~26% solution). The manufacturer specifies that a 1% solution of TSP in water has 12 pH. The higher concentration solution was used after no results were seen with the 1% TSP solution. At these high concentrations, the solution would become cloudy every 1-2 hours. When this occurred, 250 mL of the solution was removed and replaced with an equal amount of fresh, heated 40% TSP solution. The dissolved ST-130 would create a gel-like substance as it was dissolved. This was removed from the test cube whenever the solution was changed. The gel-like material is shown in figure

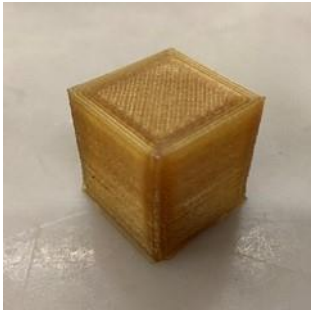
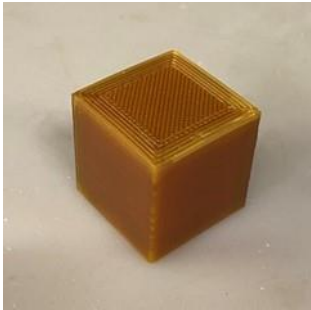
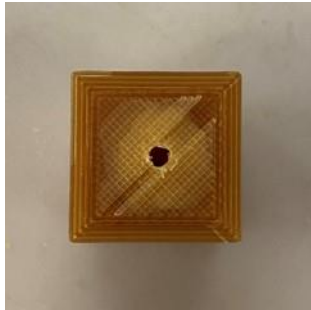
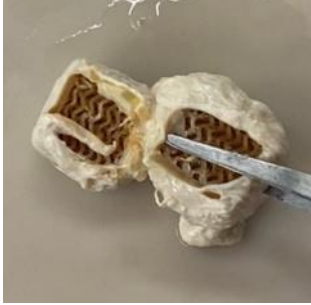
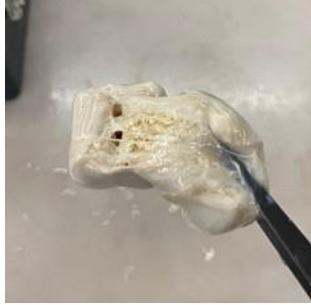
29. After about 12 hours, a hole was noticed on the external corner meaning solution could flood the interior of the infill region. At the 17.5-hour mark, the part was removed from the solution and easily broken into two pieces. The infill region had coalesced into solid gel-like material. It was at this point that the test was stopped because, in practice, the tooling material could be physically broken up and removed.



Figure 29 The gel-like substance forming on the surface of the ST-130 sample during dissolution trials.

Stratasys reports a dissolution rate for ST-130 of 12g/minute using WaterWorks detergent, and 6g/minute using EcoWorks. The washout rate using the TSP solution was much slower than the values reported by Stratasys, indicating it was an ineffective alternative to either WaterWorks detergent or EcoWorks detergent. The AQ-120 and AQ-180 required less preparation of the solution used for dissolution because they both used tap water. During dissolution, these materials also developed a gel material on the surface, which unlike the ST-130 cube, was not removed during the test. The AQ-120 and AQ-180 cubes are seen in Table 22 at various stages during their dissolution.

Table 22 The dissolution process is shown below for the AQ-120, AQ-180, and drilled AQ-180 samples.

Dissolution Stage	AQ-120	AQ-180	AQ-180 with hole
Pre-Test			
During Dissolution			
After Dissolution			

The AQ-180 cube with drilled holes had completely softened, including the infill, after 3 hours, while the cube without drilled holes had intact infill after 7.2 hours when it was physically broken apart. The introduction of the drilled holes is consistent with the original plan to use the Gyroid infill to allow the dissolution fluid to contact a greater surface area, which would be very effective for reducing the washout time.

CHAPTER 3: COMPOSITE MANUFACTURE ON PARTIALLY DENSE TRUNCATED PYRAMID TOOLING

After completing the small-scale Temperature Pressure Vacuum (TPV) tests and determining that ST-130 was the most robust material choice, and that infill percentage was an important structural parameter, these findings were taken to a composite tooling study. A truncated pyramid geometry was used to 3D-print tools that were used to cure carbon fiber epoxy prepreg composites. Even though sacrificial tooling media was used, the tooling was designed to be removable for evaluation. These medium-scale, partially dense tools were evaluated for deformation both before and after composite processing using a 3D scanner. The composites were manufactured in previously tested autoclave conditions of 121°C and 345kPa. Additionally, while 3D printing, one tool used a surface smoothing routine that uses the deposition nozzle to smooth the top surface. The top surfaces of the tools and the molded top surface of the composites were evaluated using surface profilometry both before and after composite manufacture to understand the interaction between the composite and the tool. These tools were compared against a baseline sample that was CNC machined from a billet of sacrificial ceramic tooling media by Ability Composites. It was important to determine how a tool deforms during composite manufacture, and if a secondary sealing step is required to produce composites. If no secondary sealing step is required, this would eliminate a significant step from the manufacturing process when using sacrificial tooling media.

COMPOSITE MANUFACTURE ON TRUNCATED PYRAMID GEOMETRY

Experimentation

The purpose of these tests was to evaluate the processing of prepreg composites on printed dissolvable tooling as compared to traditional washout tooling. It was important to understand the challenges of using 3D printed tooling as they relate to CTE and autoclave integrity. Attention was also given to any epoxy ingress, poor part release, or mold release reactivity, as these were thought to be potential issues. Additionally, an investigation of improving surface finishes using a smoothing routine

was completed. Two truncated pyramid specimens were additively manufactured. Only one printed truncated pyramid sample used the surface smoothing routine and was compared to the sample that did not use surface smoothing.

Materials

A total of three truncated pyramid tools were generated for this portion of the study. Two were manufactured additively using ST-130, and one was CNC machined from a billet of washout ceramic tooling material, Solcore 100, by Ability Composites. The ceramic washout tool was used as a high-quality baseline material as it was known to be successful for composite manufacture. The ceramic tool was covered with PTFE tape to prevent epoxy ingress, provide a high-quality surface finish, and allow easy part release. ST-130 was chosen for the 3D printed tools based on its favorable performance in the prior TPV studies.

The truncated pyramid tools were treated with a mold release prior to the prepreg layup. A different mold release was applied to each tool. They were Chemlease® 41-90 EZ Semi-Permanent Release Agent and Stoner Molding Solutions G471 XK-22 LV.5 Mold Release. The pyramid that was printed with a smoothing routine used the Stoner Molding Solutions Release agent.

The prepreg used for the manufacture of composite articles on the 3D-printed tooling was Toray F2673C-07M plain weave carbon fiber epoxy prepreg. The prepreg used for the composite manufactured on the ceramic tool was a carbon fiber plain weave with TCR UF3362 resin that was supplied and cured by Ability Composites.

Equipment

The 3D printed tools used Cura 4.6 to generate the G-Code. After printing, the same autoclave at CSU that was previously used for the TPV specimen trials was used to manufacture composite articles on the 3D printed tools. This autoclave was capable of 200°C (400°F) and 690kPa (100psi), so was adequate for composite manufacture. Ability Composites used their autoclave to manufacture a composite on the

ceramic tool. Both before and after composite manufacturing, the tools were scanned by Ability Composites using a FaroArm Edge with an LLP HD 3D scanner to create 3D point cloud data that could be compared to the original CAD model. FaroArm systems accurately create point cloud datasets by combining the relative position of the 3D scanner in space with the scan results. Encoders in each axis of the arm are used to locate the scanner. The comparison of the point cloud data to the CAD model was done with PolyWorks Inspector software. The surface roughness of the tools was evaluated using a Taylor Hobson Surtronic S-100 series drag profilometer using a standard type 112-1502 pickup, which operates by dragging a small needle across the surface of the component that gathers the height of the profile.

Preparation of Truncated Pyramid Tooling

The truncated pyramid geometry was a square pyramid, with a base dimension of 152.4mm, a height of 25.4mm and a top flat square dimension of 101.6mm, as shown in figure 30. This change from the round specimen of the tooling stability trials was made to ease the draping of the prepreg during composite laminate preparation. The truncated square pyramid geometry included nominally 3.3mm thick solid outer surfaces that are shown shaded in figure 30, with an enclosed 40% dense gyroid infill region. The tool was designed to be removable from the cured composite, even though a soluble material was used, to allow evaluation of the tool after composite manufacturing.

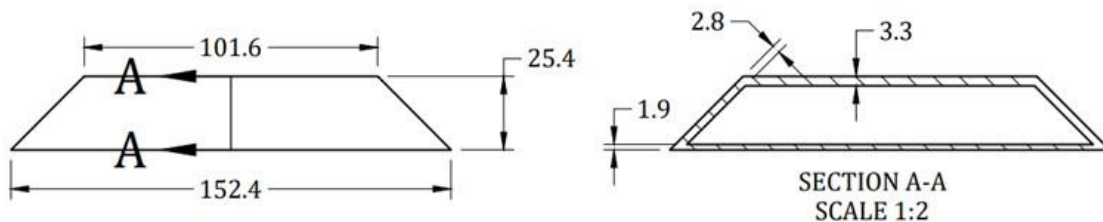


Figure 30 Cross-section of truncated square pyramid specimen geometry. A complete drawing is in Appendix A.

Two tools were 3D printed from ST-130 using Cura Ultimaker 4.6. Cura has a feature called ironing, which was utilized to explore surface smoothing. The samples were printed using an enclosure temperature of 105°C, an extruder temperature of 280°C, and a build plate temperature of 126°C, which was near the maximum temperature that the stock heat bed could reach. The build plate had Kapton tape

applied to improve bed adhesion. Additional print parameters included a 20mm/s print speed, a 0.3mm layer height, a 0.8mm nozzle size, and a 40% density gyroid infill pattern. The higher 40% density infill was chosen in response to the deformation and print-through noted during the Temperature Pressure Vacuum (TPV) trials, and to better support the larger top surface of the truncated square pyramid specimens. The gyroid infill pattern was chosen as it has continuous open spaces which were of interest in terms of moving the dissolution fluid through the tool to ultimately reduce dissolution time. Only one specimen used ironing to modify the surface finish. The routine adds many final passes over the part surface with very small stepovers and a small amount of material extrusion with the goal of improving the finish of the flat horizontal surface. The parameters used for ironing were determined by manufacturing a large quantity of smaller samples. The resulting parameters were: ironing flow = 10%, ironing speed = 16.7mm/s, line spacing = 0.1mm, and ironing pattern = 'zig-zag'. A photograph of one of the tools during manufacture can be seen in figure 31.

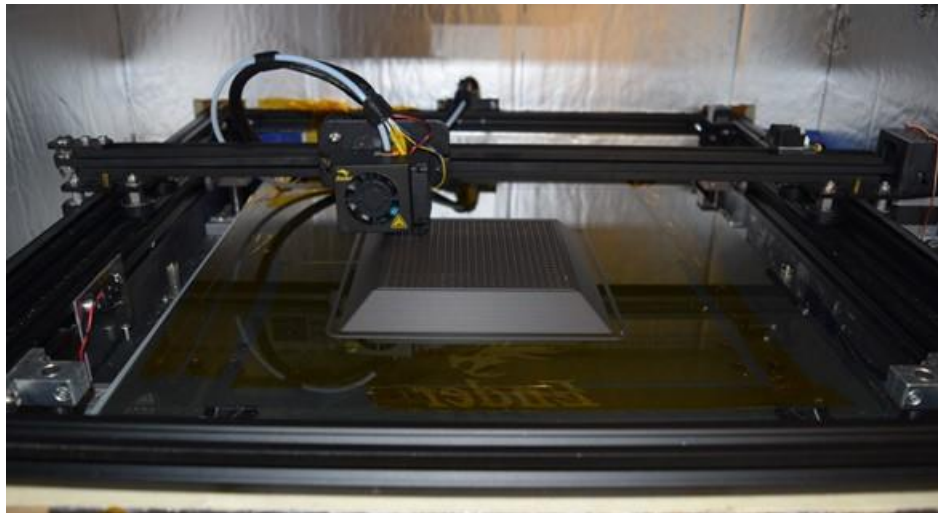


Figure 31 One of the tools during manufacture inside the heated enclosure.

The three tools will be referred to as the Rough Pyramid, the Smooth Pyramid, and the Ceramic Pyramid, where the Rough and Smooth Pyramids were 3D printed, and the Smooth Pyramid utilized surface smoothing/ironing. The Rough Pyramid was treated with Chemlease® 41-90 EZ Semi-Permanent Release Agent and the Smooth Pyramid used Stoner Molding Solutions G471 XK-22 LV.5 Mold Release,

to ensure easy separation to allow for post-process measurements. Both mold releases were tested because Ability Composites commonly uses the Stoner Mold Release, and there was an interest in evaluating mold release compatibility. No other form of surface sealing was used prior to autoclave processing.

Autoclave Processing of Truncated Pyramid Tooling

The composites were processed on the truncated pyramid tools using a typical autoclave cure cycle at CSU. The layup involved an aluminum tooling plate, a layer of peel ply, and a layer of breather/bleeder. The prepreg material recommended non-porous release film, not peel ply, however this was not available at the time. The vacuum bag was pleated to prevent the bridging at the corners of the tool. The composites were approximately 1.2mm thick, made from 6 plies of Toray F2673C-07M plain weave prepreg. Two composites were made on the Rough Pyramid, and one on the Smooth Pyramid. Two composites were made on the Rough Pyramid to evaluate deformation after an additional manufacturing cycle.

The autoclave cure cycle for the Smooth and Rough Pyramid started with a ramp to 121°C (250°F) at 2.77°C/minute (5°F/minute) that was then held for 150 minutes to complete the cure under full vacuum. The pressure was increased to 345kPa (50psi) once the cure temperature hold started. After the 150-minute cure temperature hold, the composites were cooled at a rate of approximately 2.77°C/minute (5°F/minute) and removed for evaluation. The layup, vacuum bagging, autoclave cure, and demolding steps are shown in figure 32.

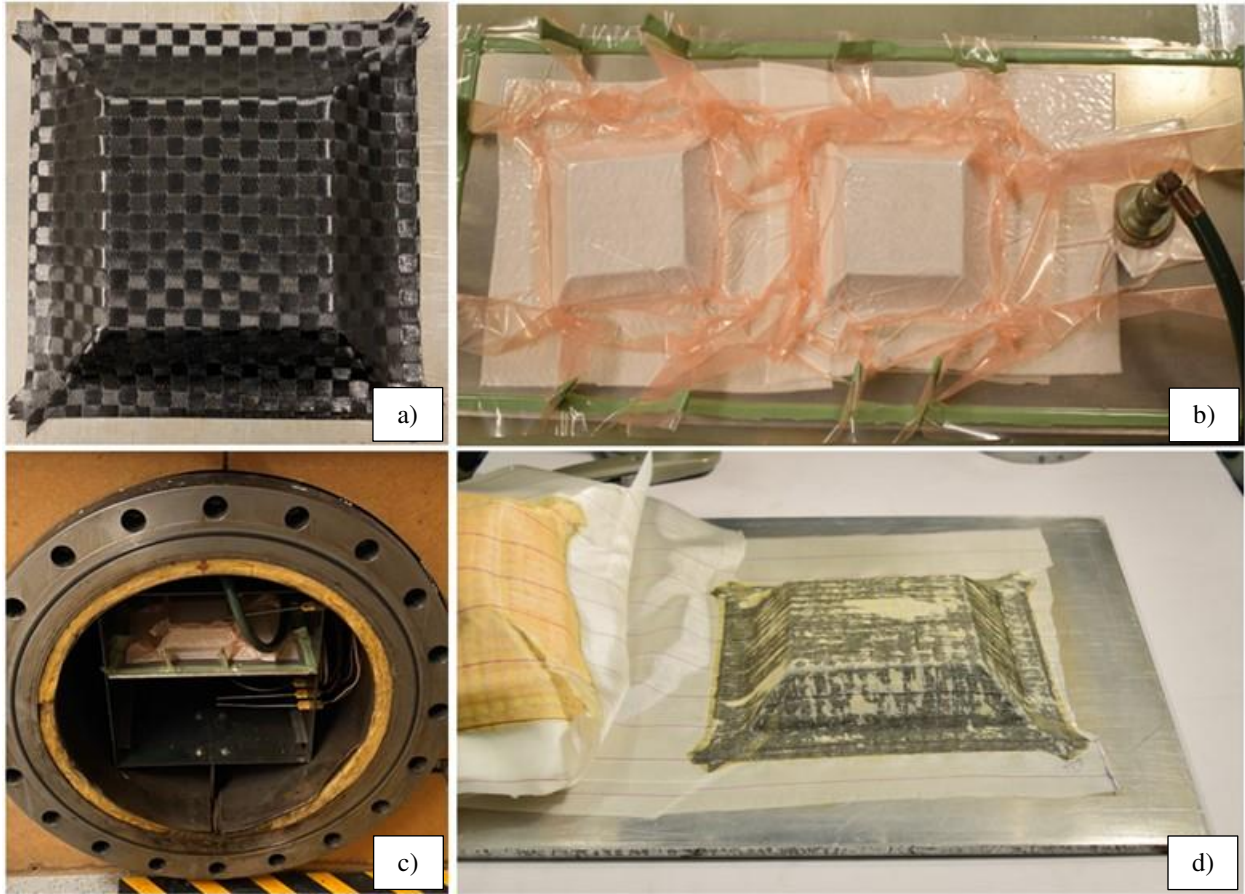


Figure 32 Representative layup (a), vacuum bagging (b), autoclave cure (c), and demolding (d) steps of the composite manufacturing process.

It was noted that upon process completion and cooldown to ambient temperature the 3D printed tools had already fully released from the composite laminate. This is assumed to be a result of the relatively high CTE of the ST-130 tooling material of $177\mu\text{m}/\text{m}/^\circ\text{C}$ as given in table 3.

Evaluation of Truncated Pyramid Tooling

The truncated pyramid tools and composite parts were photographed, and 3D scanned using a FaroArm to document any changes in surface quality or deformation. The top surfaces of the tools and the molded surfaces of the respective composites were evaluated using a drag profilometer both before and after cure to give insight into any changes to the surface quality. The surface roughness data was taken at 9 evenly spaced points on the surface of the tool, with each point being measured in four orientations that were 45° apart ($0, 45, 90,$ and 135°). This aligned one measurement direction with the

final print path or the ironing direction and resulted in 36 measurements per tool or part on the top surface only. The surface roughness of the conventional tool was not evaluated, as it depends on the surface roughness of the sealant used. A diagram showing measurement locations and orientations can be seen in Figure 33.

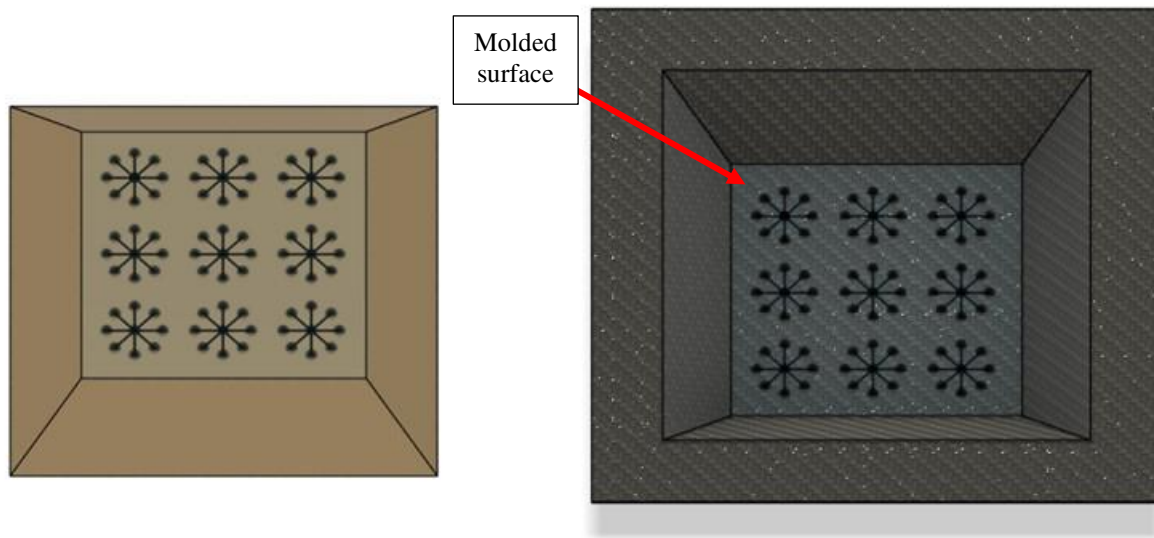


Figure 33 The approximate locations and orientations used to record the surface roughness data on the tool (left) and composite (right).

The profilometer used a 20mm stroke length over which data was recorded. Additionally, the sides of the composite were removed using a Dremel tool to take these measurements, as the profilometer did not have any extensions that would allow it to reach inside the composite cavity to take measurements.

Truncated Pyramid Results and Discussion

After 3D printing, the tools had high-quality surfaces with no indications of warping or abnormal process induced defects. It was noticed that the smoothing routine improved the tactile feel of the surface finish for the Smooth Pyramid; however, it also left regions of excess material and appeared to discolor the top surface, likely from material degradation as the rate of extrusion was so low during the ironing procedure that the filament had more residence time inside the heated region of the extruder. The seam is

seen as a diagonal line running across the front of both tools, as seen in figure 34, that was caused by the start and stop points of the 3D printer path. This is a common defect in 3D printing. In general, the seam would be located on a corner or edge of a part to hide the seam. However, in this study it was intentionally placed on a face to allow for observation of the surface texture that was transferred to the composite part.



Figure 34 The as-printed Rough Pyramid tool (left) and the Smooth Pyramid tool (right).

After 3D-printing, the Smooth Pyramid was scanned with a FaroArm. The scan showed that the tool was undersized (indicated by the blue color of the scan on the angled edges) in the horizontal plane by nominally 0.1-0.3 mm and too tall (indicated by the green/yellow tones of the horizontal top surface) by about 0.3-0.5 mm. These deviations are measured as distances of the point cloud data to the nominal surface, so for the sides of the tool the distances are measured normal to the scanned point cloud data. The 3D scan of the smoothed tool can be seen in figure 35.

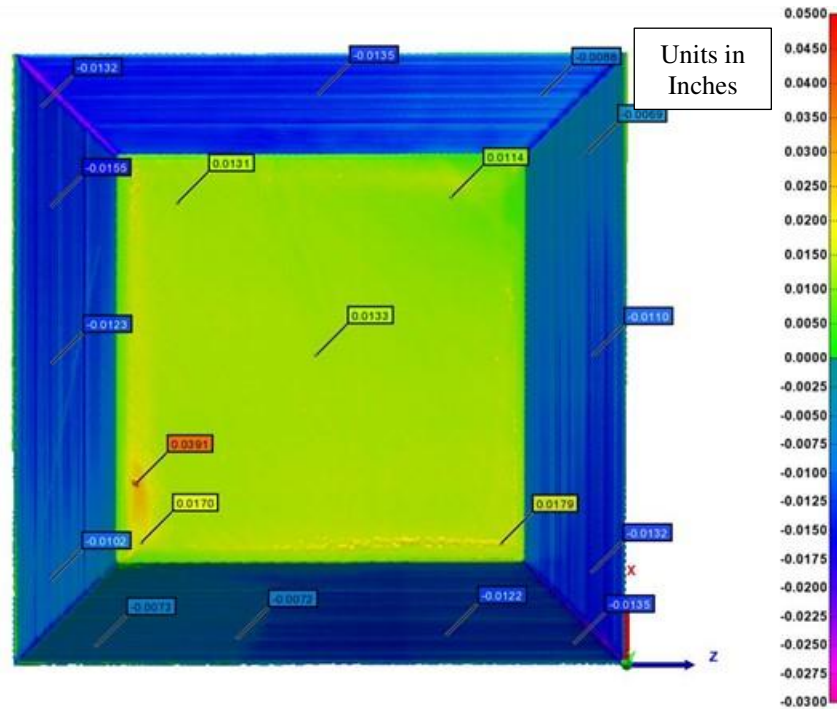


Figure 35 The FaroArm scan of the Smooth Pyramid prior to composite manufacture.

Both the Rough and Smooth Pyramid Tools were assumed to have similar deviations from nominal, as caused by the 3D-printing inaccuracies. The 3D printer was not precisely calibrated prior to tool manufacture. The calibration process would involve accounting for machine and part size change due to CTE by creating a test sample with the same process conditions. Then, by comparing the actual dimensions of the test sample to the nominal dimensions, it would be possible to eliminate this error. However, it was not accounted for and can explain the deviations seen in figure 35. Compared to the ceramic Control Pyramid, the deviations from nominal were worse. The Control Pyramid Tool was undersized on the sides (as indicated by the light blue sides) and too tall (as indicated by the yellow top surface) by only around 0.1mm as seen in figure 36.

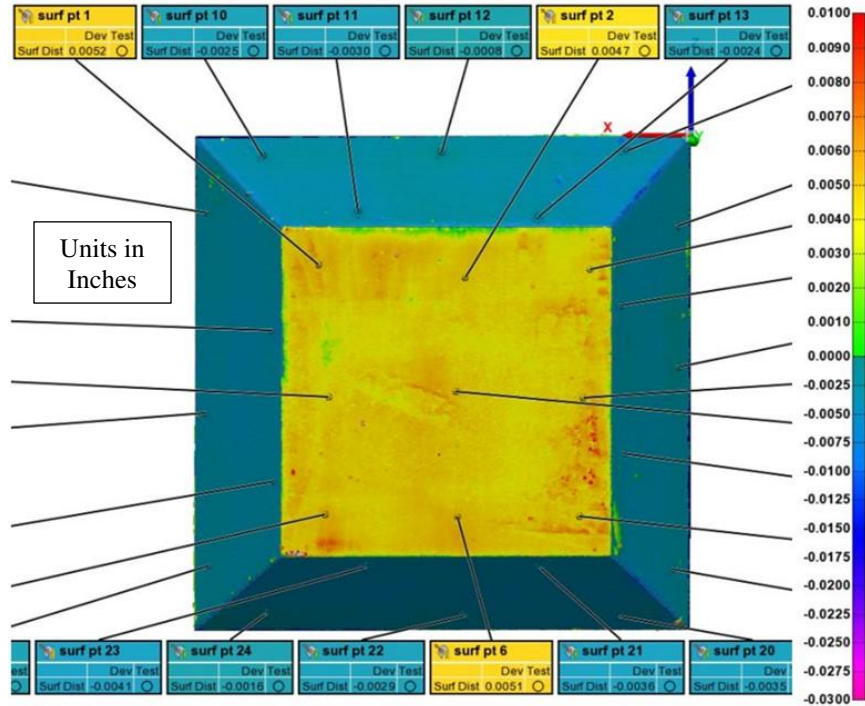


Figure 36 The FaroArm scan of the ceramic tool prior to composite manufacture. Complete scans are listed in Appendix B.

After composite manufacturing, it was noticed that there was some epoxy transfer to the printed tool surface on both tools, as well as damage to the Smooth Pyramid tool on one corner. While some epoxy was transferred to the tool surface, as seen in figure 37, there was no indication of epoxy ingress into any unseen porosity of the tool surface. This suggests that there may not be a need to seal 3D printed tooling to prevent epoxy ingress, which provides significant time savings over traditional sacrificial tooling materials that tend to be somewhat porous.

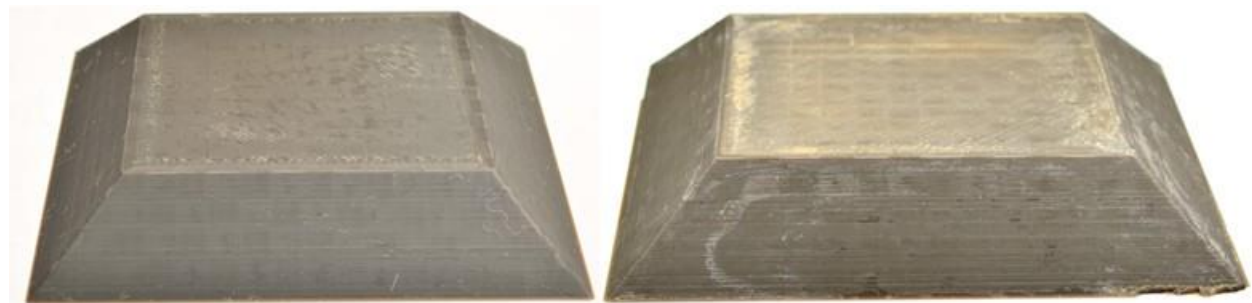


Figure 37 The Rough Pyramid (left) and Smooth Pyramid (Right) tools shown after composite processing.

The damage seen on the corner of the Smooth Pyramid was likely caused by epoxy flowing under the bottom surface, creating a mechanical lock around the removed material. This type of damage is typically seen as the tool shrinks due to the CTE of the material during cooldown. The surface texture created by the discrete layers likely contributed to the situation. While these tools are sacrificial, if the tools had been intended for reuse the mechanical locking could cause tool damage. So, if tool reuse is required, then it would be advantageous to improve the surface texture by reducing the layer heights. To evaluate the effects of multiple cure cycles to represent the reusable tooling scenario, another composite was manufactured on the Rough Pyramid tool. The sequence of tool and composite manufacture are shown in figure 38.

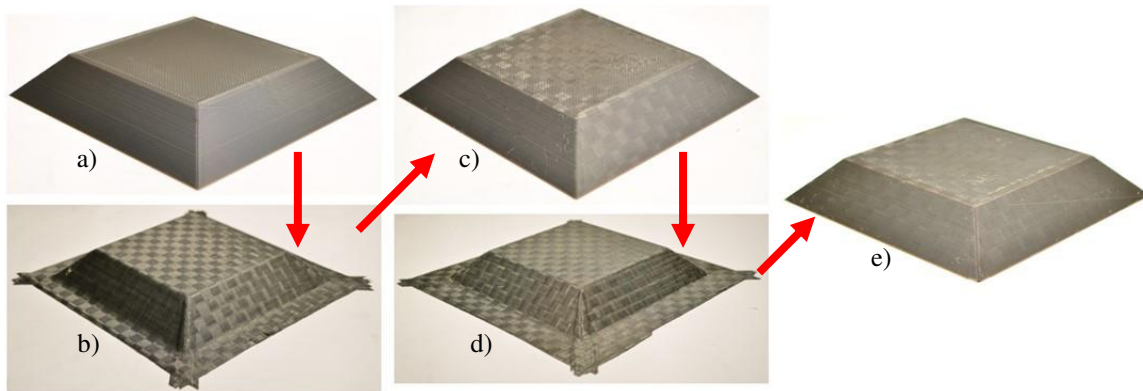


Figure 38 The Rough Pyramid tool and the resulting composite parts are shown before composite manufacture (a), after one production cycle (b, c), and after two production cycles (d, e).

As can be seen in Figure 38c and 38e, the surface texture from the weave of the composite prepreg material was transferred to the completed tool. This was noticed for both the Smooth and Rough Pyramid tools. This surface texture seemed to primarily affect the sheen of the surface, and not the surface profile. The imparted texture was not detectible tactilely or using surface profilometry. The epoxy on the cured composite likewise shared the surface texture of the tools, capturing the layer lines and top surface finish clearly. If the molded surface finish was important in design, it would be advantageous to improve this finish. The molded surface of the composites created with the Rough,

Smooth, and Ceramic Pyramid tools are shown in figure 39. The image of the composite surface created by the Rough Pyramid tool is from the second composite production cycle completed on this tool.

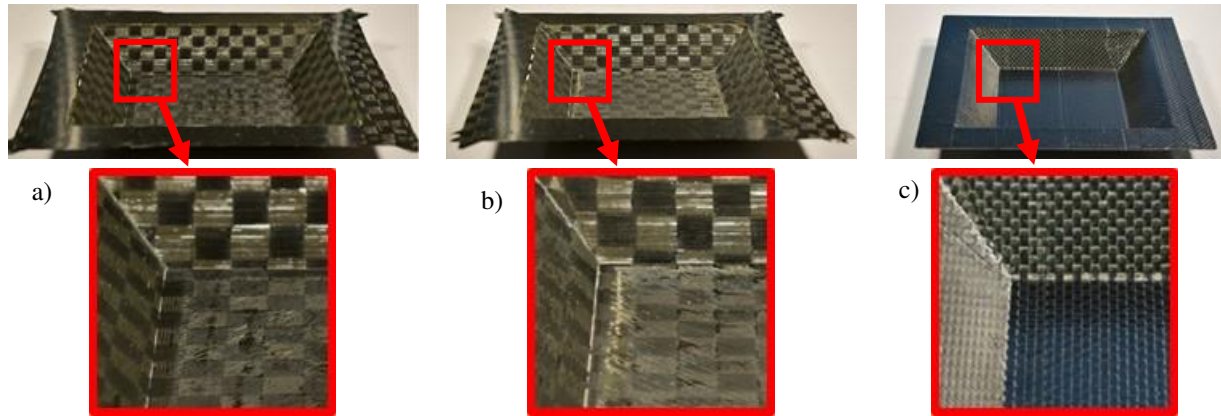


Figure 39 The molded surfaces of the composites created by the Rough (a), Smooth (b), and Ceramic (d) Pyramid tools are shown.

The surface finish created by each of the 3D Printed tools was poor when compared to the surface finish imparted by the PTFE tape that was used to seal the Ceramic Pyramid tool. This is no surprise, as the PTFE tape has a gloss texture. However, the seams from the tape were present on the final surface finish of the control sample. Further investigation into improving the surface finish of 3D printed tooling may provide sufficient improvements to be acceptable for composite processing without a secondary sealing procedure like applying PTFE tape, sanding, or machining.

After these cure cycles, the tools and composites were 3D scanned using a FaroArm. The scans created before and after composite manufacturing are shown for the Smooth Pyramid in figure 40, and the complete set of 3D scans are listed in Appendix B.

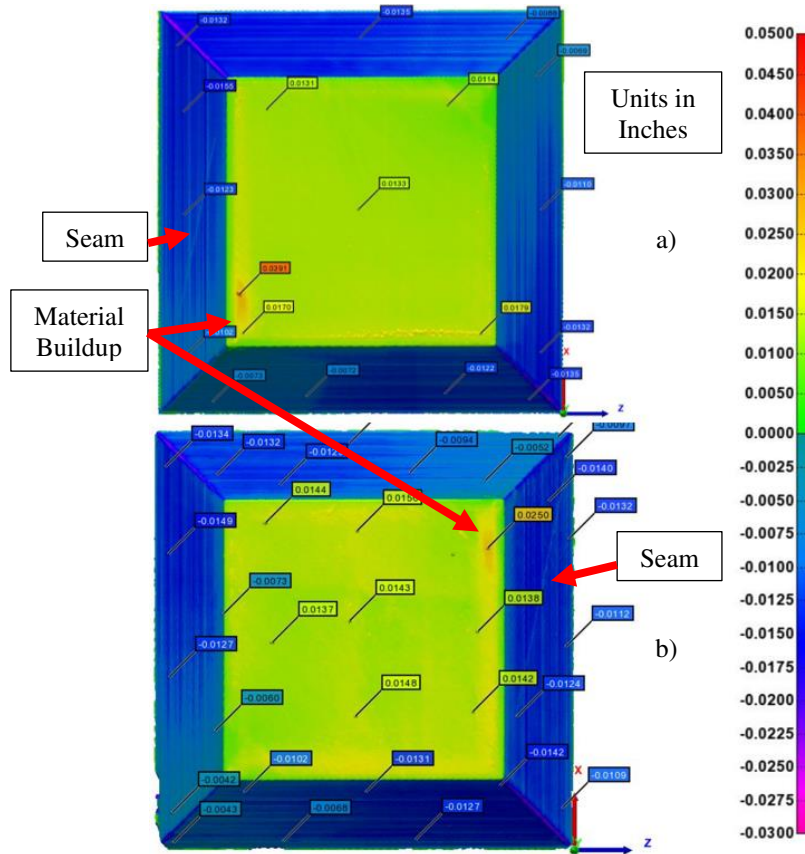


Figure 40 The FaroArm scans of the 3D Printed Smooth Pyramid tool are shown before (a) and after (b) composite manufacture.

It should be noted that the tool was rotated 180° between FaroArm scans. To point this out, the seam can be seen on the left side of the scan in Figure 40a, and on the right side of 40b. The Smooth Pyramid tool showed minimal deformation after composite manufacture. However, prior to manufacture, there was local deviation recorded at the corners of the tool top surface due to material build-up related to the smoothing routine, which is most obvious as the orange shades in the lower left corner of the FaroArm scan, in Figure 40a. The material buildup is undesirable, but further tuning of ironing parameters may have provided a solution to that issue. The composite that was produced on the Smooth Pyramid tool is shown in figure 41, which also shows where the material buildup on the tool surface transferred to the composite part produced on the Smooth Tool.

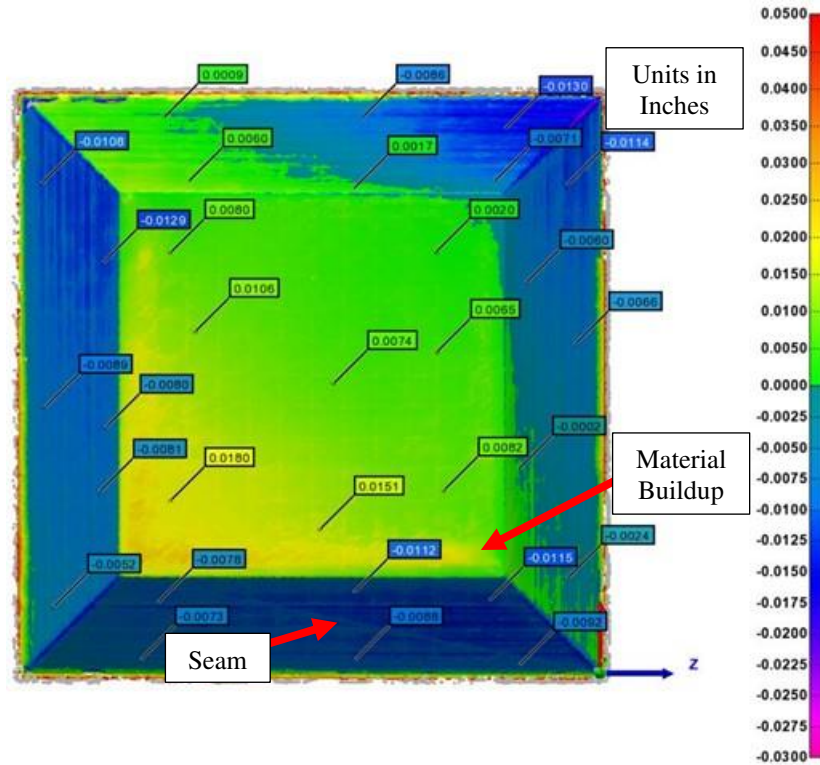


Figure 41 The FaroArm scan of the composite manufactured on the Smooth Pyramid tool showing the seam and region with excess material did transfer to the cured composite.

The scan shows the slightly deformed top surface, where the lower left side of the top surface is approximately 0.5mm higher than the upper right surface. There was no known cause for this uneven top surface. The Rough Pyramid tool was used to manufacture composites as well, but 3D scans were not completed prior to the first composite was processed. However, scans were made after the first and second composite processing cycles. These scans are shown in figure 42.

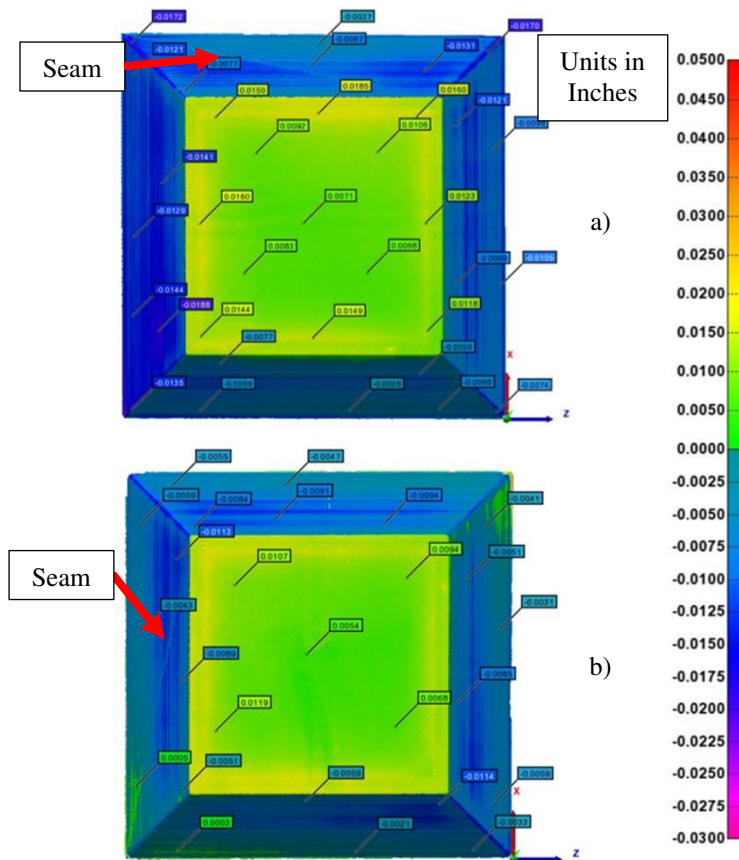


Figure 42 The Rough Pyramid tool scans after one processing cycle (a) and two processing cycles (b).

Like the previous scans, the tool was rotated between scans. However, this time the tool was rotated 90° counterclockwise, as indicated by the seam locations. However, in both cases the top surface appeared to be similar, with little to no deformation induced by the composite process cycle. The center of the top surface was depressed, which may have either been from composite processing deformation or from manufacturing process error. One possible explanation could be from the printhead changing directions. It is common for 3D printed components to have excess material whenever the printhead changes direction due to the printhead slowing down and speeding up. Typically, this is accounted for so that as the printhead direction changes and the printhead slows down, the extrusion rate is reduced as well. However, the printhead speed and the extrusion rate are often not accounted for perfectly, so excess material can be deposited at the edges. This is like what was seen in the scans of the Smooth Pyramid tool, except the ironing speed was slower than the print speed, so there was a smaller region where the

printhead was changing speeds. Alternatively, the tool may have deformed during the cure of the composite and the center was depressed then. However, this seems less likely as there was no progression of tool deformation between the first and second autoclave cure cycles. Like the smooth tool, many features from the tool were transferred to the cured composites. The scan in figure 43 clearly shows the undersized sides, the oversized top surface, and the seam.

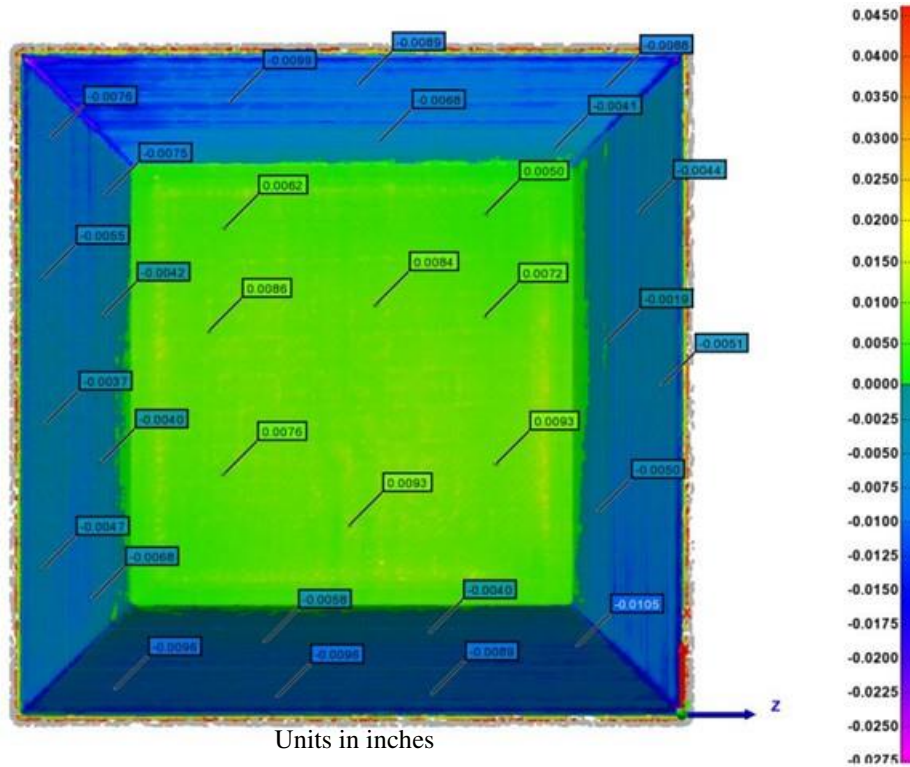


Figure 43 The first composite manufactured on the Rough Pyramid.

After the first manufacturing run, the Rough Pyramid was used to make a second composite part to evaluate how the tooling changed after multiple autoclave cycles. The scan of the second composite part produced on the Rough Pyramid is shown in figure 44.

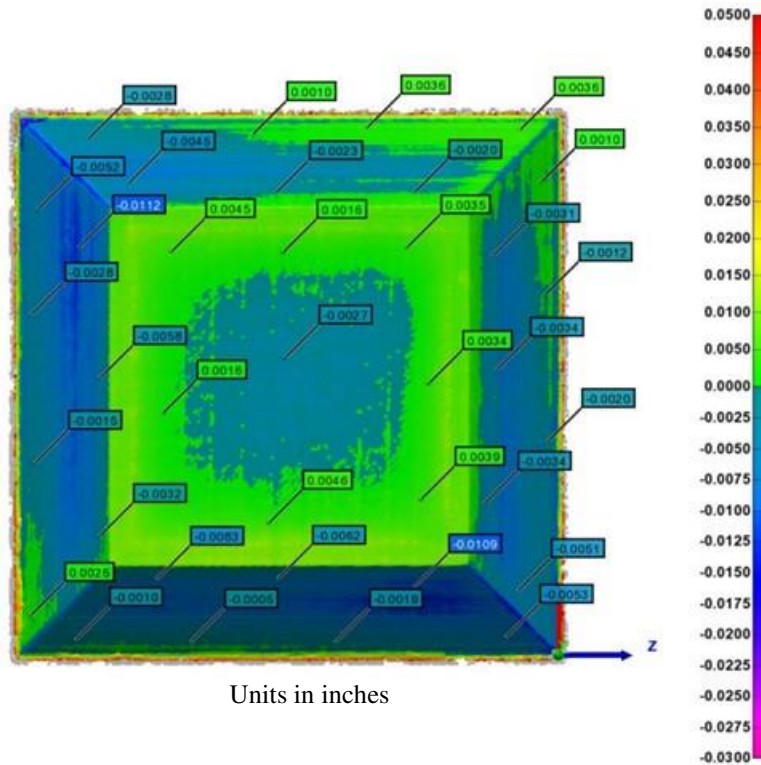


Figure 44 The second composite cured on the Rough Pyramid tool.

The scan of the second composite shows a slightly deformed geometry from the first composite scan. This composite tended to have a deviation of approximately $\pm 0.13\text{mm}$, as compared to the last composite which had an approximate deviation of $\pm 0.25\text{mm}$. While the agreement between this composite and the nominal geometry is improved from the previous composite manufactured on the Rough Pyramid, it shows that some deformation occurred. It is unlikely that a soluble tooling material would ever be used to manufacture more than one composite due to the sacrificial nature of the tooling; however, this test suggests that this material is near the limit of its processing conditions, and it may slowly deform at elevated temperatures or after multiple cycles.

The two tools showed good thermal stability and did not deform significantly between cures. The satisfactory performance of the tools indicates that the surface thickness, 40% gyroid infill, and material choice were sufficient to maintain the desired geometry. However, given the small deformation of the second composite, the tools are near the limit of their capabilities in terms of processing temperature and

pressure. These results suggest that the infill density and outer thicknesses should be increased for improved geometric fidelity, or that with increased infill density increased autoclave conditions could be pursued. In future applications of 3D printed tooling to autoclave cured composites, it would be beneficial to ensure the machine is calibrated to produce the correct size of geometry, account for the size change during autoclave processing caused by the CTE of the thermoplastic tooling material and improve the printer firmware to better account for the speed change when the printhead changes directions, resulting in less material extruded on the edges of the tools.

The surface roughness of the tools and parts were also measured to give insight into any changes before and after cure. Table 23 shows average surface roughness values measured for the top, horizontal surfaces of the truncated pyramids throughout the manufacturing process. Both Ra and Rz were recorded. Ra represents the average height between peaks and valleys relative to the mean measured height, while Rz is a measure of the maximum height difference between the highest peak and lowest valley in the measurement region. These were assumed to be good representations of the surface quality.

Table 23 The surface profilometry data for the truncated pyramid tooling

Sample	Ra (μm)	Rz (μm)
Rough Tool after 1 st cure	4.2	25.8
Rough Tool after 2 nd cure	3.3	20
Composite cured on Rough Tool (1 st cure)	4.7	29.3
Composite cured on Rough Tool (2 nd cure)	4.9	27.8
Smooth Tool before cure	7.5	35.2
Smooth Tool after cure	5.7	22.8
Composite cured on Smooth Tool	4.7	24.7

The results of surface profilometry indicate a decrease in roughness of the tool after the composite part is processed. This result could be from residual epoxy or from local surface deformation of the tool surface occurring during the prepreg cure. The composites manufactured on the Rough Tool both had increased roughness compared to the tool. The composite manufactured on the Smooth Pyramid tool had Ra lower than that of the tool surface, but a medial Rz value compared to the roughness values of

the tool both before and after processing. This suggests that ironing can be effective in improving the final composite part surface finish, even though the effect on the tools surface seemed minimal. The reduction in surface roughness after composite processing seems consistent with local flattening of the peaks on the tool surface during composite processing.

CHAPTER 4: COMPOSITE MANUFACTURE ON PARTIALLY DENSE BENT DUCT TOOLING

The truncated pyramid studies indicated that partially dense ST-130 tooling could be used to manufacture composite structures with minimal deformation at cure temperatures of 121°C at 345kPa, and that they did not require secondary sealing to prevent epoxy ingress. However, because the truncated pyramid tools did not represent a trapped tooling situation, a bent duct geometry was studied that was larger, more complex, and could not be removed from a cured composite without removable or sacrificial tooling. The bent duct geometry was manufactured additively using a partially dense infill structure based on the results of previous truncated pyramid trials. A baseline bent duct tool was CNC machined from a solid billet of conventional washout tooling material by Ability Composites. Both processes manufactured the tool in halves that were then bonded together.

Ability Composites was interested in further elevated processing conditions of 160°C at 414kPa, which were significantly higher than previously tested and much higher than the T_g of ST-130 which is 132°C. In previous studies, the T_g of ST-130 had not been exceeded, however these cure conditions were desirable because they were more typical of those used by Ability Composites, and of many advanced composite systems with elevated temperature requirements. Ability Composites again assisted in composite layup, cure, and 3D scanning of the baseline and 3D printed tools. There was little knowledge of how these tools would perform at the elevated temperatures, because all the prior tooling samples had been tested at 121°C at 345kPa. The two composite parts produced were scanned externally using a FaroArm that accounts for the thickness of the composite to determine the approximate tool deformation.

Experimentation

Materials

The 3D printed tool was manufactured from ST-130, and the corresponding bent duct washout tool was made Solcore 100 by Ability Composites. These are the same materials that were used previously in the truncated pyramid studies. Ability Composites also indicated that some voids had been

exposed during machining of the baseline Solcore tool and these had to be filled by mixing excess tooling media with water to form a paste that was then pressed into the exposed voids. Both the printed and CNC machined bent duct tools were wrapped with PTFE tape to prevent epoxy ingress. The prepreg used for the composite articles was a carbon fiber plain weave with TCR UF3362 resin, supplied and cured by Ability Composites.

Equipment

These tools were manufactured on the modified Ender 5 Plus. This printer was modified to use an enclosure temperature of up to 105°C. The composite articles were processed in the autoclave at Ability Composites. Once manufactured, the composites were photographed, and the outer surfaces were scanned with the same FaroArm Edge that was used in the truncated pyramid trials to create point cloud data of the samples both before and after composite manufacturing.

Preparation of Bent Duct Tooling

The bent duct tool geometry involved a 101.6 mm x 152.4 mm (4 in x 6 in) cross section that was swept in two directions. The length of the tool was designed to fit onto the print bed of an Ender 5 Plus 3D printer, so its length was 317.5 mm (12.5 in). The bent duct tool geometry is shown in figure 45.

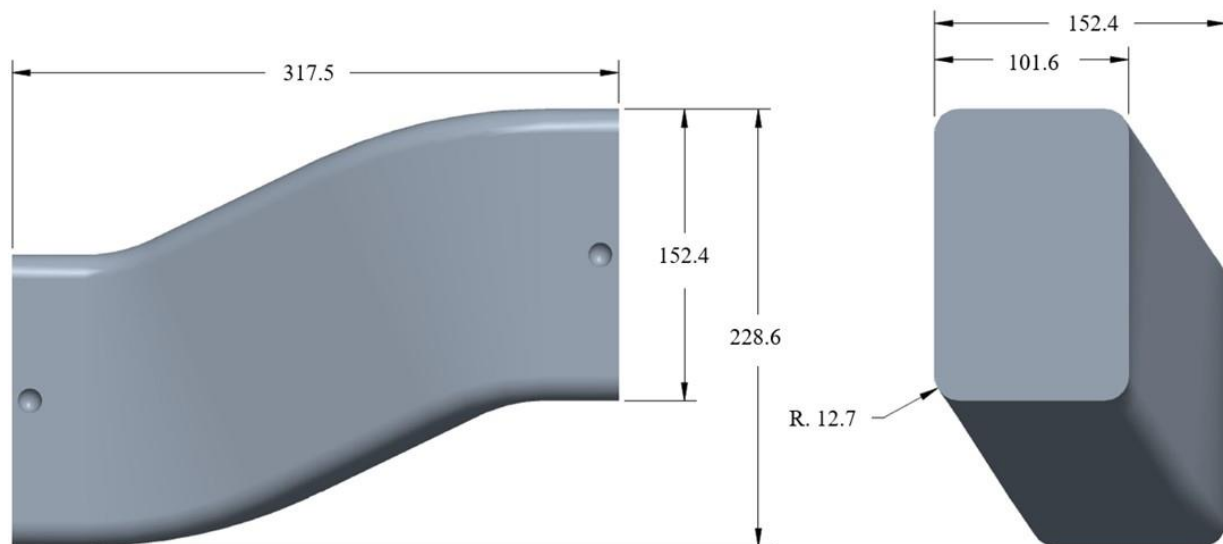


Figure 45 Geometry of the complex tooling.

Two ducts were manufactured, one as a baseline from sacrificial tooling media, and one from ST-130 using 3D-printing. Both ducts were manufactured in two halves, then bonded together at the midplane. The midplane can be seen in figure 46, and detailed geometry can be found in Appendix A.



Figure 46 The bent duct geometry showing the two halves.

The tool that was manufactured using ceramic tooling media will be referred to as The Control Duct (0) and the tool made from ST-130 will be referred to as the Split ST-130 Duct (1). The two halves of the Control Duct (0) were manufactured using a CNC process by Ability Composites. After machining, the tool halves were bonded together, then wrapped with PTFE tape to seal the tools.

The Split ST-130 duct (1) halves were printed separately in a horizontal build orientation. This tool was printed using a 40% dense gyroid infill, 3.2mm wall thickness, 3.3mm top thickness, and 1.3mm thickness on the bottom print surface (which would become the bonding plane). The thinner bottom surface would eventually be bonded to the other half, effectively doubling the thickness of that surface of the tool. These structural configurations were determined from the prior studies of autoclave robustness.

Ironing was additionally used on the horizontal regions of the duct to attempt to improve the surface finish. The same 0.3mm layer height and 0.8mm nozzle were used to manufacture this tool, like the truncated pyramid trials. The relatively large layer height and nozzle size, as well as the partially dense infill were chosen to reduce the manufacturing time of this tool. The manufacture of one half of the Split ST-130 Duct (1) on the Ender 5 Plus is shown in figure 47. Additionally, the tools included fiduciary 12.7 mm (½ in) hemispherical impressions to seat ball bearings that would allow for easier

locating of the composite after manufacturing. This would represent a common approach used by Ability Composites for locating a composite for trimming operations after autoclave processing.

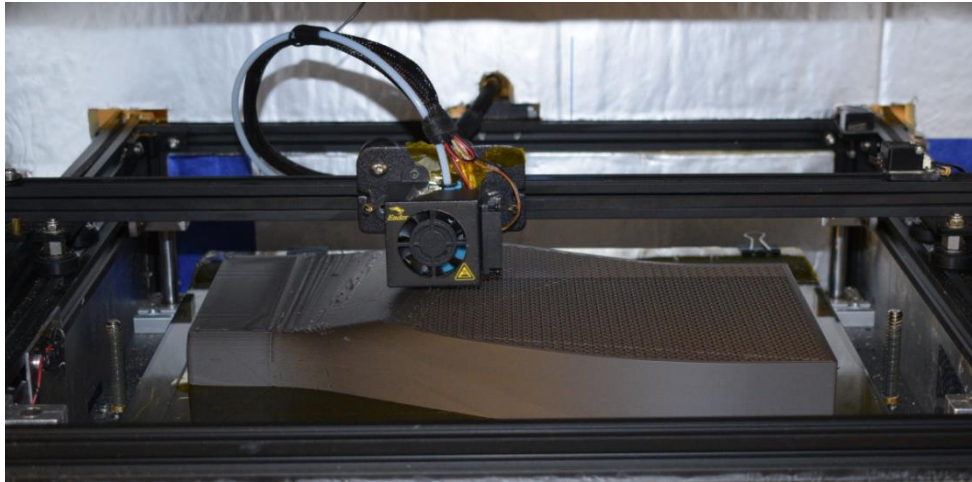


Figure 47 Printing the Split ST-130 Duct (1).

In total, the two halves of the Split ST-130 duct took approximately 4 days, 17 hours, and 46 minutes of print time and used 3.08kg (6.8lb) of material, even with the large layer heights and nozzle size. After printing, the two halves of the duct were match drilled to aid in washout before being bonded together using EPON 828 epoxy resin and EPIKURE 3140 hardener. The match drilling process involved drilling holes on each half of the printed tool that would align once bonded to allow dissolution media to pass between the tool halves. The bonding process was made difficult due to a small amount of warping that developed on each print. The warping created a 1-3 mm gap at the bonding plane that did not completely fill with the first application of epoxy. During bonding, the two tool halves were clamped together, and the clamps applied enough force to slightly close the bond line. However, it still required additional epoxy thickened with glass microspheres to completely fill the bond line. The thickened epoxy was applied and allowed to cure at room temperature, then sanded to be flush with the tool surface. The room temperature cured epoxy was post-cured at 100°C for 1 hour after a 2.8 °C/minute ramp up. The manufactured duct halves, as well as the bonding process, are shown in figure 48.

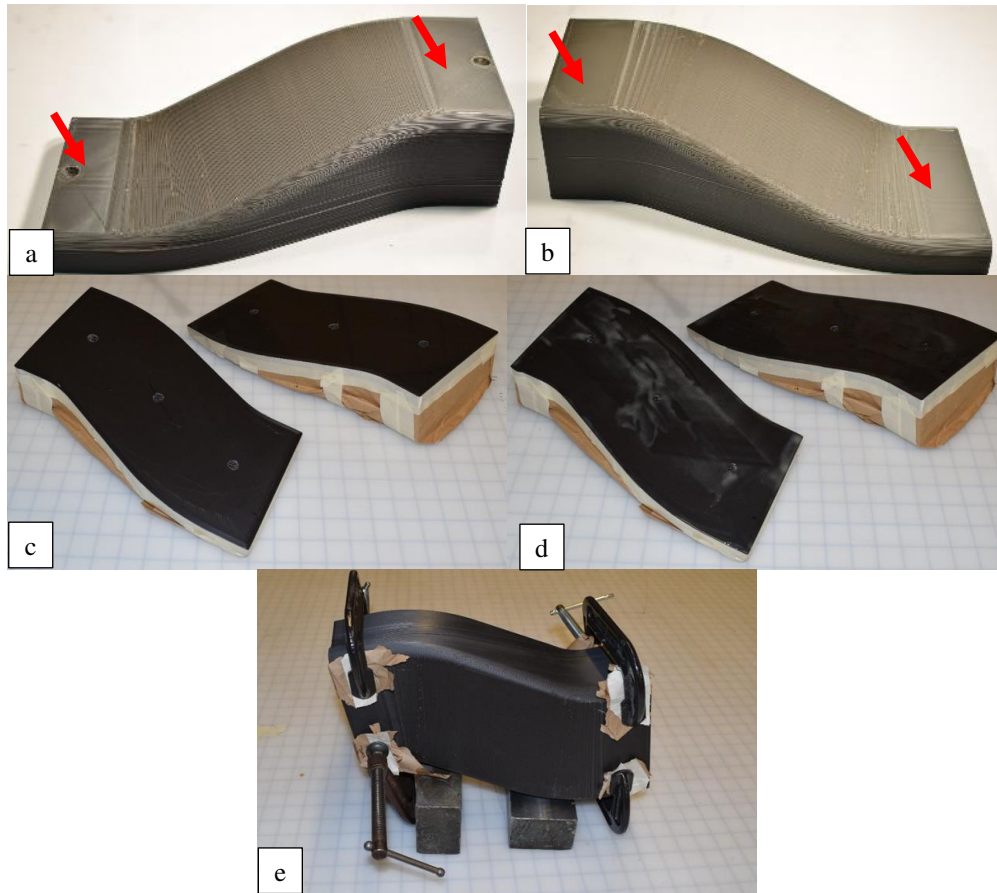


Figure 48 The ST-130 Split Duct (1) was printed in two halves and utilized ironing on the surfaces indicated by the red arrows (a, b), had holes drilled in the bottom bonding surface (c), was bonded together (d) and clamped to cure (e).

The bonded tool was post-cured to improve the bond strength, but upon cooldown the tool fractured along layer lines. The crack opened along one end of the duct. A combination of thermal stresses from printing, stresses introduced from the clamps during bonding, and thermal loading during the post-cure likely caused this failure. The developed crack was filled using the same thickened epoxy. The result of post-curing the filled crack was another small crack that appeared in the tool. Instead of attempting to repair the second smaller crack, the tool was wrapped with PTFE tape to seal the surface, and a composite was manufactured on the cracked tool with minimal negative impact from the defect. The completed tool (without PTFE tape) is shown in figure 49.

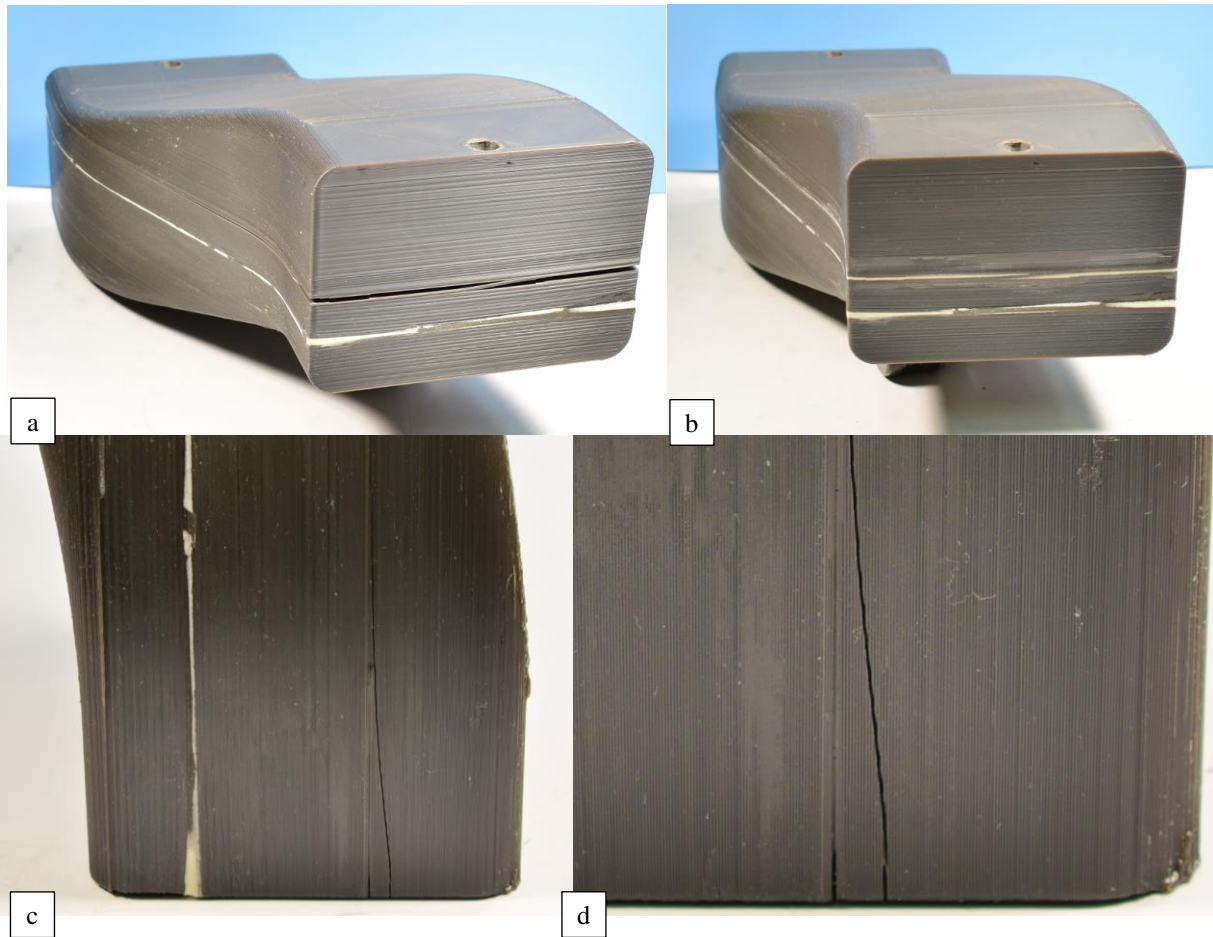


Figure 49 The tool had a significant crack form during the post cure of the epoxy used to bond the two halves together (a). This crack was then filled, and post cured again (b). During the second post cure, a new crack formed (c) and can be seen traversing multiple layers (d).

ST-130 has a relatively high coefficient of thermal expansion, making the environment temperature an important printing parameter to prevent thermal stresses, warping, and cracking. The enclosure temperature was at 105 °C for the manufacture of this duct, which was deemed the limit to avoid damaging the plastic components within the heated chamber. However, had the enclosure temperature been closer to the CTE of the material, the warping that occurred likely could have been prevented which would have reduced the chances of cracking during the bonding process

Autoclave Processing of Composites on the Bent Duct Tooling

The Split ST-130 Tool was delivered to Ability Composites for composite manufacturing. The Control Duct (0) and the Split ST-130 Duct (1) were both manufactured using 12 plies of prepreg. The

layup procedure involved debulking after the first ply, and then again after every 3-4 plies. The plies used 13-25 mm ply overlaps in the corners, resulting in more prepreg material and a thicker resulting composite in the corner regions. The layup included release film and breather/bleeder material to maintain a vacuum path. Then the tools were vacuum bagged using an envelope bag, which is where the bagging material envelopes the entire part applying both vacuum pressure and the autoclave pressure evenly on all outer surfaces of the tool. This would be similar in concept to how a food item could be vacuum sealed.

The nominal cure cycle for these ducts included a 2-stage temperature and pressure cycle while maintaining full vacuum throughout the cure. The initial hold temperature was 82°C (180°F), at a pressure of 207kPa (30psi) for 2 hours, followed by a second hold at 160°C (320°F) for 5 hours at a pressure of 414kPa (60psi). This programmed cure cycle is shown schematically in figure 50.

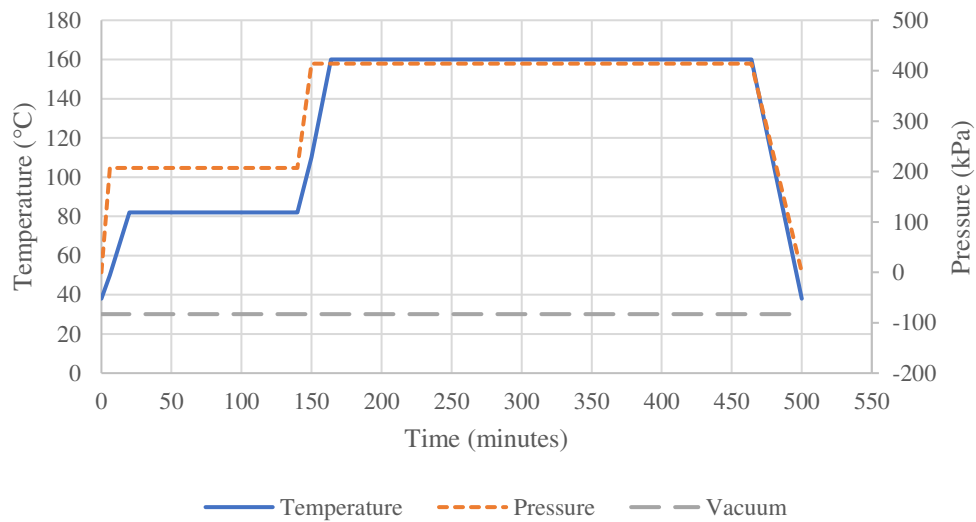


Figure 50 The nominal autoclave conditions programmed for the cure of the Control Duct (0) and the Split ST-130 Duct (1), which used a carbon fiber plain weave with TCR UF3362 resin.

After composite manufacture, the components were allowed to cool and then moved to 3D scanning for evaluation.

of the outside of the composite. The PTFE tape was 0.13mm (0.005 in) thick, so in design, this extra thickness could be accounted for. In this case, it was not considered. The duct showed overall good consistency after autoclave processing. There were some regions in the corners of the tool where the prepreg wrinkled during cure, creating high spots in the scan. The tool was soaked in water for 6 hours allowing it to soften, then removed manually. The tool was easily removed, but in the future a pressurized water jet would make removal much easier. Figure 52 shows the Control Duct (0) before and after tool removal.



Figure 52 The completed duct before and after washout tooling material removal.

The Control Duct (0) performed as expected, providing a rigid structure to mold the composite throughout the entire cure with no indication of structural deficiency.

Bent Duct Tooling Geometric Fidelity – Split ST-130 Duct (1)

A composite was manufactured on this tool by using an envelope bag around the whole part and curing in the autoclave. This was the same vacuum bagging approach that was used for the Control Duct (0). The completed duct with the tool trapped inside is shown in figure 53.

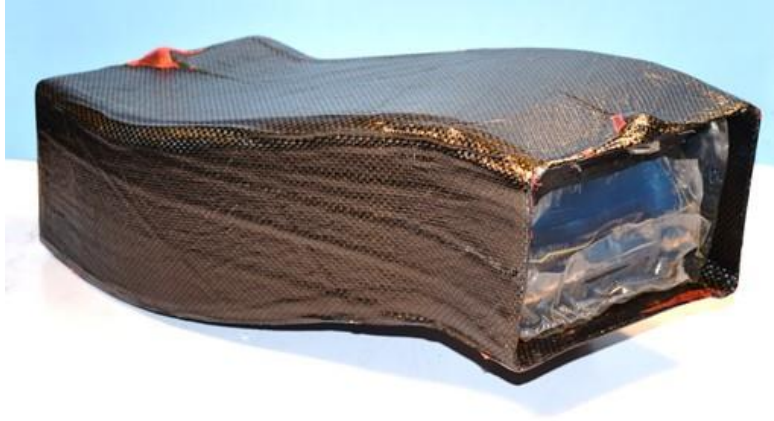


Figure 53 The cured part and tool used for duct 1.

The cured composites shown in both Figure 52 and 53 showed that the adhesive used to bond the two tooling halves together protruded from the surface, showing up on the outer surface of the composite. This was also noticed in the composite manufactured on the Control Duct (0). This may have been due to the adhesive not being sanded exactly flush with the tools. The Split ST-130 Tool collapsed completely during processing. The tool became smaller in all directions, likely collapsing into the infill region. The tool, still wrapped in PTFE tape, can be seen in figure 53. Ability Composites recorded the cure conditions for this composite, and a vacuum bag leak was recorded that can be seen developing at around the 290-minute mark in the vacuum trace shown in figure 54.

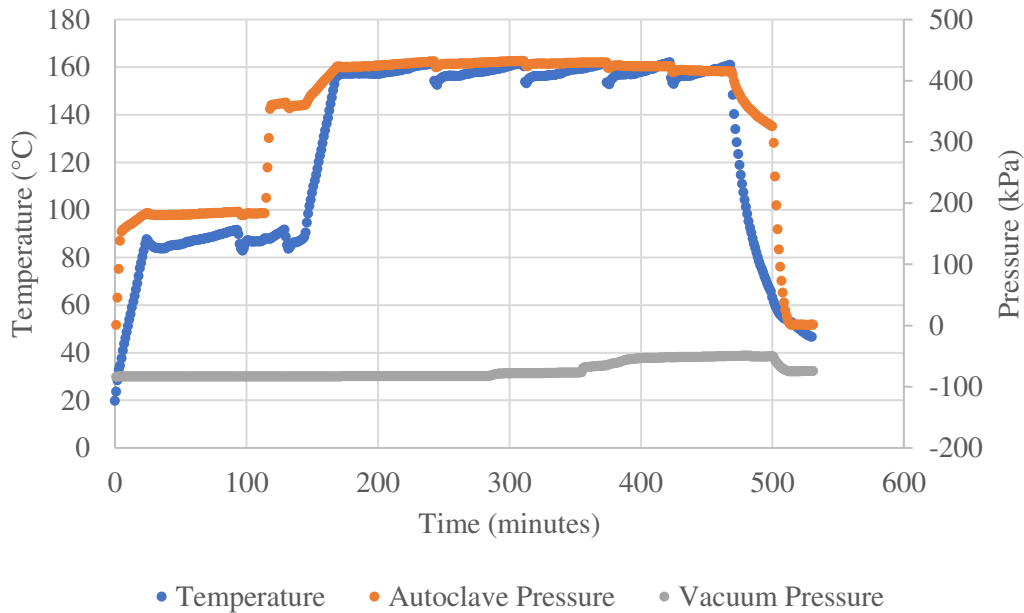


Figure 54 Cure cycle used to manufacture duct 1 showing a loss of vacuum.

The loss of vacuum, beginning around the 290-minute mark, is assumed to be associated with the timing of the tool failure. It is assumed that the tool remained intact through the initial 1 hour hold at 82°C, which is well under the previously tested conditions where ST-130 was found to be stable. However, after nearly 2 hours of the 160°C hold, the vacuum was lost. Given that the composite shape was relatively accurate, it is assumed that the tool remained stable long enough for the composite to develop a high enough degree of cure that the composite remained rigid even when the tool collapsed. Upon collapse, it is thought that the sharp corners on the ends of the partially cured composite could have compromised the vacuum bag. 3D-scans were completed using a FaroArm before and after manufacturing the part. These are shown side-by-side in figure 55.

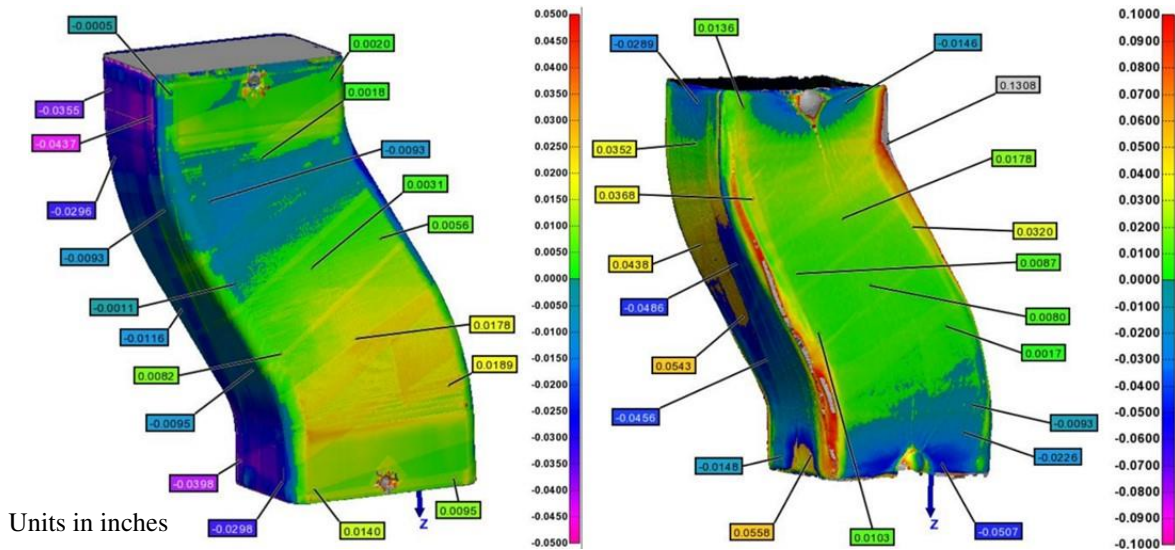


Figure 55 Scans of the tool (left) and part (right) were made using a FaroArm by Ability Composites.

The tool scan showed the tool was oversized by 0.5mm (+0.020”) over much of the front face of the tool. There was one low spot that appeared 0.25mm (0.010”) too small. Additionally, the sides of the tool were also too small by up to 1mm (0.040”). This geometric disagreement with the CAD model was likely due primarily to the bonding process that attempted to account for warping during manufacturing. It may have also been compounded by 3D printer inaccuracy. The composite deformation was around 0.25mm (0.010”) over large regions of the duct, further indicating that the tool maintained structural integrity long enough that the composite was able to rigidize and withstand the autoclave pressure. The corners had high spots, which can be attributed to the overlaps of plies at the corners and resulting wrinkling. The ends of the part deformed the worst, resulting in up to 1mm of composite part deformation in some regions. The PTFE tape is also clearly visible in the scan of the tool. The collapse of this tool indicated that the 160°C (320°F) cure temperature tested was too high for this tooling material. The hold temperature of 160°C (320°F) and pressure of 414 kPa (60 psi) were notably higher than the values used in the preliminary TPV trials or the truncated pyramid tooling. However, considering the significant challenges in bonding the two duct halves together and the catastrophic failure of the tool, the general geometric agreement between the composite and the CAD model was surprisingly good.

CHAPTER 5: COMPOSITE MANUFACTURE ON HOLLOW BENT DUCT TOOLING

EXPERIMENTATION

The Split ST-130 Duct (1) was produced with an internal 40% dense infill region, a 0.3mm layer height, and a 0.8mm nozzle to reduce the weight, the material use, and the manufacturing time. However, it still consumed over 3kg of material and took more than 4.5 days to print. It was then used to process a composite article at a hold temperature of 160°C and 414kPa, but these conditions were much higher than the tooling material was expected to perform well at and the tool failed catastrophically, collapsing in on itself. The failure motivated an investigation into an alternate tool design that was intended to reduce the likelihood of the tool itself crushing. A hollow tool, with solid walls, was designed that could utilize a vacuum bagging approach that allowed the bag to cover both the inner and outer surfaces of the tool. This concept was intended to allow a nominally equal autoclave induced pressure on the inside and outside surfaces of the tool, thus reducing the likelihood of deformation. Further, since the tool walls in this concept were solid, there were no partially dense infill regions that were prone to collapse, and thus reducing the chances of deformation. This was a significant deviation from the approach used for the previous Temperature Pressure Vacuum tests, the Truncated Pyramid tests, and from the trial with the Split ST-130 Duct (1), which all used partially dense infill structure. This tool concept and vacuum bagging approach are shown in figure 56.

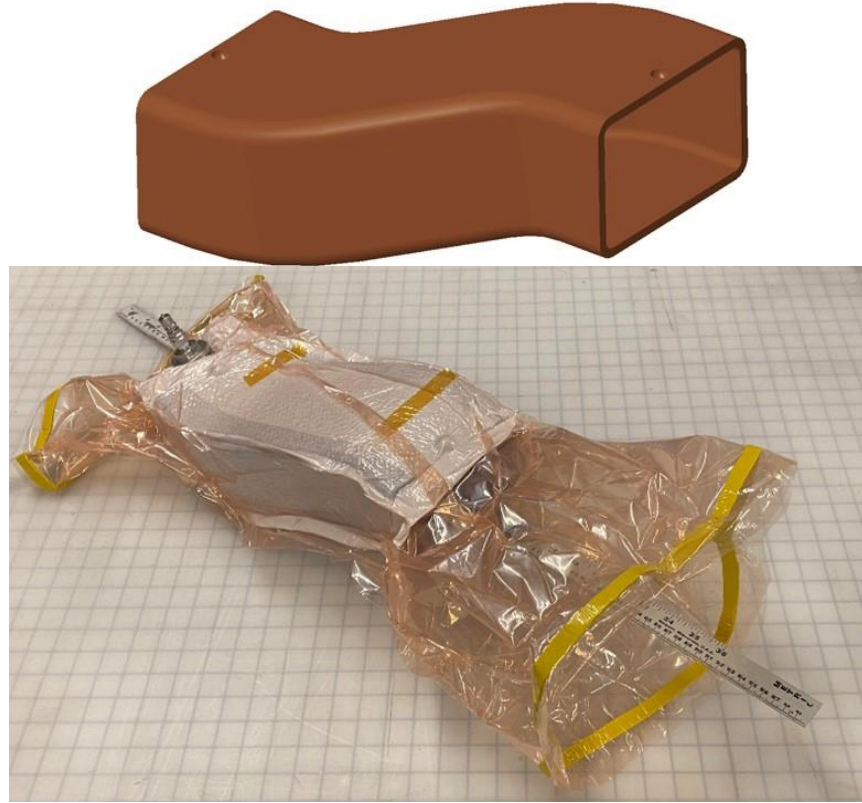


Figure 56 The hollow duct geometry and the new vacuum bagging approach, with a straightedge inserted through the vacuum bagged component to better visualize the approach.

Additionally, there were added benefits of the new approach related to manufacturing and tool quality. These hollow tools could be printed in a vertical orientation in single print which reduced the need for a bonding step. Additionally, the improvements from the Split ST-130 Duct (1) related to weight, material, and time savings, which were significant. By moving from the 40% dense Split ST-130 Duct (1) to the hollow configuration, the time savings allowed a refinement from a 0.3mm layer height to a 0.17mm layer height for the hollow ducts (2-6) and 0.16mm layer height for tools 7 and 8, which substantially improved the as-printed surface finish. For example, the Split ST-130 duct was manufactured in 4 days, 17 hours, and 46 minutes of print time and used 3.08kg (6.81lb) of material. In comparison, even with a reduced layer height, the print time and material usage for the 6.4mm Thick ST-130 Duct (2) were reduced to 2 days, 17 hours, and 45 minutes and 1.17 kg (2.59lb), respectively. The Extra Thick ST-130 Duct (7) with 12.4mm thick walls only used 2.24kg of material and took 3 days, 15 hours, and 25 minutes. Most importantly, the hollow geometry was predicted to allow improved tool

performance in the autoclave due to the reduced structural requirements of the tool when vacuum bagged on both inner and outer surfaces, as depicted in figure 57.

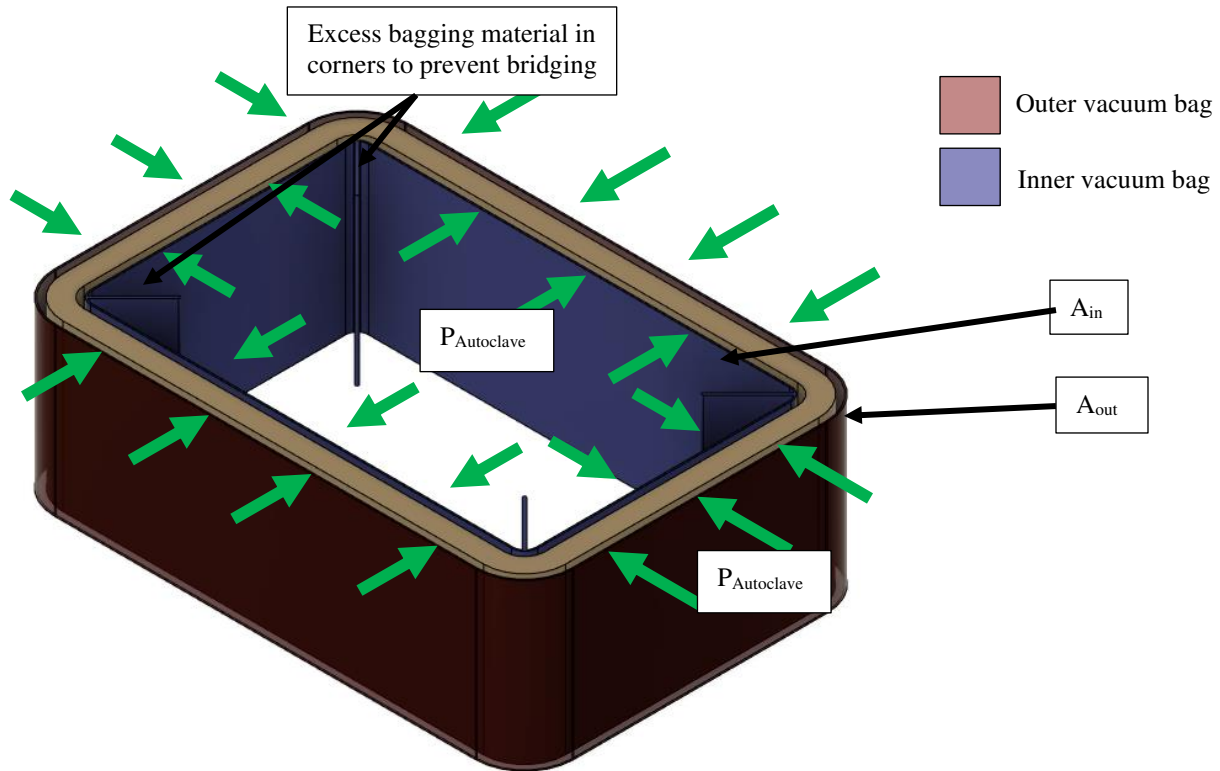


Figure 57 Depiction of the vacuum bagging scheme on the hollow duct geometry.

The reduced structural requirements can also be shown mathematically, by considering the surface area of the vacuum bag on external and internal sides of the tool. If the outer surface area, A_{out} , is greater than the inner surface area, A_{in} , but the autoclave pressure is equivalent on both surfaces, then the net force can be shown to be greater on the outer surface of the tool; however, this difference may not be very large with thin-walled tools. By using equations 1.1-1.3, it can be shown that for a 12.4mm thick tool (the highest thickness and worst-case scenario tested) the outer perimeter is 486mm and the inner perimeter is 408mm. This difference in perimeter length corresponds to a net force difference of approximately 20%, with more force being applied to the outside of the tool.

$$F_{out} = P_{autoclave} \cdot A_{out} \quad (1.0)$$

$$F_{in} = P_{autoclave} \cdot A_{in} \quad (1.1)$$

$$\begin{aligned} \text{if } A_{out} > A_{in} & \quad (1.2) \\ \text{then } F_{out} > F_{in} & \quad (1.3) \end{aligned}$$

As the tool thickness approaches zero then $A_{in} = A_{out}$ and $F_{in} = F_{out}$, indicating that the optimal tooling would be infinitely thin. However, since the tool would still be processed at temperatures significantly above the glass transition temperature (T_g) and would behave rubbery, it would likely fail due to the weight of the consumables, the composite materials, and the tool itself. So, various materials and wall thicknesses were evaluated to understand the impacts of the new vacuum bagging scheme on autoclave robustness at temperatures that exceed the T_g of the material. This was the fundamental approach to processing composites on tools above the upper limit of the tooling material stability. These ducts were printed using 3.2mm (0.125 in), 6.4mm (0.25in), or 12.4mm (0.49in) wall thicknesses. A summary of the different tool configurations, including the previously evaluated Control (0) and Split ST-130 (1) ducts can be found in table 24.

Table 24 Various duct geometries and materials used for manufacturing composite parts for this project.

Duct	Tooling Material	Prepreg Material	Wall Thickness	Maximum Autoclave Conditions	3D Printer Chamber Temperature
Control (0)	Ceramic Washout Tooling	Plain Weave TCR UF3362	N/A – Control Duct	160°C at 414kPa	105°C
Split ST-130 (1)	ST-130	Plain Weave TCR UF3362	N/A – Split Duct Approach	160°C at 414kPa	105°C
Thick ST-130 (2)	ST-130	Plain Weave TCR UF3362	6.35 mm (0.25 in)	160°C at 414kPa	105°C
Thin ST-130 (3)	ST-130	Plain Weave TCR UF3362	3.2 mm (0.125 in)	160°C at 414kPa	105°C
Thick AQ-120 (4)	AQ-120	Plain Weave TCR UF3362	6.35 mm (0.25 in)	160°C at 414kPa	~55°C
Thin AQ-120 (5)	AQ-120	Plain Weave TCR UF3362	3.2 mm (0.125 in)	160°C at 414kPa	~55°C
Thin AQ-180 (6)	AQ-180	Plain Weave TCR UF3362	3.2 mm (0.125 in)	160°C at 414kPa	90-75°C
Extra Thick ST-130 (7)	ST-130	Satin Weave CYCOM 5320-1	12.4mm (0.49in)	160°C at 414kPa	122°C
Thin Low Temperature ST-130 (8)	ST-130	Plain Weave Toray F2673C-07M	3.2mm (0.125in)	121°C at 345kPa	122°C

The ducts 2-6 were initially manufactured and evaluated to understand the impact of material type and wall thickness on the success of the tooling. However, later in the study it became apparent that the evaluation of ducts 7 and 8 would be useful. The Extra Thick ST-130 tool (7) had a 12.4mm wall thickness to attempt to minimize deformation. Duct 8 was prepared to evaluate the more complex geometry at the same cure conditions that had been previously tested in the Temperature Pressure Vacuum tests and the Truncated Pyramid trials using the new vacuum bagging approach. Each of these ducts would provide new information regarding autoclave tooling stability.

Materials

Ducts 1-8 were manufactured using 1.75mm feedstock materials using nominal processing conditions for each material unless stated otherwise. In some cases, the print parameters were slightly modified to improve print performance. The 3D printing materials used were Stratasys ST-130, Infinite

Material Solutions AquaSys-120 (AQ-120) and AquaSys-180 (AQ-180), and the individual tool materials were listed in table 24. For AQ-120, challenges with heat creep in the extruder that occurred during the duct prints necessitated the switch to a direct drive extruder. Heat creep is a printing malfunction where the filament binds in the extruder, preventing material flow. The enclosure was left vented for AQ-120, so that the approximate chamber temperature was only passively heated by the bed and reached an approximate temperature of 55°C.

Most of the composites were made from the same carbon fiber plain weave prepreg using TCR UF3362 resin supplied by Ability Composites. However, two tools were used to manufacture composites using different prepregs, namely Toray F2673C-07M plain weave carbon fiber epoxy prepreg and a CYCOM 5320-1 resin prepreg system with T650-35 3K 8HS Fabric 36% RW reinforcement. The CYCOM satin weave prepreg is processable using the same cure cycle as TCR UF3362 and was meant to be a similar prepreg and was used to manufacture the composite on the Extra Thick ST-130 Tool (7). The Toray prepreg was used as a lower temperature curing material, which would be used to process the Thin Low-Temperature ST-130 Duct (8) at reduced autoclave conditions of 121°C at 345kPa. Mold release was typically not used due to the trapped nature of the tooling; however, some tools and composites were destructively separated and in these cases, the tools were treated with Stoner Molding Solutions G471 XK-22 LV.5 Mold Release to allow easy release.

Equipment

The tools for ducts 1-6 were all manufactured using a modified Ender 5 Plus that had a maximum enclosure temperature of 105°C, which allowed reduced warping during manufacturing. However, it became clear after manufacturing the Control Duct (0), which had a large footprint, that this chamber temperature was insufficient at reducing thermal stresses, leading to warping and cracking. Thus, the decision was made to further modify the enclosure to reach elevated chamber temperatures prior to the manufacture of the Extra Thick ST-130 duct (7), which had 12.4mm thick walls that would be prone to cracking. The target temperature was 122°C, which was deemed advantageous because this temperature

was closer to the glass transition temperature of ST-130 (132°C) which helps to reduce thermal stresses. This upgrade was only completed prior to the manufacture of the tools for Ducts 7 and 8.

Ducts 2-6

Tools for manufacture of ducts 2-6 were manufactured on the modified Ender 5 Plus. This printer was modified to use an enclosure temperature of up to 105°C. The composite articles were processed in the autoclave at Ability Composites. Once manufactured, the composites were photographed, and the outer surfaces of the composites were scanned with the previously used FaroArm Edge. The outer surfaces of the composites were scanned, and the laminate thicknesses were accounted for in software.

Ducts 7 and 8

The Ender 5 Plus was upgraded to have increased chamber temperatures and higher flowrates, which would allow higher quality and faster printing of high temperature materials like ST-130. The belts and other non-metallic components inside the print chamber were replaced with higher temperature alternatives. One change included adding forced air cooling using a DC motor diaphragm air pump known as 'Berd-Air Cooling'. This approach uses air that is directed through tiny holes drilled in a metal pipe at the printed material which cools the material. The air exits these orifices very quickly, providing rapid cooling. Ideally this should cool the materials to near their glass transition temperature so that they can rigidize, while still being able to dissipate thermal stresses. Cooling becomes especially important in high temperature enclosures that approach the material T_g , where natural passive cooling becomes sluggish. Without cooling, it was found that ST-130 prints were slow to rigidize and began to droop. The extruder cooling block and fan was replaced with a water-cooled extruder cooling block, to prevent the fans from needing to be replaced after short periods of use at elevated temperatures. Additionally, the nozzle was changed to a Bondtech CHT nozzle with a 1.0mm orifice size instead of the previously used 0.8mm brass nozzle. This nozzle has a unique internal geometry that splits the filament into three channels that allows increased heat conduction to the filament through a larger surface area, as seen in figure 58. This results in much faster melting and flowrates.

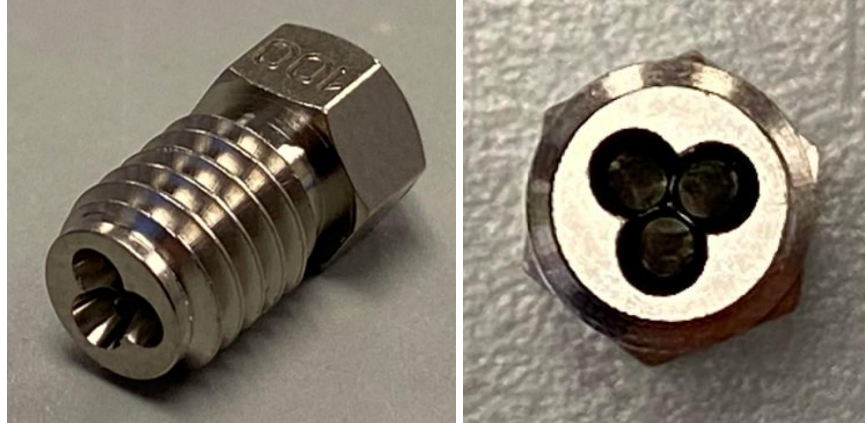


Figure 58 The Bondtech CHT nozzle has three filament channels, increasing material flowrate.

These modifications allowed the rapid manufacture of the final two ST-130 ducts (3.175mm and 12.4mm thicknesses) without developing significant thermal stresses, which was most important for the 12.4mm thick tool that would be prone to cracking. The modified hotend is shown in figure 59.

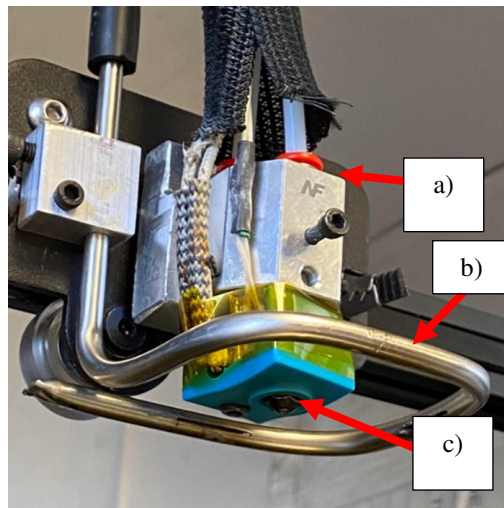


Figure 59 The upgraded extruder can be seen with a water cooled heatsink (a), Berd Air Cooling (b), and a high flow 1mm Bondtech CHT nozzle (c).

The limit switches were moved outside the chamber and triggered remotely by flexible rods in PTFE tubes, running from the homing point inside the chamber to the limit switch on the outside of the chamber. The prototype design of this approach best shows the limit switches outside the enclosure, with the PTFE tubes containing the flexible plungers running to the homing locations inside the chamber, as in

Figure 60. The flexible plungers were made from PEI (Ultem 1010) 3D printing filament, as PEI has a glass transition temperature of 217°C which would be sufficient for this application.

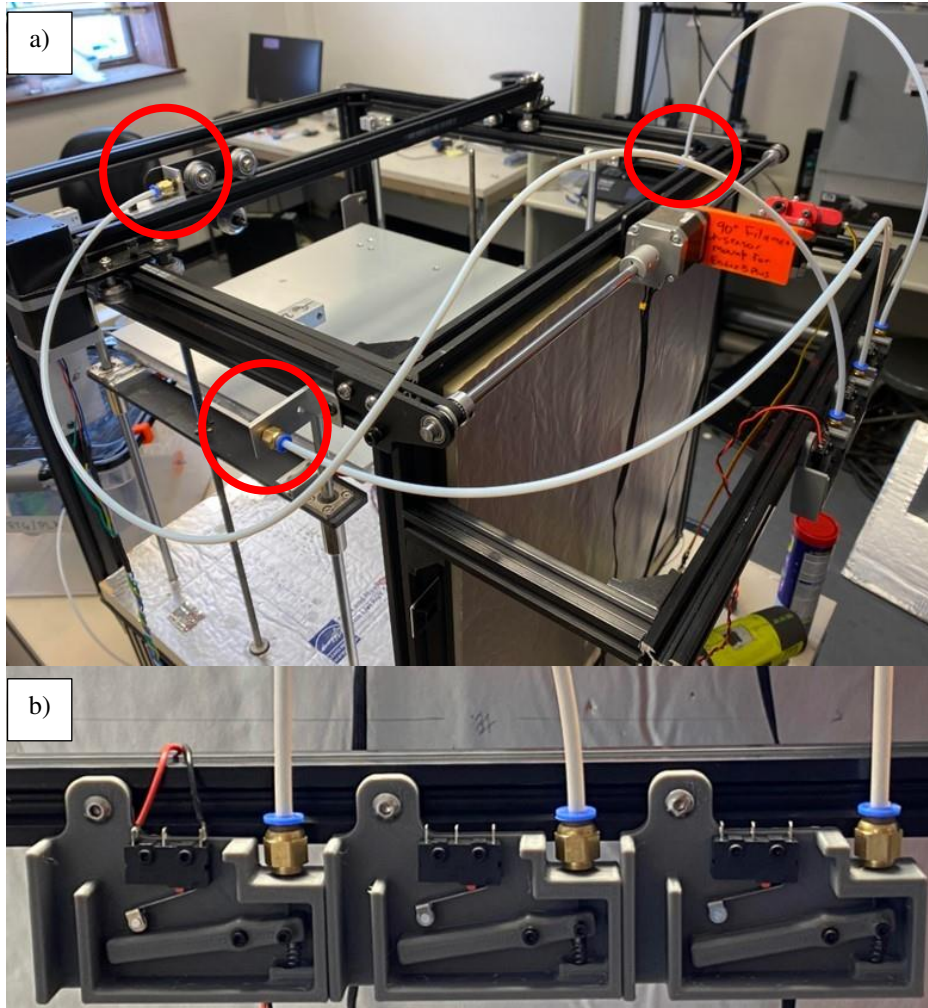


Figure 60 The ends of the flexible plungers that contact the homing surfaces in the print chamber are circled in red (a). The limit switches are shown outside the enclosure (b).

After 3D printing, composites were manufactured using the autoclave at CSU that was previously used for Temperature Pressure Vacuum and Truncated Pyramid studies. After composite manufacturing, the dimensional fidelity was documented by Ability Composites using a FaroArm to create 3D point cloud data that could be compared to the original CAD model.

Preparation of Hollow Duct Samples

Tools 2-6

The tools were manufactured in a vertical build orientation. On tools 2-6, the G-code was generated using Cura Ultimaker 4.6, and did not use a hollow CAD file. Instead, a solid CAD model was used and 0% infill, 0 top layers, and 0 bottom layers were specified. Then, the walls were made using the appropriate number of perimeter print paths to generate the wall thickness. By setting the infill, top layers, and bottom layers to 0 the walls would only be made from perimeter paths, creating concentric passes.

The sloped regions of the tool were also thinner, so in these regions, a ‘modifier mesh’ was used to locally modify the settings for the overlapping regions in the slicing software to add an extra print path to ensure the thickness of the tool was maintained. A depiction of this process is shown in figure 61.

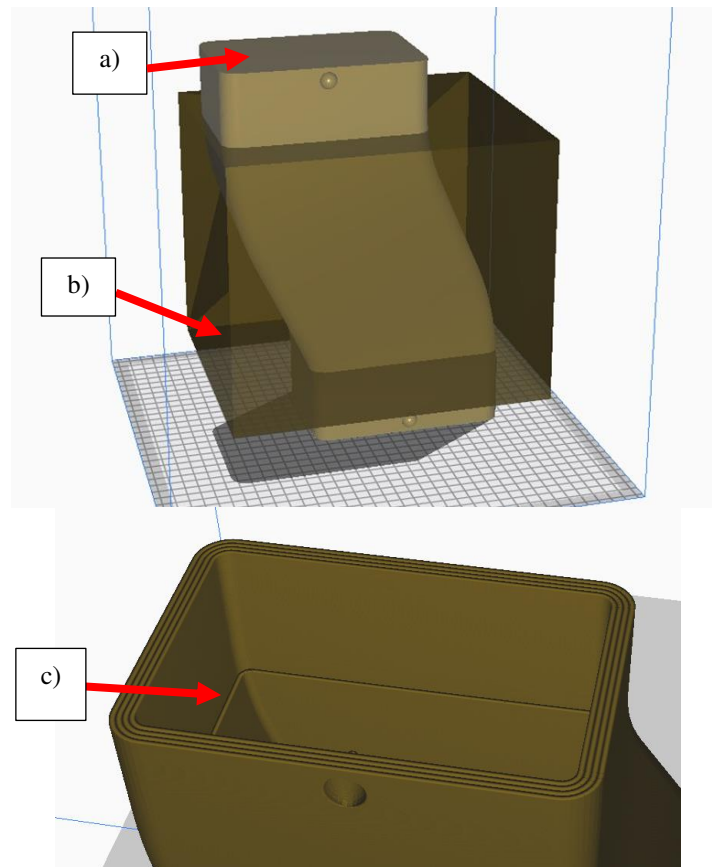


Figure 61 This shows the solid tool geometry (a) and the modifier mesh (b) that was used to add an additional perimeter road to the sloped regions of the tool (c).

Ironing was not feasible because of the vertical build orientation; however, the smaller layer height and the relatively steep surfaces reduced the stair-stepping effect between layers making ironing less critical. The vertical print orientation is shown for the 6.4 mm wall thickness Thick ST-130 Duct (2) in figure 62.



Figure 62 Hollow bent duct printing process for the Thick ST-130 Duct (2).

The manufacturing process of each of the hollow ducts (ducts 2-8) was completed in a single step, unlike the process used for the Split ST-130 Duct (1).

Tools 7 and 8

The hollow tools for ducts 7 and 8 were manufactured using the upgraded Ender 5 Plus, and they used modified print parameters. First, the new ducts used a chamber temperature of 122°C, which was closer to the T_g of ST-130. The layer height was reduced from 0.17mm to 0.16mm, which was optimized

for the leadscrew pitch and motor combination for the z-axis to further improve surface quality using a layer height calculator by Prusa Research [52] .

Ducts 7 and 8 also did not use the modifier mesh approach that was used for previous ducts. Instead, the CAD model was adjusted to have the correct wall thickness, and the printer spent more time per layer filling in gaps on the sloped wall regions. While somewhat slower, it resulted in an improved surface finish on the inner surface of the tool by allowing all non-printing motion to occur in the solid infill regions. Previously, there was not an infill region that could be selected to make motion moves through, as the tool was made using only perimeters, so the inside surface of the duct had stringing issues. These two ducts were manufactured with a 100.4% scale on the X-direction or the nominally 152.mm (6in) side and a 100.1% scale on the Y-direction or the nominally 101.6mm (4in) side. This was done in response to concerns over undersized tools 2-6. The tools were thought to have shrunk due to CTE upon cooling from the print chamber temperature of 105°C. Both the tooling and the 3D Printer change size due to CTE when in the print chamber, so simply calculating the size change based on the CTE of the material is not feasible. Therefore, the exact numbers used to scale ducts 7 and 8 were determined by printing a cross section of the duct, then measuring the outer dimensions to determine the scaling factor. After this calibration, the printed geometry was measured with calipers to be within +/-0.03mm (+/- 0.001”) of nominal along the X and Y directions.

Additionally, Cura Ultimaker 4.13 was used, which offered a unique setting that was utilized to decrease the manufacturing time. The infill was printed every other layer, at double the layer thickness. This modification allowed the perimeter roads to be printed every 0.16mm to maintain the outer surface quality, but the internal structure to be manufactured every 0.32mm, reducing the print time. The print speed was set to 30mm/s for the perimeters and 22mm/s for the infill, however the flow rate was still higher for the infill regions. A depiction of this can be seen in figure 63.

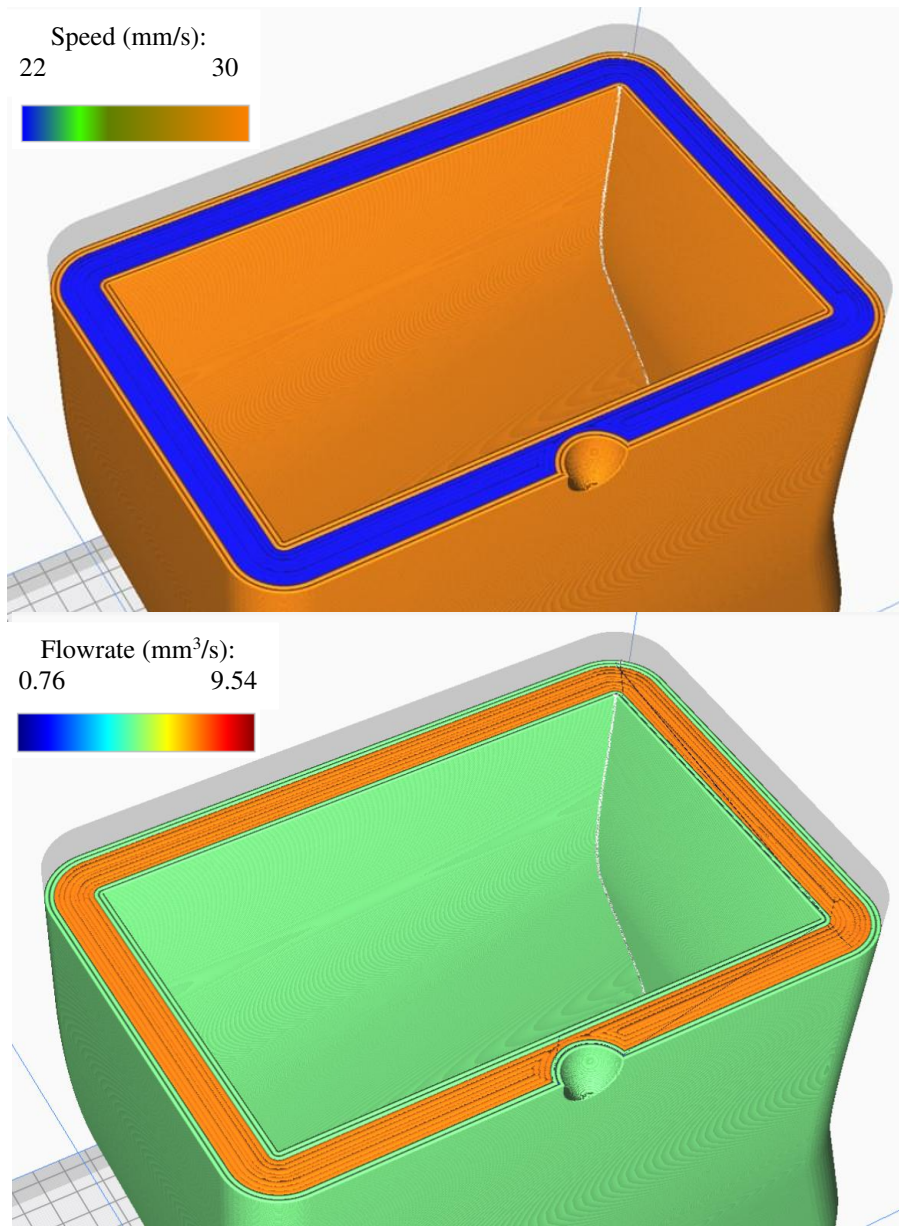


Figure 63 The speed and material flowrates for duct 7.

The infill approach and other modifications reduced the manufacturing time of the Extra Thick ST-130 tool (7) and the Thin Low Temperature ST-130 tool (8) to be approximately 3 days 15 hours and 25 minutes and 1 day 16 hours and 35 minutes, respectively. The Extra Thick ST-130 Tool used an estimated 2239g of material, and the Thin Low Temperature ST-130 Tool used an estimated 635g. A comparison of print time, material weight, and print rate for each 3D printed tool is shown in table 25.

Table 25 The material usage, print time, and overall print rates for the 3D printed ducts.

Duct	Estimated Material Use (g)	Estimated Material Use (cc)	Estimated Print Time (dd:hh:mm)	Total Print Rate (g/hr)	Total Print Rate (cc/hr)
Split ST-130 (1)	3087	2594	04:17:46	27.1	22.8
Thick ST-130 (2)	1175	987	02:17:45	17.9	15.0
Thin ST-130 (3)	714	600	01:15:57	17.9	15.0
Thick AQ-120 (4)	1303	987	02:17:45	19.8	15.0
Thin AQ-120 (5)	792	600	01:15:57	19.8	15.0
Thin AQ-180 (6)	756	600	01:15:57	18.9	15.0
Extra Thick ST-130 (7)	2239	1881	03:15:25	25.6	21.5
Thin Low Temperature ST-130 (8)	635	534	01:16:35	15.6	13.2

In table 25, the volumetric print rate was the highest for the Split ST-130 duct (1) and followed by the Extra Thick ST-130 duct (7). This was caused by a high spring force, which controls the pressure applied by the filament feed gear, for ducts 1-6. This resulted in increased print rates but also caused frequent feedstock breakage requiring restart. By upgrading to a high-flow nozzle prior to printing ducts 7 and 8, the printer could be run more reliably, with a reduced spring force and no feedstock breakage. Ducts 7 and 8 had a reduced layer height with comparable speed, resulting in further reduction of print rate, and they used a 1mm nozzle instead of the 0.8mm nozzle which increased the print rate. The Thin Low Temperature ST-130 Tool did not benefit from the infill being printed every other layer, because the perimeter beads were wide enough to make up the entire thickness. However, the Extra Thick ST-130 (7) tool benefited significantly, due to the large number of infill roads. As a comparison, the Extra Thick ST-130 tool was nearly twice as thick as the Thick ST-130 Tool (2), which were 12.4mm and 6.4mm, respectively, but the Extra Thick Tool (7) only took 1.3 times as long even with the slightly reduced layer height and speed (which both improved the quality of the print).

Autoclave Processing of Composites on Hollow Bent Duct Tooling

Tools 2-6 were delivered to Ability Composites for composite specimen manufacture. Ducts 0, 1, and 2 used 12 plies of prepreg, while ducts 3-6 used 6 plies, and ducts 7 and 8 used 4 plies to save time on layup. The different composite thicknesses will have some impact on the stiffness of both the uncured and

cured composites, however this effect was assumed to be minimal. CSU aided with the layup of ducts 3-6, and the layup and cure of Ducts 7 and 8 were completed by CSU. Each composite was made using a symmetric layup, with 0/90° plies on the molded tool surface as well as the visible external surface, and +/-45° plies in between. Ducts 0-6 used a plain weave carbon fiber prepreg with TCR UF3362 resin. Duct 7 used Cycom 5320-1 satin prepreg. This prepreg was chosen because it can be cured using the same cure cycle that Ability Composites used for curing composites on tools 0-6. Duct 8 used Toray 2510 spread tow carbon fiber epoxy prepreg, the same that had been used in the truncated pyramid trials that can be cured at the lower process conditions of 121°C and 345kPa. The layup procedure for all samples involved debulking after the first ply, and then again after every 3-4 plies. The plies used 13-25 mm ply overlaps in the corners, resulting in more prepreg material and a thicker resulting composite in the corner regions. The composite layup process is shown in figure 64.

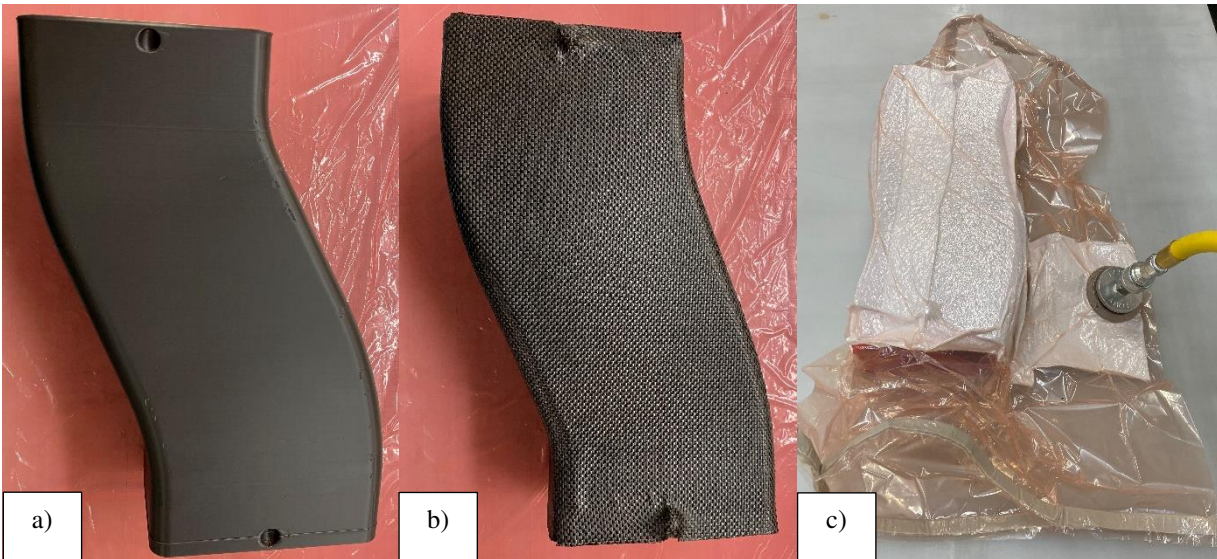


Figure 64 A representative composite manufacturing process of one of the hollow ducts at steps: bare tool (a), during layup (b), and during debulk (c).

During the layup, the first step was to prepare the tool. The tools were first cleaned using dry compressed air and/or isopropyl alcohol, as needed. Then, Stoner Molding Solutions mold release was applied to tools 2, 7, and 8. After this, the laminate was applied, debulking after the first ply and then every 3-4 plies as necessary. Next, nonporous release film and breather/bleeder were applied to allow a

high-quality vacuum path. Finally, the composites were sealed within the vacuum bag paying special attention that pleats (folds made using excess bagging material) were located on the internal and external corners of the tool to prevent the bag from bridging and inducing deformation. Tools 2-7 used the cure cycle in figure 65.

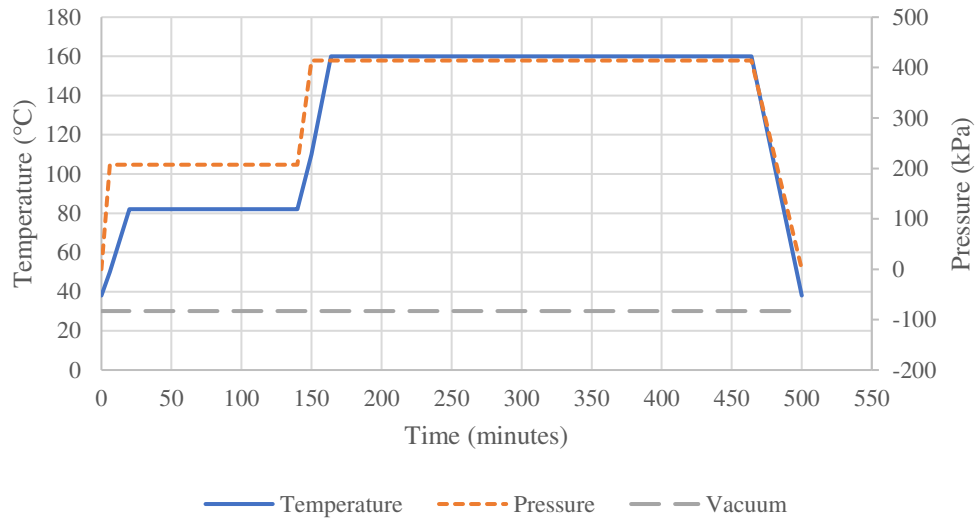


Figure 65 The nominal autoclave conditions programmed for the cure of ducts 2-7. This is the cure cycle that was used to process Ducts 0 and 1 in previous studies that also used prepreg with TCR UF3362 resin.

The Thin ST-130 Low Temperature Duct (8) used 3.175mm wall thicknesses and was processed at reduced temperatures. It used the same Toray prepreg and cure cycle that the 3D printed Truncated Pyramid tools used, and first involved a 10-minute hold at 38°C to stabilize the autoclave. Then, it underwent a 30-minute ramp up to 121°C where it was held for 150 minutes. Once the hold temperature was reached, the autoclave was pressurized to 345kPa, which took about 8-minutes to reach the hold pressure. When the hold was completed, the autoclave was depressurized and cooled, and the part was removed from the autoclave.

After composite processing, both composites were planned to be destructively removed so that the tool could be directly scanned, eliminating the need to account for the composite thickness in software. The composite on the Extra Thick ST-130 Tool (7) was successfully removed using a Dremel tool. However, the Thin Low Temperature ST-130 Tool (8) cracked in several places during composite

processing, likely due to CTE mismatch between the tool and the composite causing fracture during cooldown. It was worried that removing the composite would result in the tool breaking into pieces, which would prevent any scan data from being captured at all. So, the ply thickness was accounted for in the 3D scan of Tool 8, using the same approach that was used for Tools 2-6.

Evaluation

RESULTS AND DISCUSSION

Thick ST-130 Duct 2

The second 3D printed tool that was manufactured and tested was made from ST-130 and was manufactured using a 6.35mm thick hollow geometry. This geometry was printed upright, and only required one print to complete rather than the two prints required for Duct 1. It had slight geometry deviations from filament changes during printing primarily related to pauses in the print and inadequate cooling on some of the overhanging edges. Cooling was a challenge for long prints at the 105°C enclosure temperature because the fan would overheat and begin to fail, reducing the effectiveness of the cooling. Prior to composite manufacturing, the tool was coated with Stoner Molding Solutions Mold Release. The tool and the completed composite are shown in figure 66. After manufacturing the composite, the tool was destructively sectioned and removed by using a Dremel tool to inspect the molded surface finish.



Figure 66 The printed tool (a), the composite manufactured on the tool (b), and the composite part after the tooling was removed (c).

The FaroArm scan of the composite showed relatively good agreement with the CAD geometry, indicating that the tool performed well during composite processing, even at the elevated temperature of 160°C (320°F) and 414kPa (60psi). The resulting composite had slight deviations at the ends of the part that appeared to be concave along the long edges of the end profile, as seen in figure 67.

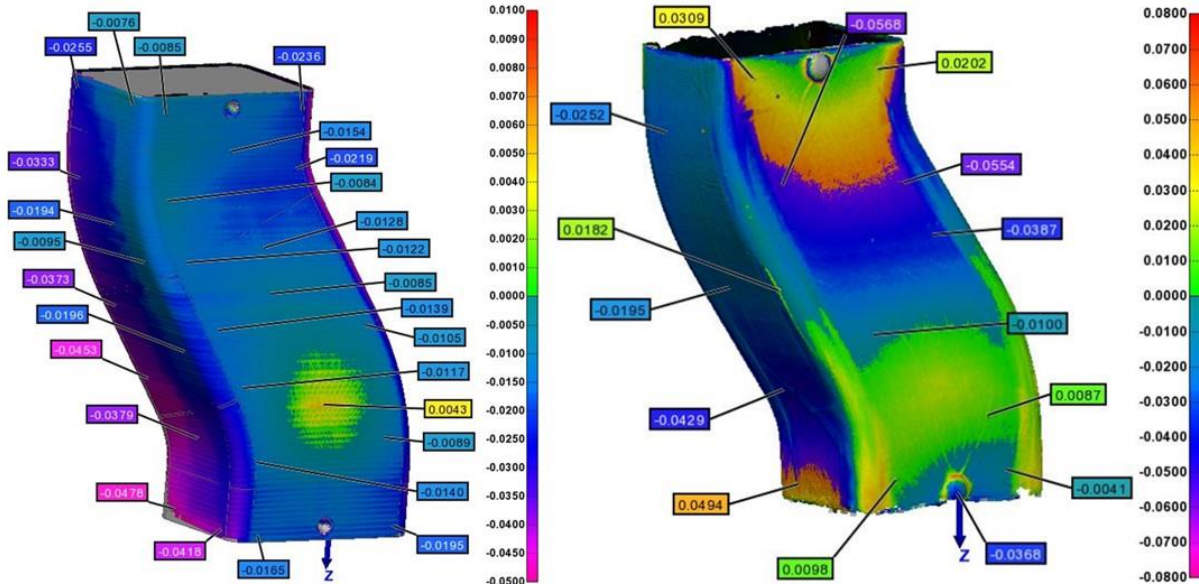


Figure 67 FaroArm scans of the Thick ST-130 Tool (2) both before (left) and after (right) composite processing.

The tool prior to composite processing showed an overall undersized geometry of approximately +0.1/-0.5mm. This overall undersized geometry was also seen in the truncated square pyramid tools and could be attributed to many systematic errors. Two obvious error sources could be the CTE of the material and the 3D printer accuracy. Additionally, the size change of the 3D printer itself was not accounted for in the high temperature enclosure. So, the deformations prior to composite production should be accounted for, but are not critically important for judging the structural robustness in this study. However, the composite that was produced did have deformation that was inconsistent with the tool inaccuracies. Some undersized regions could be attributed to the undersized geometry of the tool, but the oversized regions cannot be easily explained. The top-down view of this duct is shown in figure 68 and the slight deformation is clearly present.



Figure 68 The top-down view of the Thick ST-130 Duct (2).

Figures 67 and 68 show a slight concavity on the edges of the duct that was caused by either a manufacturing error or by another process occurring during cure that was causing deformation. The cause of this deformation is unknown and was originally assumed to be caused by bridging of the bagging material on the inside corners of the part, causing slight concavity of the long edges. The performance of this duct was promising considering the material was processed at temperatures around 40°C higher than the HDT, but left unanswered questions about the tool thickness, tool thermal properties, and the cause of the deformation. The promising outcome can be attributed to the hollow geometry and the vacuum bagging technique used. The Split ST-130 Duct (1) did not perform well at this temperature, and the relative success of this tool was likely due to the vacuum bagging material passing on both the inner and outer surfaces of the tool.

The outcome of this 6.4mm thick tool prompted the manufacturing of ducts 3-8. The assumption made at this point was that the hollow tool approach would allow approximately equal loading from the vacuum bag on the inside and outside of the duct during cure. This would allow materials with reduced thermal properties to be used as tooling, reducing the cost and printing conditions required to print. The hollow ducts three through six were initially 3D printed and tested to investigate these assumptions.

Thin ST-130 Duct 3

The Thin ST-130 Duct was manufactured from ST-130 using 3.2 mm (0.125 in) thick walls to determine the impact of wall thickness on deformation. It was hoped that this tool would indicate if the tooling structural requirements could be reduced, allowing thin, lightweight, and cheap tools or materials with lower use temperatures to be used with the vacuum bagging approach. Figure 69 shows the manufactured tool which was printed in approximately 31 hours and required slightly less than 0.6 kg (1.3lb) of ST-130.



Figure 69 The manufactured thin-walled ST-130 tool.

The Thin ST-130 Duct had one primary defect located near the ball bearing insert. The filament ran out at this location in the print, resulting in the start of a filament run-out routine where the printer pauses to allow the user to reload filament. At some point during this routine, the location of the printhead was misaligned. The composite part cured on the Thin ST-130 Duct (3) is shown in figure 70, with the tool still trapped inside.



Figure 70 The cured composite with the tool left inside.

The manufactured composite showed significant deformation; however, the general form of the duct was still intact. The performance of the Thin ST-130 Duct (3) was significantly worse than the Thick ST-130 Duct (2), indicating that the bagging scheme utilized does not eliminate tool stiffness requirements entirely. However, this scheme largely resulted in a duct that maintained its form throughout the cure. This is promising for future efforts because it may be possible to apply this bagging technique at reduced temperatures, significantly reducing the chances of deformation occurring. The FaroArm scans of the tool before and after composite manufacture are shown in figure 71.

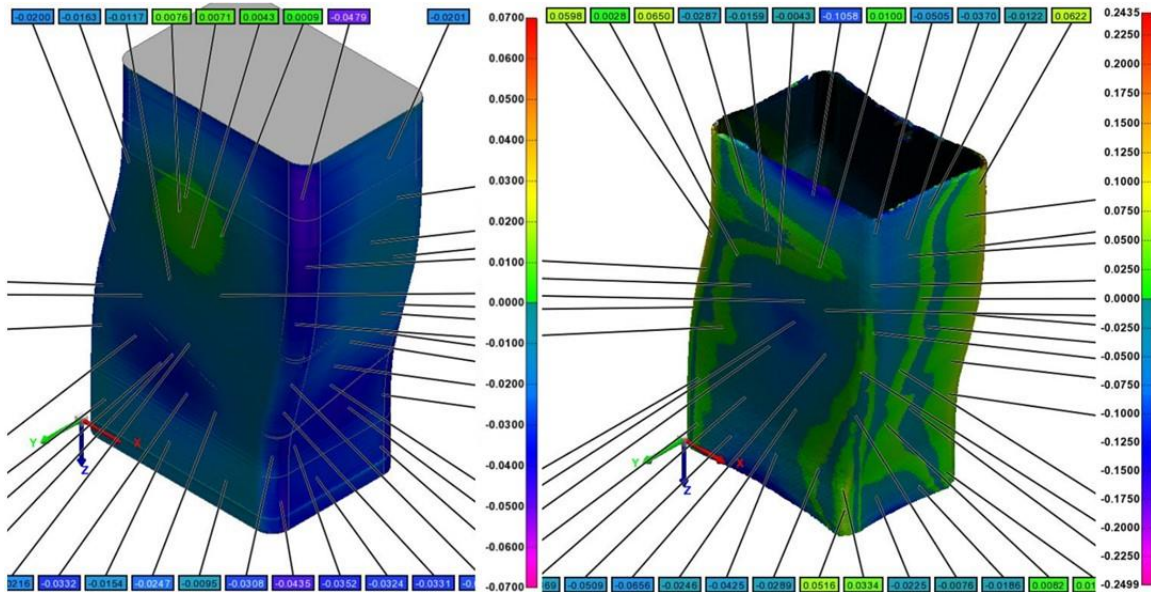


Figure 71 FaroArm scans of the Thin ST-130 Tool before (left) and after (right) composite manufacturing.

The FaroArm scans of the Thin ST-130 Duct (3) shows undersized geometry, especially on the corners, and a high spot on the front face. This is very similar to the 3D scan of the Thick ST-130 Duct (2), indicating some sort of systematic error introduced during manufacture. The composite shows high regions on the corners, but low regions on the faces. The concave regions at the ends of the tool appear to be too small by up to 2.54 mm (0.1 in). This tests again indicates that the materials were tested far above their use temperature.

Thick AQ-120 Duct 4

Duct 4 was 3D printed from AQ-120, considered to be a low temperature material as indicated by the T_g of approximately 92°C, and used 6.35mm thick walls. This Thick AQ-120 Duct (4) would allow a comparison to the Thick ST-130 Duct (2), which also used 6.4mm thick walls, and indicate if the vacuum bagging scheme used would allow lower use temperature materials to be used at elevated cure temperatures of 160°C. The use of a water-soluble tooling material is desirable to avoid the caustic solutions used for ST-130. Additionally, AQ-120 can be manufactured on low-cost 3D printers without a heated enclosure and can be printed with low-cost extruders that do not need to exceed 250°C. The as manufactured tool is shown in figure 72.



Figure 72 The manufactured tool for Duct 4.

The Thick AQ-120 Duct (4) had some slight printing defects, namely a layer shift near the top of the part. This was likely caused by the drive gear for one axis slipping. The gear was tightened on the motor shaft, and the error was not seen again with other ducts. Additionally, there were some small regions where under extrusion caused voids in the tool surface. All the AQ-120 and AQ-180 ducts have similar horizontal banding of color occurring parallel to the build plate. This color shift was discussed with the technical support engineers at Infinite Material Solutions (the manufacturer of the AquaSys products) who indicated that the cause of the banding is unknown, but that the bands are typical and should not impact part performance. Figure 73 shows the composite manufactured on the Thick AQ-120 Duct (4).



Figure 73 The completed part and tool used to manufacture Duct 4.

The results of the Thick AQ-120 duct showed worse results than the previous two hollow ducts, which were both made from ST-130. This duct had significant deformation, primarily located at the ends of the part, and the same lozengeing failure mode was also present down the length of the duct where the sides collapse inwards. There was more wrinkling at the corners of the composite, but that was decided to be caused by improper consolidation during layup. The concave deformation mode is depicted clearly in the FaroArm scan of the composite as shown in figure 74.

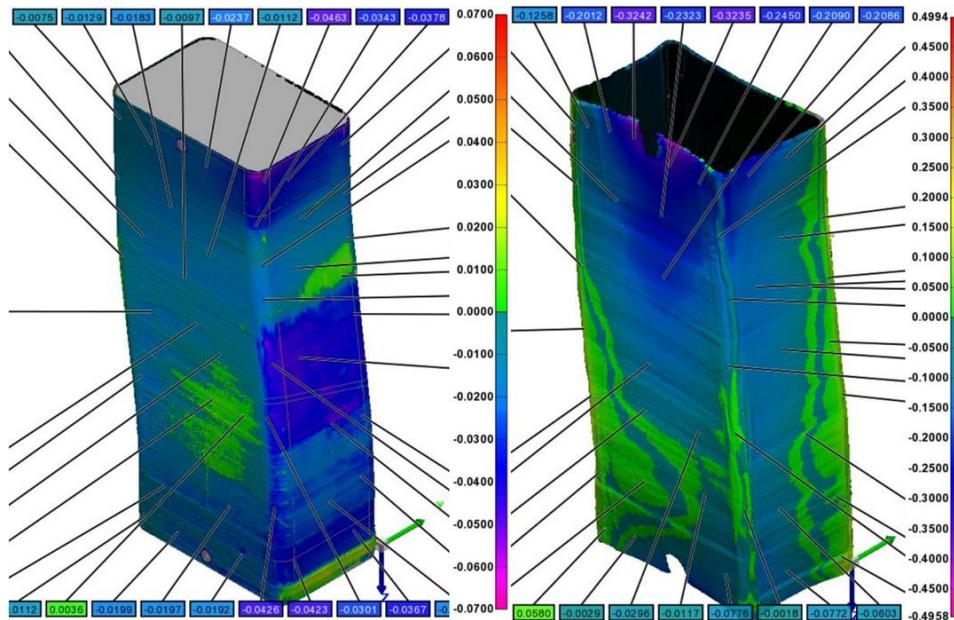


Figure 74 The FaroArm scans of the Thick AQ-120 Duct (4) tool (left) and composite (right).

The FaroArm scan of the as-printed Tool 4 shows similar characteristics to the previous hollow printed ducts with undersized geometry, except for a high spot on the front face. The scan of the duct after manufacture shows corner regions that are oversized by around 1.5 mm (0.06 in), and low face regions on the ends that are too small by up to 13 mm. Some of the regions in the center of the duct do not have as severe of deformation, but overall the tool performed poorly. The deformation of this Thick AQ-120 tool was greater than that measured for the Thin ST-130 tool. The deformation of the low temperature tooling material, AQ-120, provided evidence that the vacuum bagging scheme used still requires a higher degree of overall tool stiffness than was provided at the autoclave process temperature, which is primarily derived from the tooling material.

Thin AQ-120 Duct 5

This duct was manufactured similar to the Thick AQ-120 Duct (4), just with a reduced 3.2 mm wall thickness. Therefore, it is not surprising that many of the results and discussion points for ducts 4 and 5 are similar, except with worse performance for the Thin AQ-120 duct. The 3D printed tool for duct 5 is shown in figure 75.



Figure 75 The manufactured tool for the Thin AQ-120 Duct (5).

The Thin AQ-120 Tool did not have any significant printing defects, however minor surface imperfections on overhanging regions were caused by insufficient part cooling. This likely had no impact

on composite production and was only related to the molded surface finish. Figure 76 shows the composite manufactured using this tool.



Figure 76 The completed part and tool for the Thin AQ-120 Duct (5).

The Thin AQ-120 Duct had the most severe deformation out of all the ducts tested. The deformation was much worse than the Thin ST-130 Tool (3), which used the same 3.2mm wall thickness. This comparison shows that the rigidity provided by the material stiffness at temperature is a critical factor in tooling stability. The poor performance of the Thin AQ-120 Tool (5) is consistent with the use of the low temperature material and the lowest wall thickness tested creating the worst-case scenario for tool rigidity during cure. The associated FaroArm scan is shown in figure 77.

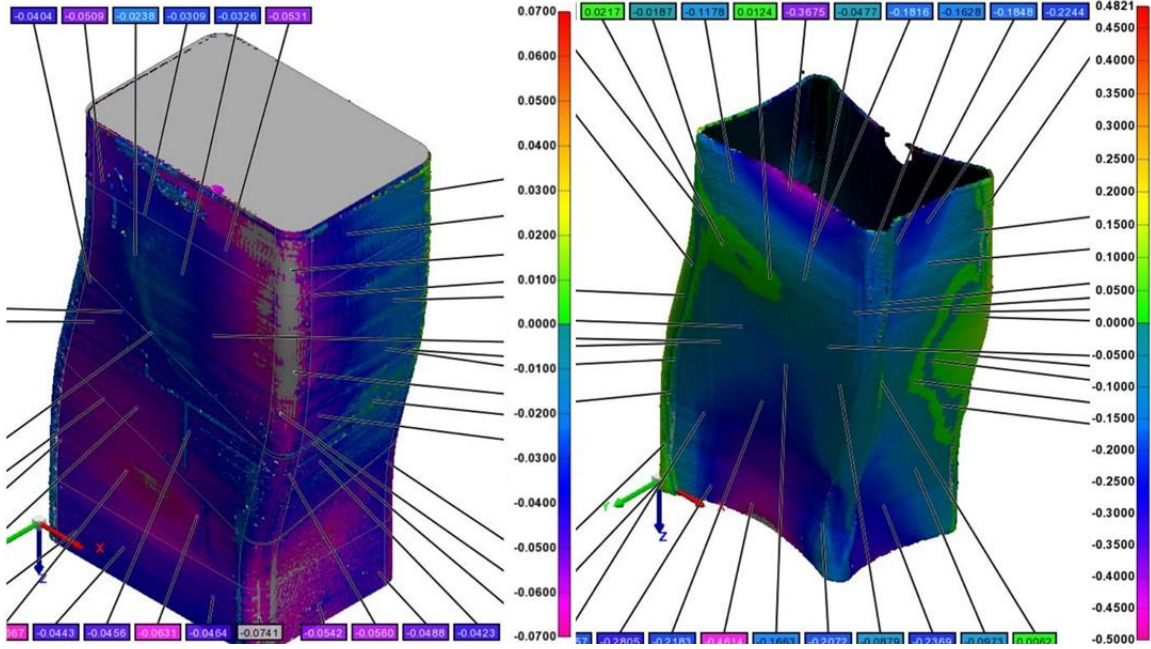


Figure 77 The FaroArm scans of the Thin AQ-120 tool before (left) and after (right) composite manufacture.

The results from manufacturing the Thin AQ-120 tool and composite were more-or-less conclusive that the vacuum bagging technique does not provide sufficient support by itself, and rather the tool needs to maintain higher rigidity than what was used in these tests with improving results occurring at decreasing temperatures beneath the glass transition temperature. However, it has yet to be seen if the same tooling configurations would provide sufficient results at lower temperatures like the 121°C (250°F) conditions used in preliminary TPV testing and truncated square pyramid trials.

Thin AQ-180 Duct 6

Duct 6 was manufactured using a thin-walled AQ-180 configuration, with wall thicknesses of 3.2mm. The manufactured tool can be seen in figure 78.



Figure 78 The manufactured Thin AQ-180 tool (6).

This tool was the only tool tested that utilized AQ-180, the second-best performing material to ST-130 in prior trials, and the best performing water-soluble printed material. Tool 6 had a rough surface texture on the overhanging regions of the printed tool as seen in figure 78 and in the close-up photos in figure 79. This was likely caused by insufficient cooling and deposition on material that was not yet fully rigid from the previous layer. This defect would likely be addressed by lowering the processing temperature and increasing the cooling. For this tool, a combination of printing with no part cooling fan (it would fail after prolonged use at elevated temperatures), high enclosure temperature, and high print speeds caused this defect. After the rough surface finish was noticed, it was addressed by lowering the enclosure temperature from 90°C to 75°C and reducing the speed from 32mm/s to 19mm/s during the print. It is likely that 32mm/s would be sufficient for part manufacturing with adequate cooling, however the speed was lowered to allow more time for the tool to naturally cool between extruder passes. Additionally, while the manufacturer had originally stated there should be no adverse effects from the regions of color banding on part quality for AquaSys 120, undersized tooling was observed in these regions as seen next to a straightedge in figure 79 for AquaSys 180. So, it is assumed that the color banding does have some impact on tool quality, but it may be small enough in many applications to not have a notable impact.

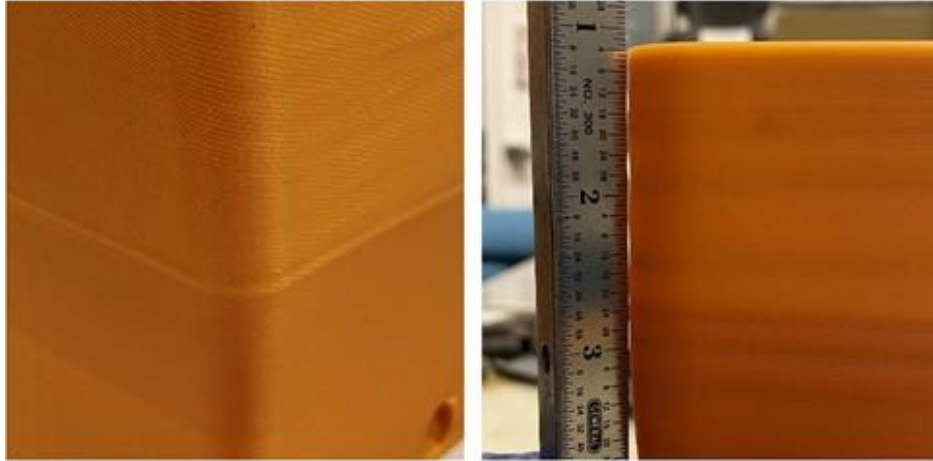


Figure 79 Duct 6 had a rough surface texture on overhanging regions (left) and a wavy surface located where the color banding occurred (right).

The composite produced on the Thin AQ-180 duct showed less deformation than the AQ-120 tools, and similar deformation to the ST-130 tool of the same thickness. Figure 80 shows the as manufactured composite using this tool.

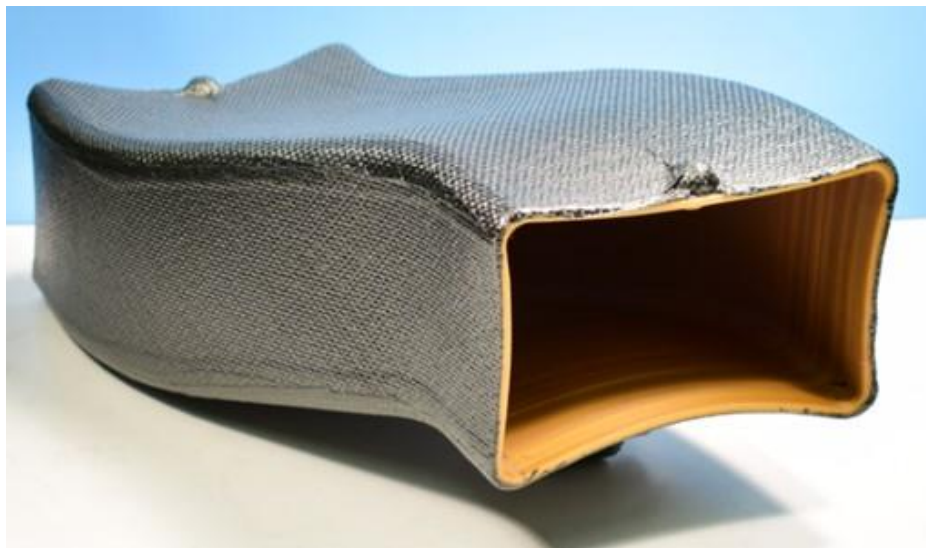


Figure 80 The cured composite cured on the Thin AQ-180 Duct (6).

The composite that resulted from the Thin AQ-180 Duct performed similarly to the Thin ST-130 Duct (3) with the same 3.2 mm wall thickness. This agrees well with the previous conclusion that AQ-180 is a suitable alternative to ST-130 in scenarios where water solubility is necessary. Figure 81 shows the FaroArm scan of the tool before and after composite manufacture.

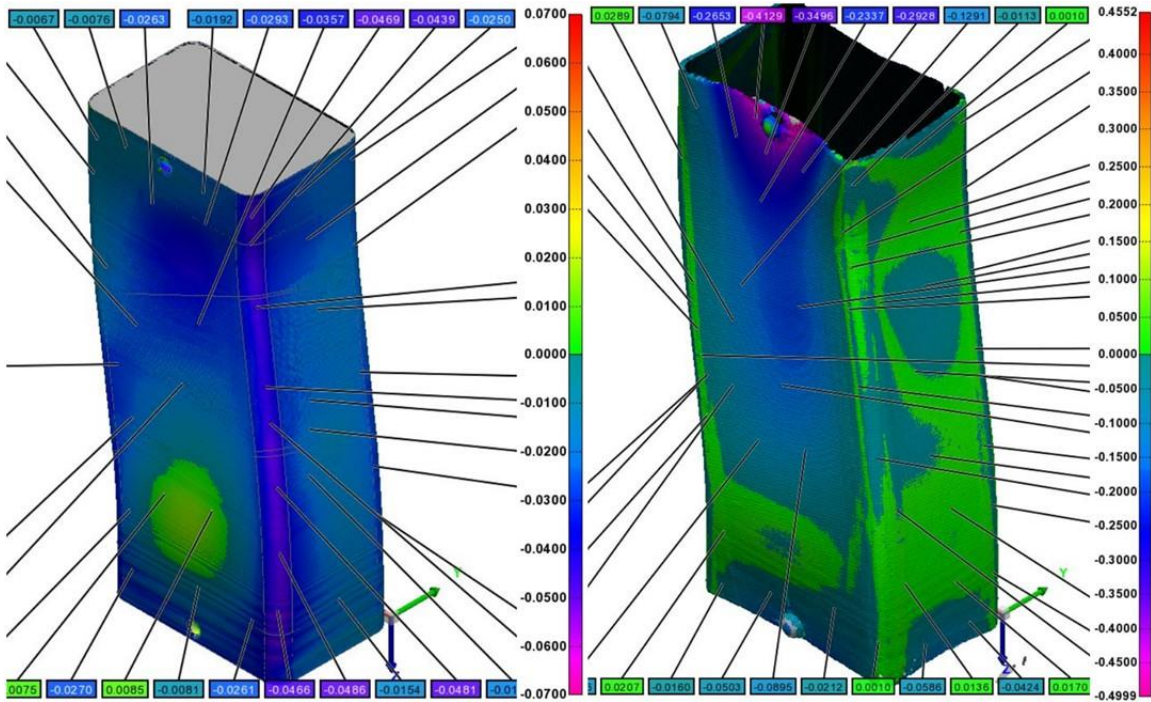


Figure 81 The FaroArm scans of the Thin AQ-180 Duct (6) before (left) and after (right) composite manufacture.

The tool had uniform and undersized geometry by around 0.5mm with a high spot located in a similar region to the prior ducts. The scan of the duct after composite manufacturing had local high regions near the corners that may have been caused by the ply overlaps in those regions. It is unlikely the high regions were caused by the tooling material, given those regions were undersized prior to composite processing. Additionally, one end of the duct performed much worse than the other, deforming as much as 13mm and the other deforming closer to 1.3mm. One possible explanation for this is the vacuum hose could have been resting on this region, and due to the low stiffness of the heated tool it deformed locally. Alternatively, the tool may have been propped up and resting on that location, causing the deformation. However, the exact reason for this inconsistency is unknown.

Extra Thick ST-130 Duct 7

The Extra Thick ST-130 Duct (7) had 12.4mm wall thicknesses and was manufactured in response to the results of the Thick ST-130 Duct (2), which performed relatively well with 6.4mm wall thickness. The extra wall thickness was expected to reduce deformation at 160°C at 414kPa. The size of this tool was adjusted slightly, in that an attempt to account for the prior tools all being undersized. To

make this adjustment, a cross section of the duct was manufactured with standard settings then measured to arrive at scaling factors for each axis that should allow the tool to be accurately sized. These factors were 100.4% along the long edge (x-direction) and 100.1% along the short edge (y-direction). The height of the tool was not changed. The photos of the manufactured duct are shown in figure 82.

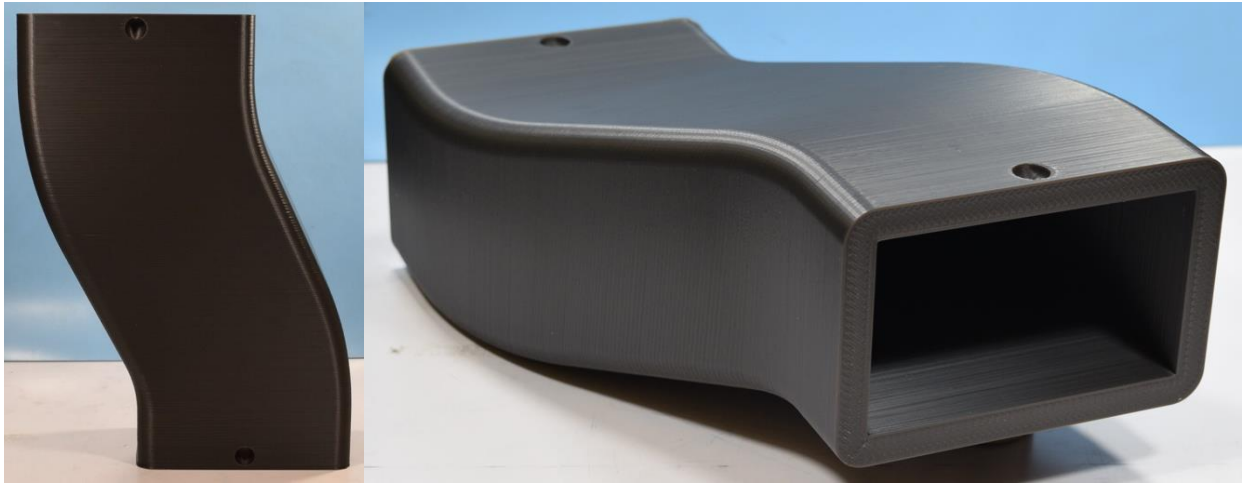


Figure 82 The manufactured Extra Thick ST-130 Tool (7).

The duct in figure 82 had excellent print quality and print time, which came from a combination of new printer modifications. For reference in future endeavors, the settings that were successfully implemented included: upgraded high flow 1mm nozzle, 100% air cooling rate using a Berd air cooling setup, high chamber temperatures of 122°C, retractions of 1.5mm, combing mode set to ‘not in skin’, z-hop of 0.5mm when retracted, 1mm outer wall wipe distance (to hide the z-seam), a 99.9% dense infill (to approximate 100%, while still allowing certain infill settings to be relevant), concentric infill pattern, extruder temperature of 280°C, bed temperature of 140°C, infill speed of 22mm/s, wall speed of 30mm/s, layer thickness of 0.16mm, and infill layer thickness of 0.32mm. The composite that was manufactured on this tool is shown in figure 83.



Figure 83 The composite cured on the Extra Thick ST-130 Tool 7.

The composite that was cured on the Extra Thick ST-130 tool performed well, indicating that tools with thick walls can perform satisfactorily using the vacuum bagging approach, even when used above the T_g 132°C. The long edges of the tool at the ends of the duct did collapse inwards slightly, sharing the same lozenge deformation mode that has been seen previously. This tool was separated from the cured composite by using a Dremel tool to cut the composite into two halves. This allowed the tool to be scanned directly, which allowed for a direct comparison of the tool both before and after composite manufacture as shown in figure 84.

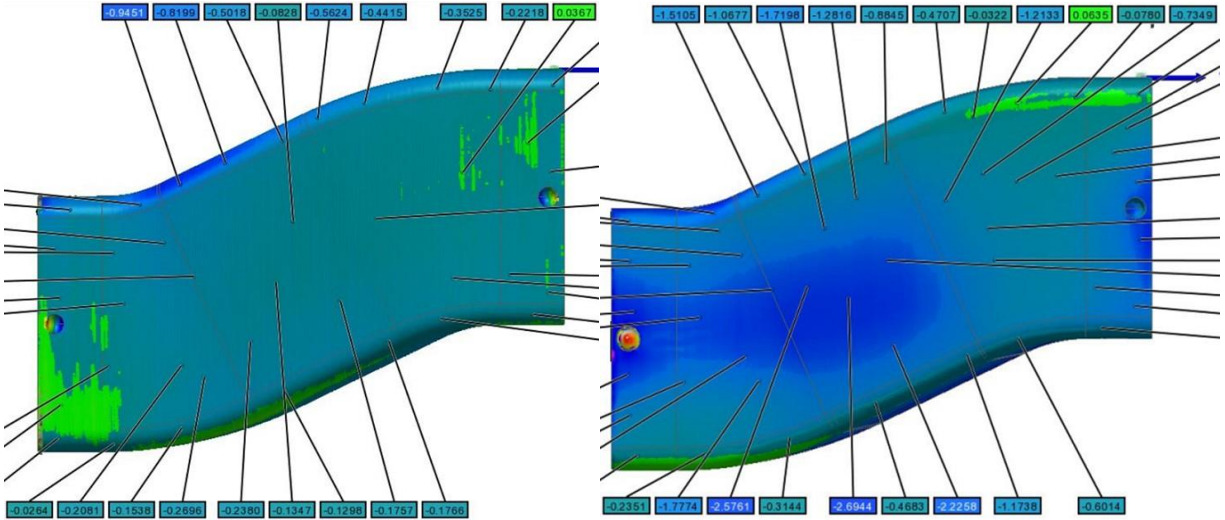


Figure 84 The FaroArm scans of the Extra Thick ST-130 Tool (7) both before (left) and after composite manufacture (right).

In these scans, the tool has been shown to deform, at worst, by around 2.3mm between the two scans. The location of the deformation was in the center of the tool, as well as on the long edges towards the ends of the tool. Deformation at the ends has been seen in most scans of each tool, so this is not surprising.

Low Temperature Thin ST-130 Duct 8

The Low Temperature Thin ST-130 Duct (8) was manufactured to attempt to demonstrate acceptable deformation with a thin wall thickness using ST-130, based on the reduced temperature requirements of 121°C at 345kPa. At these process conditions, prior TPV testing and Truncated Pyramid trials indicated that ST-130, as well as AQ-180, should be able to be successfully scaled to a larger part size with acceptable deformation, which is what this duct was designed to test. The photos of this duct prior to composite manufacture are showed in figure 85.



Figure 85 The manufactured Low Temperature Thin ST-130 Tool (7).

This print had good print quality, with some defects on the internal and external surfaces caused by a lack of retraction. The lack of retraction allowed material to leak out of the extruder during travel moves, resulting in missing material at the start of the following print path, as shown in figure 86.

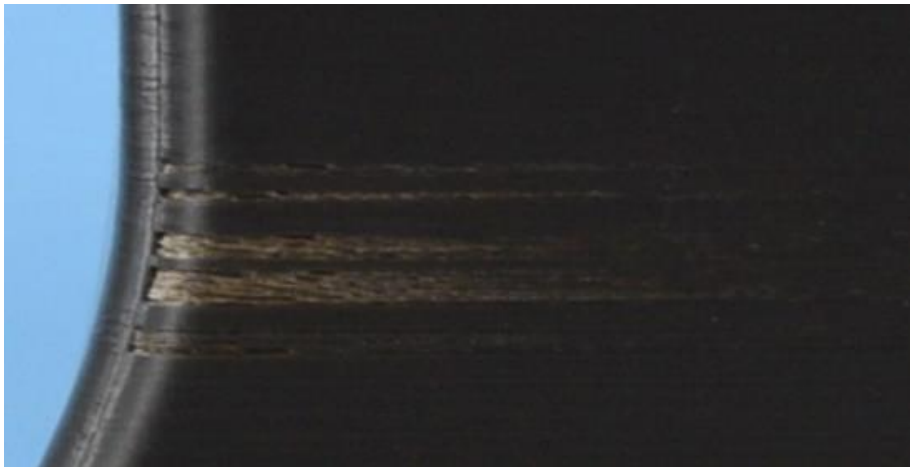


Figure 86 The surface porosity caused by no retractions present on the backside of the tool.

There was also insufficient cooling on the overhanging regions. Initially, the extruder temperature was set to 290°C with a fan speed of 50% using the forced air cooling. This was changed to an extruder temperature of 285°C and fan speed of 100% at a Z-height of approximately 195mm. This defect can be seen clearly in Figure 87, as well as when the fan speed and temperature were changed, improving the quality at that point.

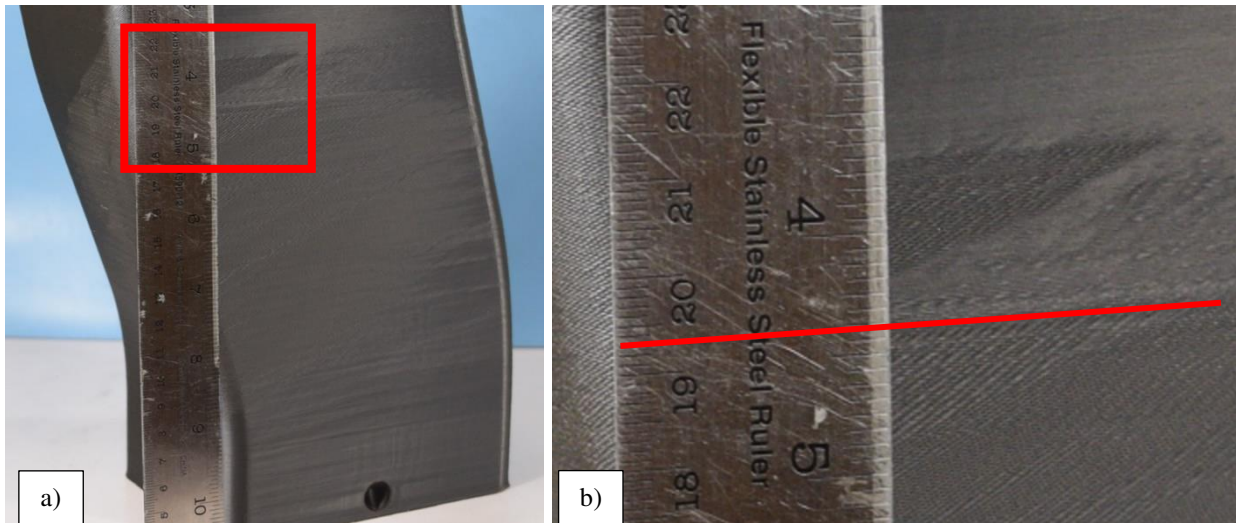


Figure 87 The printing defect caused by insufficient cooling on overhanging regions (a), and the layer position at 195mm where the fan speed and extruder temperature were modified (b).

This print had been completed prior to the Extra Thick ST-130 Tool (7), so these issues were addressed in that print, and in addition the extruder temperature was dropped to 280°C for the manufacture of Tool 7. The composite that was manufactured on this tool used Toray F2673C-07M plain weave prepreg for the 121°C cure and is shown in Figure 88.

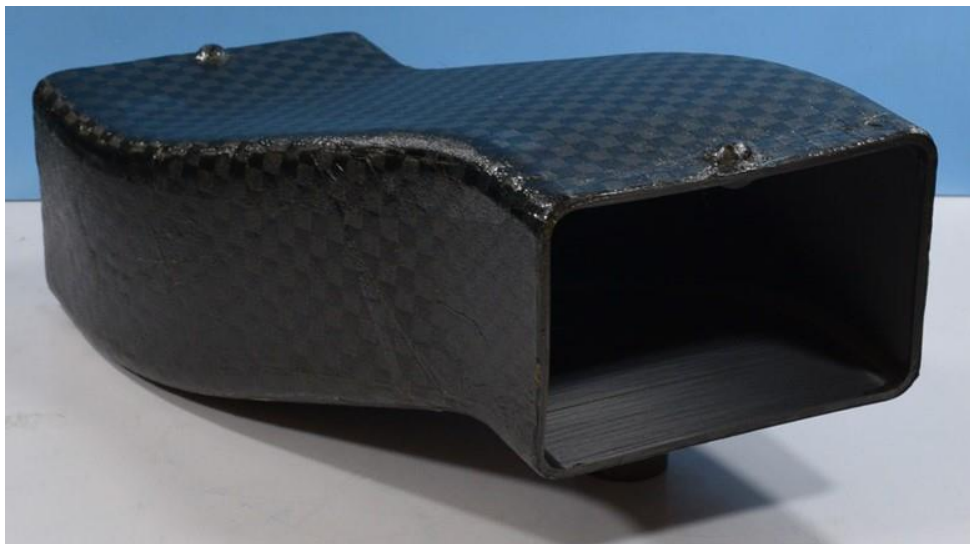


Figure 88 The composite cured on the Low Temperature Thin ST-130 Tool.

The composite that was cured at 121°C for the Low Temperature Thin ST-130 tool performed well compared to the Thin ST-130 Tool (3) that had a 160°C cure. This test indicated again that ST-130

could be used at 121°C with minimal deformation, and that the 160°C used for the Thin ST-130 tool (3) was too high for the stiffness of that tool. Even still, the Low Temperature Thin ST-130 tool presented a slight concaving of the long edges near the ends of the tool. The tool before composite manufacturing, as well as the external scan of the composite with the thickness of the laminate subtracted are shown in figure 89.

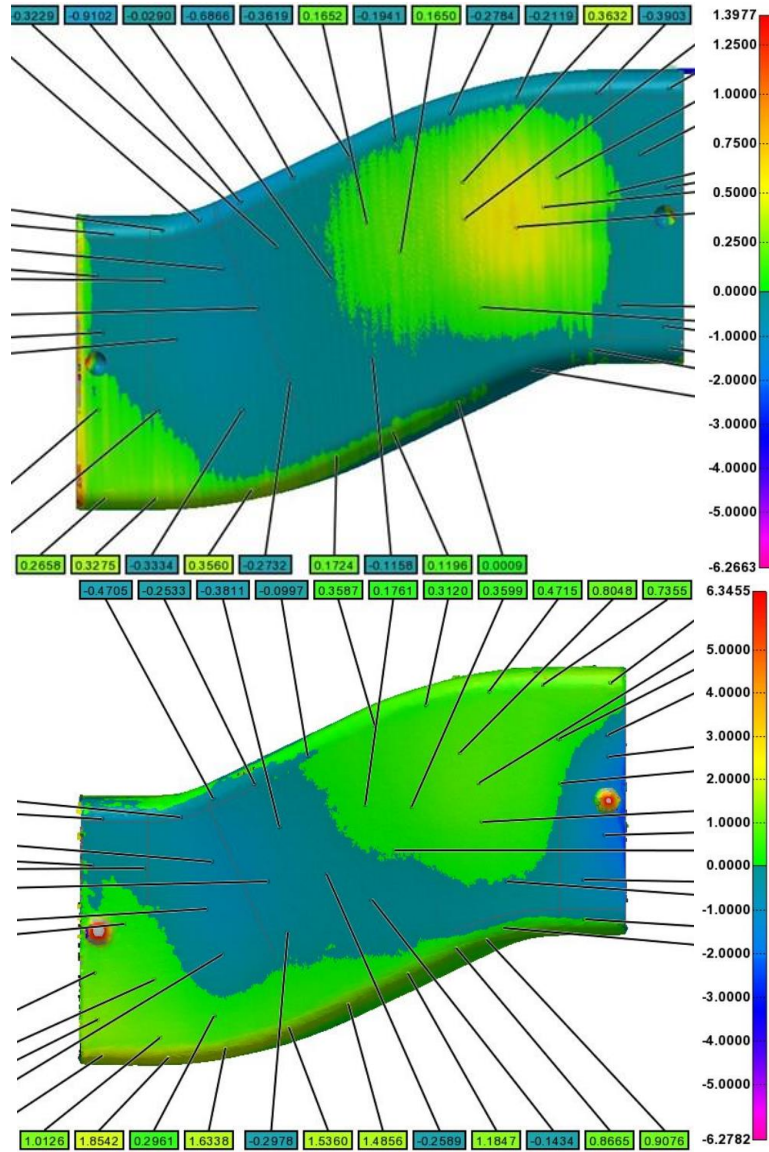


Figure 89 The FaroArm scans of the Low Temperature Thin ST-130 Duct (8) both before (top) and after composite manufacture (bottom).

Direct Comparison of Ducts and Additional Discussion

The as-manufactured 3D geometry of all the ducts showed relative repeatability, along with repeatable deviation from the specified duct geometry. Figure 90 shows the FaroArm scans of tools 3 through 6 after printing, which were all scanned in the same orientation and clearly show the repeatability of the process.

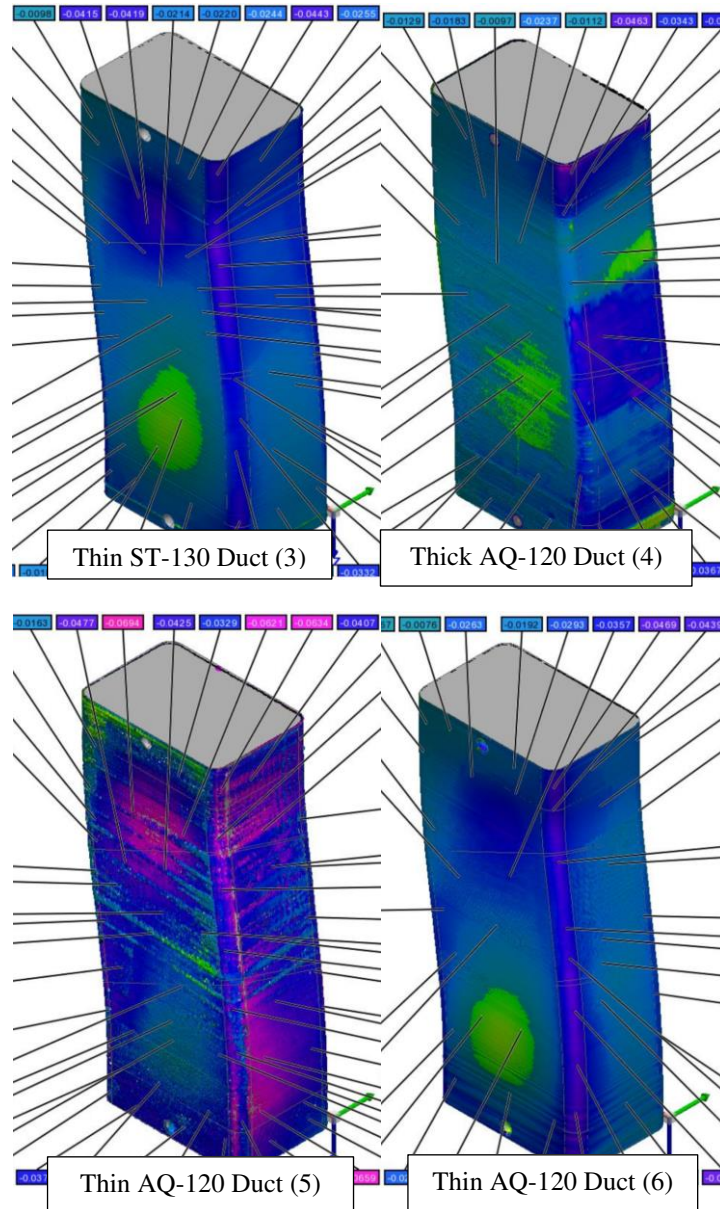


Figure 90 The FaroArm scans of the hollow ducts 3-6. The remaining scans showed similar results but were scanned in different orientations. The entire set of scans can be found in Appendix B.

It does appear that each printed tool was manufactured smaller than desired, especially on corner regions. This is important to note because uniform and consistent geometry deviations are easier to correct than local geometry deviations. The tools that were manufactured within the heated chamber likely changed size in part due to CTE as they cooled and shrank. The tools without a heated environment still appeared small in the FaroArm scan, so it is likely there is some amount of machine error as well, and this is most likely the dominant factor in part size deviation. The most severely undersized tool was the Thin AQ-120 duct (5) shown in figure 90 above. It did not have any significant printing defects; however, its geometry was the most undersized which is likely due to improper printer calibration. It was also noted by Ability Composites that during the 3D scans, the partially transparent surfaces of both AQ-120 tools were difficult to scan with the FaroArm which lead to the granulated appearance of these tools in the scans. In order to address the undersized printed Tools 3-6, Tools 7 and 8 used a scaling factor to increase the size of the ducts in the X and Y directions, parallel to the build surface, by 100.4 and 100.1% respectively. The 3D scan of Tools 7 and 8 prior to composite manufacture are shown in figure 91.

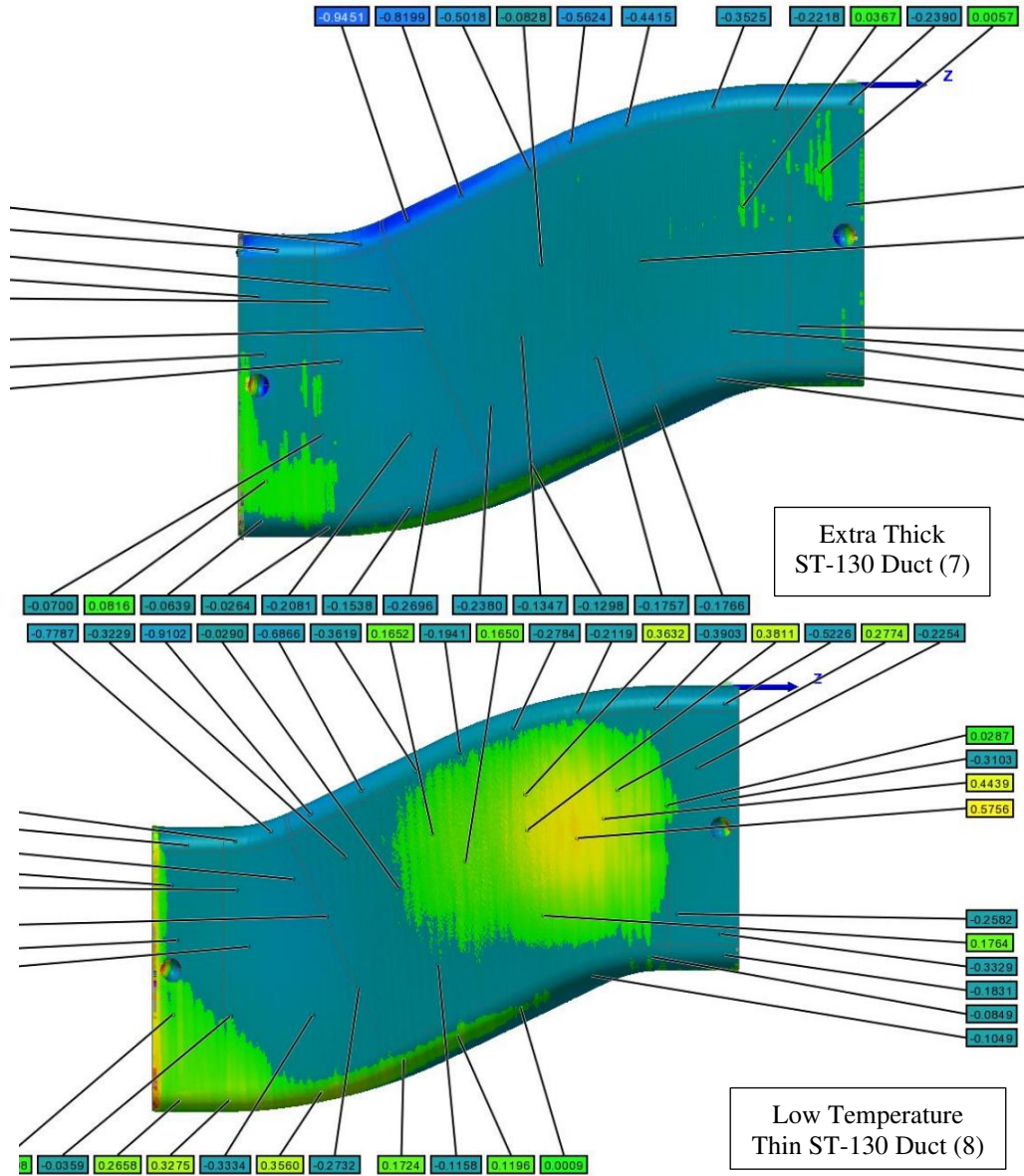
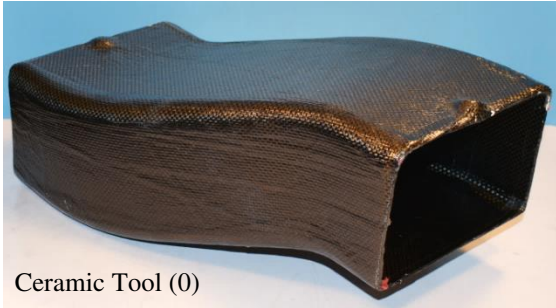


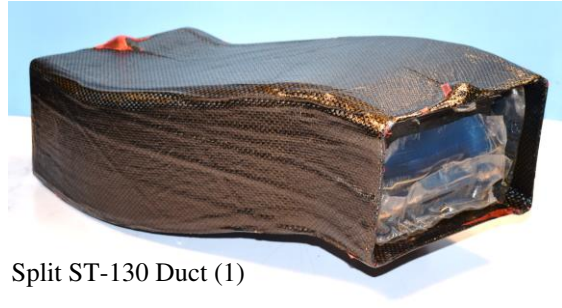
Figure 91 The FaroArm scans for Ducts 7 and 8, which used scaling to adjust the size of the printed geometry.

Both tools 7 and 8 had relatively good agreement with the CAD model. Like previous scans of the tools, the corners on tool 7 were inset from the CAD by about 0.5mm, however the scan of the faces of the tool showed geometry that maintained high accuracy to within approximately +/-0.2mm. Tool 8 stayed within 0.4mm, but did have a region that appeared to protrude from the CAD model by around 0.5mm on the front face. The approach taken to compensate for the size change of the tool using scaling prior to manufacture is useful but may be neglecting other sources of machine error.

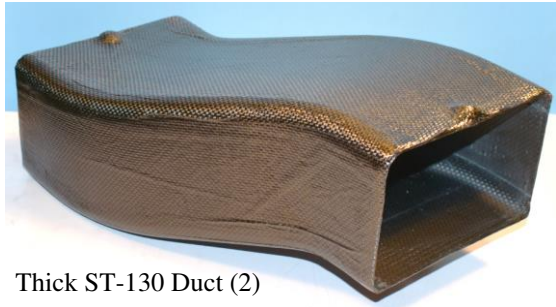
In general, the hollow tools did not fare well during the 160°C cure. The glass transition temperature (T_g) of each material is 132°C for ST-130 and 92°C for AQ-120 and AQ-180. The 160°C cure pushed each material far past its T_g , significantly reducing the stiffness of the tools. Thus, the tools deformed much further than what had been observed in the earlier TPV tests and Truncated Pyramid trials at 121°C. The deformation was present for all tools, but minimal for the Extra Thick ST-130 tool (7) and the Low Temperature Thin ST-130 tool (8). Photographs of each cured composite are shown in Figure 92.



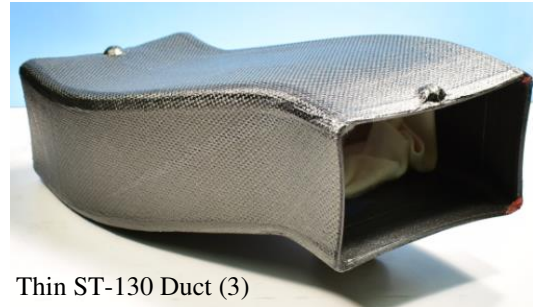
Ceramic Tool (0)



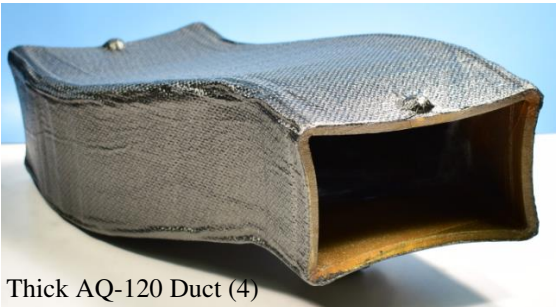
Split ST-130 Duct (1)



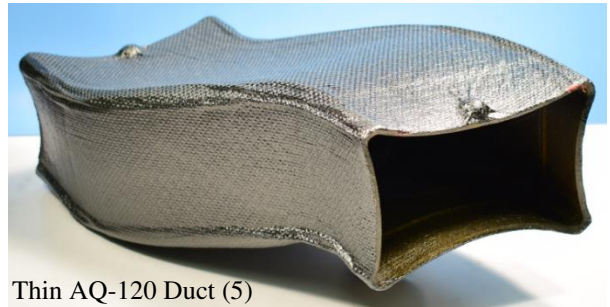
Thick ST-130 Duct (2)



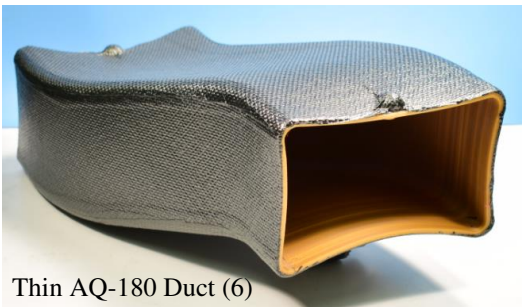
Thin ST-130 Duct (3)



Thick AQ-120 Duct (4)



Thin AQ-120 Duct (5)



Thin AQ-180 Duct (6)



Extra Thick
ST-130 Duct (7)



Low Temperature
Thin ST-130 Duct (8)

Figure 92 The photograph of each cured duct can be compared for deformation.

The Extra Thick ST-130 tool utilized the higher 160°C autoclave process temperature but was manufactured with 12.4mm thick walls. This extra thickness improved the stiffness enough that deformation was minimized to within 2.3mm. The Low Temperature Thin ST-130 tool was used in a 121°C autoclave process temperature, which was a temperature that the material was expected to survive at. Even still, this tool presented a small amount of deformation, indicating that process temperature, material type, and tool thickness should all be carefully considered if composite tooling is to be used near the T_g of the tooling material.

A comparison of the FaroArm scans of the outer surfaces of each composite and the associated deformations is provided in figure 93. The composite was left on the tool and the thickness of the laminate was subtracted for comparison in all cases, except for Duct 7, which had the composite removed so that the scan is of the tool after composite processing.

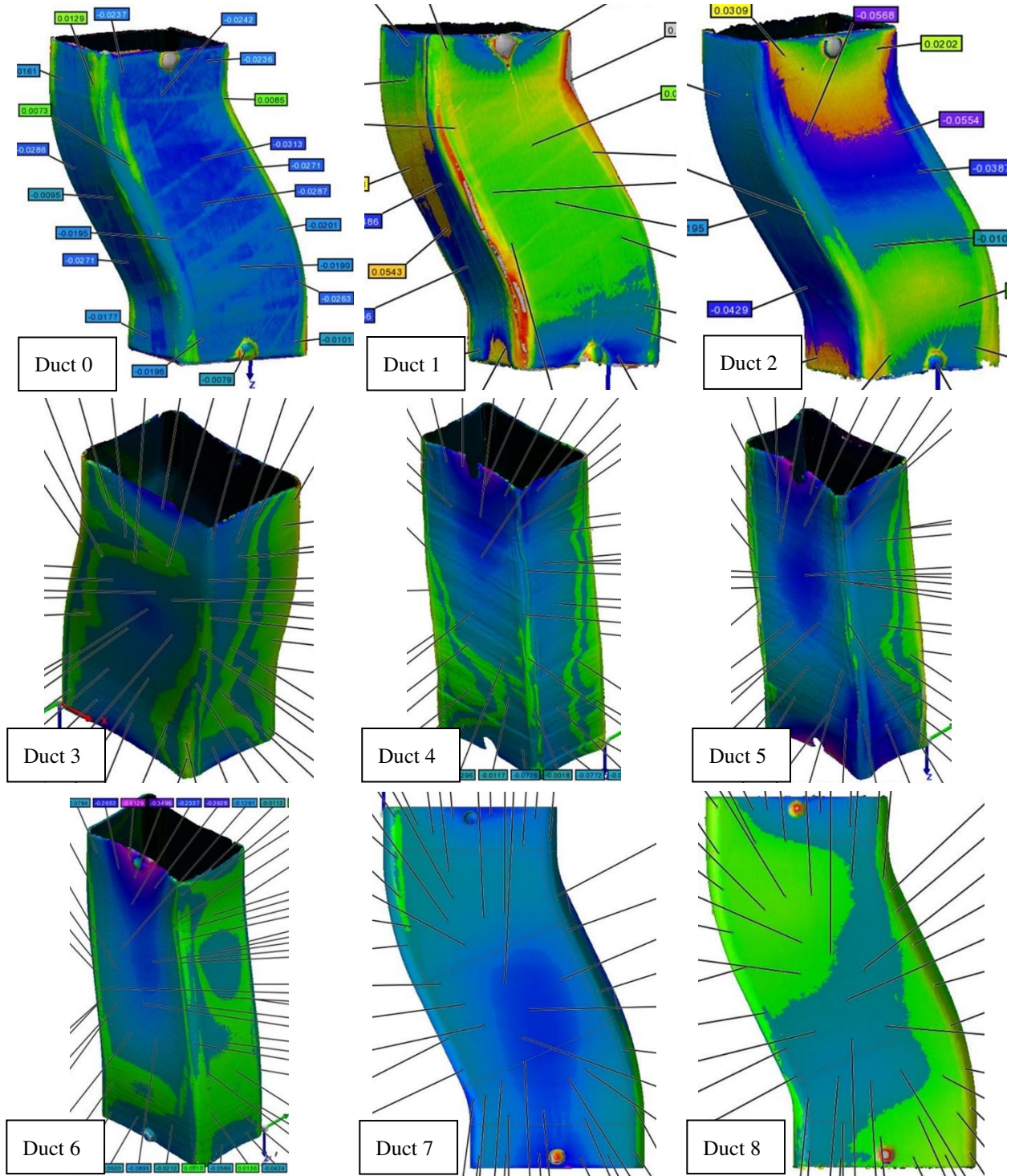


Figure 93 The FaroArm scans of the ducts after composite processing.

In the 3D scans of the composites after processing, the scale bars did not use the same color representation, so the above figure does not represent relative deformation between ducts. However, the

general trends show that the corner regions of the composite ducts had extra thick corners due to the composite laminate. Additionally, the edges at the ends of each duct seem to cave towards the center of the tool, indicating that these unsupported edges are the most sensitive to loading condition. This was especially true of the long edges, as the extra span length increases the total deflection.

The FaroArm scanning technique used for all ducts except Duct 7 had shortcomings related to the scan approximating the tool surface through the composite part. Had the scan been completed on the outside of the tool rather than the composite, the representation of the tool would have been more accurately captured. However, for most of these scans, features like the PTFE tape, the overlapping plies in the corner regions, and wrinkles appear in the scan making the results less clear. The lozenge deformation mode can be clearly seen in the cross-sectional view of the ends of each duct in figure 94.

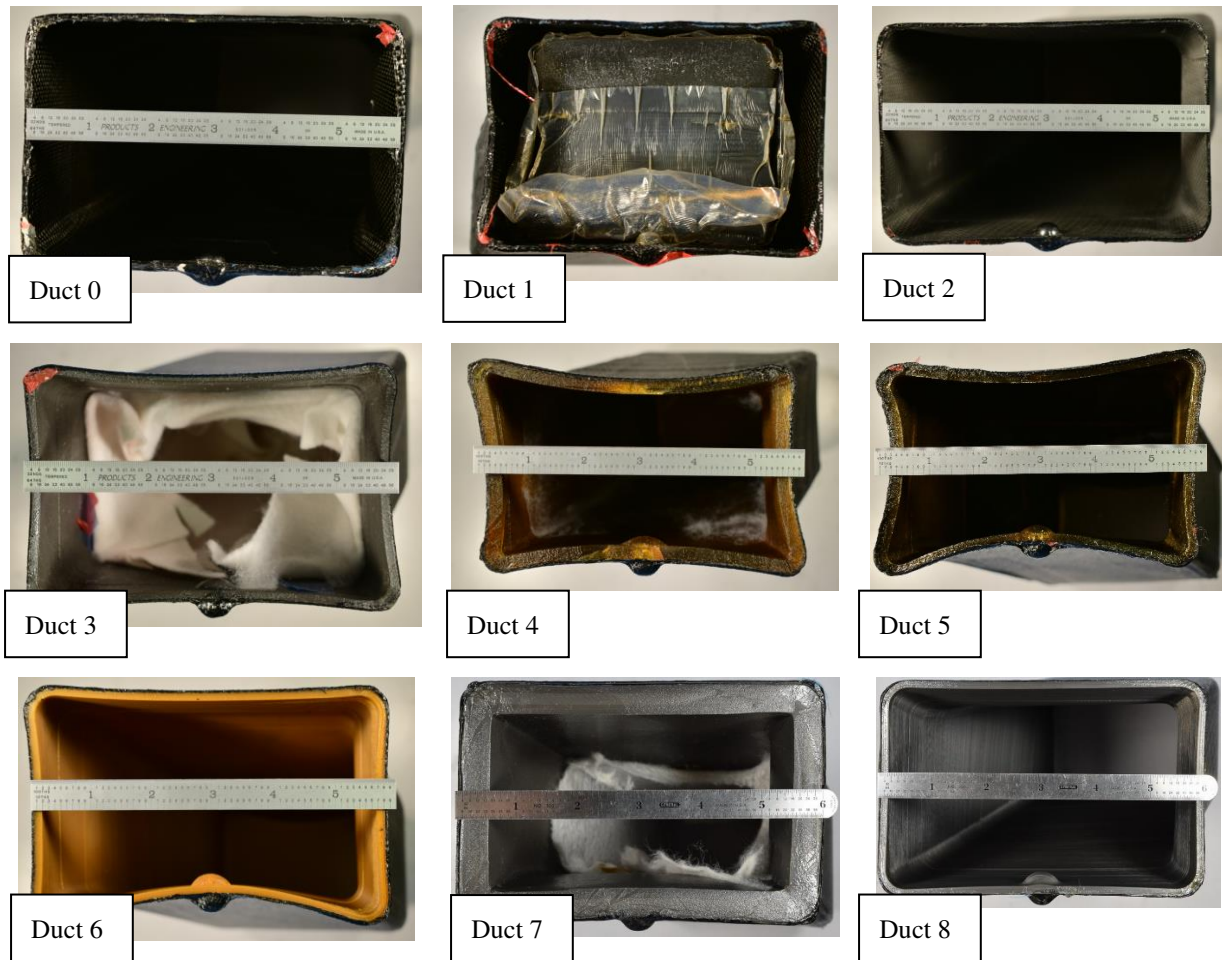


Figure 94 Views showing relative distortions of the manufactured ducts 0-8.

In a comparison of ducts 0-7 that were manufactured using 160°C cure temperature and 414 kPa (60 psi) pressure, the Control Duct (0) performed the best. Following this, the Extra Thick ST-130 duct (7) with 12.4mm wall thickness and the Thick ST-130 duct (2) with 6.4mm wall thicknesses were also very good. The performance of the Extra Thick ST-130 Duct (7) was one of the most stable 3D printed ducts due to the increased tool wall thickness and the use of ST-130, the material with the highest T_g and HDT that was evaluated. The deformation seen as the thickness increased seemed to go down, indicating that similar composite structures made using 3D printed tools should use increased tool thicknesses to support composite cures at temperatures of 160°C at 414kPa. The Low Temperature ST-130 Duct (8) performed well, and at reduced temperatures tools can be made much thinner to reduce material usage and print time.

While the vacuum bagging scheme used seemed to significantly improve results, the assumption that the tools did not experience any unequal loading was incorrect. The cause of the lozenge mode of deformation had previously been assumed to do with bridging on the internal vacuum bag, however bridging was not observed during the manufacturing of tools 3-8, and pleats of excess bagging material were left near the internal corners to prevent bridging. One possible cause of this deformation and deformation mode may be due to unequal distribution of pressure on the internal and external surfaces of the vacuum bag, leading to a greater net force applied to the external surface of the tool. For a 12.4mm thick tool, the net force was shown previously to be around 20% greater on the outside than the inside surface of the tool using equations 1.1-1.3. Additionally, after the applied thickness of the vacuum bagging materials, the difference between the outer and inner surface areas of the tool become even greater. However, the hollow tooling approach was still very valuable because it allowed a reduction in structural requirements and improved the manufacturing process. The benefits of this approach included: (i) a reduction of the visibility of 'stair stepping' caused by discrete layer heights over the gradually sloped surface of the split duct geometry; (ii) the elimination of the need to bond two halves of the duct together; and (iii) the reduction in print time and weight. Most importantly, it was demonstrated that by removing the infill regions and enveloping the tool using vacuum bagging on both inner and outer tool surfaces, there would be less tendency to collapse due to processing temperatures that exceeded the maximum use temperature of the tooling materials.

The results of this testing indicate that 3D printed tooling seems to be a reasonable approach for lower temperature and pressure curing prepreg material systems. To reduce deformation to a minimum, the cure temperature should be limited to lower than the T_g of the material, and the tool should use as high of thicknesses as is reasonable to maintain sufficient stiffness during cure. For this study, autoclave cure cycles should be limited to 121°C (250 °F) and 345 kPa (50 psi) or less for ST-130 and AQ-180, as indicated by the earlier Temperature Pressure Vacuum trials and the results of the complex tooling studies. Ducts should be printed in a hollow configuration so that their print time and material usage is

reduced, and the bagging material can be applied to both the inside and outside of the tool resulting in an improved loading condition. The sum of these studies indicated that ST-130 and AQ-180 could be used up to 121°C at 345kPa with vacuum bagging surrounding the tool on the inside and outside, even with low wall thicknesses and partially dense infill structures. However, if processing conditions are elevated above the T_g of the materials, like the 160°C cure completed for the ducts, tools with increased thicknesses should be used to prevent deformation.

CHAPTER 6: CONCLUSIONS

The desire to move toward rapid manufacture of tooling for the processing of composite parts is complimented well by the benefits of additive manufacturing. As an alternative to CNC machining or casting traditional ceramic washout molds, 3D printing of molds using dissolvable thermoplastic materials may be valuable for complex shapes produced in low volumes. The benefits of AM of molds relate to the low cost of geometric complexity and the ability to address several of the drawbacks of traditional ceramic molds. Ceramic molds by nature are often brittle and monolithic, making them slow to heat up. Additionally, the surfaces are porous and require a sealing step to prevent resin ingress during cure. Additively manufactured molds can be thin walled and faster to heat than monolithic, ceramic molds, and thermoplastics are typically less brittle. Additionally, secondary sealing steps are not needed as the printed surfaces prevent resin ingress. AM also has the advantage of being able to easily add useful features to the design, such as fiduciary markings, channels for dissolution, and integrated heating channels in the mold. For example, in this work an interconnected gyroid internal structure was used that allows dissolution media to pass through the entire volume of a tool, allowing a reduction in washout times. Finally, it was shown that AM tools can be used at temperatures up to 40°C above their use temperature by using a vacuum bagging scheme that passes the bag through the inside and outside of the tool, allowing nominally equal autoclave pressure induced force. This was demonstrated with deformation limited to 2-3mm or less, which may be sufficient for many low volume or prototyping situations.

Temperature Pressure Vacuum (TPV) studies were completed for both material and structural evaluation. Of the dissolvable candidate materials examined, the most successful tooling material, from a geometric fidelity standpoint, was Stratasys ST-130. However, it also requires a basic solution for washout, and it has a high CTE that requires careful incorporation into tool design to generate accurate dimensions in the final composite part. Infinite Material Solutions AquaSys 180 was also identified as a successful dissolvable tooling material, but it was slightly less robust than ST-130. However, it can be dissolved in water and has a lower CTE. AquaSys 180, in circumstances where slightly lower

temperature cure cycles are permissible, may be preferable to ST-130 due to the water solubility. Additionally, moving to higher infill densities or solid structures may extend the composites processing window to limit deformation. The greatest challenge for manufacturing tooling from ST-130 and AQ-180 was the need for a heated build chamber that could approach the glass transition temperatures of the materials to avoid distortion. Additionally, all the soluble feedstocks tested were sensitive to moisture absorption, so careful feedstock handling practices were developed. The TPV tests also indicated that the most important parameter for controlling the robustness of partially dense tooling was infill density. Gyroid infill pattern was determined to be a great infill pattern from both a thermal stability and a washout perspective, due to the interconnected structure that would allow dissolution media to flow through the entire part.

The dissolution studies included AQ-120, AQ-180, ST-130, and the conventional washout material, Solecore 100. The conventional washout material could be removed from a composite duct with little effort using hand tools after soaking the washout material in water for several hours. By drilling a hole in an AQ-180 sample, it was shown that the gyroid infill could successfully be flooded, greatly reducing the washout time. The ST-130 washout approach used a trisodium phosphate solution, but this was extremely time consuming and future trials including WaterWorks or EcoWorks may improve washout times.

The results of curing composites on the Truncated Pyramid Tools showed that the tool remained rigid enough to support the composite during the 121°C at 345kPa cure. The tool was printed with deviations from the nominal geometry limited to approximately +/-0.4 mm (0.015”) and deformations due to composite processing were negligible. The deviations from the nominal part geometry were likely caused by a combination of 3D printer inaccuracy and CTE driven deformation during cooldown. It was seen that the surface geometry and roughness of the tool transferred to the cured part. The use of surface smoothing showed a small improvement in the molded surface of cured composites, but holds promise for improving the surface finish of completed parts.

The complex bent duct tooling studies required cure conditions of 160°C at 414kPa, which far exceeded the capabilities of the 3D printed mold materials in this study. A partially dense mold was first manufactured, which failed catastrophically during autoclave processing by collapsing inwards. However, this spurred the development of a hollow mold configuration with 100% dense walls that, as compared to the partially dense mold, had numerous benefits. This new approach provided significant savings in manufacturing time and material usage, even with reduced layer heights that improved the surface finish of the mold and composite. By moving from the partially dense tool to hollow tools with wall thicknesses equal to 3.2mm, 6.4mm, and 12.4mm, time savings of 65%, 42%, and 23%, respectively were seen. Additionally, the hollow construction allowed a nearly equal autoclave pressure induced load that significantly reduced the mold structural requirements and enabled satisfactory composite part production. This was most successful with thick-walled ST-130 molds, where the autoclave temperature was nearly 40°C higher than the HDT of ST-130 but mold deformation was still limited to less than 2.5mm. The successful manufacture of composite parts with limited mold deformation at elevated temperatures could be sufficient for many applications. In this study, it was found that the wall thickness, cure temperature, and material selection are all important parameters for the mold rigidity during cure.

Overall, this research demonstrated that commercially available dissolvable 3D printing materials exist that can be used to produce washout 3D printed molds capable of performing well during prepreg composite fabrication under autoclave conditions approaching 121°C (250°F) and 345kPa (50psi) with minimal deformation. Both AquaSys 180 and ST-130 were found to perform similarly with equal wall thicknesses. However, ST-130 showed slightly less deformation but also required washout in an 80°C 11-13pH solution, whereas AquaSys 180 used 80°C water which may be advantageous for concerns related to disposal and handling. Additionally, it was found that a secondary machining or sealing step was not required prior to composite manufacture, which is a significant advantage over traditional washout tooling materials. For duct-like geometries used at temperatures far exceeding the use temperature of the material, it was found that thick-walled hollow tools create nominally equal force on

the inner and outer surfaces of the tool which prevents deformation, and the hollow construction reduces the washout time, material usage, and manufacturing time. The hollow tooling approach also provides faster heat-up rates in autoclave processes. While this structural configuration showed an improved performance at temperatures that far exceed the material use temperature, there is still a need for highly structural tools. A manufacturer should carefully consider the mold material, structural integrity, infill density, infill pattern, cure temperature, CTE, thermal stability, and vacuum bagging approach in order to ensure the geometric fidelity of the printed tool. Using additive manufacturing of dissolvable thermoplastics may provide an excellent option for manufacturers when low volumes of complex washout tools are required, alleviating many of the challenges related to traditional washout tooling.

REFERENCES

- [1] S.-J. Park, Carbon Fibers, Singapore: Springer Nature Singapore Pte Ltd., 2018.
- [2] B. K. Post, B. Richardson, R. Lind, L. J. Love, P. Lloyd, V. Kunc, B. J. Rhyne, A. Roschli, J. Hannan, S. Nolet, K. Veloso, P. Kurup, T. Remo and D. Jenne, "Big Area Additive Manufacturing Application in Wind Turbine Molds," in *International Solid Freeform Fabrication Symposium - An Additive Manufacturing Conference*, Austin, 2017.
- [3] T. G. Gutowski, Advanced Composites Manufacturing, New York: John Wiley & Sons, Inc, 1997.
- [4] P. Malnati, "Composites World," 2 February 2021. [Online]. Available: <https://www.compositesworld.com/articles/invar-wire-additive-manufacturing-expand-aerocomposite-tooling-options>. [Accessed 23 February 2022].
- [5] D.-A. Turk, A. Ebnother, M. Zogg and M. Meboldt, "Additive Manufacturing of Structural Cores and Washout Tooling for Autoclave Curing of Hybrid Composite Structures," *Journal of Manufacturing Science and Engineering*, vol. 140, no. 10, 2018.
- [6] D.-A. Turk, R. Kussmaul, M. Zogg, C. Klahn, B. Leutenecker-Twelsiek and M. Meboldt, "Composites Part Production with Additive Manufacturing Technologies," *Procedia CIRP*, vol. 66, pp. 306-311, 2017.
- [7] M. Wallen, J. Rossfeldt, C. Aune and Z. N. Wing, "Flexible Manufacturing of Hollow Composites Via Soluble Tooling," in *SAMPE*, Long Beach, 2013.

- [8] E. J. Thompson, *Design of a Multi-Piece Removable Mandrel Mold Tool to Fabricate and Control Inner Mold Surface Contour of Composite Wing Spar*, Morgantown: The Research Repository @ WVU, 2010.
- [9] S. Alam, G. R. Yandek, R. C. Lee and J. M. Mabry, "Design and development of a filament wound composite overwrapped pressure vessel," *Composites Part C: Open Access*, vol. 2, no. 100045, 2020.
- [10] C. Pfladderer, S. Shewchuk, C. Nelsen, E. Loiacono, T. Margraf and M. Matlack, "Performance and Durability Assessment of Shape Memory Polymer Tools for Closed Composite Structures," in *SAMPE neXus Proceedings*, 2021.
- [11] Easy Composites Ltd, "How to Make Complex Split/Multi-Part Mould for Composites," 2022. [Online]. Available: <https://www.easycomposites.co.uk/learning/how-to-make-complex-multi-part-split-moulds>. [Accessed 6 June 2022].
- [12] Z. N. Wing and R. K. Vaidyanathan, "Evaluation of Out of Autoclave Composite Properties Manufactured From Soluble Self-Pressurizing Tooling," in *SAMPE*, Long Beach, 2016.
- [13] D.-A. Turk, L. Triebe and M. Meboldt, "Combining Additive Manufacturing with Advanced Composites for Highly Integrated Robotic Structures," *Procedia CIRP*, vol. 50, pp. 402-407, 2016.
- [14] A. Bandyopadhyay and S. Bose, *Additive Manufacturing*, Boca Raton: CRC Press, 2016.
- [15] Stratasys, "3D Learning Content Glossary," Stratasys.

- [16] ASTM International, *Standard Terminology for Additive Manufacturing Technologies*, West Conshohocken: ASTM International, 2013.
- [17] V. Kunc, A. A. Hassen, J. Lindahl, S. Kim, B. Post and L. Love, "Large Scale Additively Manufactured Tooling for Composites," in *SAMPE Japan*, Tokyo, 2017.
- [18] T. Duda and L. V. Raghaven, "3D metal printing technology: the need to re-invent design practice," *AI & Society*, no. 33, pp. 241-252, 2018.
- [19] M. Leschok and B. Dillenburger, "Dissolvable 3DP Formwork," in *ACADIA*, Austin, 2019.
- [20] S. E. Doyle and E. L. Hunt, "Dissolvable 3D Printed Formwork," in *ACADIA*, Austin, 2019.
- [21] I. Mitropoulou, M. Bernhard and B. Dillenburger, "Nonplanar 3D Printing of Bifurcating Forms," *3D Printing and Additive Manufacturing*, vol. 00, no. 00, 2021.
- [22] H.-C. Song, N. Ray, D. Sokolov and S. Lefebvre, "Anti-aliasing for fused filament deposition," *Computer-Aided Design*, vol. 89, no. 8, pp. 25-34, 2017.
- [23] M. K. Thompson, G. Moroni, T. Vaneker, G. Fadel, I. R. Campbell, I. Gibson, A. Bernard, J. Schulz, P. Graf, B. Ahuja and F. Martina, "Design for Additive Manufacturing: Trends, opportunities, considerations, and constraints," *CIRP Annals*, vol. 65, no. 2, pp. 737-760, 2016.
- [24] P. Ohldin, "Series Production of CE-Certified Orthopedic Implants with Integrated Porous Structures for Improved Bone Ingrowth," in *21st International DAAAM Symposium*, Zadar, 2010.

- [25] C. Tosto, A. Latteri, E. Pergolizzi, D. Giordano, G. Abramo, R. Catenaro, N. Pignotti and G. Cicala, "Additive Manufacturing of Plastics: An Efficient Approach for Composite Tooling," *Macromolecular Symposia*, vol. 389, no. 1, 2020.
- [26] E. M. Sachs, J. S. Haggerty, M. J. Cima and P. A. Williams, "Three-dimensional printing techniques". United States Patent 5,204,055, 20 April 1993.
- [27] ExOne, "Sand 3D Printers," [Online]. Available: <https://www.exone.com/>. [Accessed 26 February 2022].
- [28] B. Shassere, A. Nycz, M. W. Noakes, C. Masuo and N. Sridharan, "Correlation of Microstructure and Mechanical Properties of Metal Big Area Additive Manufacturing," *Applied Sciences*, vol. 9, 2019.
- [29] F. Calignano, D. Manfredi, E. P. Ambrosio, S. Biamino, M. Lombardi, E. Atzeni, A. Salmi, P. Minetola, L. Iuliano and P. Fino, "Overview on Additive Manufacturing Technologies," *Proceedings of the IEEE*, vol. 105, no. 4, pp. 593-612, 2017.
- [30] M. Pagac, J. Hajnys, Q.-P. Ma, L. Jancar, J. Jansa, P. Stefek and J. Mesicek, "A Review of Vat Photopolymerization Technology: Materials, Applications, Challenges, and Future Trends of 3D Printing," *Polymers*, vol. 13, no. 4, pp. 598-618, 2021.
- [31] M. Biedermann, M. Widmer and M. Meboldt, "Additive Manufactured Break-Out Cores for Composite Production: A Case Study with Motorcycle Parts," in *Munich Symposium on Lightweight Design*, Munich, 2020.

- [32] D.-A. Turk, H. Einarsson, C. Lecomte and M. Meboldt, "Design and Manufacturing of High-Performance Prostheses with Additive Manufacturing and Fiber-Reinforced Polymers," *Production Engineering*, no. 12, pp. 203-213, 2018.
- [33] C. Tosto, A. Latteri, E. Pergolizzi, D. Giordano, G. Abramo, R. Catenaro, N. Pignotti and G. Cicala, "Additive Manufacturing of Plastics: An Efficient Approach for Composite Tooling," *Macromolecular Symposia*, vol. 389, no. 1, p. 1022, 2020.
- [34] Stratasys, "FDM Sacrificial Tooling for Composite Part Fabrication," 2017. [Online]. Available: www.stratasys.com. [Accessed 21 February 2022].
- [35] G. Cicala, C. Tosto, G. Recca and A. Patti, "Additive Manufacturing Processing of Plastics for Mass Production of Composites Tooling: Technical and Economic Analysis," *Macromolecular Symposia*, vol. 395, 2021.
- [36] UMaine News, "umaine.edu," 10 October 2019. [Online]. Available: <https://umaine.edu/news/blog/2019/10/10/umaine-composites-center-receives-three-guinness-world-records-related-to-largest-3d-printer/>. [Accessed 28 February 2022].
- [37] Thermwood, "LSAM - Large Scale Additive Manufacturing," [Online]. Available: https://www.thermwood.com/lam_home.htm#moreinfo. [Accessed 28 February 2022].
- [38] V. Kunc, J. Lindahl, R. Dinwiddie, B. Post, L. Love, C. Duty, M. Matlack, R. L. Fahey Jr. and A. A. Hassen, "Investigation of In-Autoclave Additive Manufacturing of Composite Tooling," in *CAMX*, Anaheim, 2016.

- [39] J. N. Strickland, P. S. Martinez, A. Noel, P. Nolan, A. Cheung and D. Ursenbach, "Design, Analysis, and Manufacturing of a Fiber Reinforced Composite Hard Upper Torso for the Exploration Space Suit," in *SAMPE*, Long Beach, 2021.
- [40] T. Schniepp, "Additively Manufactured Composite Tooling," Stratasys, Eden Prairie, 2017.
- [41] Omnexus - The material selection platform, "HDT @0.46Mpa (67psi)," 2022. [Online]. Available: <https://omnexus.specialchem.com/polymer-properties/properties/hdt-0-46-mpa-67-psi#PE-PL>. [Accessed 10 June 2022].
- [42] L. J. Love, V. Kunc, A. M. Elliott, B. K. Post, R. J. Smith and C. A. Blue, "The importance of carbon fiber to polymer additive manufacturing," *Journal of Materials Research*, vol. 29, no. 17, pp. 1893-1898, 2014.
- [43] A. M. Baker, J. McCoy, B. S. Majumdar, B. Rumley-Ouellette, J. Wahry, A. N. Marchi, J. D. Bernardin and D. Spornjak, "Measurement and Modelling of Thermal and Mechanical Anisotropy of Parts Additively Manufactured Using Fused Deposition Modelling (FDM)," in *Eleventh International Workshop on Structural Health Monitoring*, Stanford, 2017.
- [44] P. Pibulchinda, E. Barocio and B. R. Pipes, "Influence of Fiber Orientation on Deformation of Additive Manufactured Composites," in *CAMX - The Composites and Advanced Materials Expo*, Dallas, 2021.
- [45] A. A. Hassen, A. Lambert, J. Lindahl, D. Hoskins, C. Duty, S. Simunovic, C. Chin, V. Oancea, L. Love, V. Kunc and S. Kim, "Simulation Assisted Design for an Additively

Manufactured Autoclave Tool Accounting for an Anisotropic Expansion," in *CAMX - The Composites and Advanced Materials Expo*, Anaheim, 2019.

- [46] W. J. Swanson, P. W. Turley, P. J. Leavitt, P. J. Karwoski, J. E. LaBossiere and R. L. Skubic, "High temperature modeling apparatus". United States of America Patent 6722872, 20 April 2004.
- [47] S. Maidin, J. H. U. Wong, A. S. Mohamed and S. B. Mohamed, "Effect of Vacuum Assisted Fused Deposition Modeling on 3D Printed ABS Microstructure," *International Journal of Applied Engineering Research*, vol. 12, no. 1, pp. 4877-4881, 2017.
- [48] V. Kishore, C. Ajinjeru, A. Nycz, B. Post, J. Lindahl, V. Kunc and C. Duty, "Infrared preheating to improve interlayer strength of big area additive manufacturing (BAAM) components," *Additive Manufacturing*, vol. 14, pp. 7-12, 2017.
- [49] A. Uthaman, G. Xian, S. Thomas, Y. Wang, Q. Zheng and X. Liu, "Durability of an Epoxy Resin and Its Carbon Fiber-Reinforced POLYmer COMposite upon Immersion in Water, Acidic, and Alkaline Solutions," *Polymers*, vol. 12, no. 3, 2020.
- [50] A. Amaro, P. Reis, M. Neto and C. Louro, "Effects of Alkaline and Acid Solutions on Glass/Epoxy Composites," *Polymer Degredation and Stability*, vol. 98, no. 4, pp. 853-862, 2013.
- [51] Infinite Material Solutions, "Water-Soluble Support Materials," 2021. [Online]. Available: <https://infinitematerialsolutions.com/us/en/support-materials>. [Accessed 1 March 2022].

- [52] Prusa Research, "Rep Rap Calculator," [Online]. Available: https://blog.prusa3d.com/calculator_3416/. [Accessed 31 May 2022].
- [53] J. Halladay, "Guide to Sealing Additive Manufacturing Porosity," 4 July 2020. [Online]. Available: <https://www.spotlightmetal.com>. [Accessed 19 February 2022].
- [54] A. A. Hassen, J. Lindahl, X. Chen, B. Post, L. Love and V. Kunc, "Additive Manufacturing of Composite Tooling Using High Temperature Thermoplastic Materials," in *SAMPE*, Long Beach, 2016.
- [55] A. Mass, "thingiverse," 9 September 2018. [Online]. Available: <https://www.thingiverse.com/thing:3091560>. [Accessed 19 January 2022].
- [56] F. Lora, "Thingiverse," 10 February 2019. [Online]. Available: <https://www.thingiverse.com/thing:3419869>. [Accessed 19 January 2022].
- [57] D. H, "Thingiverse," 21 February 2018. [Online]. Available: <https://www.thingiverse.com/thing:2802474>. [Accessed 19 January 2022].
- [58] ABB, "Product Specification - IRB 4600," 2021.
- [59] Creality, "Ender-3 Pro 3D Printer," [Online]. Available: <https://www.creality.com/goods-detail/ender-3-pro-3d-printer>. [Accessed 20 February 2022].
- [60] D. Ahlers, F. Wasserfall, N. Hendrich and J. Zhang, "3D Printing of Nonplanar Layers for Smooth Surface Generation," in *IEEE 15th International Conference on Automation Science and Engineering (CASE)*, Vancouver, 2019.

- [61] M. Sardinha, C. M. Vicente, N. Frutuoso, M. Leite, R. Ribeiro and L. Reis, "Effect of the Ironing Process on ABS Parts Produced by FDM," *Material Design and Processing Communications*, vol. 3, no. 2, p. e151, 2020.
- [62] Y. Gao, L. Wu, D.-M. Yan and L. Nan, "Near support-free multi-directional 3D printing via global-optimal decomposition," *Graphical Models*, vol. 104, p. 101034, 2019.
- [63] C. Dai, C. C. L. Wang, C. Wu, S. Lefebvre, G. Fang and Y.-J. Liu, "Support-Free Volume Printing by Multi-Axis Motion," *ACM Transactions on Graphics*, vol. 37, no. 4, pp. 1-14, 2018.
- [64] E. Ulu, E. Korkmaz, K. Yay and O. B. Ozdoganlar, "Enhancing the Structural Performance of Additively Manufactured Objects Through Build Orientation Optimization," *Journal of Mechanical Design*, vol. 137, no. 11, 2015.
- [65] G. Fang, T. Zhang, S. Zhong, X. Chen, Z. Zhong and C. C. Wang, "Reinforced FDM: Multi-Axis Filament Alignment with Controlled Anisotropic Strength," *ACM Transactions on Graphics*, vol. 39, no. 6, 2020.

APPENDICES

APPENDIX A: COMPONENT DRAWINGS

This appendix contains the engineering drawings of the geometries manufactured by the CMMS Lab at CSU and by Ability Composites to support the studies presented in this thesis.

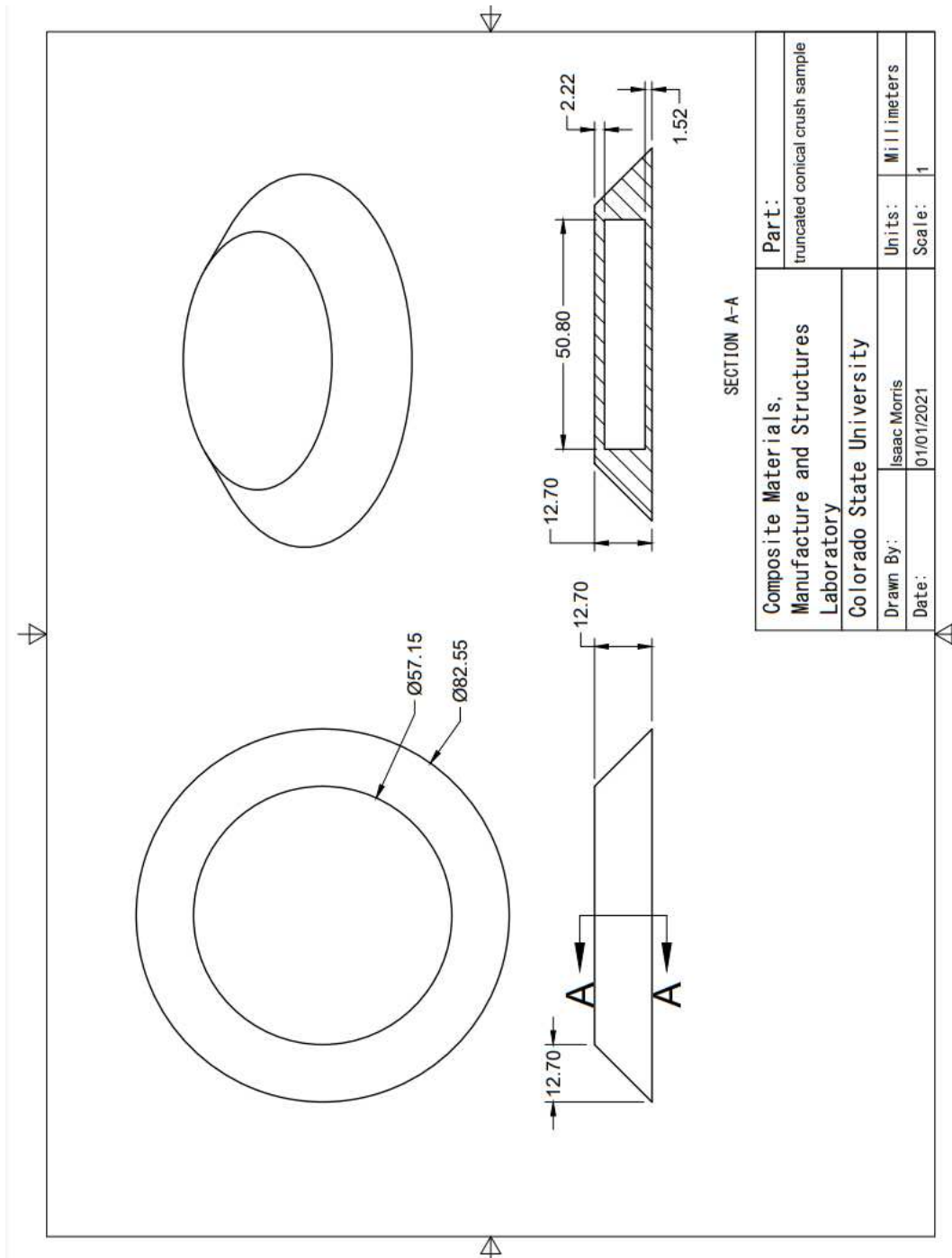


Figure A 1 Crush sample geometry

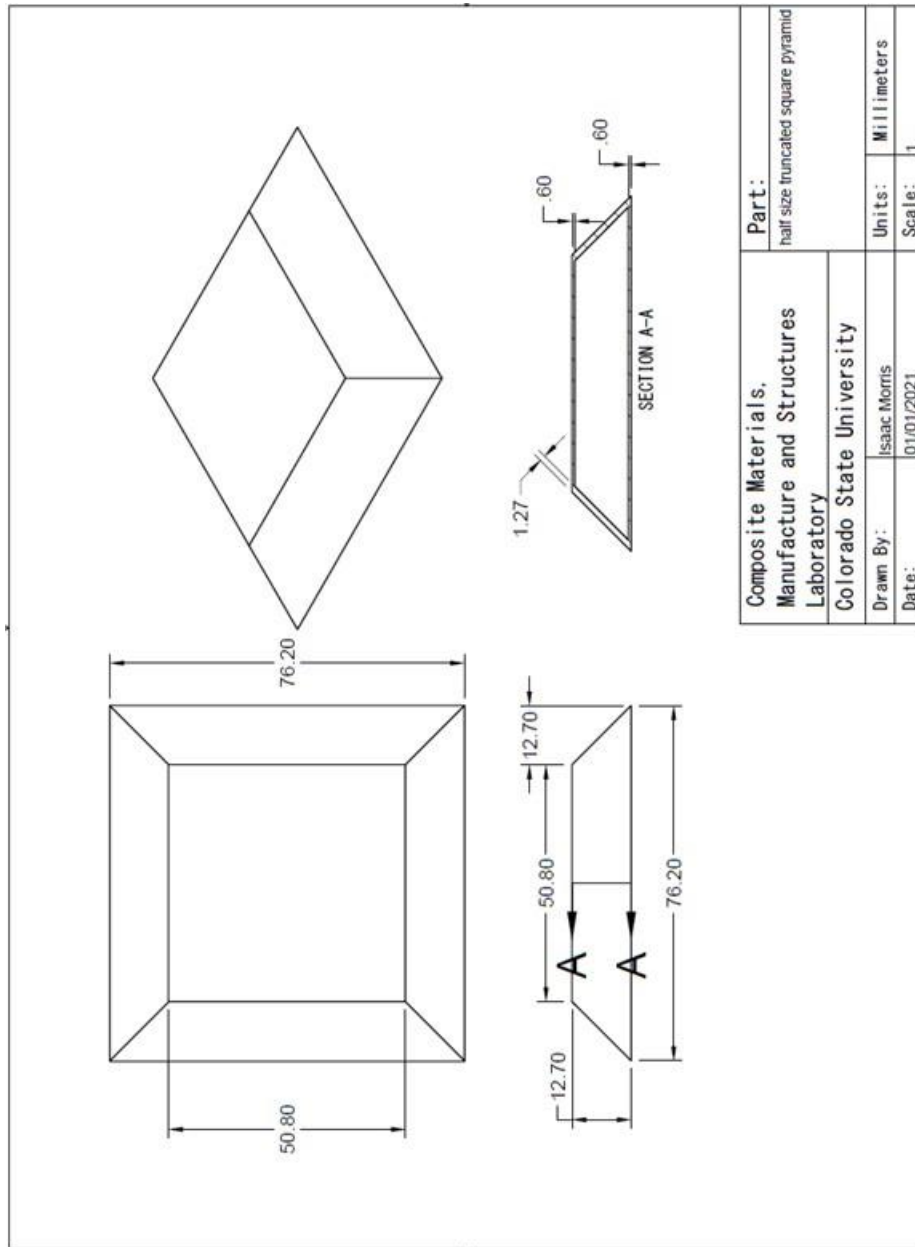
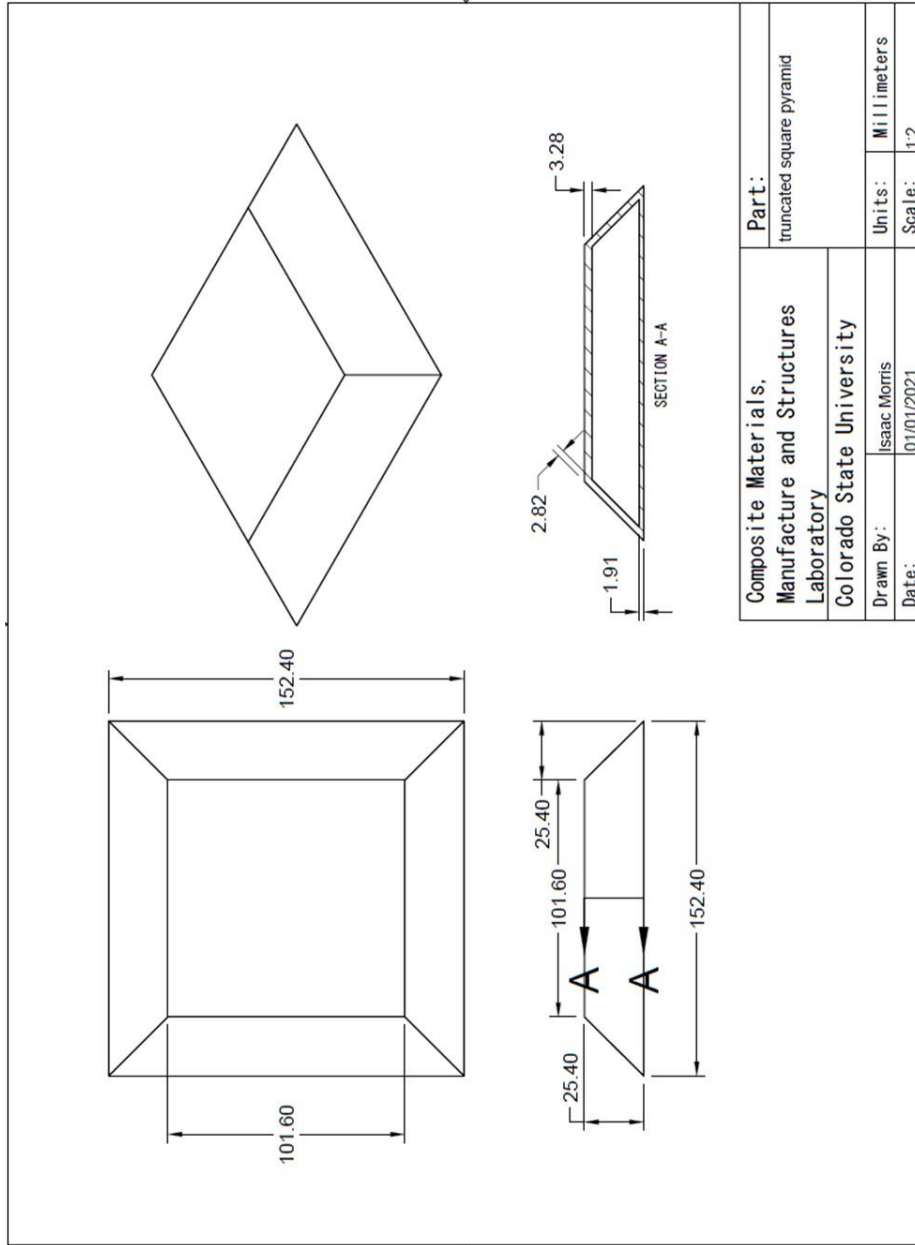


Figure A 2 Truncated square pyramid geometry for PETG sample studies



Composite Materials, Manufacture and Structures Laboratory Colorado State University	Part: truncated square pyramid	
	Drawn By: Isaac Morris	Units: Millimeters
Date: 01/01/2021	Scale: 1:2	

Figure A 3 Truncated pyramid geometry for composite manufacturing trials

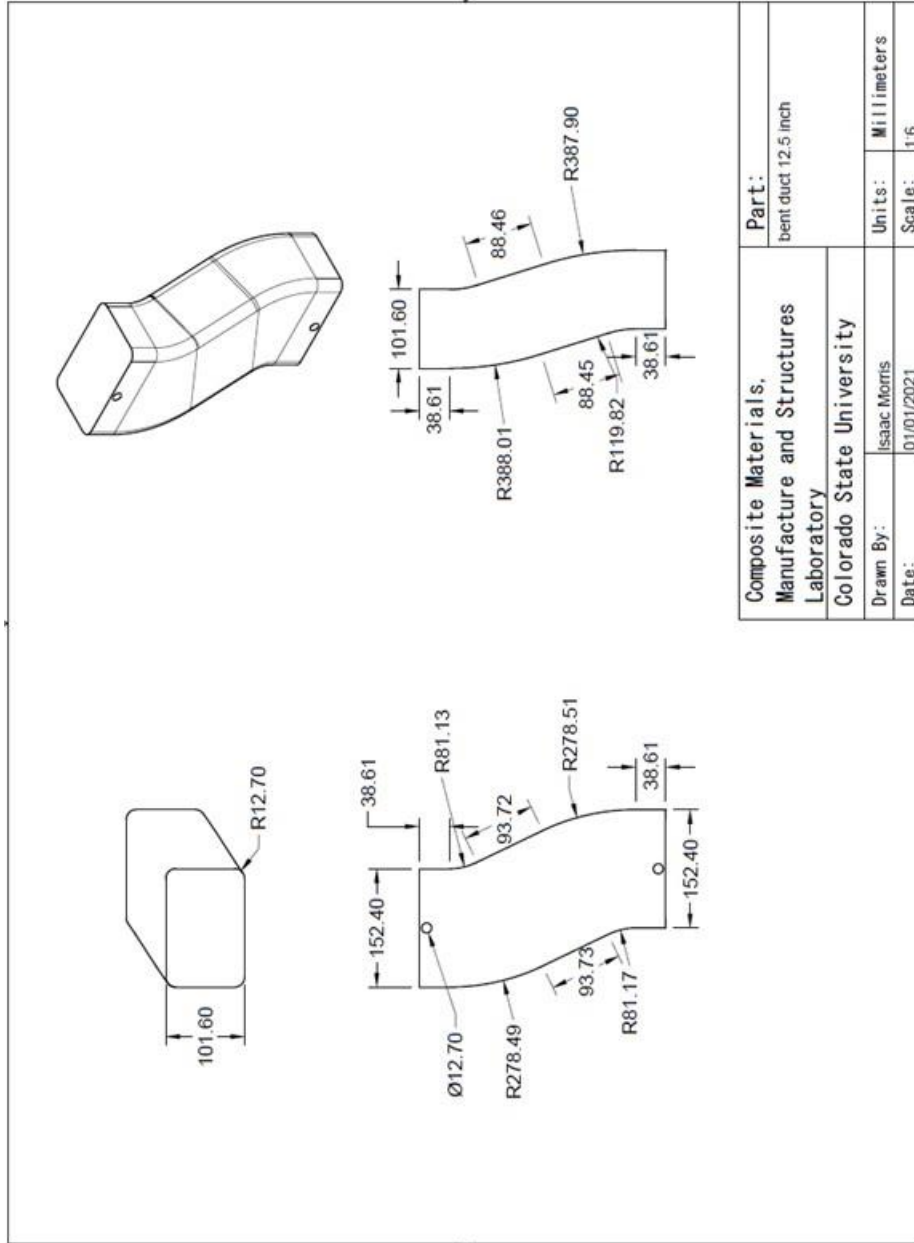


Figure A 4 Bent duct tooling geometry

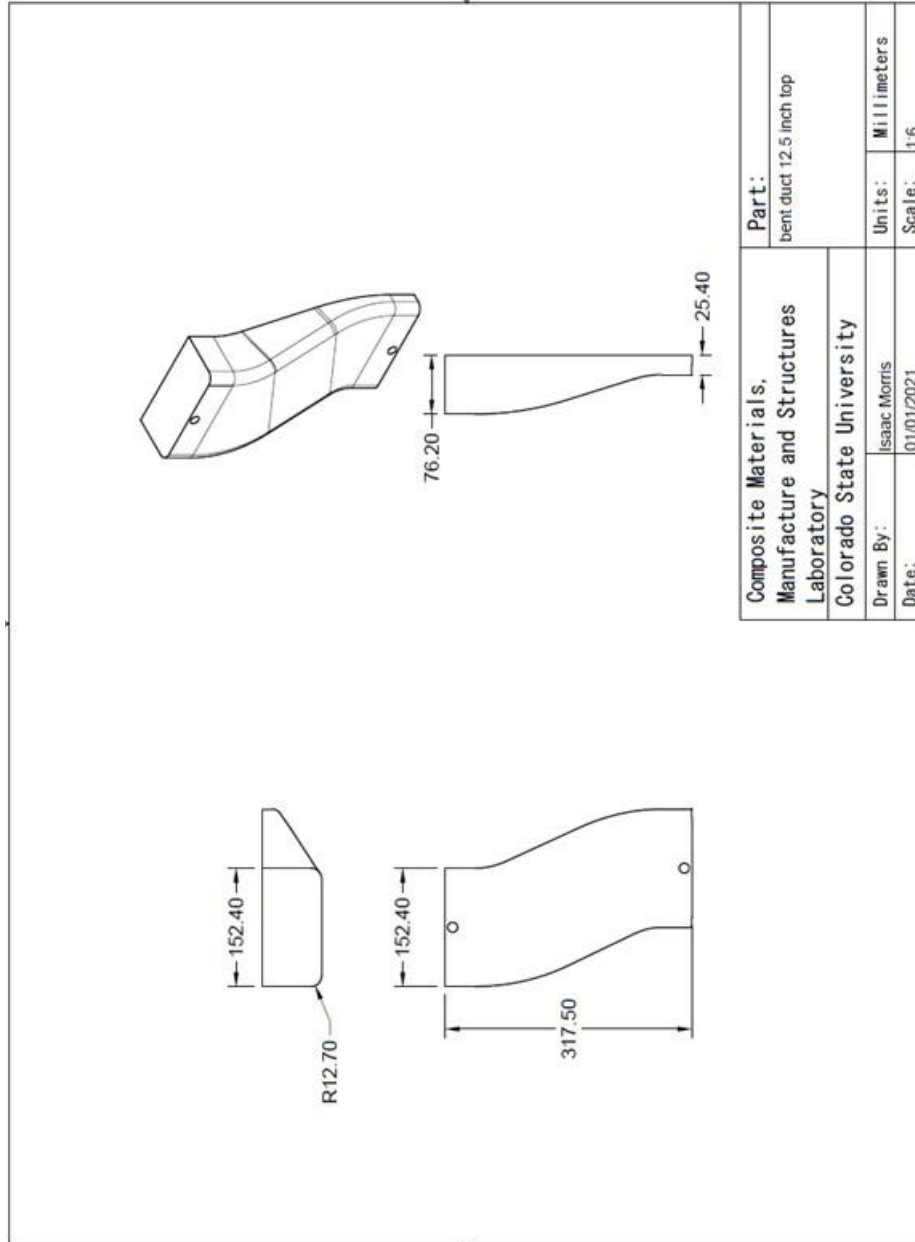


Figure A 5 Top half of longitudinally split bent duct

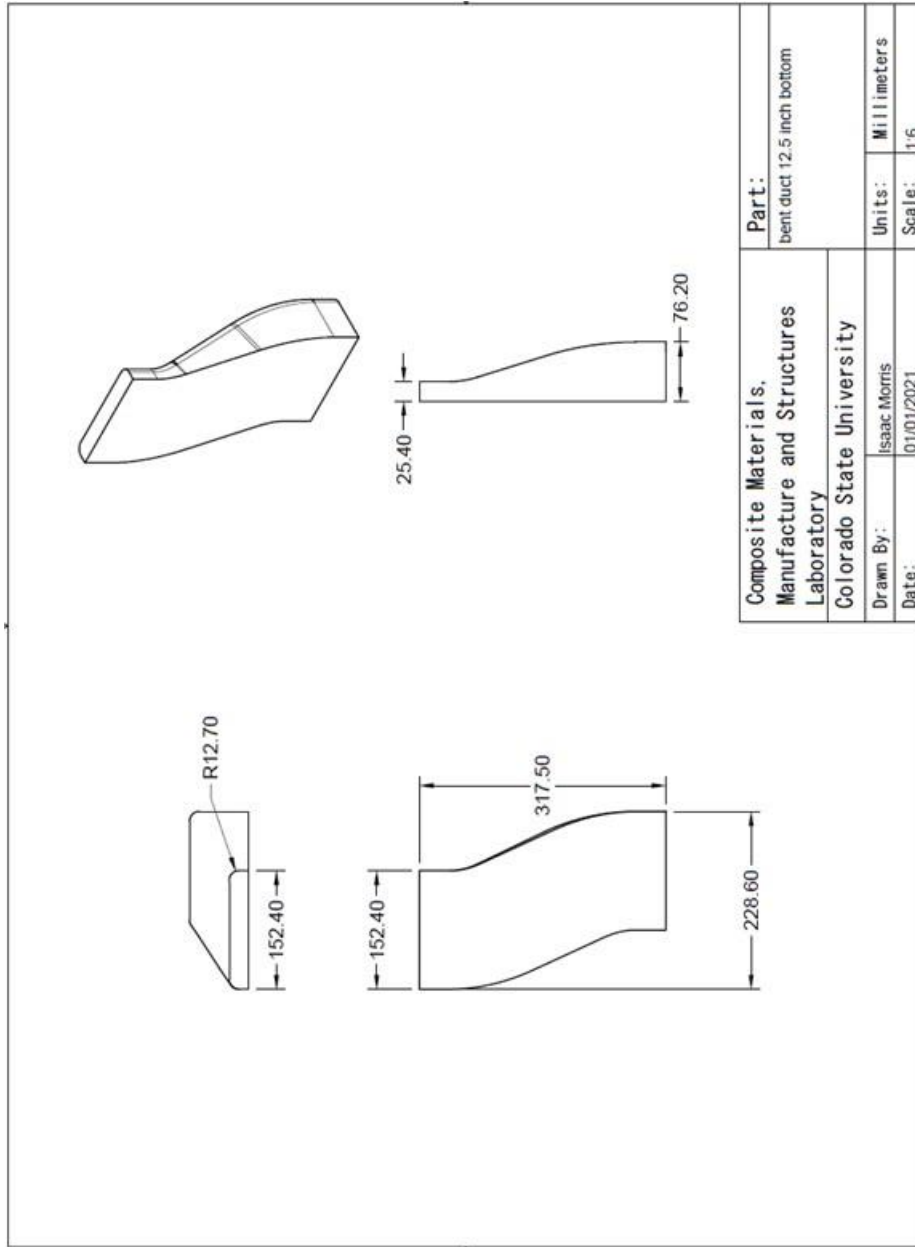


Figure A 6 Bottom half of longitudinally split bent duct

APPENDIX B: 3D SCANS

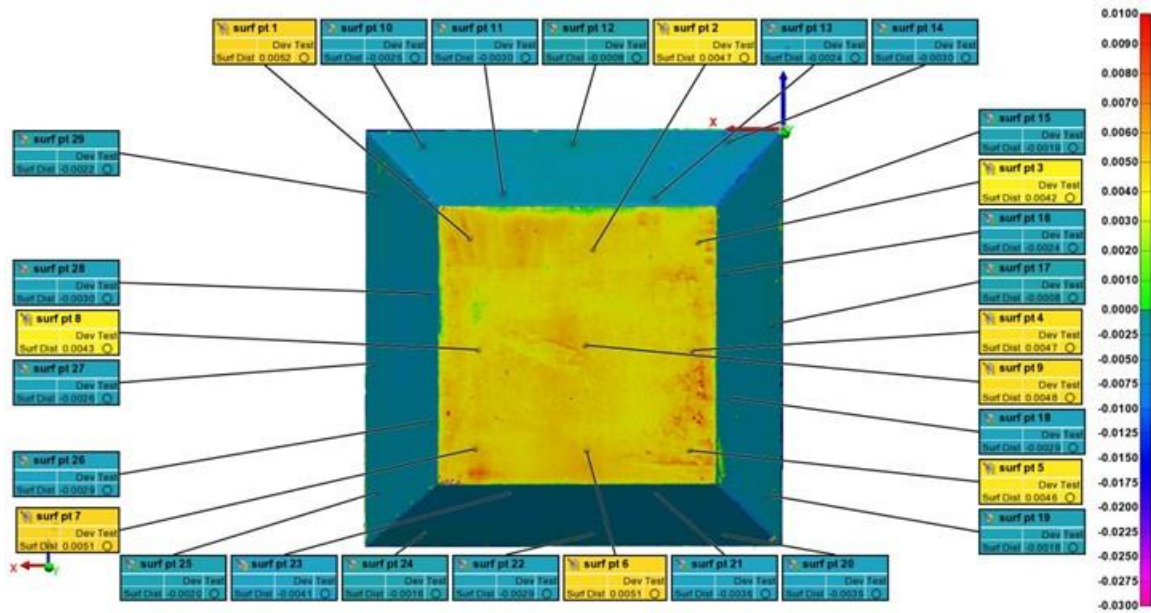


Figure B 1 The ceramic pyramid tool FaroArm 3D scan prior to composite manufacture.

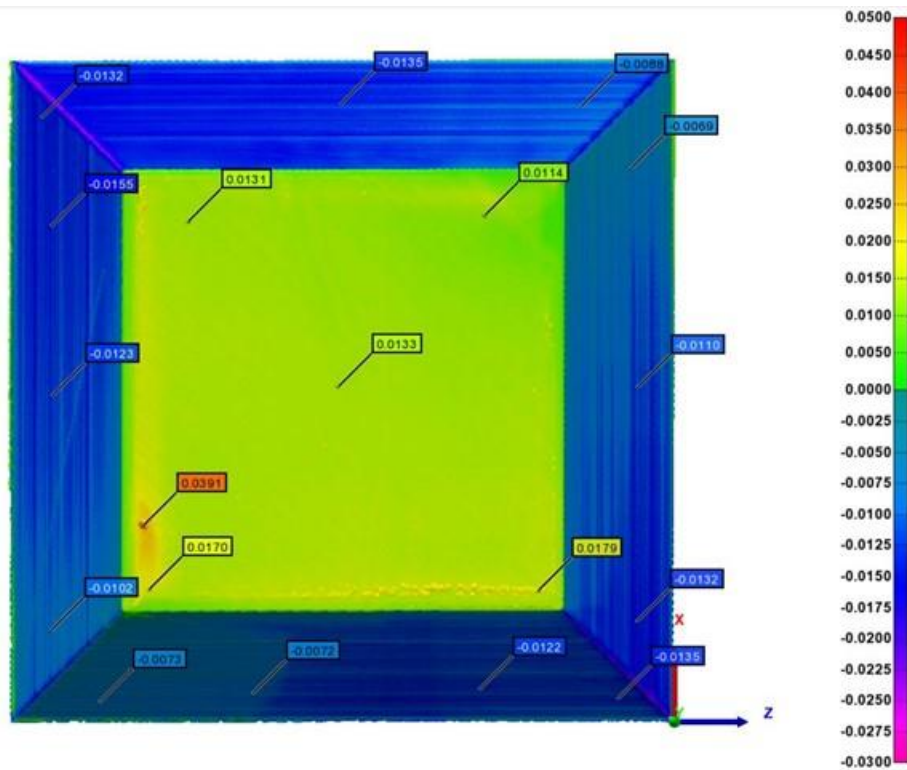


Figure B 2 The Smooth Pyramid tool FaroArm 3D scan prior to composite manufacture.

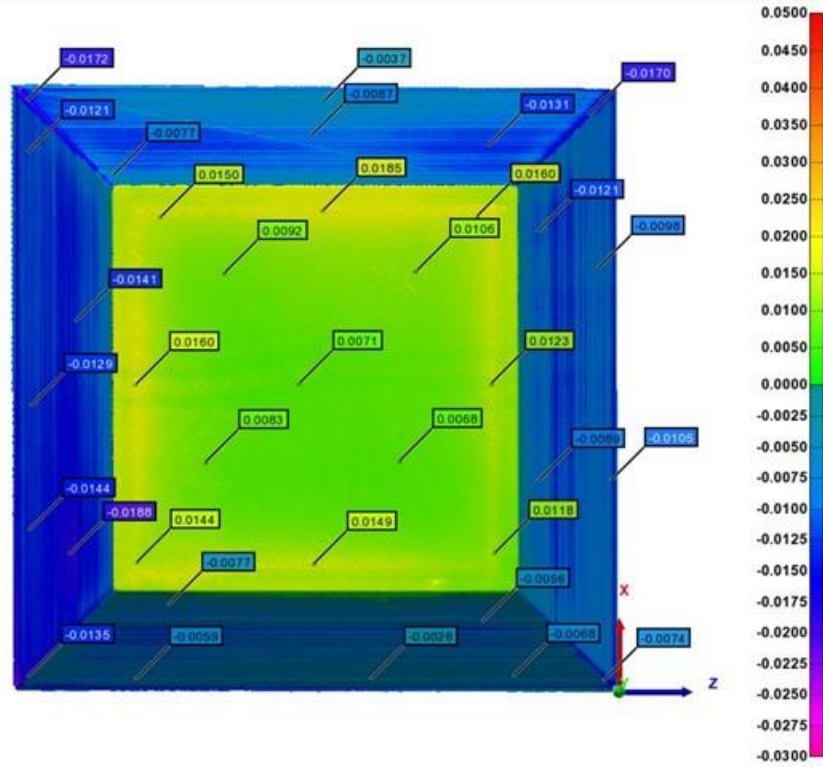


Figure B 3 The Rough Pyramid tool FaroArm 3D scan after one composite was manufactured.

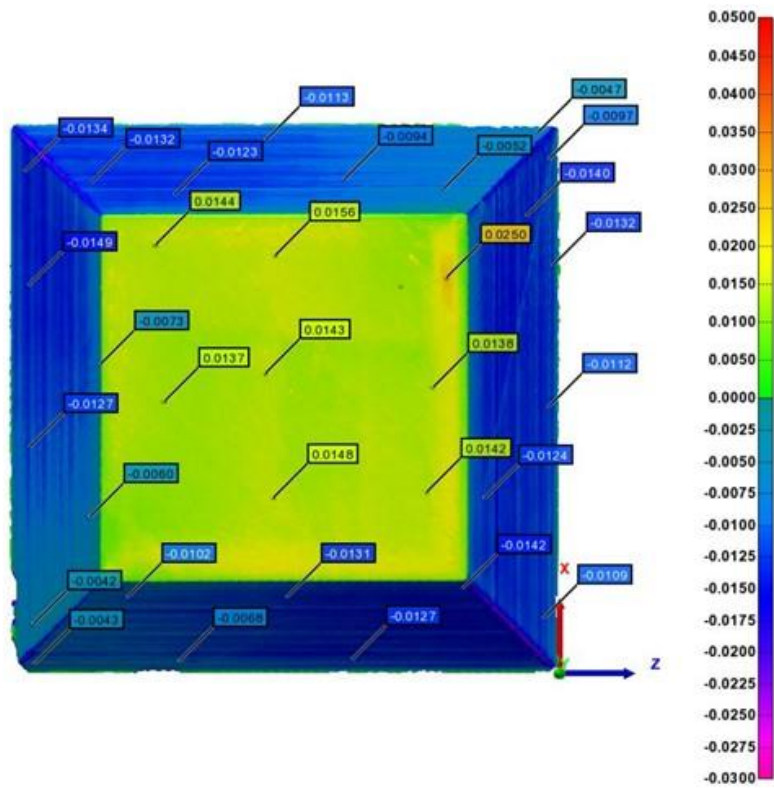


Figure B 4 The Smooth Pyramid tool FaroArm 3D scan after one composite was manufactured.

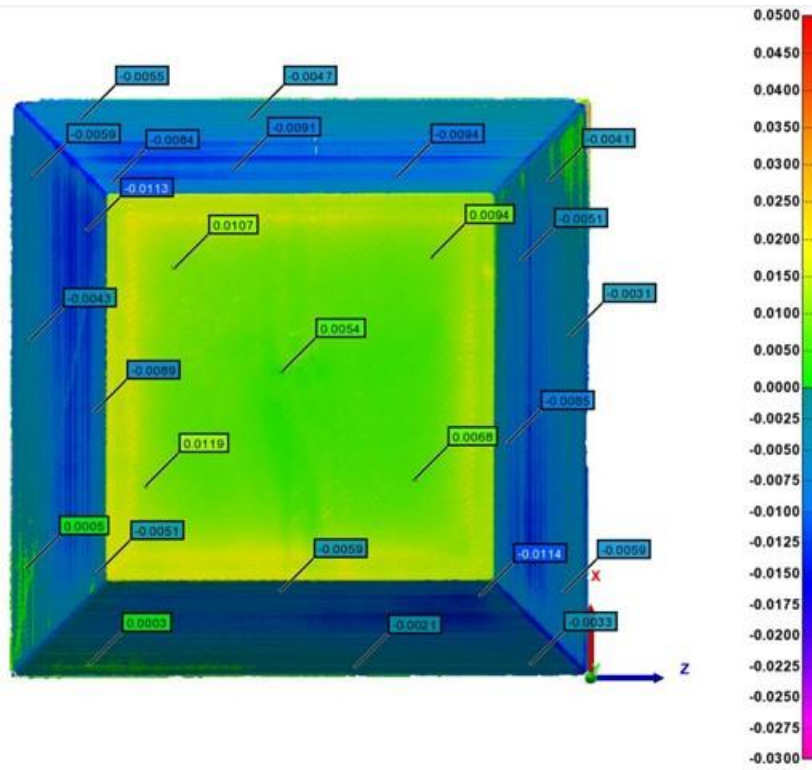


Figure B 5 The Rough Pyramid tool FaroArm 3D scan after two composites were manufactured

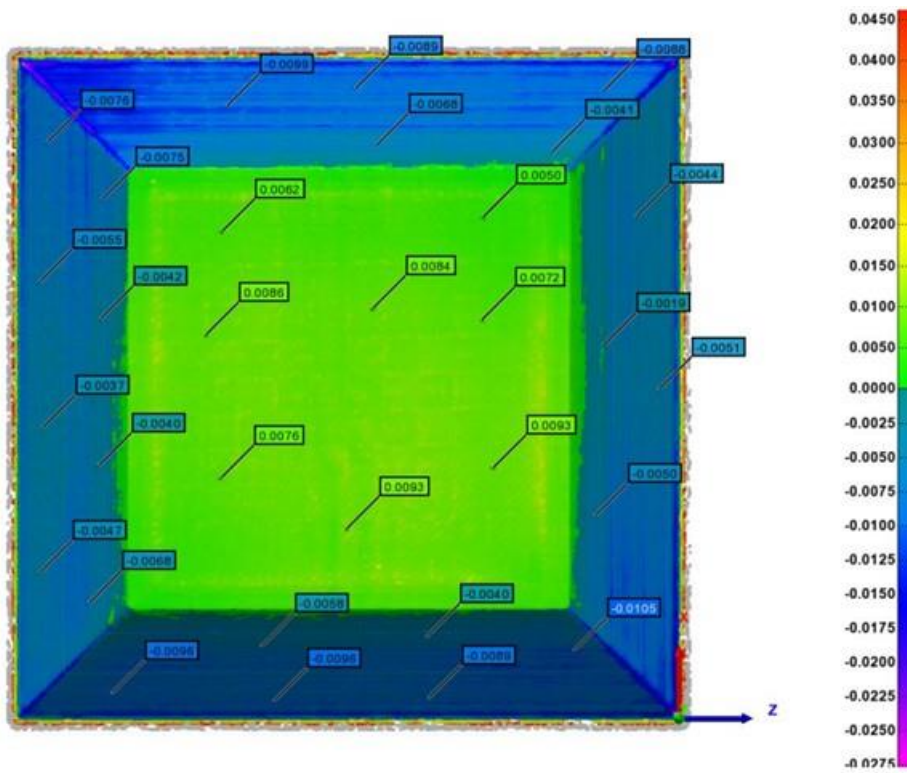


Figure B 6 The FaroArm scan of the first composite cured on the Rough Pyramid tool.

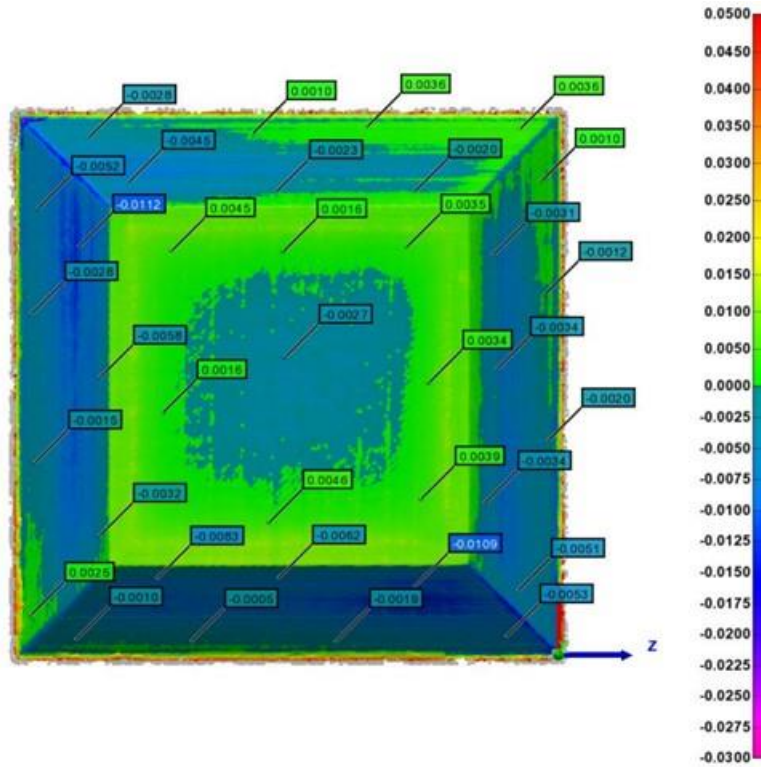


Figure B 7 The FaroArm scan of the second composite cured on the Rough Pyramid tool.

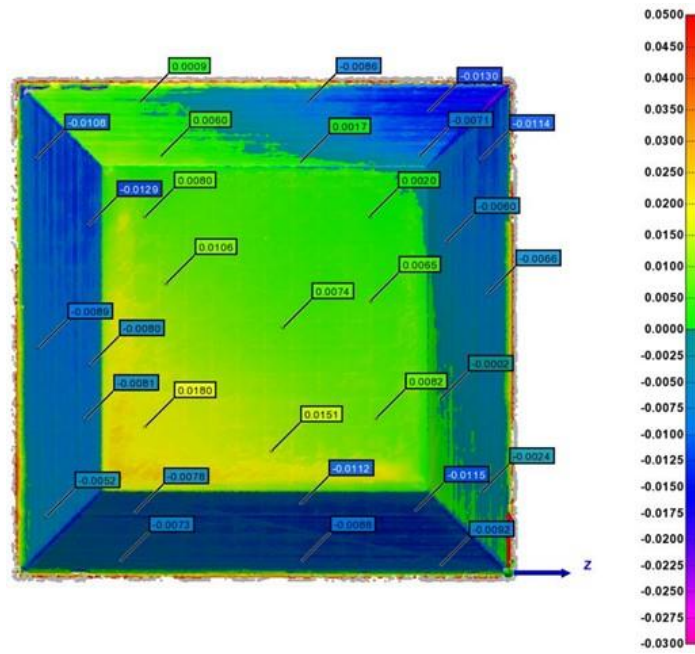


Figure B 8 The FaroArm scan of the composite cured on the Smooth Pyramid tool.

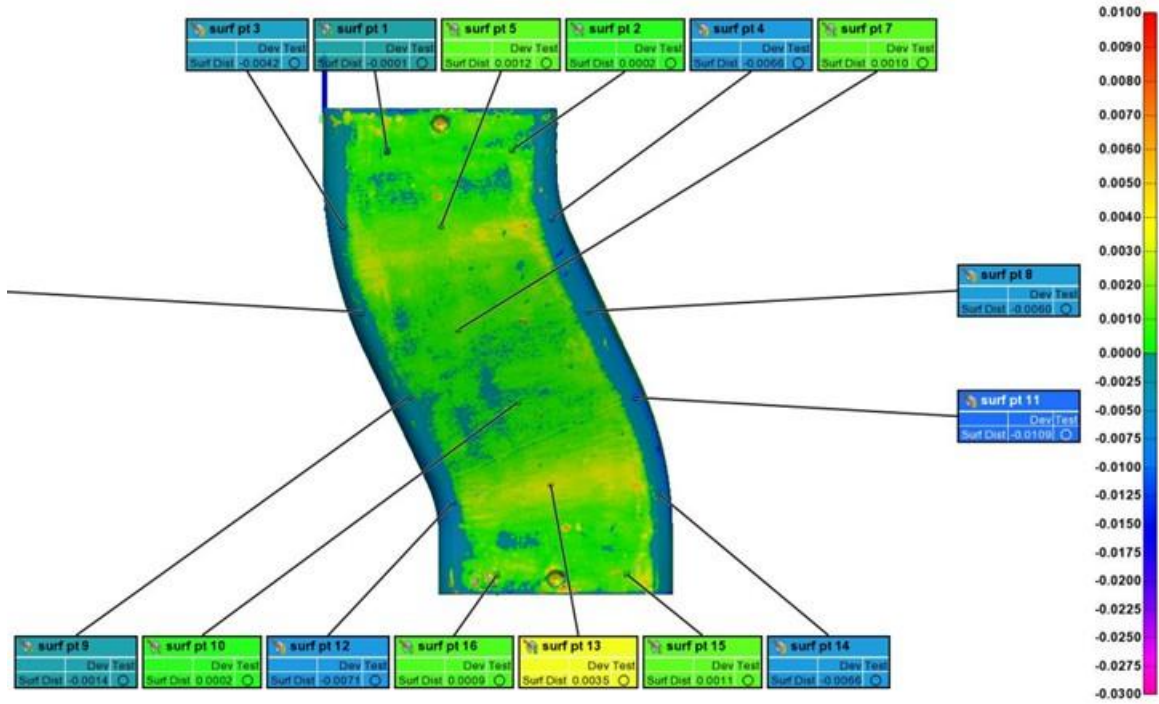


Figure B 9 The FaroArm scan of the top half of the tool used for the Control Duct (0).

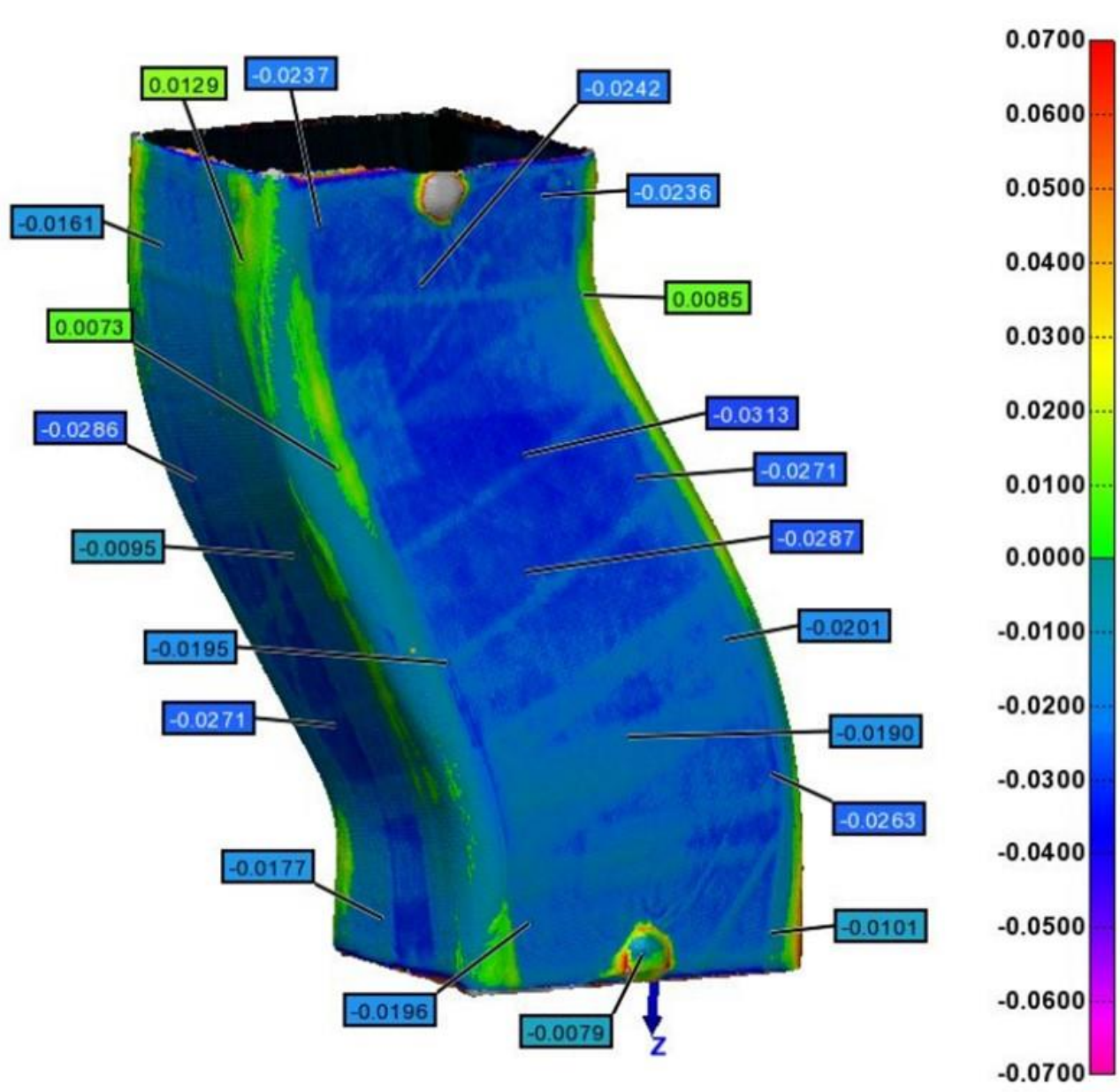


Figure B 10 The FaroArm scan of the composite manufactured on the Control Duct Tool (0).

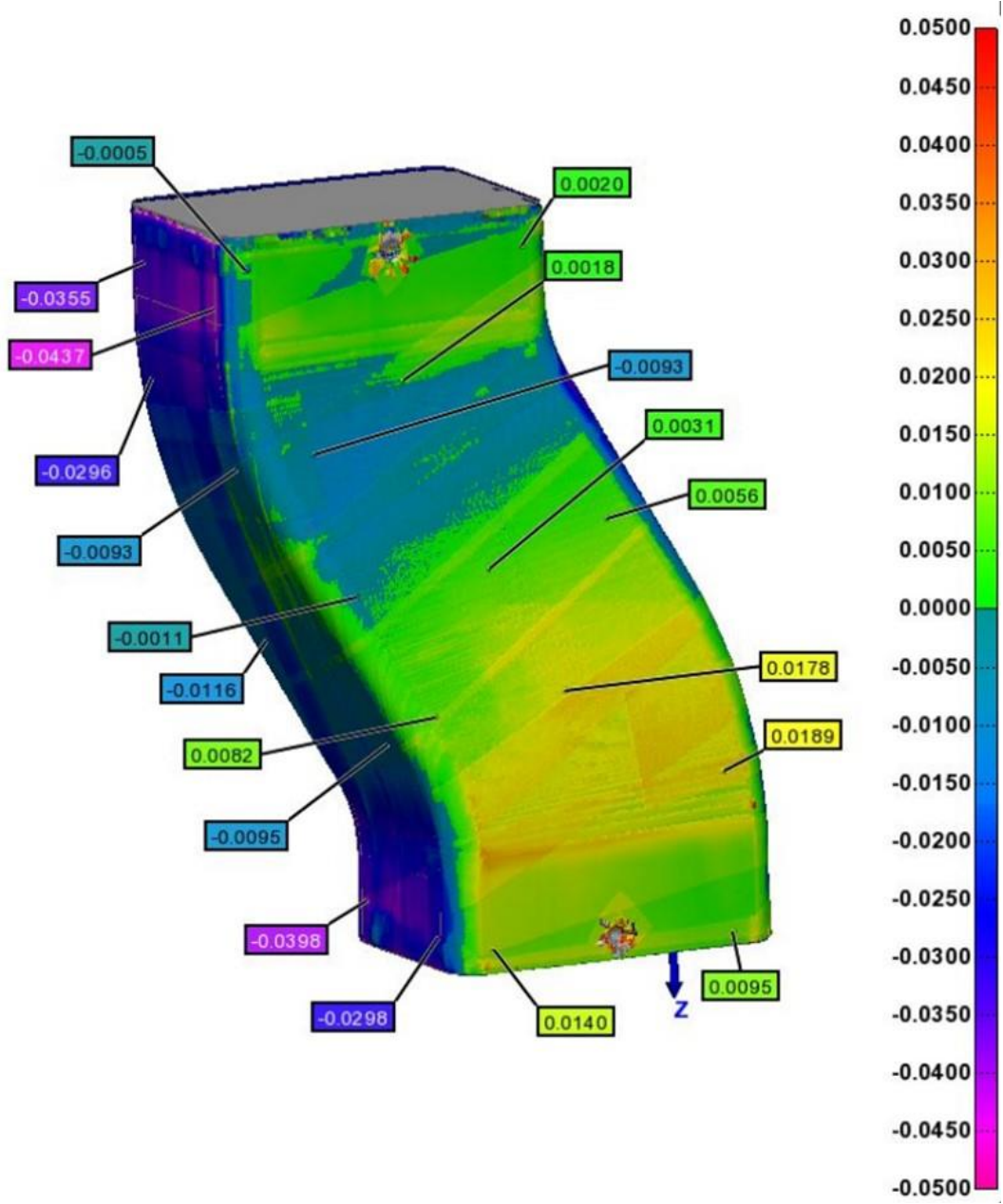


Figure B 11 The FaroArm scan of the Split ST-130 Tool (1).

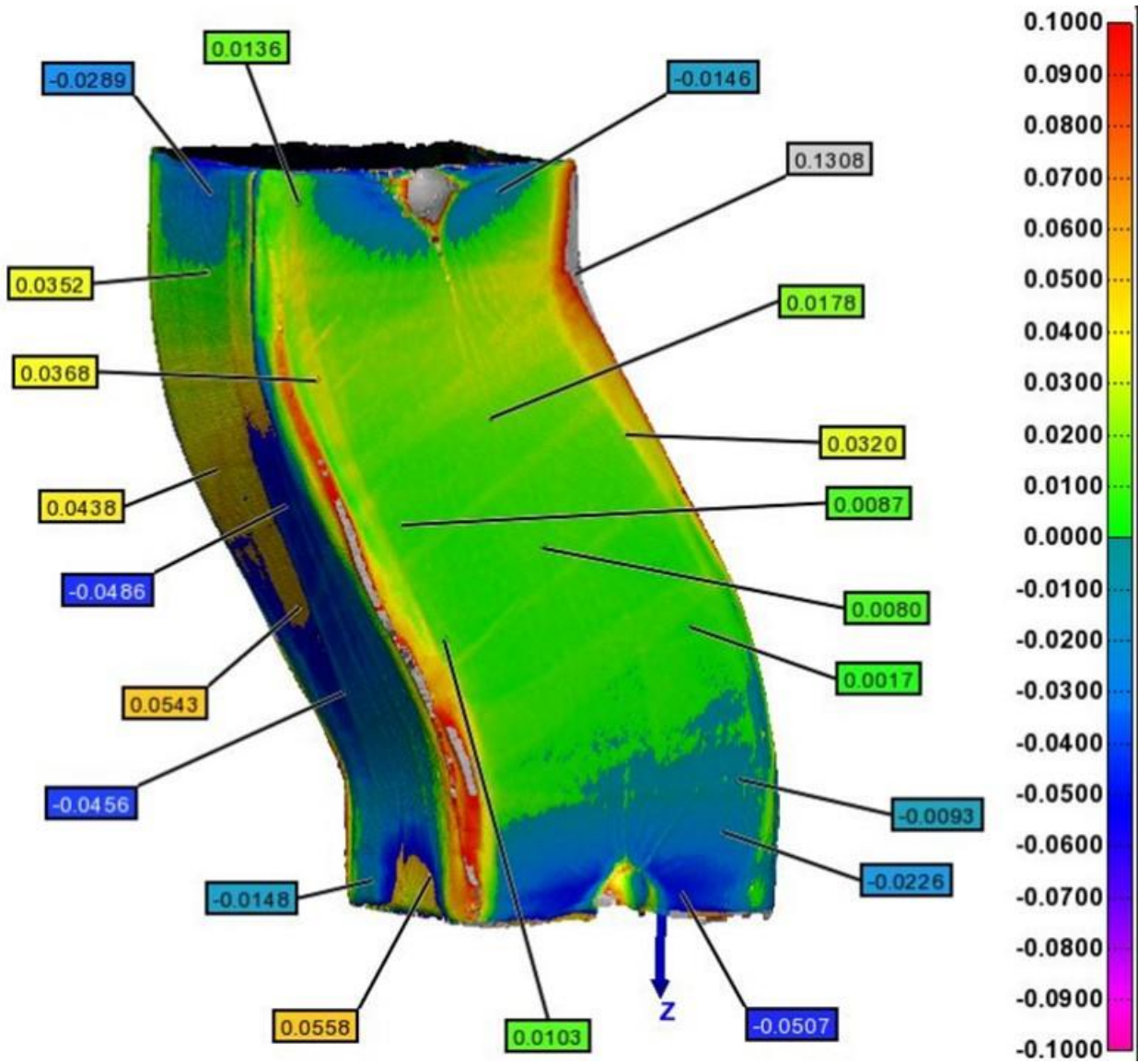


Figure B 12 The FaroArm scan of the composite manufactured on the Split ST-130 Tool (1).

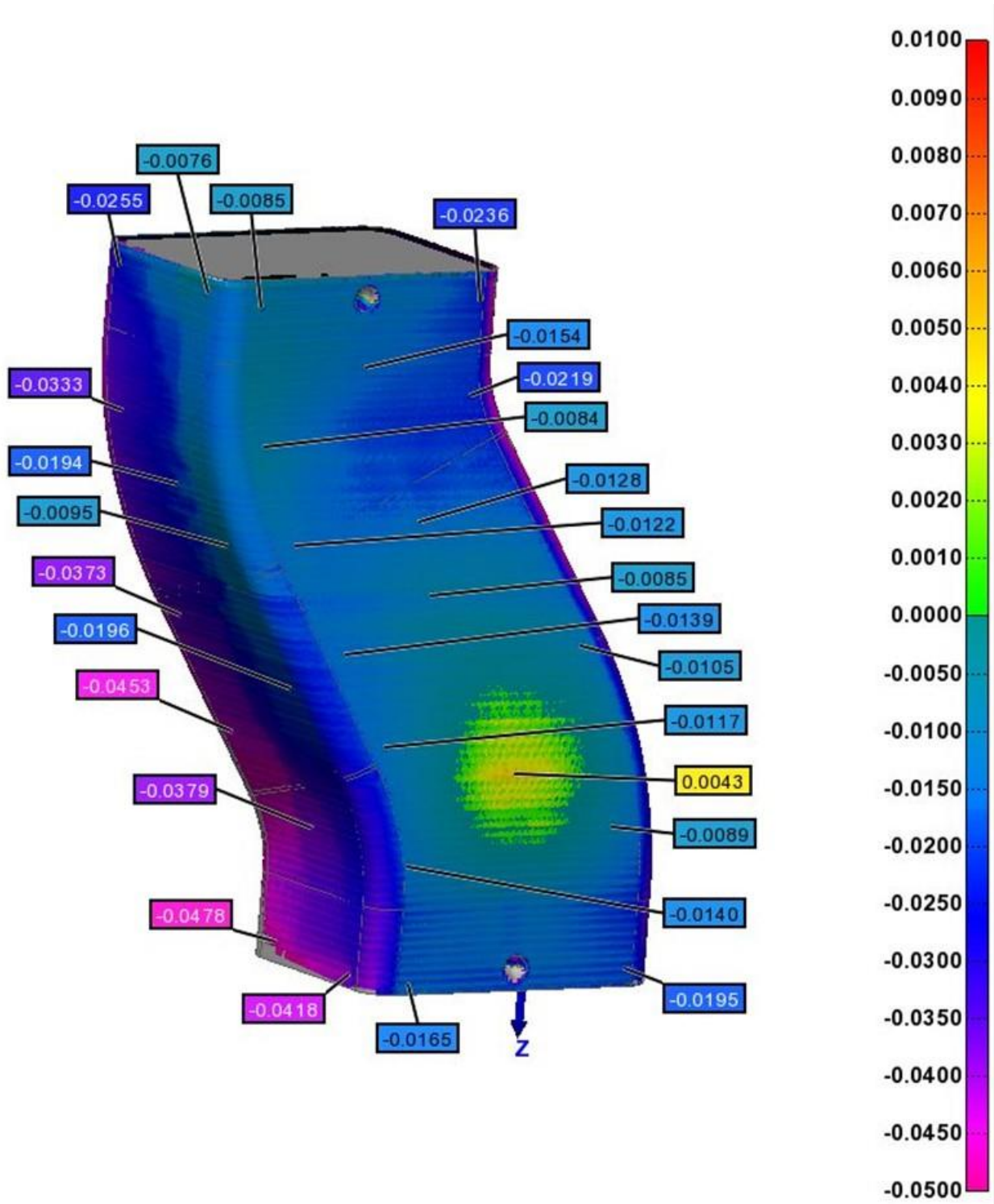


Figure B 13 The FaroArm scan of the Thick ST-130 Tool (2).

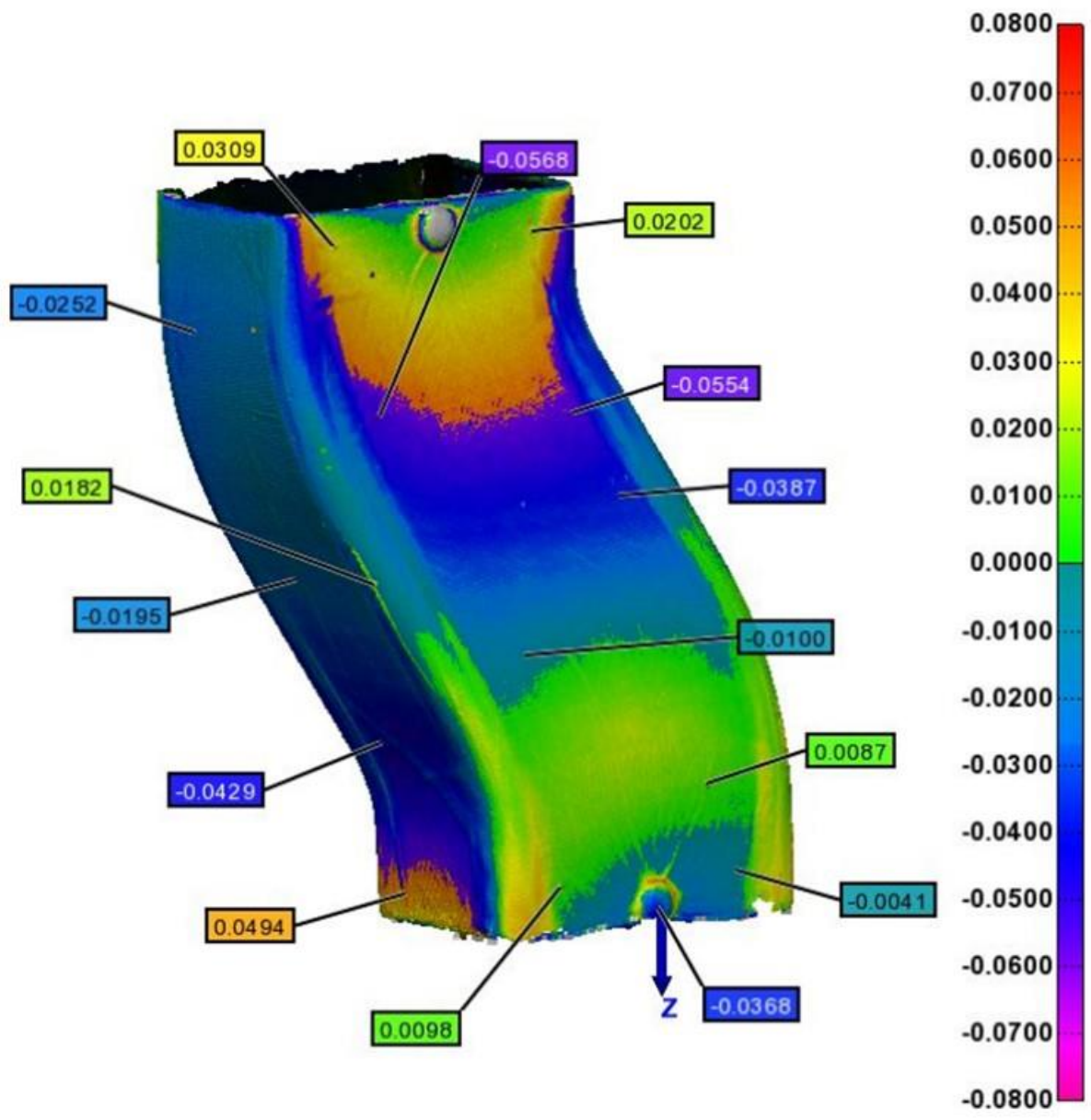


Figure B 14 The FaroArm scan of the composite manufactured on the Thick ST-130 Tool (2).

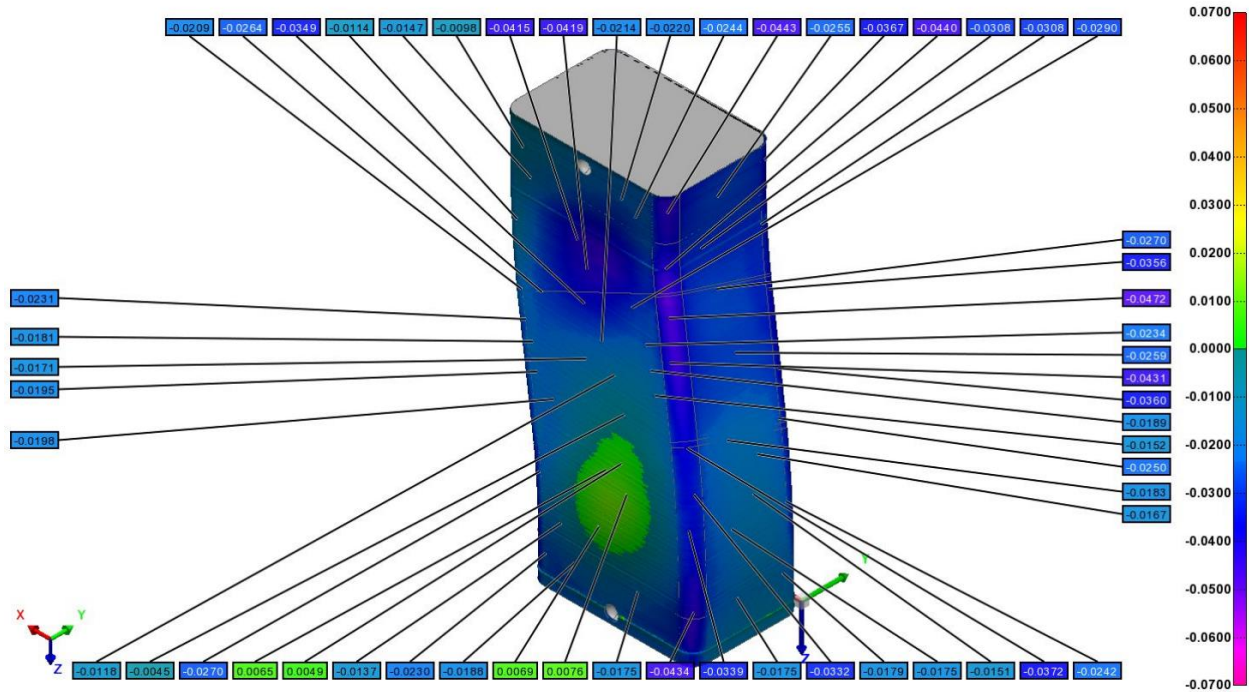


Figure B 15 The FaroArm scan of the Thin ST-130 Tool (3).

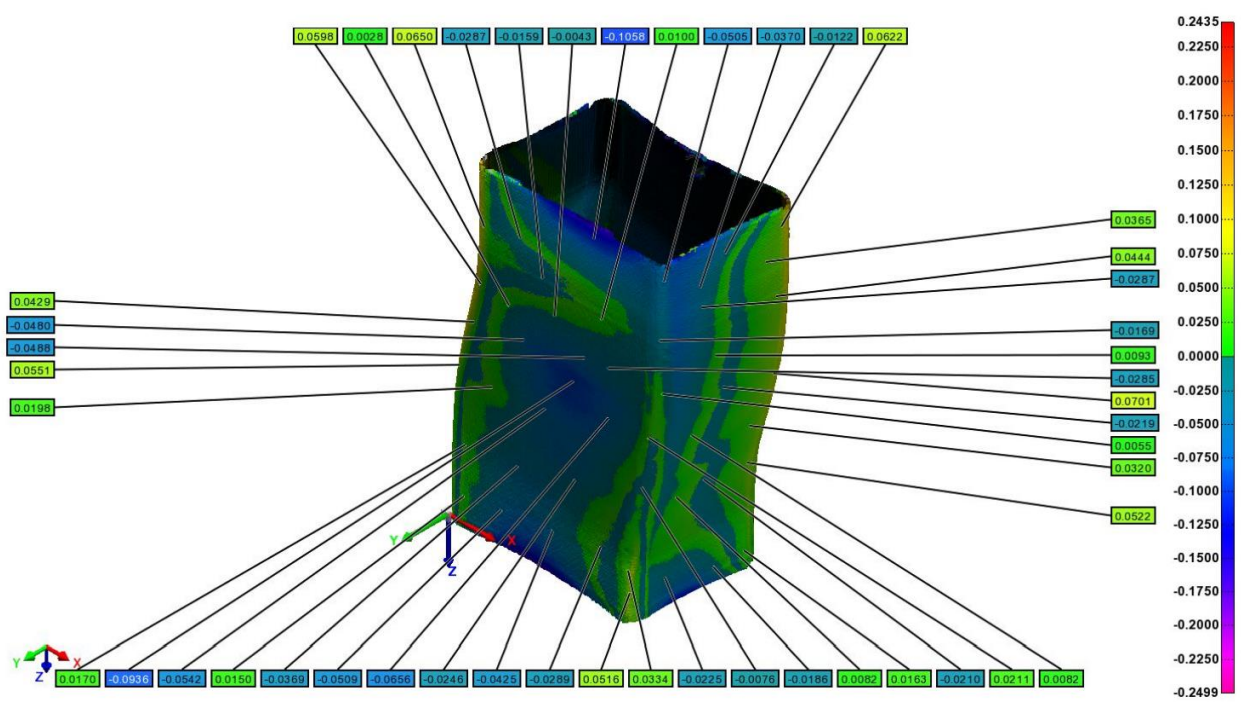


Figure B 16 The FaroArm scan of the composite manufactured on the Thin ST-130 Tool (3).

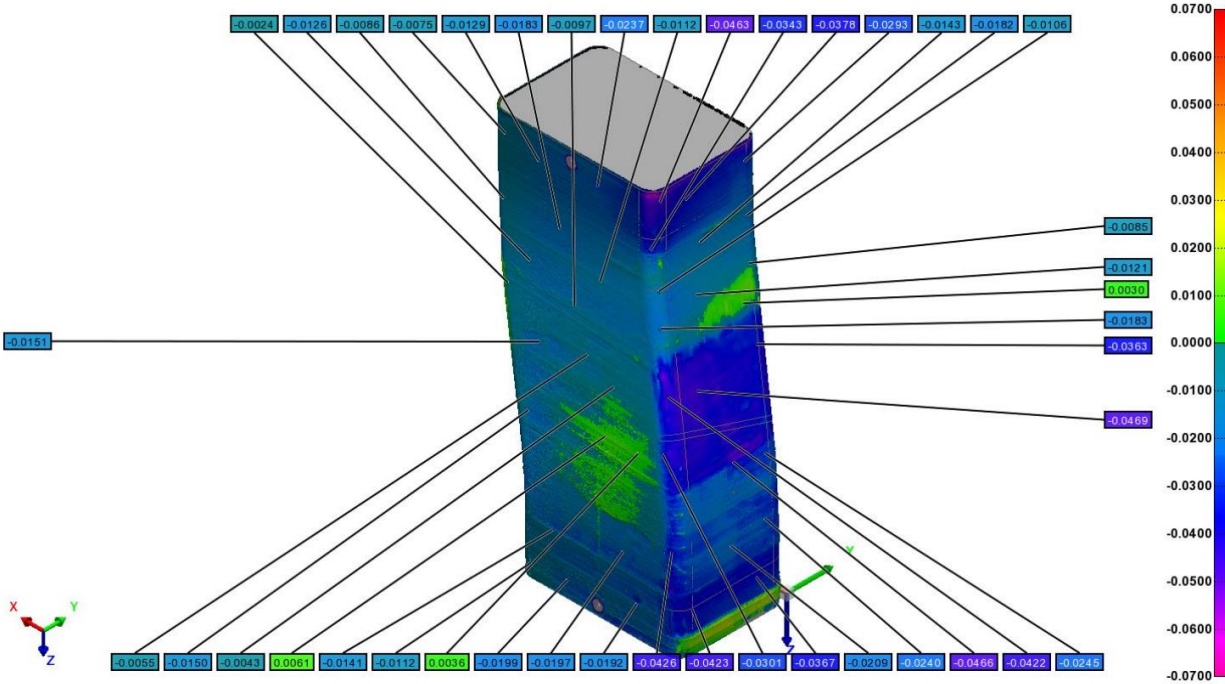


Figure B 17 The FaroArm scan of the Thick AQ-120 Tool (4).

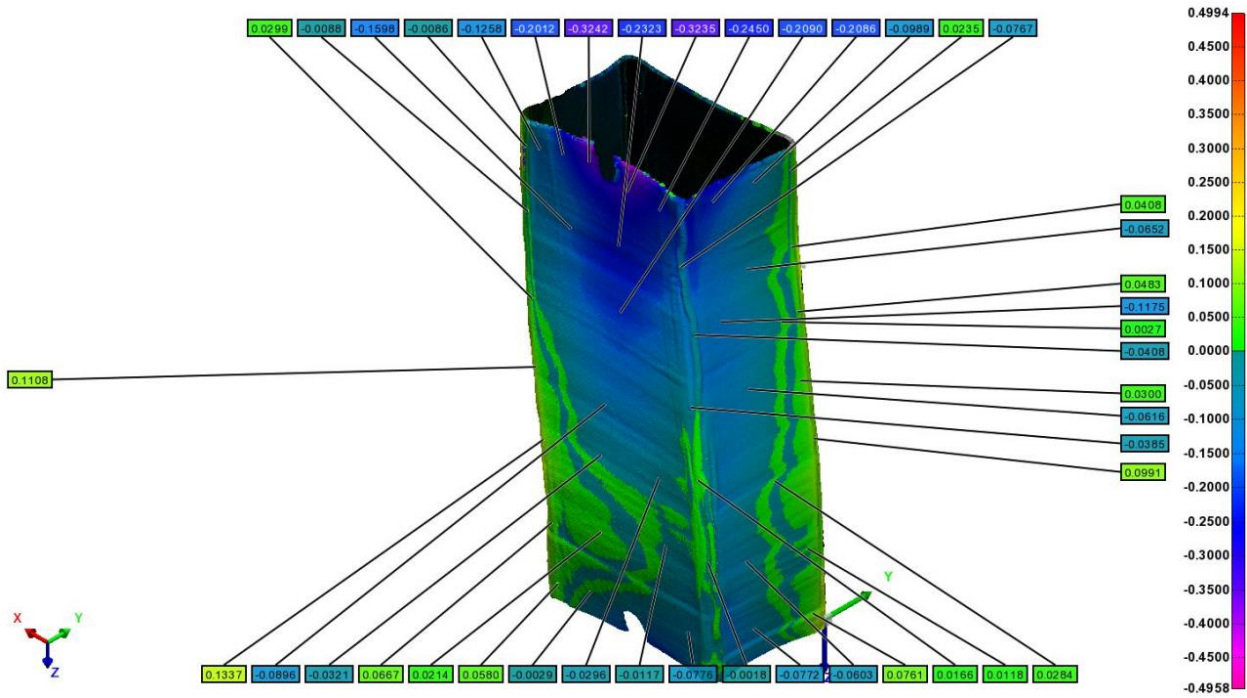


Figure B 18 The FaroArm scan of the composite manufactured on the Thick AQ-120 Tool (4).

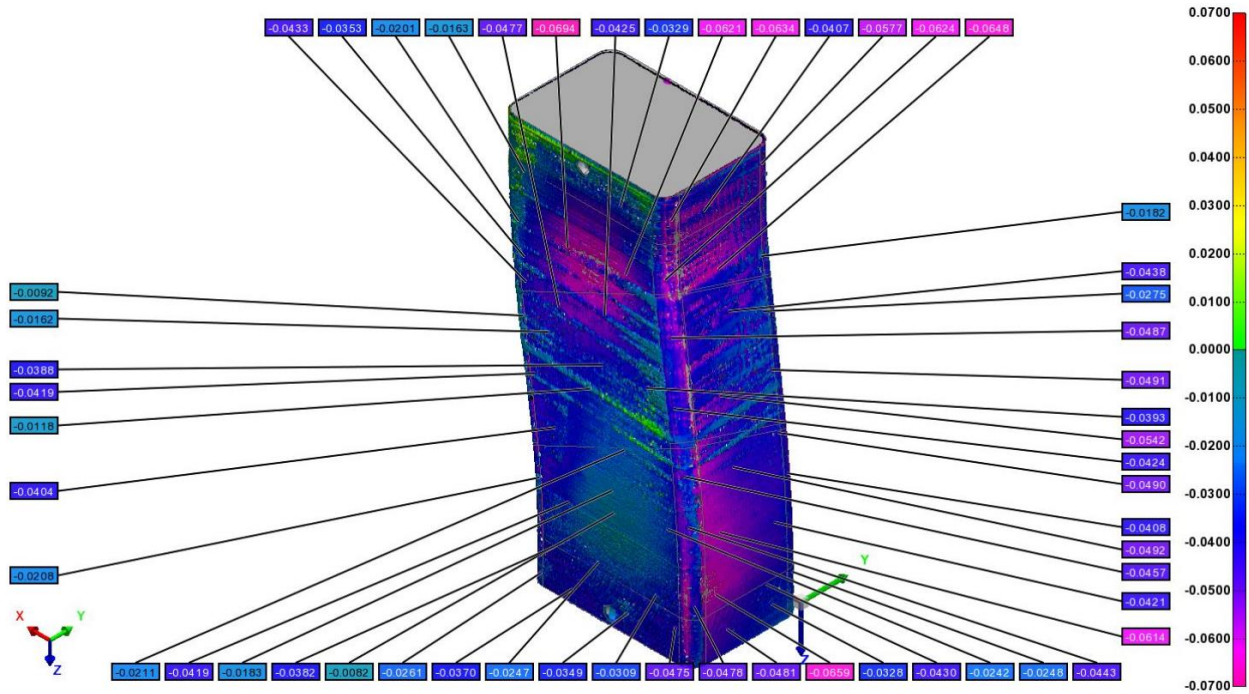


Figure B 19 The FaroArm scan of the Thin AQ-120 Tool (5).

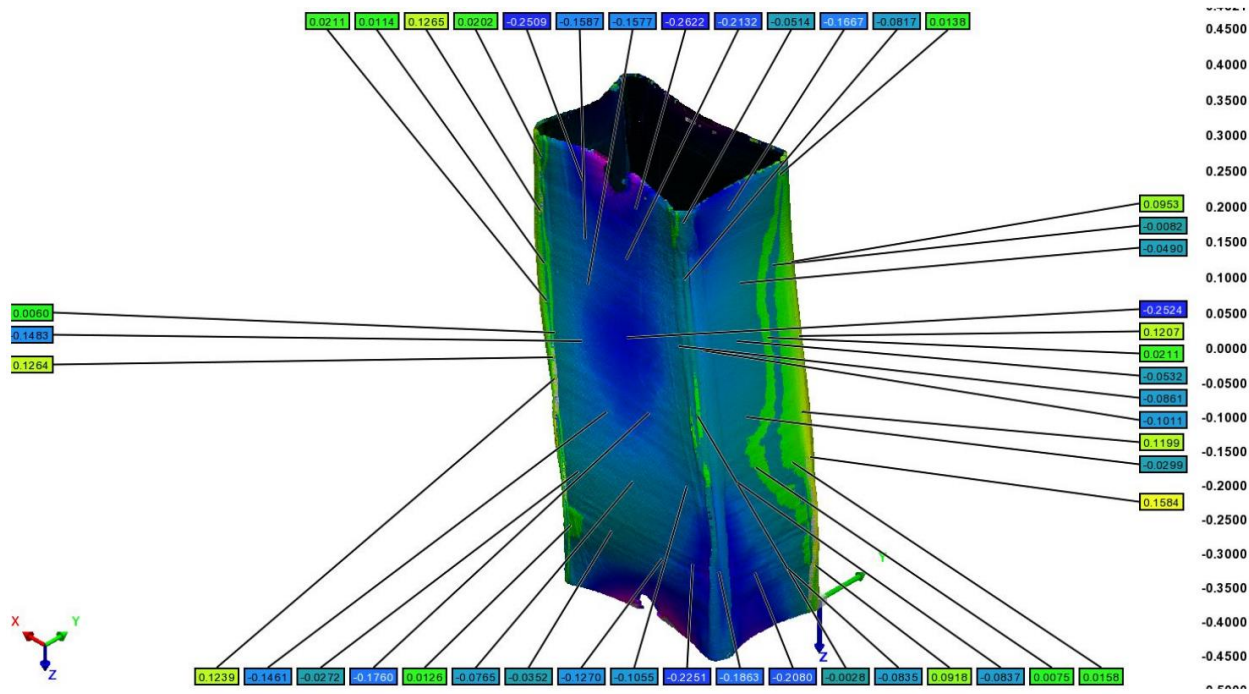


Figure B 20 The FaroArm scan of the composite manufactured on the Thin AQ-120 Tool (5).

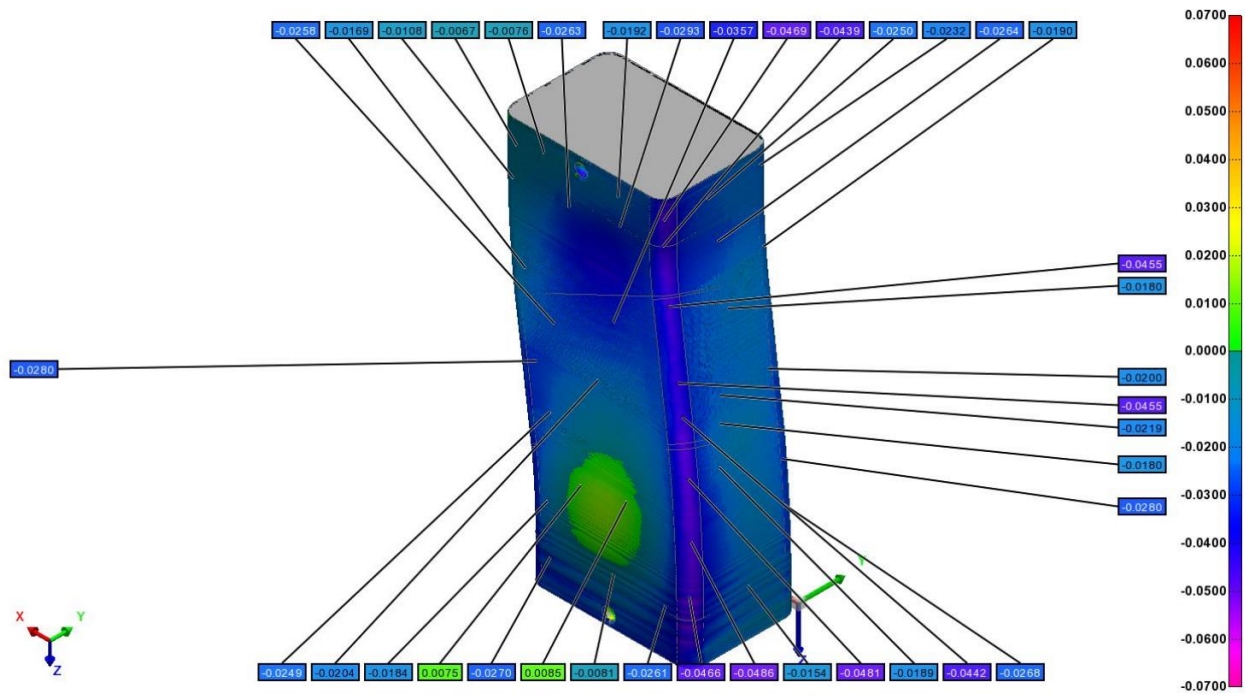


Figure B 21 The FaroArm scan of the Thin AQ-180 Tool (6).

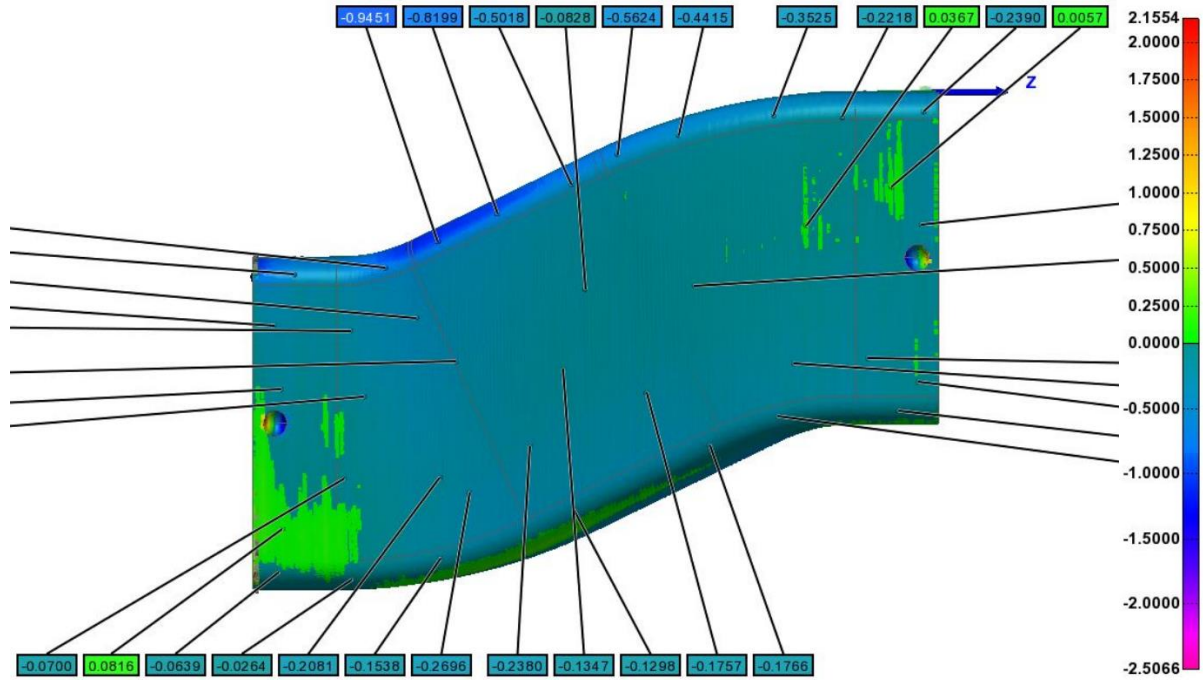


Figure B 23 The FaroArm scan of the Extra Thick ST-130 Tool (7).

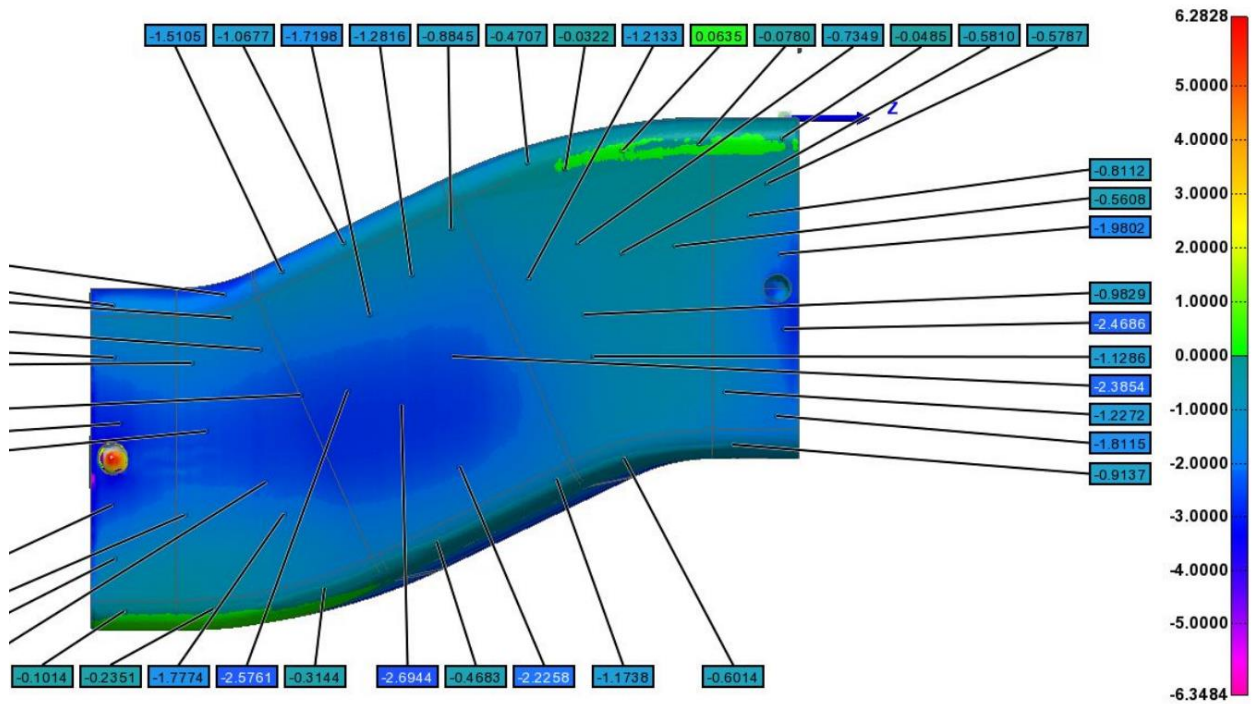


Figure B 24 The FaroArm scan of the Extra Thick ST-130 Tool (7) after composite manufacture.

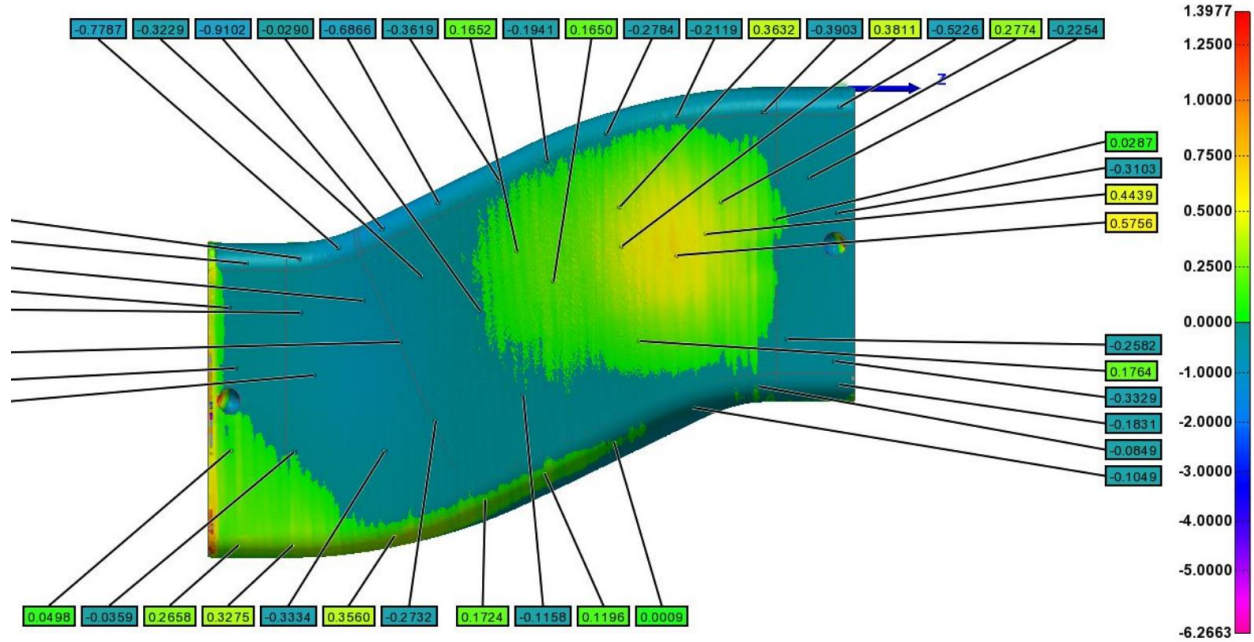


Figure B 25 The FaroArm scan of the Low Temperature Thin ST-130 Duct (8).

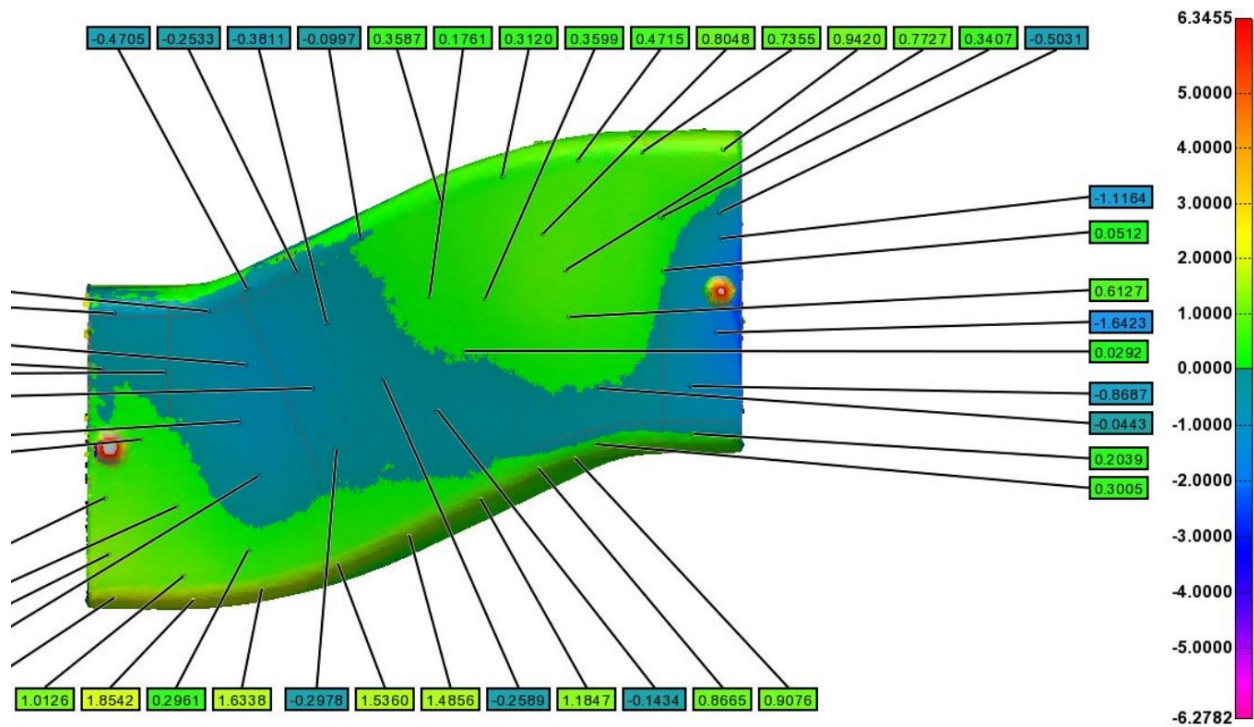


Figure B 26 The FaroArm scan of the composite manufactured on the Low Temperature Thin ST-130 Tool (8).